An Improved Static Seismic Design Method for Podium Structures with Vertical Irregularity of Mass and Stiffness

by

Daniel Lahey

A thesis
presented to the University of Waterloo
in fulfillment of the
thesis requirement for the degree of
Master of Applied Science
in
Civil Engineering

Waterloo, Ontario, Canada, 2020

Author's Declaration

I hereby declare that I am the sole author of this thesis. This is a true copy of the thesis, including any required final revisions, as accepted by my examiners.

I understand that my thesis may be made electronically available to the public.

Abstract

Owing to potentially reduced costs and faster project timelines, North American designers are increasingly opting for novel structural systems that are not well-addressed by the current model codes. Specifically, mid-rise structures are increasingly incorporating a vertical combination of seismic force-resisting systems, in which a stiff and massive lower podium structure (e.g. a reinforced concrete moment resisting frame) is used to support a less massive, less stiff upper tower structure (e.g. of cold-formed steel). These structures are vertically irregular in both their mass and stiffness and thus subject to restrictions and complications if designed according to modern design codes. In particular, the design procedure is generally both dynamic and iterative, not static and closed-form. These restrictions are imposed based on the justifiable expectation that such a vertically irregular structure behaves differently than a regular one. Research has repeatedly demonstrated that such structures exhibit more severe higher-mode effects, differences in inelastic action and a response that is sensitive to the relative stiffness and mass of the two structures. To remedy this, previous studies by Yuan & Xu (Xu & Yuan, 2015; Yuan, 2016; Yuan & Xu, 2016, 2014) propose a methodology to assess the feasible storey-stiffness distributions and equivalent static loads appropriate to such as structure, both for NBCC 2010 (National Research Council of Canada (NRCC), 2010). and ASCE 7-10 (American Society of Civil Engineers (ASCE), 2010). Based on the work of Yuan & Xu, the current study aims to both improve the ease of use and the scope of these methods. This includes extending them to NBCC 2015 (NRCC, 2015c), larger mass ratios and storey counts.

The first half of the current study concerns the feasible storey-stiffness distributions, as first proposed by Yuan & Xu (Xu & Yuan, 2015; Yuan, 2016; Yuan & Xu, 2014). By approximating the expected magnification of the upper structure's first mode shear as a function of the mass and stiffness ratios between the two structures and by applying the code-specified limitation on interstorey drift to the upper structure, the procedure relates the degree of irregularity in a given structure to the required stiffness of the upper structure. the stiffnesses of the upper and lower structures are confined to those ranges for which the interstorey drift is tolerable for the expected amplification. In other words, the relationship between the higher-mode and first-mode base shears for the upper structure is used to characterize the feasible stiffness distribution subject to all other variables being known a priori. Compared to Yuan (2016), the critical points that define the relationship between the overall stiffness ratio and the amplification ratio are redefined and simplified, and the approximation to the NBCC spectral relationship is abandoned in favour of a direct numerical or graphical solution. Two

examples demonstrate the proposed procedure, with the second also comparing the results to Yuan (2016).

The latter half of the current study concerns the estimation of equivalent static loads on a mid-rise structure with a vertical combination of framing systems. Neither ASCE 7 nor NBCC 2015 incorporate irregularity into their static procedures –they consider the default procedure applicable to irregular structures subject to period and/or height requirements, except for cases where the lower structure is much stiffer than the upper one. If this is the case, the ASCE 7 two-stage procedure may be used. The procedure allows that each structure can be analyzed separately via the static procedure and reassembled to obtain the full structural loads. Unfortunately, Yuan & Xu (Yuan, 2016; Yuan & Xu, 2016) and others note that both the two-stage procedure and default static procedures do not well-represent the load distribution on an irregular structure.

Instead, the current study proposes two approaches. The first is applicable only for a one-storey upper structure (appendage) and is based on Yuan (2016). In this method, the proposed higher-mode amplification factor is used to characterize the increased loads applied to the top storey, and the lower structure is analyzed as though regular per the NBCC. Despite the removal of the requirement on the stiffness ratio imposed by Yuan (2016), the revised method performs well with the redefined amplification factor. Meanwhile, the second method is wholly new and more generally applicable than the two-stage procedure proposed by Yuan (2016). By extending the amplification factor concept to the top storey and modifying the assumed force distribution accordingly, the proposed method conservatively estimates the loads on even fairly irregular structures. Altogether, the proposed changes to both the stiffness procedure and the calculation of the equivalent static loads represent a marked improvement to the methods proposed by Yuan (2016). Despite an expanded domain and applicability and an updated acceleration spectrum, the proposed procedures are both easier to use and more widely applicable than the previous iteration.

Acknowledgements

A project of this length and complexity is impossible without the numerous contributions of many others. It is, then, of paramount importance that I thank all of those without whom the completion of this thesis would be impossible. First and foremost, I extend my sincere gratitude to my supervisor Professor Lei Xu, without whose academic and financial contributions this project would never have existed. His suggestions, feedback and support have been invaluable.

In addition, for their role on my thesis and defence committee, I would like to thank Dr. Scott Walbridge and Dr. Bruce Hellinga for their commentary and advice. My thesis is inevitably improved with their and Dr. Xu's feedback.

For their financial contributions, I also sincerely thank CSSBI, Professor Reinhold Schuster and the University of Waterloo's Department of Civil and Environmental Engineering. Without the research funding from CSSBI, the Reinhold M. Schuster Graduate Scholarship and multiple Teaching Assistantships with the Department of Civil and Environmental Engineering, I would have been unable to pursue my studies.

Likewise, the assistance of the University of Waterloo's library in obtaining research materials, no matter how arcane, has been very helpful. Special thanks also to the Structural Engineers Association of California, SEAOC, who generously provided me with every edition of their lateral force recommendations for my research.

Finally, I would be remiss not to thank everyone else who in one way or another contributed to my success. To my friends, my family, former colleagues and everyone else to whom I owe my success, thank you.

Table of Contents

Abstract iii
Acknowledgements v
Table of Contents vi
List of Figures ix
List of Tables xii
Nomenclature xiv
Chapter 1 Introduction 1
1.1 Background 1
1.2 Research objectives 3
1.3 Applicability 3
1.3.1 Assumptions 3
1.3.2 Scope 4
1.4 Thesis structure 6
Chapter 2 Literature Review 8
2.1 Introduction 8
2.2 Characterizing vertical irregularity 11
2.3 The response of setback, stepped and soft-storey structures 13
2.4 The dynamic behaviour of other vertically irregular structures 16
2.5 The response of structures having a vertical combination of framing systems 18
2.6 Commentary on previous research 22
Chapter 3 Characterization of the Effect of Higher Vibration Modes on the Upper Structure of Podium Structures 25
3.1 Introduction 25
3.2 Design criterion 26
3.3 Revised stiffness ratio and amplification (R_k-α_U) relationship 30
3.3.1 Simplified 2DOF model 31
3.3.2 Analytical results based on the 2DOF model 34
3.3.3 Analytical results based on the MDOF model 39
3.3.4 Proposed equations to evaluate shear-force-amplification factor α_U 41
3.3.5 The rationale for proposed equations to evaluate upper structure base shear amplification factor α_U 43

3.4 Error of the proposed R_k-α_U relationship 47
3.5 Revised formulation for design stiffness k_U 55
3.6 Summary of R_k-α_U relationship and procedure to evaluate upper structure stiffness k_U 67
3.7 Design examples 69
3.7.1 Example 3-1 70
3.7.2 Example 3-2 76
3.8 Conclusions 89
Chapter 4 Equivalent Static Loads on Vertically Irregular Structures 91
4.1 Introduction 91
4.2 The NBCC 2015 Equivalent Static Force Procedure 91
4.2.1 Regular structures 95
4.3 Using α_U to estimate the upper base shear on an irregular structure 100
4.4 Appendage structures 100
4.4.1 The Yuan (2016) modified equivalent lateral force method 101
4.4.2 Newly proposed method to evaluate appendage structures 103
4.4.3 Efficacy of the newly proposed method to evaluate appendage structures 104
4.5 Newly proposed method 106
4.5.1 Top storey higher mode amplification factor α_{Utop} 107
4.5.2 Error associated with α_{Utop} 111
4.5.3 Evaluating loads on the upper structure via α_U and α_{Utop} 112
4.5.4 Evaluating loads on the lower structure: 114
4.5.5 Error of proposed procedure 116
4.5.6 Error considering non-uniform storey stiffness of the upper structure 118
4.6 Design Procedure 121
4.7 Design examples 123
4.7.1 Example 4-1 124
4.7.2 Example 4-2 126
4.7.3 Example 4-3 127
4.7.4 Example 4-4 129
4.8 Conclusions 132
Chapter 5 Conclusions and Recommendations 135
5.1 Summary 135

5.2 Conclusions 136
5.3 Recommendations 138
Appendix A Modal Response Spectrum Analysis to Evaluate α_U of Simplified 2DOF Model 154
Appendix B Analytical Study on α_U 157
Appendix C Determination of Revised Critical Stiffness Ratios and Amplification Factors 171
Appendix D α_U-k_U Relationship Derived by Yuan (2016) 194
Appendix E Tabulated values of R_{kU1}, A_{U1}, B_{U1}, A_{Umax} and B_{Umax} 208
Appendix F The Yuan (2016) two-stage procedure 213
Appendix G Stiffness of CFS shear wall and RC moment-resisting frame 223

List of Figures

Figure 1.1: Mid-Rise structures with a vertical combination of framing systems 1
Figure 1.2: Sample NBCC 2015 design spectrum 5
Figure 1.3: Annotated ASCE 7 design spectrum (ASCE, 2010, 2017; Yuan, 2016) 6
Figure 2.1: *n*-th 2DOF modal system (Lin et al., 2019) 20
Figure 3.1: Model simplification (Yuan, 2016; Yuan & Xu, 2014) 31
Figure 3.2: Physical interpretation of extremely flexible and stiff lower structure (Yuan, 2016) 36
Figure 3.3: Effect of R_m and R_k on amplification factor α_U 37
Figure 3.4: Effect of period ratio T_U/0.2 on α_U (NBCC) 39
Figure 3.5: Effect of period ratio T_U/T_S on α_U (ASCE), (Yuan, 2016) 39
Figure 3.6: Idealized R_k-α_U relationship (Yuan, 2016) 46
Figure 3.7: α_U – MRS value versus approximated value (Yuan, 2016) 49
Figure 3.8: Comparison of error as a function of R_k - Proposed versus Yuan (2016), previous scope 51
Figure 3.9: Comparison of error - Proposed versus Yuan (2016), previous scope 51
Figure 3.10: Comparison of error as a function of R_k - Proposed, previous versus expanded scope .. 52
Figure 3.11: Comparison of error – Proposed, previous versus expanded scope 52
Figure 3.12: Schematic representation of the graphical solution for k_U 62
Figure 3.13: Graphical Illustration of Bounds on Design Stiffness k_U in terms of R_k and α_U 66
Figure 3.14: Sample graphical illustration of the feasible range of stiffness k_U and k_L 67
Figure 3.15: Graphical solution for critical stiffnesses k_U 73
Figure 3.16: Graphical illustration of bounds on design stiffness k_U in terms of k_U and k_L 74
Figure 3.17: Graphical illustration of bounds on design stiffness k_U in terms of system properties 74
Figure 3.18: Graphical illustration of bounds on design stiffness k_U in terms of system properties – Victoria, BC 75
Figure 3.19: Floor plan of the lower RC structure (Yuan, 2016) 77
Figure 3.20: Graphical solution for critical stiffnesses k_U 80
Figure 3.21: Graphical illustration of bounds on design stiffness k_U in terms of k_U and k_L 81
Figure 3.22: Graphical illustration of bounds on design stiffness k_U in terms of system properties 82
Figure 3.23: Graphical illustration of bounds on design stiffness k_U in terms of system properties 85
Figure 3.24: Graphical solution for critical stiffnesses k_U 88
Figure 4.1: Maximum overestimate associated with NBCC 2015 ESFP 96
Figure 4.2: Error at base of upper structure using α_U to scale the first-mode shear 100

Figure 4.3: Error at base of the upper structure for appendage structure 105
Figure 4.4: Error for appendage structure 106
Figure 4.5: α_{Utop} versus calculated results for $N_U = 2$, $N_L = 6$ and $r_m = 4$ 111
Figure 4.6: Error of proposed approximation of α_{Utop} 111
Figure 4.7: Error for the proposed method and NBCC – specific locations 117
Figure 4.8: Worst-case overestimate for the proposed method and NBCC 118
Figure 4.9: Variation of storey stiffness in the upper structure ($N_U = 5$) 119
Figure 4.10: Error for proposed method considering upper structure with stiffness variation 121
Figure 4.11: Example 4-1 force distribution and error 126
Figure 4.12: Example 4-2 force distribution and error 127
Figure 4.13: Example 4-3 force distribution and error 129
Figure 4.14: Example 4-4 force distribution and error 132
Figure B.1: Variation of φ_{L1} as a function of R_k and R_m 158
Figure B.2: Variation of φ_{L2} as a function of R_k and R_m 159
Figure B.3: Variation of M_{U1} and M_{U2} as a function of R_k and R_m 160
Figure B.4: Variation of α_U relative to $S_a(T_1)/S_a(T_U)$ 162
Figure B.5: Variation of T_U/T_1 and T_U/T_2 relative to R_k and R_m 164
Figure B.6: Variation of $S_a(T_1)/S_a(T_U)$ relative to R_k and R_m 165
Figure B.7: Variation of $S_a(T_2)/S_a(T_U)$ relative to R_k and R_m 166
Figure B.8: Variation of T_2/T_1 relative to R_k and R_m 167
Figure B.9: Variation of ρ as relative to R_m and R_k 168
Figure B.10: Effect of period ratio T_2/T_1 and damping ratio ζ on ρ 169
Figure C.1: Interstorey drift and Displacement Transition Characterizing R_{kU1} 172
Figure C.2: Mode shape associated with R_{kU1} - Yuan (2016) vs calculated as $f(N_L/(N_U + N_L))$ 175
Figure C.3: Mode shape associated with R_{kU1} - Yuan vs calculated as $f(N_U, N_L)$ 175
Figure C.4: Error histogram - R_{kU1} as defined by Yuan (2016) 177
Figure C.5: Error histogram - R_{kU1} as defined by $f(N_U, N_L)$ 177
Figure C.6: Error histogram - R_{kU1} as defined by $f(N_U, N_L, r_m)$ 178
Figure C.7: Comparison of R_{kU1} error histograms 178
Figure C.8: Sensitivity of $R_{kU1} = f(N_U, N_L, r_m)$ 179
Figure C.9: Comparison of existing two-stage criteria 183

Figure C.10: Effective mass distribution of simplified 2DOF model with extremely stiff lower structure (two-stage assumption) (Yuan, 2016) 184
Figure C.11: Relative modal masses in the 2DOF model versus proposed R_{kU2stg} 185
Figure C.12: Comparison between calculated and proposed α_{U1} (N_U = 4, N_L = 5, r_m = 2) 190
Figure C.13: Comparison between calculated and proposed α_{Umax} (N_U = 4, N_L = 5, r_m = 2) 192
Figure C.14: Comparison between proposed and Yuan (2016) α_{U2stg} 193
Figure D.1: NBCC 2010 design spectrum (Yuan, 2016) 200
Figure D.2: EXP-2 design spectrum (Yuan, 2016) 200

List of Tables

Table 2.1: Relevant structural irregularities (NRCC, 2015c) 9
Table 3.1: Normalized first mode circular frequency of uniform structure 32
Table 3.2: Comparison of α_U approximation error 53
Table 3.3: Minimum error for α_U - Proposed, $N_U+N_L \leq 10$, $r_m \leq 3$ 54
Table 3.4: Maximum error for α_U - Proposed, $N_U+N_L \leq 10$, $r_m \leq 3$ 54
Table 3.5: Minimum error for α_U – Proposed, expanded scope 55
Table 3.6: Maximum error for α_U – Proposed, expanded scope 55
Table 3.7: NBCC 2015 spectral acceleration for St. Catharines, Ontario (NRCC, 2015a) 71
Table 3.8: Input characteristics of Example 3-1 71
Table 3.9: Example 3-1 critical intermediate parameters 72
Table 3.10: NBCC 2015 spectral acceleration for Victoria, British Columbia (NRCC, 2015a) 75
Table 3.11: Input characteristics of Example 3-2 77
Table 3.12: NBCC 2010 spectral acceleration for Vancouver (Yuan, 2016) 78
Table 3.13: NBCC 2015 spectral acceleration for Vancouver City Hall (NRCC, 2015a) 79
Table 3.14: Critical intermediate parameters 79
Table 3.15: Comparison of critical stiffness values – Proposed versus Yuan (2016) 84
Table 3.16: Critical stiffness ratio values – Yuan (2016) 86
Table 3.17: Critical values of α_U – Yuan (2016) 87
Table 3.18: EXP-2 fit parameters – Yuan (2016) 87
Table 3.19: Critical k_U as evaluated by different methods 88
Table 4.1: NBCC 2015 higher mode factor M_v – Other Systems (NRCC, 2015c) 92
Table 4.2: Minimum overestimate for shear – NBCC 2015 ESFP, regular structure 98
Table 4.3: Maximum overestimate for shear – NBCC 2015 ESFP, regular structure 98
Table 4.4: Maximum error for Shear – NBCC 2015 ESFP, regular structure, $T_1 < 2$ s 99
Table 4.5: Values of A_{top} 109
Table 4.6: Values of B_{top} 110
Table 4.7: NBCC 2015 spectral acceleration for Montreal City Hall (NRCC, 2015a) 125
Table 4.8: Calculation of proposed force distribution 128
Table 4.9: Calculation of proposed force distribution 130
Table D.1: Values of α_{U12} and α_{U12} for the case where $R_{kU1} < R_{kU2}$ (Yuan, 2016) 197
Table D.2: Values of α_{Umax1} for NBCC 2010 (Yuan, 2016) 198

Table D.3: Values of α_{Umax2} for NBCC 2010 (Yuan, 2016) 199
Table D.4: Numerical solution of y_i (Yuan, 2016) 206
Table E.1: Values of R_{kU1} 208
Table E.2: Values of A_{U1} 209
Table E.3: Values of B_{U1} 210
Table E.4: Values of A_{Umax} 211
Table E.5: Values of B_{Umax} 212
Table F.1: i-th mode normalized effective modal masses M_{Ni} for top storey of uniform structure.... 216
Table F.2: i-th mode normalized circular frequencies $\boldsymbol{\omega i}$ of uniform structures 216
Table F.3: Empirical values of critical T_U/T_L and T_U/T_S (Yuan, 2016)..... 219
Table F.4: Values of η_{min1} and η_{min2} for two-stage analysis procedure (Yuan, 2016) 220

Nomenclature

Abbreviations

Abbreviation	Description
AISI	American Iron and Steel Institute
ASCE, ASCE 7	American Society of Civil Engineers and the standard that they publish
AWC	American Wood Council
CQC	Complete quadratic combination method, common technique to combine modal responses to estimate peak response. See Chopra (2012).
ESFP	Equivalent static force procedure, as used by the NBCC
EXP-2	Exponential approximation of NBCC-specified spectral acceleration relationship
FEMA	United States Federal Emergency Management Agency
IBC	International Building Code
ICBO	International Conference of Building Officials
ICC	International Code Committee
NBCC	National Building Code of Canada
NRCC	National Research Council of Canada
SDOF, 2DOF, MDOF	Single, two and multiple degrees of freedom
SEAOC	Seismology Committee, Structural Engineers Association of California and associated publication, also known as the *blue book*
SFRS	Seismic force-resisting system (also referred to as lateral load-resisting system)
SRSS	Square-root-sum-of-squares, common technique to combine modal responses to estimate peak response. See Chopra (2012).
UBC	Uniform Building Code, historical building code published by ICBO.

Variables

Variable	Description
$\mathbf{1}$	Vector of ones [-]

A_c	Gross cross-sectional area of chord member of cold-formed steel shear wall, defined by AISI S400-15 (2015) [mm^2]
A_i	Fit parameter for EXP-2 exponential approximation to NBCC 2010 $S_a(T)$ proposed by Yuan (2016) [-]
$A_n(t)$	Pseudo-acceleration function, as defined by Chopra (2012)
A_{max}	Fit parameter associated with amplification factor α_{Umax} [-]
A_{U1}	Fit parameter associated with amplification factor α_{U1} [-]
b	Length of cold-formed steel shear wall (AISI, 2015) [m]
b_i	Coefficient associated with i-th term of Yuan (2016) solution for critical stiffnesses k_U [-]
B_{max}	Fit parameter associated with amplification factor α_{Umax} [-]
B_{U1}	Fit parameter associated with amplification factor α_{U1} [-]
$\boldsymbol{C}$, C_U, C_L	Damping matrix of structure, damping associated with upper and lower structures [Nm]
C_i	Generic coefficients in Appendix D that are used to describe the formulation given by Yuan (2016). [-]
C_d	Deflection amplification factor used to determine design deflections in ASCE 7-16 (2017). Analogous to R_dR_o in NBCC 2015 (NRCC, 2015c) [-]
C_{U1}	Scaling factor applied to α_U for $R_k < R_{kU2}$ [-]
E	Modulus of elasticity of steel, defined by AISI S400-15 (2015) as 203,000 MPa [MPa]
$f(x)$	Mathematical shorthand to abbreviate equation that is function of some input x [-]
f_c'	Specified compressive strength of concrete, defined by CSA A23.3-19 (2019) [MPa]
f_y	Specified yield stress of compression non-prestressed reinforcement, defined by CSA A23.3-19 (2019) [MPa]
$\boldsymbol{F}$	Vector of external forces [N, kN]
F_a	Site coefficient defined by NBCC 2015 (NRCC, 2015c). Equal to unity for current study. [-]
F_t	Portion of seismic base shear V to be concentrated at top of a structure, defined by NBCC 2015 (NRCC, 2015c) [kN]

F_U, F_L	Equivalent static force applied at the upper and lower structures in the 2DOF model for Yuan (2016) interpretation of two-stage procedure [kN]
F_x	Lateral force applied to level x, defined by NBCC 2015 (NRCC, 2015c) [kN]
g	Gravitational acceleration, assumed to be 9.8 m/s^2 [m/s^2]
$Gt_{sheathing}$	For oriented strand board panels acting as sheathing to a cold-formed steel shear wall, the product of the shear modulus G [MPa] and the sheathing panel thickness $t_{sheathing}$ [mm], defined by AISI S400-15 (2015). Assumed to be equal to panel rigidity-through-the-thickness ($G_v t_v$) specified by the 2018 AWC Manual for Engineered Wood Construction and National Design Specification for Wood Construction (2017, 2018). [MPa·mm]
h	Height of cold-formed shear wall, defined by AISI S400-15 (2015) [m]
h_i, h_x	Height above the base ($i = 0$) to level i or x, defined by NBCC 2015 (NRCC, 2015c) [m]
h_s	Interstorey height ($h_i - h_{i-1}$), defined by NBCC 2015 (NRCC, 2015c) [m]
I_E	Earthquake importance factor of a structure, defined by NBCC 2015 (NRCC, 2015c). Equal to one for normal structures. [-]
k	Exponent which is applied to equivalent static force distribution to modify the assumed mode shape to account for the effect of higher modes. [-]
$\boldsymbol{K}$	Stiffness matrix of structure [N/m, kN/m]
k_L	Storey stiffness of one storey of lower structure [kN/m]
K_L	Total stiffness of lower structure [kN/m]
k_U	Storey stiffness of one storey of upper structure [kN/m]
K_U	Total stiffness of upper structure [kN/m]
$k_{U,required}$	Minimum stiffness of upper structure satisfying drift-based storey criterion [kN/m]
$k_{U,unconditional}$	Minimum stiffness of upper structure for which drift-based storey criterion is satisfied for any selection of k_L, subject to the scope of α_U [kN/m]
k_{U1}, k_{Umax}, k_{U2stg}	Stiffness of upper structure corresponding to amplification factor α_{U1}, α_{Umax} and α_{U2stg}, respectively. Formerly $k_{\alpha U1}$, $k_{\alpha Umax}$ and $k_{\alpha U2stg}$ (Yuan, 2016) [kN/m]

k_{U01}, k_{U02}, k_{U03}	Intermediate variables used in the solution of $k_{\alpha U1}$, $k_{\alpha Umax}$ and $k_{\alpha U2stg}$ by Yuan (2016) [kN/m]
$\boldsymbol{M}$	Mass matrix of structure [kg]
m_L	Storey mass of one storey of lower structure [kg]
M_L	Total mass of lower structure [kg]
m_U	Storey mass of one storey of upper structure [kg]
M_U	Total mass of upper structure [kg]
M_n^*, M_{Un}^*, M_{Ln}^*	n-th mode effective mass of full structure, upper structure and lower structure in 2DOF model [-]
M_n, M_{Un}, M_{Ln}	n-th mode normalized effective mass of full structure, upper structure and lower structure in the 2DOF model. Normalized for total mass. [-]
M_v	Factor to account for higher mode effect on base shear, defined by NBCC 2015 (NRCC, 2015c) [-]
N_L, N_U	Storey count of the lower and upper structures, respectively [-]
R	Response modification coefficient, defined by ASCE 7-16 (2017) [m]
R_d, R_o	Ductility and overstrength-related force modification factor, defined by NBCC 2015 (NRCC, 2015c). Related to R and C_d given by ASCE 7-16 (2017) [-]
r_k, R_k	Storey and overall stiffness ratio of lower and upper structure [-]
r_{kb1}, R_{kb1}	Storey and overall stiffness ratio at which the effective mass associated with the first mode is 90% of the total mass of the full structure. Used in Yuan (2016) modified equivalent lateral load procedure.
r_{kU1}, R_{kU1}	Minimum storey and overall stiffness ratio. Defines point at which interstorey drift at the base of the upper structure is approximately equal to maximum interstorey drift. [-]
r_{kU2}, R_{kU2}	Storey and overall stiffness ratio associated with lower bound of the region for which it is assumed that $\alpha_U = \alpha_{Umax}$ [-]
r_{kU2stg}, R_{kU2stg}	Storey and overall stiffness ratio associated with the two-stage procedure's requirements and beyond which α_U is approximately constant. Formerly defined as beyond which $\alpha_U \approx 1$; merged with R_{k2stg}, which formerly defined bound on the two-stage procedure (Yuan, 2016) [-]

$r_{kU2stg,Yuan}$, $R_{kU2stg,Yuan}$	Storey and overall stiffness ratio beyond which α_U is approximately constant. (Yuan, 2016) [-]
$r_{k2stg,Yuan}$, $R_{k2stg,Yuan}$	In Yuan (2016) formulation, storey and overall stiffness ratio beyond which two-stage procedure is applicable. Merged with r_{kU2stg}, R_{kU2stg} for newly proposed procedure. [-]
r_{kU3}, R_{kU3}	Storey and overall stiffness ratio associated with the upper bound of the region for which it is assumed that $\alpha_U = \alpha_{Umax}$ [-]
r_m, R_m	Storey and overall mass ratio of lower and upper structure [-]
$S_a(T)$	5% damped spectral response acceleration, expressed as ratio to gravitational acceleration, for a period of T. Both defined by NBCC 2015 (NRCC, 2015c), or ASCE 7-16 (2017) equivalent, as applicable [g]
T'_s	Fit parameter for EXP-2 exponential approximation to NBCC 2010 $S_a(T)$ proposed by Yuan (2016) [-]
T_i, T_j, T_1, T_2	Periods associated with i-th, j-th, first (fundamental) and second period of structure, respectively. [s]
T_L, T_{singL}	Period associated with entire lower structure, and with one storey of the lower structure, respectively [s]
T_s	Period associated with the transition from constant acceleration region to constant velocity region of $S_a(T)$, defined by ASCE 7-16 (2017). Analogous to 0.2 seconds for most locations in NBCC 2015 (NRCC, 2015c). [s]
T_U, T_{singU}	Period associated with entire upper structure, and with one storey of the upper structure, respectively [s]
t_{stud}	Cold-formed steel stud designation thickness, defined by AISI S400-15 (2015) [mm]
v	Shear demand, defined by AISI S400-15 (2015) [N/mm, kN/m]
V	Lateral earthquake design force at the base of the structure as defined by NBCC 2015 (NRCC, 2015c). [kN] Total lateral load applied to a cold-formed shear wall, defined by AISI S400-15 (2015) [kN]
V_{Ub}	Lateral earthquake force at the base of the upper structure [kN]
W	Weight of structure, as defined by NBCC 2015 (NRCC, 2015c) [kN]

W_i, W_x	The portion of W that is located at or is assigned to level i or x, respectively, as defined by NBCC 2015 (NRCC, 2015c) [kN]
W_U	Weight of upper structure [kN]
W_{Ui}, W_{Uj}	The portion of W_U associated with i-th or j-th mode of vibration, respectively. [kN]
$\boldsymbol{x}$, $\dot{\boldsymbol{x}}$, $\ddot{\boldsymbol{x}}$	Displacement, velocity and acceleration co-ordinates [m, m/s, m/s^2]
y_i	Parameter used in i-th term of numerical solution of critical k_U in the procedure proposed by Yuan (2016). [-]
α_U	Factor to account for higher mode effect on base shear of the upper structure. Analogous to M_v used by NBCC 2015 (NRCC, 2015c) [-]
α_{U1}	Value of α_U corresponding to critical stiffness ratio R_{kU1} (r_{kU1}) [-]
α_{U11}	Lower bound on the value of α_{U1} in Yuan (2016) formulation for α_U [-]
α_{U12}	Upper bound on the value of α_{U1} in Yuan (2016) formulation for α_U [-]
α_{U2stg}	Value of α_U corresponding to critical stiffness ratio R_{kU2stg} (r_{kU2stg}) [-]
α_{Ulim}	Value of α_U corresponding to the interstorey drift limit Δ_{Ulim} [-]
α_{Umax}	Value of α_U for stiffness ratios lying between R_{kU2} (r_{kU2}) and R_{kU3} (r_{kU3}) [-]
α_{Utop}	Factor to account for higher mode effect on the top storey of the upper structure. [-]
β	Parameter specified by AISI S400-15 (2015) [N/mm$^{1.5}$]
Γ	Modal participation factor [-]
δ	Calculated deflection of cold-formed steel shear wall, defined by AISI S400-15 (2015) [mm]
δ_v	Vertical deformation of anchorage/attachment details of cold-formed steel shear wall, defined by AISI S400-15 (2015) [mm]
Δ	Interstorey drift (relative displacement) [m]
Δ_{jn}^{st}	The static portion of interstorey drift corresponding to DOF j and mode n, as defined by Chopra (2012) [m]
Δ_{jo}, $\Delta_{io,}$ Δ_{no}	Peak interstorey drift corresponding to DOF j, mode i or mode n evaluated at DOF j, respectively, as defined by Chopra (2012) [m]
Δ_U	Interstorey drift at the base of the upper structure [m]

Δ_{Ulim}	Interstorey drift limit at the base of the upper structure, 2.5% of storey height for regular importance structures per NBCC 2015 (NRCC, 2015c) [m]
ζ	Damping ratio, assumed to be 5% in all modes [%]
ρ	Correlation coefficient for CQC modal combination method, between modes *i* and j
	Parameter specified by AISI S400-15 (2015) [-]
τ_i	Fit parameter for EXP-2 exponential approximation to NBCC 2010 $S_a(T)$ proposed by Yuan (2016) [-]
Φ	Modal matrix of eigenvectors (mode shapes) [-]
φ_{jn}	Value of eigenvector (mode shape) associated with *j*-th DOF and *n*-th mode
$\varphi_{L1}, \varphi_{U1}, \varphi_{L1}, \varphi_{U2}$	Value of eigenvector (mode shape) associated with first mode and lower structure, first mode and upper structure, second mode and lower structure, and second mode and upper structure, respectively, in 2DOF model [-]
$\varphi_{L1,min}$	Value of eigenvector (mode shape) for the lower structure's first mode in the 2DOF model, corresponding to R_{kU1} [-]
ω_i	*i*-th mode circular frequency of structure [rad/s]
	One of several parameters for cold-formed shear walls specified by AISI S400-15 (2015) [-]

Chapter 1
Introduction

1.1 Background

Mid-rise residential/commercial building structures with a vertical combination of seismic force-resisting systems (SFRS), such as those in Figure 1.1, are increasingly common throughout North America. Such a structure, often referred to as a podium structure by commercial proponents, is characterized by a lower structure of stiff, massive construction (e.g. structural steel or reinforced concrete (RC)) which supports an upper structure of less stiff, less massive construction (e.g. cold-formed steel (CFS) or wood). To architects, engineers and building owners, the mix of materials suits a mix of building uses – for example, where commercial or parking space is desired near grade, the stiffer lower structure allows larger structural spans and larger open spaces. Meanwhile, for residential occupancy in the upper structure, lighter-weight materials can be used. The result is a structure that is more efficiently matched to the loads imposed by its occupancies – this is understood by commercial proponents, who are increasingly endorsing the approach to suit project requirements. (Hoesly, 2019; Ni et al., 2016; Nitterhouse Concrete Products, 2019; Podesto, 2017; Think Wood, 2019; Warr, 2019).

Figure 1.1: Mid-Rise structures with a vertical combination of framing systems

(Left: RC and CFS (D. Allen & Wills, 2017), Right: RC and wood (Think Wood, 2019))

By the loose industry use of the term, podium buildings are characterized by vertical irregularity in any or all of mass, stiffness, strength and geometry, encompassing both structures with a combination of framing systems and a regular floor plan, and structures with a single structural system but a shrinking floor plan at higher elevations. While in practice these cases overlap, the focus herein is on

structures with a combination of framing systems and thus irregularity of mass and stiffness, as opposed to the geometric irregularity characteristic of setback or stepped structures.

Given the growing popularity of combining seismic force-resisting systems vertically, one might naively expect that the code provisions and designer knowledge have improved to match. This, however, is not the case. The 2015 National Building Code of Canada (NBCC) (National Research Council of Canada (NRCC), 2015c) and American Society of Civil Engineers (ASCE) 7-16 (2017) code do not articulate the effect of irregularity either qualitatively or quantitatively. Both characterize irregularity only by a set of independent limits which according to research are not effective in characterizing the expected behaviour of vertically irregular structures (more on this in Chapter 2). The codes recommend only that irregular structures be preferentially designed using dynamic analysis but give no further guidance regarding the expected behaviour.

On account of these irregularity limits being questionably effective and potentially ambiguous, it is often left to engineering judgement to determine how to analyze these types of structures. For mid-rise structures, designers may then embrace simpler static approaches to inform their dynamic design, or to replace dynamic design altogether. In NBCC 2015 and ASCE 7-16, there are two alternatives – the equivalent static force procedure (or its ASCE 7 equivalent) and the ASCE 7 two-stage procedure. But these procedures are derived for relatively regular structures and rely on the first mode of vibration being dominant – this is not always the case for irregular structures (Rosenblueth et al., 1980). This is true also of the two-stage procedure. Despite being intended for irregular structures, it can produce unconservative results, given differences in the dynamic behaviour compared to a regular structure (Chen & Ni, 2020; Yuan & Xu, 2016).

The crux of the problem is that these existing methods do not incorporate irregularity. Research has repeatedly observed that higher mode effects are potentially more substantial for irregular structures than regular structures, particularly as the extent of the irregularity increases. Depending on the distribution of mass and stiffness in the structure, the relative value of modal periods, and the applied earthquake excitation, this means that the storey shears may be amplified relative to those predicted by the first mode alone. For example, a relatively lightweight upper structure may experience much larger storey shears if attached to a more massive lower structure. This amplification effect is of primary concern for this research. Based on earlier work by Yuan & Xu (Xu & Yuan, 2015; Yuan, 2016; Yuan & Xu, 2014, 2016), this study aims to provide a set of static approximations which will address the higher-mode amplification effect neglected by current codes and designers.

1.2 Research objectives

Given that existing static design methods specified by NBCC 2015 do not incorporate the effect of vertical irregularity and neglect the effect of different modes of vibration interacting with one another, this study has three objectives:

1. quantify the higher-mode amplification effect on the base shear of the upper structure,
2. select the storey stiffness of the upper and lower structures such that the NBCC-specified interstorey drift limit is satisfied, and;
3. conservatively estimate the equivalent static seismic loads – the storey shears – associated with a vertically irregular structure.

As opposed to Yuan (2016), this study is focused exclusively on application to NBCC 2015, rather than ASCE 7-16 (2017).

1.3 Applicability

1.3.1 Assumptions

To simplify the procedure by which mid-rise structures with combined framing systems are designed, assumptions are made to facilitate analysis. The assumptions can be defined in two categories – those which are commonly adopted, and those which are specific to the current study.

The following assumptions are commonly adopted by simplified methods:

1. The combined framing systems are modelled as discrete, lumped-mass models, with each storey (in the case of the MDOF model) or each of the upper and lower structures (in the simplified 2DOF model) being represented by a single mass at the appropriate storey height. Consequently, it is assumed that mass and stiffness are uniformly distributed within a given storey. Torsional effects, effects due to vertical displacements and out-of-plane effects are neglected. It is also assumed that each storey height is identical and that each storey mass of the upper structure is equal to all other storey masses in the upper structure, and similarly for the lower structure.
2. The model is a pure shear model – all load is resisted in shear only and all storeys are assumed to act as rigid diaphragms. Consequently, vertical displacements and joint rotations

are neglected, but this requires a smaller number of DOFs and avoids the problem of coupled DOFs.

The following assumptions are specific to the current study:

1. Only vertical combinations of seismic force-resisting systems are considered.
2. The model is evaluated and calibrated using code-specified linear modal response spectrum analysis using the CQC (complete quadratic combination) rule to combine modal responses via the NBCC 2015 spectrum.
3. The spectral acceleration, $S_a(T)$, specified by NBCC 2015 (NRCC, 2015b) is adopted. This is based on soil class C and 5% (Rayleigh) damping in each mode, as associated with the default spectrum in the NBCC. Any differences in damping or soil conditions from this baseline are neglected.
4. The effect of overstrength and ductility factors (R_o and R_d) are neglected in the design examples. For practical application, R_dR_o values should be taken as the minimum of the two systems being combined per the recommendation of NBCC 2015 (NRCC, 2015b).
5. The model assumes that the interstorey drift at the base of the upper structure is larger than that at the base of the lower structure. Specifically, that the interstorey drift between the top storey of the lower structure and the bottom storey of the upper structure is the largest of any storey in the structure. This requirement is explained more in-depth in Chapter 3 and Appendix C along with the overall stiffness ratio requirement R_{kU1}, as R_{kU1} defines the limits at which this assumption is true. As the interstorey drift between the top storey of the lower structure and the bottom storey of the upper structure is the largest, it is therefore the critical design variable. It is assumed that no slippage occurs between the different framing systems – e.g. between storeys of the upper structure or between the upper and lower structures.

1.3.2 Scope

The simplified approach proposed in this study is applicable only for mid-rise buildings with a vertical combination of framing systems having the following characteristics:

1. It is assumed that the number of storeys is no greater than twelve., Compared to Yuan (2016), the storey count is increased by two. This is partially on account of NBCC (NRCC, 2015c) limits on seismic force-resisting system heights – timber and cold-formed steel systems are

often limited to 20-30 metres in height (≈ 6-10 storeys) depending on the system in question. For CFS, fire-related considerations are often more onerous than seismic requirements, likewise limiting their height. Nonetheless, these structures do not generally exceed 12 storeys in height.

2. For this study, the single-storey periods of the lower and upper structures (T_{singL} and T_{singU}) are less than or equal to 0.31 seconds, consistent with Yuan (2016). In the 2015 NBCC (NRCC, 2015c), the largest empirical period is that of a steel moment-resisting frame, and the maximum permitted period via structural mechanics is 1.5 times the empirical value. Thus, if the maximum interstorey height is 3.3 metres, the maximum permitted period for a single storey is 0.31 seconds, as follows:

$$T_{sing} \leq 1.5(0.085)(3.3)^{3/4} = 0.31s \tag{1.1}$$

In the ASCE 7 spectrum shown in Figure 1.3, the lower bound on T_{singU} and T_{singL}, the spectral acceleration associated with $T < 0.2T_s$ is lower than that for longer periods, and therefore Yuan (2016) specifies that $0.2T_s \leq T_{singU}$ and T_{singL}. T_s is a parameter specified by ASCE 7. However, the NBCC 2015 spectrum shown in Figure 1.2 is monotonically decreasing, so this lower bound on T_{singU} and T_{singL} is not required.

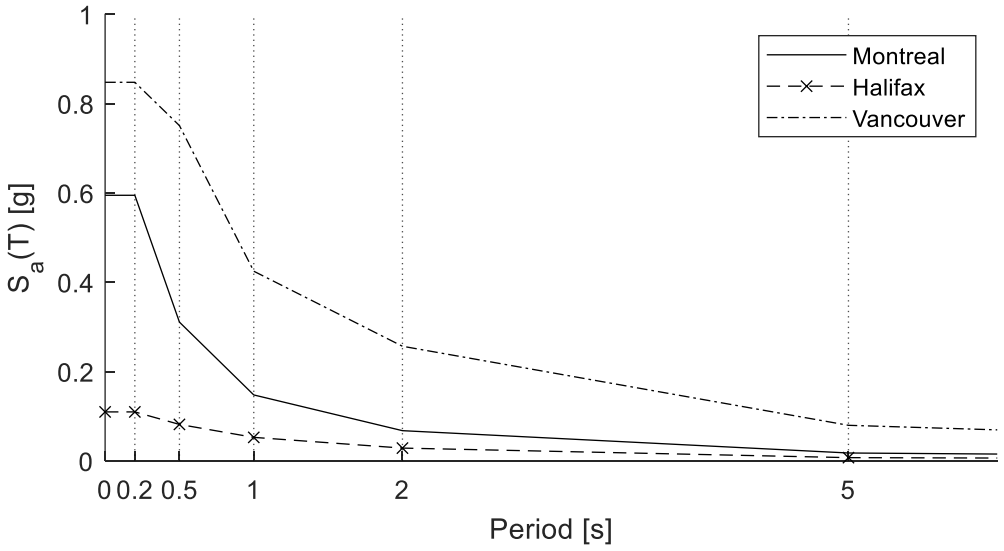

Figure 1.2: Sample NBCC 2015 design spectrum

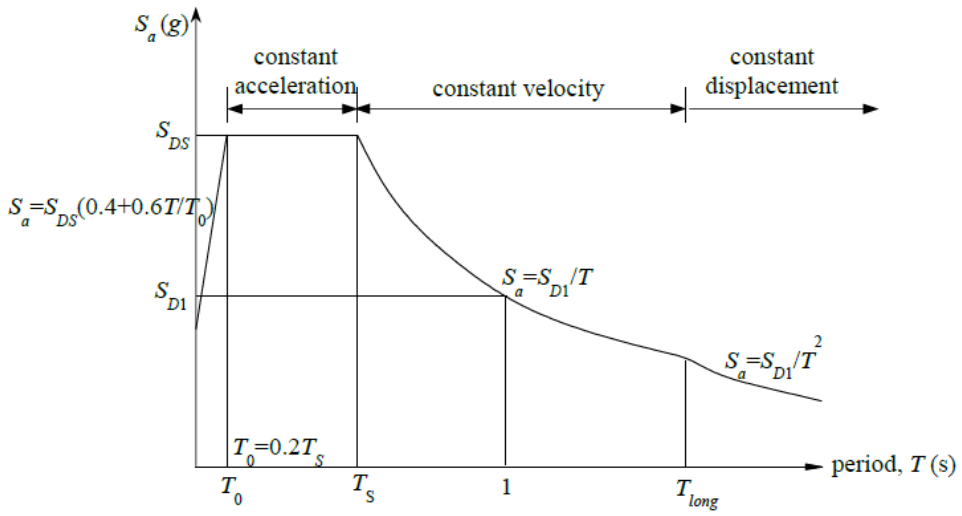

Figure 1.3: Annotated ASCE 7 design spectrum (ASCE, 2010, 2017; Yuan, 2016)

3. The storey-mass ratio $r_m = m_L/m_U$, where m_U and m_L are the mass of one storey of the upper and lower structures, respectively, is limited to $1 \leq r_m \leq 5$. This is increased from the previous formulation, which is capped at 3.

4. Storey-stiffness ratio $r_k = k_L/k_U$ is limited to $\max(r_{kUI},1) \leq r_k \leq 20$, where the minimum storey stiffness ratio r_{kUI} is the minimum stiffness ratio at which the maximum storey-drift ratio occurs at the first storey of the upper structure. R_{kUI} and r_{kUI} are defined in Chapter 3.

The limits on r_m and r_k exclude a soft storey scenario - each storey of the lower structure must be more massive and stiffer than each storey of the upper structure. However, the mass ratio in a setback structure may be greater than five where the change in dimension is significant. This study is concerned primarily with vertical combinations of seismic force-resisting systems and thus may not apply to a variety of setbacks structures.

1.4 Thesis structure

The thesis is organized as follows:

- Chapter 2 consists of a review of the relevant literature relating to vertically irregular structures. The focus is on vertically irregular structures with mass and stiffness irregularity and on vertical combinations of framing systems, but both code-specified irregularity limits and setback structures are also discussed.

- Chapter 3 concerns the derivation of the upper structure amplification factor α_U. In combination with a drift-based design criterion, this amplification factor is used to derive adequate distributions of storey stiffness on a vertically irregular structure. Two examples are provided to demonstrate the feasible stiffness distributions associated with the proposed method.
- Chapter 4 concerns the specification of equivalent static loads on vertically irregular mid-rise structures with stiffness and mass irregularity. It begins with an investigation of the efficacy of the NBCC 2015 spectrum and ends with a method for a single-storey upper structure (appendage structure) and another more general method applicable to other structures.
- Chapter 5 presents the study's conclusions and recommendations.

Chapter 2
Literature Review

2.1 Introduction

Vertically irregular structures have been considered in one form or another since the very first seismic design codes in North America, beginning with the first edition of the Structural Engineers Association of California (SEAOC) Recommended Lateral Force Requirements (also known as the Blue Book), which featured in an appendix a brief characterization of the expected behaviour of setback structures (Blume et al., 1960). In the time since, the concept of irregularity has progressed from considering only soft storey and setback irregularity, and now incorporates not only differences in stiffness, mass and strength but also discontinuity of the SFRS and other configuration issues. Categories continue to be added to the NBCC as they become relevant – inclined columns, for example, have appeared in proposals for the 2020 edition of the NBCC in response to industry demand (Canadian Commission on Building and Fire Codes, 2018).

But despite the ever-expanding list of irregularity types, the design of vertically irregular structures with a combination of framing systems remains a complicated process, hindered by three main obstacles:

1. code-imposed limitations on the design of vertically irregular structures,
2. the characterization of vertical irregularity in building codes and design standards lacks a theoretical basis and may not be effective, and
3. lack of familiarity and understanding regarding the complex response of vertically irregular podium structures.

The first point is a practical one – designers face additional requirements and restrictions on the design of vertically irregular structures. This is internationally and near-unanimously the case, and in the case of North American codes is predicated on whether the structure satisfies the numerical limits on irregularity set out by the code. The specific requirements vary from code to code and may include the amplification of design forces, added detailing requirements, or prohibition of irregular configurations based on criteria such as building importance, design limit states, structural characteristics (e.g. fundamental period) or soil conditions. Analysis techniques, too, are limited - dynamic analysis (e.g. linear modal response spectrum analysis) is generally required at a minimum

for analysis. Only in limited scenarios are static procedures provided by various codes considered applicable, and often only for short structures (e.g. less than 20 metres in height).

Naturally, these limitations are not unfounded – irregular structures experience more complicated inelastic action and failure modes, often featuring damage concentrated at the location of irregularities (Federal Emergency Management Agency (FEMA), 2009b; NRCC, 2015b). Likewise, static procedures are generally applicable only to first mode vibration of regular structures, and therefore less accurate as the degree of irregularity and thus the significance of higher-mode effects increases (Valmundsson & Nau, 1997). Specifically, an increase in irregularity generally results in the higher-mode response becoming more prominent, and so only in certain scenarios is the first mode dominant as assumed by static approaches.

Implicitly, even routine structures have some degree of irregularity, and so design codes must define what constitutes an irregular structure. In the National Building Code of Canada (NBCC), the American Society of Civil Engineers (ASCE) 7 code and other North American design codes and standards, these limits are quantified based on the mechanical properties of the seismic force-resisting system and characterized into multiple archetypes (ASCE, 2017; NRCC, 2015c). In the case of podium structures with a vertical combination of framing systems designed using NBCC 2015, the cases listed in Table 2.1 are the most important, with Type 1 and 2 being the focus of this study.

Table 2.1: Relevant structural irregularities (NRCC, 2015c)

Type	Type and Definition
1	Vertical stiffness irregularity – exists where lateral stiffness of a storey's SFRS is less than 70% of an adjacent storey or 80% of the average of three above or three below
2	Weight (mass) irregularity – exists where the weight of a storey is more than 150% of an adjacent storey's
3	Vertical geometric irregularity – exists where the horizontal dimension of the SFRS of any storey is more than 130% of an adjacent storey's
6	Discontinuity in capacity – weak storey – exists where a storey's shear strength is less than the storey above

But while the NBCC limits are quantitative and straightforward to calculate, little justification is provided for the limits in the commentary to NBCC 2015 (NRCC, 2015b). Furthermore, it is not clear that they are effective – a significant body of research criticizes the NBCC limits. However, despite these criticisms, there are no universally agreed-upon alternative limits, either in research or in international building codes. This discussion is the focus of Section 2.2.

Therefore, and especially so for vertically irregular (e.g. podium) structures, it can be difficult to ascertain to what degree a structure will behave as though regular (i.e. primarily in the first mode and with inelastic behaviour well-distributed through the structure), even where the individual limits on irregularity are satisfied. Putting aside the question of whether the limits themselves are appropriate, Yuan (2016) and Yuan & Xu (2016) note that podium structures are susceptible to higher-than-expected base shears in the upper structure if assessed statically, and so the naïve use of static approaches may result in unconservative design. Structural engineers are thus faced with the choice of potentially unconservative static design – either by the Equivalent Static Force Procedure (ESFP) set out in NBCC 2015 or the two-stage analysis procedure set out in ASCE 7, or dynamic design and its associated challenges. Still, while broadly applicable and required by code for many irregular structures, dynamic analysis is more cumbersome, costly and time-consuming than static analysis – this is especially true for nonlinear dynamic design, which is largely unaddressed by NBCC 2015 (NRCC, 2015c). Therefore, practitioners often prefer static approaches, owing to their relative ease of use and speed despite their limitations.

This preference for static analysis can be hazardous at the periphery of current limits on irregularity. Where irregularity types appear together, where irregularity limits are met but not exceeded over multiple storeys, or where the code as a whole is ambiguous, the engineering judgements underlying these limits break down. Ideally, where ambiguous, an analysis should proceed dynamically. Nevertheless, static analyses will continue to be preferred by practitioners where permitted by a reasonable interpretation of the code provisions. In the zone between regular structures and those requiring dynamic analysis, this decision is often subject to engineering judgement with little additional guidance from the code. Consider for example a ten-storey podium structure designed according to NBCC 2015, with a seven-storey upper structure with each storey having 80% of the stiffness, 70% of the mass and 80% of the dimension of all storeys in the lower structure. Per either of NBCC 2015 or ASCE 7-16, such a structure approximately satisfies all the regularity limits, but with the irregularities in combination and over multiple storeys, the response

may or may not behave in a sufficiently regular way that the code-specified equivalent static approaches are applicable. Indeed, owing to the upper structure's presumably much lower overall stiffness and mass, it is unreasonable to expect that the behaviour will be the same as if the structure was perfectly homogeneous in its height-wise properties, and it is unclear whether the code-specified performance is still adequate.

However, while irregularity has received some attention in the commentary and text to the NBCC, there is often limited explanation for the origins or intent of the limits assigned to each type of irregularity. Aside from soft storey and geometric irregularity (setback and stepped), vertical irregularity has received less attention both in codes and in research relative to plan irregularity. This is particularly true of non-geometric vertical irregularity, and doubly so for structures with a combination of framing systems, which have only recently gained some degree of attention.

To better inform the development of a simplified procedure to calculate loads on vertically irregular structure such as those considered in this study, it is therefore important to characterize the research and codes in the following areas:

1. The definition of vertical irregularity – what are the origins and intent of the limits given in NBCC 2015, and how does this compare to the treatment of vertically irregular structures in other international codes?
2. The behaviour of setback, stepped and soft-storey structures – Given the lack of research focused on structures with a vertical combination of framing systems, what insight do previous studies on related structural archetypes give that is relevant to the current study?
3. The behaviour of vertical irregularity as a function of stiffness, mass and strength irregularity – subsequent research has departed from exclusively considering setback, stepped and soft-storey irregularities. What further conclusions does this provide?
4. The behaviour of structures with a vertical combination of framing systems – What is the state-of-the-art regarding structures with a vertical combination of framing systems?

2.2 Characterizing vertical irregularity

As alluded to in Chapter 1, the limits of irregularity in the NBCC are somewhat ambiguous, somewhat arbitrary, and criticized by existing research. With consideration of this and the fact that the limits do not quantify the impact of the intensity of irregularity, nor the combination of types of

irregularity, a designer may look to other design code limits for guidance. Unfortunately, while other codes sometimes define vertical irregularity, they provide no more guidance than the NBCC. In the case of standards from the United States, the limits are almost the same as those in the NBCC – this is true of ASCE 7-16 (2017), FEMA P-750 (2009b), and the 2015 International Building Code (IBC) (International Code Council (ICC), 2015), all of which are generally updated in parallel (Thornburg & Henry, 2015). Likewise, Eurocode 8 provides no further information - its definition of vertical irregularity (termed irregularity in elevation) is a qualitative one, using vague terminology such as *not vary disproportionately* and *without abrupt changes* to delimit whether a structure is irregular (European Committee for Standardization, 2004). No quantitative limits or categories are provided, except for setback structures. Nor does Japan give useful information to a North American designer, for its code philosophy is wholly different than that of Europe, Canada and the United States (Teshigawara, 2012). In it, buildings are designed using working stress design principles and then checked for storey drift and rigidity – the ultimate limit state of strength is not always required. An irregular structure is defined based on a modification factor arising from the relative storey rigidities, and a storey cannot be less than 60% the rigidity of an adjacent one. Finally, the AS1170.4 code used in Australia does not specify irregularity at all, for it is assumed that in the low seismicity of Australia the majority of structures are irregular (Standards Australia, 2007; Weller, 2005). Categorically, where they exist, quantitative limits are defined in terms of engineering judgement rather than a systematic justification (Sadashiva et al., 2012). It can therefore be difficult to interpret existing provisions, and Agham & Tariverdilo (2012) conclude that this can lead to designers ignoring such provisions altogether.

However, research on alternative vertical irregularity limits is inconclusive, with authors criticizing existing limits and proposing new limits, often applicable to a single structural system. The limits currently given by NBCC 2015 and ASCE 7-16 (and similar) have been routinely criticized by numerous authors as generally poor indicators of whether a structure behaves as irregular (De Stefano & Pintucchi, 2008; Magliulo et al., 2002, 2004, 2012; Sadashiva et al., 2012; Valmundsson & Nau, 1997). Various alternative limits have been proposed by Mazzolani & Piluso (1996), Karavasilis et al. (2008b), and Roy & Mahato (2013), each of whom uses similar geometric ratios. Meanwhile, Varadharajan et al. (2013) propose an index based on the ratio of frequencies in a regular and irregular frame and Sarkar et al. (2010) propose an index based on the ratio of modal participation factors. Each focus on a different type of structure – Karavasilis et al. (2008b) focus on steel moment-resisting setback frames, Roy & Mahato (2013) and Varadharajan et al. (2013) focus on reinforced

concrete setback frames, and Sarkar et al. (2010) focus on reinforced concrete stepped frames. Nonetheless, Bhosale et al. (2017, 2018b) conclude that collectively the existing indicators do not correlate well with the seismic risk, which they aggregate from the fragility curves, probability of collapse, drift hazard and confidence level. In a separate paper (Bhosale et al., 2018a), they propose another new indicator based on relative interstorey drifts between an irregular structure and a reference regular structure.

There is, in summary, no uniquely appropriate irregularity limit for vertical irregularity. Numerous approaches have been proposed based on geometry, frequency or other first-mode parameters, and research does not agree on which is most appropriate, nor on whether geometry as a proxy to stiffness and/or mass is appropriate whatsoever. Categorically, very little guidance is given as to the limits given in NBCC 2015 and ASCE 7, and international codes give either identical limits or no quantitative limits at all. It is consequently difficult for a designer to even identify whether a structure is worth consideration beyond the NBCC's default static approach, which is derived based on a regular structure. For the current purposes, the proposed upper structure base shear amplification factor α_U given in Chapter 3 will be used as a proxy for irregularity.

2.3 The response of setback, stepped and soft-storey structures

In the introduction, a distinction is made between podium structures in the scope of this thesis (specifically, having vertical mass and stiffness irregularity) and those with a stepped or setback configuration (having vertical geometric irregularity). In reality, the distinction is less clear – often, structures with a vertical combination of framing system also have geometric irregularity and vice versa. As existing research on vertical irregularity often focuses exclusively on geometric irregularity, it is pragmatic to review research on setback and stepped structures to gain insight into the current problem. For clarity, setback structures are defined herein as those having a reduction in dimensions (equivalently, floor area) at a single location in the building, and stepped structures are those having multiple such reductions through their height. When podium structures are referred to colloquially, it is often regarding these structures which have geometric irregularity.

Setback structures began seeing significant attention in research following the first SEAOC recommendations published in 1960. Early research quickly identified the susceptibility of setback structures to an increase in higher-mode effects brought about due to the irregularity of the structure, especially given the significant damage observed during then-recent earthquakes (Humar & Wright,

1977; Penzien & Chopra, 1965; Sexton & Keith, 1965; Shibata et al., 1965; Skinner et al., 1965). Collectively, these studies conclude that the differences in higher-mode effects change the force and interstorey drift distributions relative to a regular structure. This is especially so for structures which are particularly irregular in their stiffness and/or mass, or for which the values of the modal periods are similar to each other or to the predominant period of the seismic excitation. For example, if the second modal period of the lower structure is similar to the upper structure's fundamental period or the earthquake's predominant period, the higher-mode effects are most pronounced. This is significant for the applicability of the square-root-sum-of-squares (SRSS) method for combining modal responses – the SRSS method neglects the interaction of different modes and is therefore not applicable where these effects are significant (Chopra, 2012). SEAOC (1999) recommends that the SRSS method is useful if and only if the ratio of all higher modes to that of all lower modes is 0.75 or less – otherwise, the CQC (complete quadratic combination) method should be used.

Later analyses also indicate that a setback increases the ductility demands when compared to regular structures, particularly in the storeys adjacent to the setback (Aranda, 1984; Elnashai & Soliman, 1995; Habibi et al., 2018; Humar & Wright, 1977; Jain & Sharma, 1988; Osman, 2002; Pekau & Green, 1974; Pinto & Costa, 1993; Shahrooz & Moehle, 1990; Sobaih et al., 1988; Varadharajan et al., 2014). These effects are subject not only to the stiffness/geometrical difference between the tower and the podium structure but are also sensitive to the number of storeys, the beam-to-column strength ratio and the limit state being considered (Karavasilis et al., 2008b; Varadharajan et al., 2013). Furthermore, Varadharajan et al. (2014) also indicate that a more severe setback reduces the median collapse capacity and especially when the setback occurs at a lower point in the height. Thus, the inelastic design of setbacks may require special attention towards members in the vicinity of the setback to prevent excessive damage. However, numerous authors disagree that setback structures require more stringent analysis than regular frames (Bhosale et al., 2018a; Mazzolani & Piluso, 1996; Moehle & Alarcon, 1986; Pinto & Costa, 1993; Romao et al., 2004; Tena-Colunga, 2004; Wood, 1986, 1992).

In general, the existing NBCC 2015 equivalent static force procedure (ESFP) does not apply to setback structures – it is calibrated for regular structures (Humar & Mahgoub, 2003; Humar & Rahgozar, 2000; NRCC, 2015b). Instead, many practitioners advocate for the ASCE 7 two-stage procedure, in which the podium and tower of many setback structures are evaluated as two separate structures and reassembled to evaluate the equivalent static loads on the structure (ASCE, 2017).

Despite this, the two-stage method is criticized – for its limits (Chen & Ni, 2020; Yuan, 2016; Yuan & Xu, 2016), its accuracy (Tremblay et al., 2005), and its ease of application (M. Allen et al., 2013). Given this lack of consensus, other studies have proposed alternatives (Cheung & Tso, 1987; Duan & Chandler, 1995; Pekau & Green, 1974; Shahrooz & Moehle, 1990; Valmundsson & Nau, 1997; Wong & Tso, 1994). Nonetheless, the proposed alternatives have not seen wide adoption – designers continue to rely on the ESFP and two-stage procedure for static analyses.

Given the importance of setback structures to the more general class of vertically irregular structures, the foregoing discussion is of importance. However, it would be remiss not to also briefly mention soft-storey structures, in which one or more storeys (typically, the ground floor) possess lower strength than the remaining storeys of the structure. These structures are very common in irregularity research and are characterized by their strength irregularity – Tena-Colunga & Hernandez-Garcia (2020) provide an excellent review of the current research. It is not the intent of this study to discuss soft storey structures in detail – instead, Tena-Colunga & Hernandez-Garcia (2020) indicate several problems in soft-storey research that also apply to other vertical irregularity research. Namely:

- Codes provide limited case studies of the analysis of vertically irregular structures and the appropriateness of code provisions
- Studies inconsistently check for irregularity conditions at intermediate storeys and inconsistently report storey stiffness and storey strength ratios
- Few studies are oriented to assess the impact of the stiffness and strength ratios between adjacent storeys as dictated by codes, and few studies focus on assessing the efficacy of code recommendations towards preventing failure caused by irregularity.

Many of these trends are consistent throughout vertical irregularity research. As discussed in the forthcoming section, more general research on vertical irregularity is subject to similar flaws, particularly that many studies investigate only vertical irregularity concentrated in a single storey. This lack of investigation is also reflected in the code provisions – of type 1, 2, 3 and 6 irregularities in NBCC 2015 (Table 2.1), only type 1 (stiffness irregularity) considers more than a single storey-to-storey consideration, rather than also considering irregularity distributed over several storeys.

2.4 The dynamic behaviour of other vertically irregular structures

While historically research has paid great attention to setback, stepped and soft-storey structures, studies since the 1990s have increasingly defined vertical irregularity more generically in terms of stiffness, mass and strength in an attempt to explore such irregularities in other contexts. This especially true following the 1988 UBC/SEAOC Blue Book (ICBO, 1988; SEAOC, 1988), in which stiffness, mass and strength irregularity are defined by quantitative limits as they appear today in NBCC 2015 (NRCC, 2015c). Prior to this, Moehle & Sozen (1980), Moehle & Alarcon (1986) and Dolce (1988) published research that describes mass, stiffness and strength irregularity in this generic manner. Moehle & Sozen (1980) and Moehle & Alarcon (1986) did so based on experimental tests of RC frames with shear walls, and Dolce (1988) did so following a series of nonlinear dynamic analyses. In Moehle & Sozen (1980) and Moehle & Alarcon (1986), they conclude that while dynamic and static analysis are generally equally proficient at predicting structural demands (except for displacements), elastic methods do not well-represent the distribution of ductility demands that occur when stiffness abruptly changes due to irregularity. Meanwhile, Dolce (1988) concludes that traditional static procedures are adequate for structures up to 12 stories in height and modest changes in stiffness, on account of the overestimation of first mode effective masses. This occurs as the total mass, rather than effective mass, is used in code static force procedures (e.g. ESFP in NBCC 2015).

Of studies undertaken in the 1990s, those published by Al-Ali & Krawinkler (Al-Ali, 1998; Al-Ali & Krawinkler, 1998) are the most influential. In a similar vein as Jhaveri (1967) vis-à-vis setbacks, Al-Ali & Krawinkler investigate vertical irregularities of mass, stiffness and strength both separately and in combination, using both inelastic and elastic methods. These irregularities are introduced by modifying the storey properties of a generic planar 10-storey regular structure, a technique that is used in many other studies (e.g. Cruz & Cominetti (1996), Tremblay & Poncet (2005), Pirizadeh & Shakib (2013)). In general, Al-Ali & Krawinkler (Al-Ali, 1998; Al-Ali & Krawinkler, 1998) observe that strength irregularity is the most significant, followed by stiffness and then mass irregularity. They assert that this strength irregularity may be significant even in otherwise regular buildings, on account of relatively small irregularities introduced during the design process for a variety of reasons, and that this irregularity cannot be identified without nonlinear analysis. Accordingly, they recommend that code specifications for strength irregularity consider both above and below the given storey, rather than simply above (it is only relative to the above storey in NBCC 2015's definition). Al-Ali & Krawinkler are therefore consistent with much of the research on setbacks which note that ductility

demands may be significantly affected in the vicinity of the setback level. Concerning mass and stiffness irregularity, they conclude that structures with large irregularities of stiffness (i.e. setback structures) behaving elastically are prone to significant higher-mode effects, consistent with Jhaveri (1967) and Humar & Wright (1977). Nevertheless, Al-Ali & Krawinkler (Al-Ali, 1998; Al-Ali & Krawinkler, 1998) depart from many researchers by advocating for the universal application of inelastic analysis. Finally, they also state that the complete quadratic combination (CQC) method has no advantage over the square-root-sum-of-squares (SRSS) method – both are said to underestimate time history analysis for closely-spaced modes of vibration. Specifically, considering some set of modal responses e.g. shear for n modes, the CQC response is the square root of the weighted sum of squares of every combination of products of modal responses (Chopra, 2020). These weights are applied based on the correlation between modes – if the weights are assumed to be zero for the product of different modes, it simplifies to the SRSS method. These approaches are applied in Chapter 3.1 and Appendix A – nonetheless, Al-Ali & Krawinkler (Al-Ali, 1998; Al-Ali & Krawinkler, 1998) indicate that both are inappropriate to assess the time history response of irregular structures.

However, the inherent necessity of inelastic analysis is not a universal consensus. Numerous studies including Das & Nau (2003), Tremblay & Poncet (2005), Soni & Mistry (2006) and Le-Trung et al. (2012) agree that irregular structures can be adequately evaluated using an equivalent static force method. Further still, Das & Nau (2003) and Le-Trung et al. (2012) assert that the use of quantitative limits on the use of equivalent static procedures may be unnecessary so long as additional checks are performed to prevent unwanted failure modes. Similarly, Cruz & Cominetti (1996) conclude that ductility demand is largely independent of the vertical irregularity so long as the element design strengths are proportional to the computed maximum elastic forces. Nevertheless, most studies agree that careful detailing is required to ensure a ductile response, particularly in the vicinity of the irregularity or in the lower storeys to address shifts in ductility demand, consistent with research on setbacks specifically (Cassis & Cornejo, 1996; Cruz & Cominetti, 1996; Das & Nau, 2003; Karavasilis et al., 2008a; Pirizadeh & Shakib, 2013). Some studies propose modifications to the behaviour factors for overstrength and ductility to address this (Anagnostopoulou et al., 2015). It is also near-unanimously agreed that strength irregularity is most important, followed by stiffness and then mass irregularity (Al-Ali, 1998; Al-Ali & Krawinkler, 1998; Chintanapakdee & Chopra, 2004; Fragiadakis et al., 2006; Le-Trung et al., 2012; Soni & Mistry, 2006; Valmundsson & Nau, 1997).

2.5 The response of structures having a vertical combination of framing systems

Whereas setbacks, stepped and soft-storey structures received attention beginning in the 1960s and more generic descriptions of irregularity received attention since the 1990s, vertical combinations of seismic force-resisting systems remain novel, with perhaps fewer than twenty papers having been published on the topic in the last twenty years. Nonetheless, designers have proceeded despite limited research guidance as the demand for cost-effective mixed-use designs has driven the adoption of (in particular) cold-formed steel and light timber structures atop reinforced concrete or hot-rolled steel podiums. This is despite potential issues posed by vertical combinations of framing systems, which are compounded with those related to the more general problem of vertical irregularity. There are in general three aspects of continuing interest in research: 1) experimental and numerical tests of expected behaviour 2) characterization of overstrength, ductility and damping and 3) simplified methods usable to evaluate structural demands.

Publications have been inconsistent on the terminology used – some studies refer to these structures as (vertically) *mixed* structures (Fanaie & Shamlou, 2012, 2015; Huang et al., 2015; Papageorgiou & Gantes, 2010; Pnevmatikos et al., 2019), whereas other studies prefer to call them *hybrid* structures (Guo et al., 2014; Liu et al., 2008; Xiong et al., 2015). Others still prefer to use *vertical combination of framing systems* (Xu & Yuan, 2015; Yuan, 2016; Yuan & Xu, 2014, 2016), and one uses *podium* buildings (Chen & Ni, 2020). Presumably, the inconsistent naming used in these studies, as well as the relatively short span of time between their publishing dates, is the explanation for the limited extent to which these otherwise related papers cross-reference each other. Unfortunately, the *mixed/hybrid* nomenclature often lacks specificity, as it could also refer to the use of different systems on a given storey, rather than distinct systems on distinct storeys. To maintain clarity, the current study will use *podium structures* and *vertical combination of framing systems* rather than the more ambiguous *hybrid/mixed* nomenclature.

Many investigations have focused exclusively on experimental and numerical tests of behaviour, with most of those being purely numerical, nonlinear studies. This can be attributed to the significant cost of shake table tests on scale-model structures. One exception is Xiong et al. (2015), which considers experimental tests on a set of full-scale, 3-storey wood-concrete structures, in which a two-storey wood-frame structure sits atop a one-storey concrete frame. They observe that the seismic responses are sensitive to the stiffness ratio between the upper wood and lower concrete structures and observe that responses are larger for smaller stiffness ratios (defined as the stiffness of the

concrete structure divided by that of wood structure). Another exception is Lu et al. (2018). In Lu et al., a 12-storey frame consisting of a four-storey steel upper structure, a seven-storey concrete lower structure and a one-storey transition storey designed according to the Chinese building code is subjected to seismic excitation. Similarly to Xiong et al. (2015), the acceleration response is sensitive to the relative stiffness of the upper and lower structures – where the structure changes abruptly in stiffness, there is a significant magnification of the response. They note that the response is also sensitive to the characteristic period of the seismic input, and peak accelerations are exhibited when it matches the period of the upper structure, as noted in earlier research by Jhaveri (1967).

Numerical studies often investigate specific configurations to assess design recommendations given by codes. Maley et al. (2012) performed nonlinear time-history analysis for a steel/RC system alongside displacement-based design (DDBD) and the ASCE 7-10 (ASCE, 2010) equivalent static method, the equivalent lateral force method (ELF). While the ELF method produces conservative results, the authors conclude that DBDD provides superior performance. Guo et al. (2014) similarly investigate a wood-steel structure designed using the Chinese code, concluding that the rigid diaphragm assumption is adequate for such structures. Chen & Ni (2020) investigate wood-concrete structures designed using the NBCC and the two-stage assumption, concluding that neither ASCE 7 nor the NBCC adequately delimit the two-stage behaviour. However, research is not consistent that these structures are of concern: an analysis of fragility curves for frames with a concrete lower structure and hot-rolled steel upper structure by Pnevmatikos et al. (2019) concludes that mixed concrete/steel frames designed according to code are less vulnerable than the equivalent single-material steel or concrete frame.

Furthermore, while not in the current study's scope, the calculation of modification factors (in NBCC, overstrength factor R_o and ductility factor R_d) and equivalent damping remain problematic for vertical combinations of framing systems. Few studies assess the inelastic modification factor – Fanaie & Shamlou (2012, 2015) propose simple formulas for mid-rise structures with a lower structure of reinforced concrete and an upper structure of structural steel. Equivalent damping is better addressed, with numerous authors using an equivalent 2DOF model which represents each of the upper and lower structures as a single degree of freedom. In two related papers, Jiang et al. (2015) and Huang et al. (2015) use such a model for a structural steel upper structure and reinforced concrete lower structure and define the equivalent damping ratio according to the ratio of total mass and ratio of fundamental frequencies for the upper and lower structures. Likewise using a 2DOF model, Yuan

(2016) approaches the problem more generically and proposes a combination rule which composites the upper and lower structures' stiffness ratios. Yuan (2016) derives their modal damping ratio from classical damping relationships for generic materials, while Qian et al. (2015) and Huang et al. (2015) exclusively look at steel-concrete structures. The forthgoing discussion focuses on more recent publications - a more thorough look at equivalent damping is given by Yuan (2016).

The final area of research for vertical combinations of framing systems concerns the development of simplified methods for the assessment and design of such structures. Two groups – Yuan & Xu (Xu & Yuan, 2015; Yuan, 2016; Yuan & Xu, 2014, 2016) and Lin et al. (2019) – have proposed significantly different solution methodologies. While both use an equivalent 2DOF model, the method given by Yuan & Xu is more approximate and oriented towards practical, code-specified design, whereas Lin et al.'s method is primarily concerned with simplifying nonlinear analysis rather than immediate application to design.

Specifically, concluding that a single-degree-of-freedom (SDOF) modal system as is commonly used in inelastic static (modal pushover) analysis is inadequate to characterize the inelastic response of vertical combinations of framing systems, Lin et al. (2019) propose an alternative inelastic simplification to nonlinear time history analysis – a procedure they refer to as uncoupled modal response history analysis (UMRHA). This method is similar to conventional elastic modal analysis but for the substitution of the traditional SDOF modal system with a new inelastic 2DOF modal system that represents both the stiff-and-strong lower structure and the less stiff, less strong upper structure as shown in Figure 2.1. The characteristics of each DOF of this new system are constructed using a bilinear (trilinear, for the upper structure) approximation of the *n*-th mode pushover curve of the building.

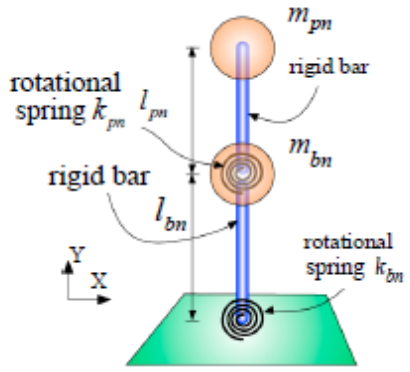

Figure 2.1: *n*-th 2DOF modal system (Lin et al., 2019)

In summary, the procedure is as follows:

1. perform eigenvalue analysis of the real/modelled structure, truncating to the desired number of modes (typically no more than three),
2. calculate the elastic 2DOF modal parameters,
3. construct the idealized bilinear/trilinear modal pushover curves in each mode,
4. calculate the inelastic 2DOF modal parameters,
5. compute each inter-storey drift ratio, and
6. repeat for each mode and combine to determine inelastic inter-storey drift ratio time history

While certainly preferable to directly performing nonlinear time history analysis, the procedure does not lend itself readily to routine or preliminary design, for which designers desire yet simpler and preferably static procedures. Furthermore, the paper gives little guidance on determining a design base shear or feasible stiffness distribution and instead focuses exclusively on interstorey drift ratios.

Fortunately, the behaviour of mid-rise structures with a vertical combination of seismic force-resisting systems can be further simplified under the right circumstances and assumptions. For example, by assuming the damping is classical and identical in each mode of vibration, and by limiting the maximum storey count. Toward this end, Yuan & Xu (Xu & Yuan, 2015; Yuan, 2016; Yuan & Xu, 2014, 2016) propose a set of linear elastic static procedures to evaluate mid-rise vertically irregular structures having ten or fewer storeys. As culminating in Yuan (2016), these methods apply to both the NBCC 2010 and the ASCE 7-10 codes and can be grouped into four categories:

1. To quantify the effect of higher modes, Yuan & Xu propose an approximation for the amplification factor α_U. α_U describes the higher-mode amplification of the upper structure's base shear as a function of the mass and stiffness ratio of the upper and lower structures.

2. To aid the pre-selection of stiffnesses satisfying the NBCC (or ASCE) interstorey drift, Yuan & Xu propose an interstorey drift criterion that is a function of both α_U and the upper structure's storey stiffness. By proxy via α_U, the criterion therefore relates the storey stiffnesses of the upper and lower structures to the interstorey drift limit, allowing a designer to identify whether a given selection of stiffnesses will satisfy the interstorey drift limit. This procedure is defined using the interstorey drift at the bottom storey of the upper structure, and on account of being static, negates most of the iteration that is otherwise

inherent in dynamic procedures (the iterative nature of the dynamic analysis is noted by Liu et al. (2008)).

3. To quantify the equivalent static loads, Yuan & Xu propose two methods for both NBCC 2010 and ASCE 7-10 to determine the seismic load distribution on a mid-rise structure with a vertical combination of seismic force-resisting systems.
4. Yuan & Xu also define equivalent damping for the structure (not in the scope of the current study).

As part of a cohesive whole, the work of Yuan & Xu provides a set of linear static methods to facilitate the preliminary design of vertically irregular structures in a variety of ways. These methods (barring equivalent damping) are the basis of the current study, and so there is no need to further elaborate on them here. Where necessary, they will be discussed in the subsequent chapters.

2.6 Commentary on previous research

The study of vertical combinations of framing systems has arisen from the wider class of vertically irregular structures much in the way that the latter arose from the study of setback, stepped and soft-storey structures. Thus, despite the relatively small number of studies specifically investigating the behaviour of vertical combinations of framing systems, there are decades of research and codes with which some conclusions can be recognized. While there is some dispute among authors, several conclusions can be said to apply generally to vertical combinations of framing systems:

1. Existing regularity limits are criticized by a large body of previous research despite being present for decades in both Canadian and American design standards. Some authors have proposed modifications or new criteria altogether, whereas others question the efficacy of such limits in a general sense and instead propose that requirements focus on ensuring acceptable failure modes rather than arbitrary limitations on specific parameters. The ultimate result is that there is no general framework in either North American or international codes for designers to determine whether a structure behaves as a regular structure - thus, designs may at times be over-conservative and at others times not fulfill the expected performance objectives (and thus be under-conservative).
2. Previous research on the elastic response of irregular structures has identified the risk of higher-mode effects arising due to the interaction of different modes of vibration. Studies have identified that this is sensitive to numerous design variables, notably the number of storeys, and

the mass and stiffness attributed to each of the upper and lower structures. This manifests most clearly in the relative values of modal periods – effects are most severe when the upper and lower structures, or the upper structure and the full structure as a whole are prone to vibrate at the same frequencies. Studies have also identified that the characteristic period of the input excitation is important.

3. Most studies on the inelastic behaviour of irregular structures agree that irregular structures are potentially subject to non-uniform distributions of ductility demand, particularly in the vicinity of the irregularity. Some studies also identify that increased ductility demand may occur in the lower structure based on the characteristics of the structure. These demands are sensitive to the location and magnitude of the irregularity, the beam-to-column stiffness ratio and the limit state being considered, as well as those factors affecting the elastic behaviour. It is in general unclear the extent to which detailing these critical sections is important to ensure adequate ductile performance in severe earthquakes.
4. There is a consensus that strength irregularity is the most severe type of irregularity, followed by stiffness and then mass irregularity, with combinations being worse than any single type.
5. Despite the importance of inelastic behaviour and strength irregularity, it is inconclusive whether elastic analysis, particularly code-specified equivalent static analysis, is adequately conservative to predict shear demands. Many studies argue that equivalent static procedures are adequate, even with little to no modification. A limited number of studies argue that irregular structures are not necessary higher-risk than regular ones, particularly setback/stepped structures and others that generally consist of a massive, stiff and strong lower structure underlying a less massive, less stiff and less strong upper structure.
6. Two-degree-of-freedom simplified models and generic regular structures are commonly used in research to compare the effects of irregularity.

Regarding vertical combinations of framing systems specifically:

1. Research on vertical combinations of framing systems features potentially ambiguous nomenclature and has currently received limited attention in research compared to other types of irregularity. Existing research explores a variety of archetypes but has focused largely on hot-rolled steel or wood atop concrete, rather than cold-formed steel as is increasingly common in North American practice.

2. Limited research has explored equivalent damping, overstrength and ductility for vertical combinations of framing systems.
3. Two major proposals exist for simplifying the analysis of vertical combinations of framing systems. One is oriented towards simplifying nonlinear analysis and the other is oriented towards improving code-specified elastic design procedures.

It is clear from the research that there is a large degree of uncertainty regarding the analysis and design of vertically irregular structures, particularly those with a vertical combination of framing systems. However, ever-improving computational and methodological techniques beg the question: why continue the development of an equivalent linear static method? The simplest answer is that, in NBCC 2015 and for the near future, linear static analysis is used as a reference for all dynamic analysis and as a minimum so that designs are sufficiently conservative (NRCC, 2015c; SEAOC, 2019). More broadly, the practice of dynamic and nonlinear analysis invites errors and difficulty of interpretation - as opined by Krawinkler (2006), "good and complex are not synonymous, and in many cases they are conflicting" rationalizations for seismic design. As pointed out by Fajfar (2018) and Terzic et al. (2015) in the context of a contest run by PEER (Pacific Earthquake Engineering Research Center), the use of advanced and sophisticated models did not necessarily ensure accurate results. Indeed, some led to wildly inaccurate results which could be easily refuted by a simple linear single-degree-of-freedom (SDOF) model. Since designers also consistently report that the guidance for nonlinear analysis is insufficient, that nonlinear analysis is excessively time-consuming, and that there is inadequate software support for such analysis, a more intuitive linear static analysis remains both desirable and necessary (Head et al., 2014). So long as nonlinear time history analysis remains esoteric, prone to errors and lacking extensive incorporation in codes, linear elastic analysis, including elastic static analysis, will serve a role in building codes.

Chapter 3
Characterization of the Effect of Higher Vibration Modes on the Upper Structure of Podium Structures

3.1 Introduction

The true behaviour of structures under earthquake excitation is a highly nonlinear, stochastic, and dynamic problem, the behaviour of which can only be exactly determined by observation of the real structure under the effects of an actual earthquake. This degree of accuracy is neither tenable nor necessary for design, and so codes often provide that the equivalent storey forces and interstorey drifts can be calculated based on a semi-empirical linear elastic static calculation. There are several essential simplifications made by the NBCC and other codes – the spectrum $S_a(T)$, the linear-to-nonlinear ductility and overstrength modification factors R_d and R_o, and some factor, e.g. M_v, to characterize the effect of the second or higher modes of vibration. These factors vary in form but are generally consistent in function between codes.

However, the use of these factors is predicated on the assumption that the structure is approximately regular in form throughout its height. Where structures vary in stiffness, mass, and/or other parameters through their height, factors such as M_v may not adequately represent the behaviour of the structure. To address this, Yuan & Xu (2014) propose a factor analogous to M_v, α_U, to characterize the amplification of the upper structure's base shear as a function of the structural irregularity. This factor serves as the basis of a simplified design method that can identify an appropriate distribution of stiffness and mass which ensures that the code-specified storey drift limits are satisfied. While originally derived for the ASCE 7-10 code (2010), the method is also adapted to the NBCC 2010 (NRCC, 2010) code.

Despite this, there remain improvements to be made to the existing method. It was originally developed for ASCE 7-10 (ASCE, 2010), not NBCC 2010 or 2015 (NRCC, 2010, 2015c), and, its application to NBCC 2010/NBCC 2015 is awkward for designers unfamiliar with the terminology of the American code. Focusing only on application to NBCC 2015 except where necessary, this chapter aims to refine the upper structure higher mode amplification factor α_U to improve its accuracy and ease of use and to expand the scope, where possible. The structure of the chapter is as follows: First, α_U and the storey drift-based design criterion are introduced, and with the help of an equivalent 2DOF model the parameters affecting α_U are described. Next, having established α_U, a simplified empirical

form is proposed and then applied to derive the required storey stiffness distribution such that the design criterion is satisfied. To end the chapter, examples are presented to demonstrate the determination of feasible stiffness distributions via the higher-mode amplification factor α_U, 2DOF model parameters (e.g. R_k) and NBCC 2015 spectral acceleration $S_a(T)$. Feasible stiffness distributions in this context are considered those which simultaneously satisfy the scope set out in Section 1.3.2, e.g. $\max(1, r_{kUI}) \leq r_k \leq 20$ and the drift-based design criterion set out in Equation (3.9).

3.2 Design criterion

As is the case in Yuan (2016), the present study is motivated by the need to reduce the iteration used for the design of vertically irregular structures. Towards this end, a design criterion is needed, and so the interstorey drift between the base of the upper structure and the top storey of the lower structure is chosen. As excessive storey drifts lead to collapse or excessive damage in a structure, the maximum interstorey drift is commonly used as a proxy for structural performance. Accordingly, both ASCE 7-16 (2017) and NBCC 2015 (NRCC, 2015c) specify a limit on interstorey drifts as a proportion of the storey height – for example, 2.5% of the interstorey height for a structure of normal importance (NBCC 2015). Considering a simplified MDOF lumped-mass model in which each storey is represented as a single mass as described in the forthcoming sections, the interstorey drift between the bottom storey of the upper structure and the top storey of the lower structure is defined as:

$$\Delta_U = \frac{V_{Ub}}{k_U} \tag{3.1}$$

where V_{Ub} is the elastic base shear force of the upper structure and k_U is the storey-stiffness of the upper structure. In this MDOF model, characterized by Figure 3.1, the lumped mass representing the bottom storey of the upper structure is associated with the seismic force-resisting system below the mass – therefore, the interstorey drift between the bottom storey of the upper structure and the top storey of the lower structure is characterized by the base shear of the upper structure acting on the storey stiffness of the upper structure. So long as the minimum overall stiffness ratio R_{kUI} as defined in Section 3.3.4 and Appendix C is exceeded, it is expected that the maximum interstorey drift will occur at the base of the upper structure and therefore Equation (3.1) is an acceptable measure of structural performance. The proposed procedure is predicated on the fact that the base of the upper structure is the only location for which interstorey drift needs to be checked.

The assumption that the interstorey drift (at least insofar as the *elastic* response) is largest at the base of the upper structure beyond a certain stiffness ratio for a fixed mass ratio and number of storeys is justified based on the behaviour of the MDOF model analyzed by MRS analysis. Assuming that the storey heights of each storey are identical, the interstorey drift of each storey is a function only of the storey stiffness of the storey and the shear force acting on the seismic force-resisting system at that storey. In a structure with constant stiffness, the shear forces accumulate towards the base of the structure, and thus the interstorey drift is largest at the base of the structure. However, if the upper structure's storey stiffness is decreased relative to the base, the interstorey drifts will increase in the upper structure, eventually surpassing those which appear at the base of the lower structure. The forces in the upper structure increase towards its base, thus the largest interstorey drift in an upper structure of constant stiffness at its base. This phenomenon as observed in the MDOF model for an arbitrary structure is illustrated by Figure C.1. That the interstorey drift is largest in the upper structure beyond a certain value of R_k can also be observed in other research (Humar & Wright, 1977; Shahrooz & Moehle, 1990; Wong & Tso, 1994; Yuan, 2016).

Note that unlike Yuan (2016) the formulation for interstorey drift is not a function of the inelastic modification factors R_d and R_o, nor the ASCE 7 drift amplification factor C_d. The definition given by Yuan (2016) is based on ASCE 7. In ASCE 7 (2010, 2017), the nonlinear scaling for forces (via R) and storey drifts (via C_d) are not equal, whereas in the NBCC the same factor (R_dR_o) is used for scaling down linear elastic forces to estimate inelastic ones, and for scaling up linear storey drifts to estimate nonlinear ones. Consequently, the design criterion is not a function of R_dR_o. However, where R_dR_o varies between the upper and lower structures, the value for the combined structure is taken as the lower of the two structures' R_dR_o, as recommended by NBCC 2015 (NRCC, 2015b). The difference between C_d and R_dR_o is not of particular concern – there are contemporary proposals to revise C_d to be equal to R in American codes, as currently assumed by NBCC 2015 (NRCC, 2015c; SEAOC, 2019).

To apply the criterion, the base shear V_{Ub} must be determined. It is well-understood that higher mode effects can be significant even for regular structures, and that it is inadequate to assume that shears are fully described by the first mode of vibration. To characterize this effect, the NBCC (NRCC, 2015c) applies a higher mode factor, M_v, to the equivalent static base shears predicted by its equivalent static force procedure (ESFP), defined as (Humar & Mahgoub, 2003; NRCC, 2015c):

$$\mathrm{M}_v = \frac{\sqrt{\sum(S_a(T_i)W_i)^2}}{S_a(T_1)W} \tag{3.2}$$

where $S_a(T_i)$ and W_i are the i-th-mode spectral values and modal weights, and $S_a(T_1)$ and W are the first-mode spectral value and the total weight of the structure. In essence, M_v describes the ratio of the total seismic force and that of only the first mode and is given in the NBCC as a function of $S_a(0.2)/S_a(5.0)$ and T_1 (NRCC, 2015c). $S_a(0.2)/S_a(5.0)$ and T_1 describe the spectral shape and fundamental period of the structure. Therefore, per the NBCC the elastic base shear of the upper structure (V_{Ub}) considering the upper structure as though fixed at its base (i.e. without the lower structure) is:

$$V_{Ub} = M_v W_U S_a(T_U) = M_v m_U N_U g S_a(T_U) \tag{3.3}$$

where W_U, m_U and N_U are the total weight, storey mass and storey count of the upper structure, $S_a(T_U)$ is the spectral acceleration at the fundamental period of the upper structure T_U, g = 9.8 m/s^2 is gravitational acceleration, and V_{Ub} is the elastic upper structure base shear.

However, M_v is derived for use with mostly regular structures and is based on the square-root-sum-of-squares (SRSS) method for combining modal contributions, which is applicable only if the modal periods of the structure are well-separated and can be considered independently (Humar & Rahgozar, 2000; Meskouris et al., 2019). This is not always true for vertically irregular structures. As observed by Xiong et al. (2015) and Yuan & Xu (2014), the amplification effect otherwise characterized by M_v varies as a function of the relative stiffness, mass and periods of the upper and lower portions of the structure, particularly for more severe irregularities. Therefore, Yuan & Xu (2014) introduce α_U to account for the effect of higher modes on the shear of vertically irregular structures:

$$\alpha_U = \frac{V_{Ub}}{m_U N_U g S_a(T_U)} = \frac{upper\ base\ shear\ from\ all\ modes}{upper\ base\ shear\ from\ first\ mode\ only} \tag{3.4}$$

where α_U is the upper structure base shear amplification factor, hereafter amplification factor for short. α_U is explicitly the ratio of the base shear of the upper structure considering all modes divided by the first-mode value and therefore characterizes the effect of higher modes on the upper structure base shear.

In both Yuan & Xu (2014) and this study, the complete quadratic combination (CQC) rule is used, and therefore α_U can also be expressed as:

$$\alpha_U = \frac{\sum_{i=1}^{N}\sum_{j=1}^{N}\sqrt{\rho_{ij}W_{Ui}W_{Uj}S_a(T_i)S_a(T_j)}}{W_U S_a(T_U)} \tag{3.5}$$

where W_U, W_{Ui}, W_{Uj} are the weights associated with the full upper structure and with the i-th and j-th modes, and $S_a(T_U)$, $S_a(T_i)$, $S_a(T_j)$ and T_U, T_i, T_j are the corresponding spectral accelerations and periods. ρ_{ij} is a correlation coefficient which is taken as (assuming equal damping ζ in each mode) (Chopra, 2012):

$$\rho_{ij} = \frac{8\zeta^2(1+\beta_{ij})\beta_{ij}^{3/2}}{(1-\beta_{ij}^2)^2 + 4\zeta^2\beta_{ij}(1+\beta_{ij})^2} \quad , \qquad \beta_{ij} = \frac{T_j}{T_i} \tag{3.6}$$

Evident from Equations (3.2) and (3.5), α_U is analogous to M_v as used in the NBCC, except that α_U is defined at the base of the upper structure rather than that of the full structure and that α_U is defined with the CQC method rather than the SRSS method (note that if $\rho_{ij} = 0$ for all $i \neq j$, the CQC method simplifies to the SRSS method). Previous authors, e.g. Jhaveri (1967), have noted that the inter-mode interaction effects are potentially significant in irregular structures on account of adjacent periods of vibration having similar modal periods. The CQC method considers both intra-modal and inter-modal contributions, whereas the SRSS method neglects the inter-modal effects caused by interactions between modes. Accordingly, it is common to see the CQC method used in research regarding irregular structures, e.g. Montazeri et al. (2012), Wong & Tso (1994) and Roy & Mahato (2013). As noted by SEAOC (1996), "the adequacy of the SRSS method depends on the ratio of the modal periods and the modal damping ratios". Meanwhile, the CQC method is said to always be acceptable. Given its robustness relative to SRSS, the CQC method is preferred.

Substituting the definition of α_U in place of M_v in Equation (3.3), the upper structure's base shear considering the vertical irregularity is as follows:

$$V_{Ub} = \alpha_U m_U N_U g S_a(T_U) \tag{3.7}$$

The design criterion given in Equation (3.1) can therefore be described as:

$$\Delta_U = \frac{\alpha_U m_U N_U g S_a(T_U)}{k_U} \tag{3.8}$$

With some manipulation of Equation (3.8) and assuming that $\Delta_U = \Delta_{Ulim}$, where Δ_{Ulim} is the storey drift limit (e.g. 2.5%) specified by NBCC 2015, the governing equation for the simplified design procedure is:

$$\alpha_U \leq \frac{k_U \Delta_{\mathrm{Ulim}}}{m_U N_U g S_a(T_U)} \tag{3.9}$$

This design criterion can be interpreted using the language of limit states design. In this sense. α_U represents a load (relative to the first-mode upper structure base shear) which is resisted by the quotient on the right-hand side of Equation (3.9). For a value of α_U exceeding the specified limit, the degree of amplification exceeds the amplification that can be resisted by the given stiffness, in which case the interstorey drift limit Δ_{Ulim} is exceeded. In other words, for any given scaling of the first-mode base shear V_{Ub} represented by α_U, there is a required stiffness k_U (with all else being held constant) required to not exceed the design interstorey drift limit Δ_{Ulim}. In essence, the goal of the simplified design procedure is to establish the range of stiffnesses k_U such that the expected amplification due to higher-mode effects as characterized by α_U is tolerable (i.e. $\Delta_U \leq \Delta_{Ulim}$). If k_U is lower than that required by Equation (3.9), the storey drift limit is exceeded, and otherwise, the structural configuration is capable of bearing the expected amplification. The stiffness of a single storey of the lower structure, k_L, is implicitly incorporated in Equation (3.9) via α_U, which is a function of the relative stiffness and mass between the upper and lower structures. With k_U as the primary design variable, the remainder of this chapter focuses on the development of a simplified approximation of α_U in terms of variables assumed to be known a priori, and the subsequent application of that relationship towards solving for appropriate distributions of k_U and k_L.

3.3 Revised stiffness ratio and amplification (R_k-α_U) relationship

Having established Equation (3.9) as the upper bound of α_U such that the interstorey drift is satisfied, the next step is to relate α_U to the parameters of the 2DOF model. The focus is on an expression for α_U which is a function of the overall stiffness ratio R_k only (The overall mass ratio R_m and the storey masses m_U and m_L are assumed to be known a priori). This relationship is developed as follows:

1. Represent the MDOF model as a simplified 2DOF model (Section 3.3.1)
2. Investigate the behaviour of α_U in the 2DOF and MDOF models (Section 3.3.2)
3. Calibrate α_U using the MDOF model (Section 3.3.3)
4. Propose equations for α_U and analyze the error between the proposed α_U and the α_U obtained from modal response spectrum analysis of the MDOF model (Section 3.3.4)

3.3.1 Simplified 2DOF model

Speaking most generally, the lumped-mass multiple-degree-of-freedom (MDOF) models used in this study are fully described given the storey mass (m_U), storey stiffness (k_U) and storey count (N_U) of the upper structure and the lower structure (m_L, k_L, N_L). However, it is desirable to possess a more general diction with which to compare otherwise different structures. To this end, Yuan & Xu (2014) introduce an equivalent 2DOF model as illustrated in Figure 3.1, in which the total mass of the upper and lower structures are lumped into two separate masses, M_U and M_L, defined analogously to their MDOF counterparts. Likewise, the upper and lower structures' total stiffnesses can be combined to obtain the total upper structure stiffness K_U and total lower structure stiffness K_L. As is the case with the mass and stiffness, this study distinguishes MDOF parameters from their 2DOF counterparts by their case – uppercase letters denote 2DOF parameters while lowercase letters denote MDOF parameters (e.g. m_U versus M_U).

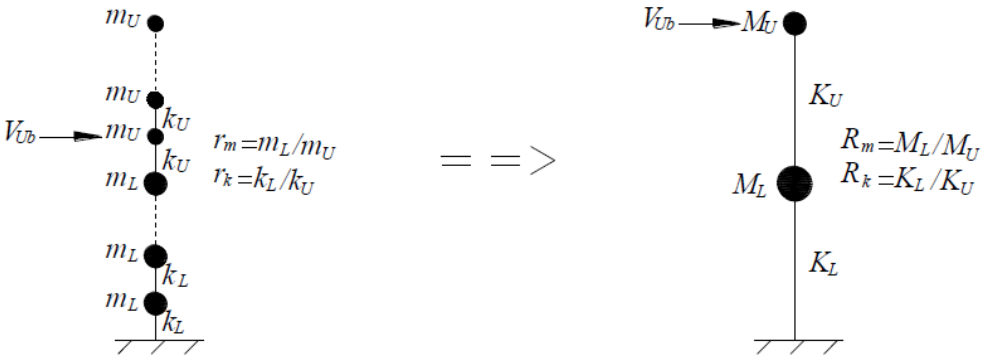

Figure 3.1: Model simplification (Yuan, 2016; Yuan & Xu, 2014)

With the MDOF and 2DOF models thusly defined, the 2DOF model masses and stiffnesses (M_U, M_L, K_L, and K_U) can be defined (Xu & Yuan, 2015):

$$M_U = m_U N_U \tag{3.10}$$

$$K_U = \left(\bar{\omega}_{1U}\sqrt{k_U/m_U}\right)^2 M_U \tag{3.11}$$

$$M_L = m_L N_L \tag{3.12}$$

$$K_L = \left(\bar{\omega}_{1L}\sqrt{k_L/m_L}\right)^2 M_L \tag{3.13}$$

where $\bar{\omega}_{1U}$ and $\bar{\omega}_{1L}$denote the normalized first-mode frequencies for the upper and lower structure, respectively. For an MDOF structure having equal mass and stiffness at each DOF, the value of stiffness and mass can be factored out of the eigenvalue problem for free vibration by assuming that the *n*-th mode circular frequency can be expressed as $\omega_n = \bar{\omega}_n\sqrt{k/m}$. $\bar{\omega}_1$, the first eigenvalue corresponding to a structure with unit mass and stiffness at each DOF can therefore be used to determine ω_1 of any uniform structure. The first mode circular frequencies are presented of $\bar{\omega}_1$, applicable to an *N*-storey uniform structure of up to 12 storeys, in Table 3.1. These can be derived for an arbitrary structure, but no structure in the current scope is beyond twelve storeys in height.

Table 3.1: Normalized first mode circular frequency of uniform structure

N	1	2	3	4	5	6	7	8	9	10	11	12
$\bar{\omega}_1$	1	0.618	0.445	0.347	0.285	0.241	0.209	0.185	0.165	0.150	0.137	0.126

The normalized first mode frequencies, $\bar{\omega}_1$, can also be used to define the fundamental period of the upper structure (T_U) and the lower structure (T_L). These periods, as well as the corresponding single-storey periods (i.e. T_{singU}, T_{singL}, associated with a single DOF of the MDOF model), are defined as:

$$T_U = 2\pi\sqrt{\frac{M_U}{K_U}} = \frac{2\pi}{\bar{\omega}_{1U}}\sqrt{\frac{m_U}{k_U}} = \frac{T_{singU}}{\bar{\omega}_{1U}} \tag{3.14}$$

$$T_L = 2\pi\sqrt{\frac{M_L}{K_L}} = \frac{2\pi}{\bar{\omega}_{1L}}\sqrt{\frac{m_L}{k_L}} = \frac{T_{singL}}{\bar{\omega}_{1L}} \tag{3.15}$$

It is also advantageous to characterize the degree of irregularity in the structure. On either a storey-versus-storey basis (as with r_m and r_k) or an overall basis (as with R_m and R_k), the mass and stiffness of the upper and lower structures in the 2DOF or MDOF model can be used to define stiffness and mass ratios:

$$r_m = \frac{m_L}{m_U} \tag{3.16}$$

$$r_k = \frac{k_L}{k_U} \tag{3.17}$$

$$R_m = \frac{M_L}{M_U} = \frac{r_m N_L}{N_U} \tag{3.18}$$

$$R_k = \frac{K_L}{K_U} = r_k \left(\frac{N_L}{N_U}\right)\left(\frac{\bar{\omega}_{1L}}{\bar{\omega}_{1U}}\right)^2 \tag{3.19}$$

where r_m is the storey mass ratio and r_k is the storey stiffness ratio, and where R_m is the overall mass and R_k the overall stiffness ratio. With r_m, r_k, R_m and R_k, the structure is defined with respect to the upper structure and the degree of irregularity rather than by the lower structure's mass and stiffness directly. Collectively, the 2DOF properties represent an approximation of the MDOF structure, such that any given input structure can be compared using the relative (total) mass and stiffness between the upper and lower structures.

Note that the interpretation of r_k and r_m concerning irregularity differs from that for R_k and R_m. A regular structure in the context of building codes such as the NBCC 2015 is a structure in which the storey stiffness and mass are approximately equal across all storeys, or otherwise vary only gradually. For such a structure, both r_k and r_m are approximately one, for the mass and stiffness of the upper and lower structure, however defined, are approximately equal. Conversely, because R_m and R_k are each a function of the number of storeys, they indicate only the relative mass and stiffness between the upper and lower structures in the collective sense. This is important in the overall behaviour because (for example) much lighter-weight penthouses are expected to behave differently than a larger and more massive upper structure, but it means that structures with equal R_k and R_m may have considerably different characteristics vis-à-vis structural regularity. For example, consider a structure with a tall, slender tower, a structure with an upper structure and lower structure of an equal number of storeys, and a tall lower structure with a one-storey penthouse. Because R_k and R_m are functions of N_U and N_L, $R_k = R_m = 1$ implies a regular structure if and only if $N_U = N_L$. For the hypothetical penthouse structure, $N_U << N_L$, and so R_m and $R_k < 1$ if the structure is regular, and for the hypothetical slender tower on a short base, $N_U >> N_L$ and thus R_m and $R_k > 1$ if the structure is regular. In addition, while R_m is a function of N_L and N_U, R_k is also a function of the normalized first mode frequencies $\bar{\omega}_{1U}$ and $\bar{\omega}_{1L}$. Therefore, while R_k and R_m both indicate the relative difference in stiffness and mass (respectively) between the upper and lower structures, they do not correspond in the same ratio to the storey ratios r_k and r_m. The interpretation of R_m and R_k should always be regarding the relative

importance of the upper and lower structure, not whether the structure is regular or not in the traditional sense.

It is precisely because R_m and R_k articulate a different view of irregularity (as opposed to being only that each storey is identical) that they are useful to further articulate the problem of vertically irregular structures. A 2DOF analogy, as well as the mass and stiffness ratios (alternatively, period/frequency ratio), has been used to great effect frequently in past research, such as by Shahrooz & Moehle (1990) and Wong & Tso (1994), The 2DOF modal approximates the responses' first two modes, and therefore lies within the range of results from the MDOF model, as the modal contributions from higher modes may exacerbate or alleviate the amplification effect observed from the 2DOF model. Therefore, while it is useful to use the 2DOF approximation to discuss and develop the approximation for the amplification factor α_U, the MDOF results are of greatest interest to the final solution.

Note also that the overall mass ratio R_m as given by Equation (3.18) and overall stiffness ratio R_k as given by Equation (3.19) are directly related to the first-mode periods of the upper and lower structure, T_U and T_L, given by Equations (3.14) and (3.15). Therefore, using these equations the period ratio of the two structures, T_U/T_L, can be expressed using R_m and R_k:

$$\frac{T_U}{T_L} = \frac{(2\pi)\sqrt{M_U/\mathrm{K_U}}}{(2\pi)\sqrt{M_L/K_L}} = \sqrt{\frac{\bar{\omega}_{1L}^2(m_U/k_U)}{\bar{\omega}_{1U}^2(m_L/k_L)}} = \sqrt{\frac{R_k}{R_m}} \tag{3.20}$$

3.3.2 Analytical results based on the 2DOF model

The shear response of the MDOF model via MRS analysis is described by seven variables: the storey stiffnesses, masses and counts (m_U, m_L, k_U, k_L, N_U, N_L), and the spectral acceleration $S_a(T)$, which itself is described by values at T = 0.2, 0.5, 1.0, 2.0, 5.0 and 10.0 seconds. Given some arbitrary values of these variables, the corresponding free vibration eigenvalue problem can be used to calculate the MRS storey shears and α_U in either the MDOF or 2DOF model, as desired. Unfortunately, an analytical solution of the eigenvalue problem is not possible, and thus it is necessary to interrogate the behaviour of α_U in the MDOF model indirectly via the inputs m_U, m_L, k_U, k_L, N_U, N_L and $S_a(T)$. This is impractical – the eigenvalues depend more on the relative values of the masses and stiffnesses rather than the absolute values. It is therefore difficult to discuss the effect of e.g. m_U independently of m_L, since changing either will affect the values of the eigenvalues and thus α_U. Accordingly, while the MDOF value of α_U is desired for design, the 2DOF model, R_m, R_k, T_U and

$S_a(T)$ can be used to generalize the trends of α_U. The 2DOF model truncates the 3rd and higher vibration modes but is sufficient to capture the overall trends.

To articulate these trends, a parameter survey of the 2DOF model is conducted and described in Appendix B, incorporating both the findings of Xu & Yuan (2015) and Yuan (2016) and additional commentary concerning the MDOF model and NBCC 2015 as applicable. Much of the survey is pre-established by Xu & Yuan (2015) and Yuan (2016) for ASCE 7-10, and so the effects of R_m, R_k, T_U and $S_a(T)$ on α_U in the 2DOF model are already well-established. In this study, R_m, R_k, T_U and $S_a(T)$ are varied according to NBCC 2015 and used to reproduce the results given by Xu & Yuan (2015) and Yuan (2016) as applicable to NBCC 2015. The results are largely identical to those of Xu & Yuan (2015) and Yuan (2016) despite the differences between ASCE 7-10 and NBCC 2015. Where they differ, additional commentary is provided. The parameter survey is described in more detail in Appendix B – the following paragraphs describe the key conclusions.

Effect of overall stiffness ratio R_k

Assuming that all variables are constant except for R_k, α_U varies between two extremes as illustrated by Figure 3.2. The theoretical relationship between R_k and α_U can be broadly characterized into three regions:

1. For values of R_k approaching zero, the lower structure damps the vibration response of the upper structure, and at the limit $R_k = 0$, the lower structure completely isolates the upper structure from the ground excitation. Thus, $\alpha_U \to 0$ as $R_k \to 0$.

2. Conversely, for values of R_k approaching infinity, the lower structure acts as a rigid body that transfers loads directly to the upper structure. In this scenario, the upper structure behaves as though rigidly fixed to the ground and can be analyzed without consideration of the lower structure. This is the two-stage assumption (as appearing in ASCE 7 (2017)), and for practical purposes, a limit R_{kU2stg} can be defined beyond which this assumption applies. This limit is subsequently defined in Equation (3.28).

   It should be emphasized that while $\alpha_U \approx 1$ beyond R_{kU2stg}, it will not generally be exactly 1. As discussed by Humar & Mahgoub (2003), regular structures are susceptible to higher-mode effects to some extent, and so too is a uniform upper structure attached to a perfectly rigid base. They refer to M_v as used in the NBCC (Equation (3.2)), but this conclusion equally applies to α_U. This is not explicitly captured by the two-stage procedure given by

ASCE 7-16 (2017), except for structures with $T > 0.5$, to which an exponent is applied to modify the force distribution.

3. The final scenario is intermediate to scenarios 1 and 2. Where R_k lies between that corresponding to a regular structure (which varies based on N_U and N_L) and R_{kU2stg}, α_U varies. While α_U for these irregular structures is sometimes less than one, it is more typically greater than one. Particularly for large values of R_m and R_k that do not exceed the two-stage limit, higher-mode effects arising due to interaction between vibration modes of the upper and lower structures may cause amplification by a factor α_U of 1.5 or more.

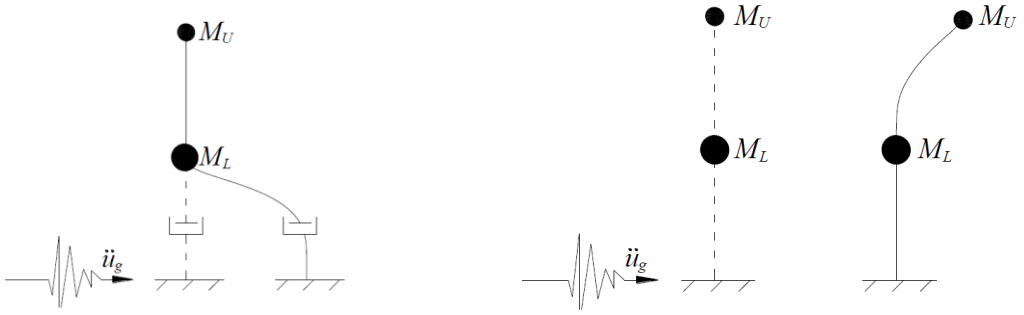

a) extremely flexible lower structure ($R_k \to 0$) b) extremely stiff lower structure ($R_k \to \infty$)

Figure 3.2: Physical interpretation of extremely flexible and stiff lower structure (Yuan, 2016)

Yuan & Xu (2014) are not the first to articulate this trend. An appendix to the first edition of the Blue Book published in 1960 by SEAOC (1960) warns of the same effect in setback (geometrically irregular) structures, namely that as a function of the masses and stiffnesses of the tower and base: 1) the base predominates, 2) the tower predominates, or 3) some intermediate condition occurs.

Effect of overall mass ratio R_m

However, it is not only the relationship for stiffness but also mass that is important in determining the amplification. As discussed in Appendix B, a larger mass ratio generally produces a larger amplification for those structures in the scope of this study. For instance, consider an appendage structure, in which a lightweight penthouse or mechanical floor adjoins a more massive lower structure. Such a structure would have a large R_m, and given the difference in the inertia, the appendage is subject to the whims of the structure below. It follows that such a structure would impose more significant higher-mode effects on the appendage (and thus, higher α_U) compared to the first-mode response of this penthouse alone.

If the value of α_U for an arbitrary structure is plotted as a function of R_m and R_k as in Figure 3.3, it is clear that a larger value of R_m corresponds to a larger amplification. The relationship for R_k is also demonstrated – the curve increases from zero and trends towards one, with varying behaviour in between. But it should also be noted that the value of R_k that is associated with the maximum changes as a function of R_m, generally increasing in conjunction with R_m. This maximum point is soon estimated by R_{kU2} and R_{kU3} in the forthcoming sections. R_{kU2} and R_{kU3} are the lower and upper bound of the region for which it is assumed that α_U is at its maximum value – they are defined in Section 3.3.4 and elaborated on in Appendix C.

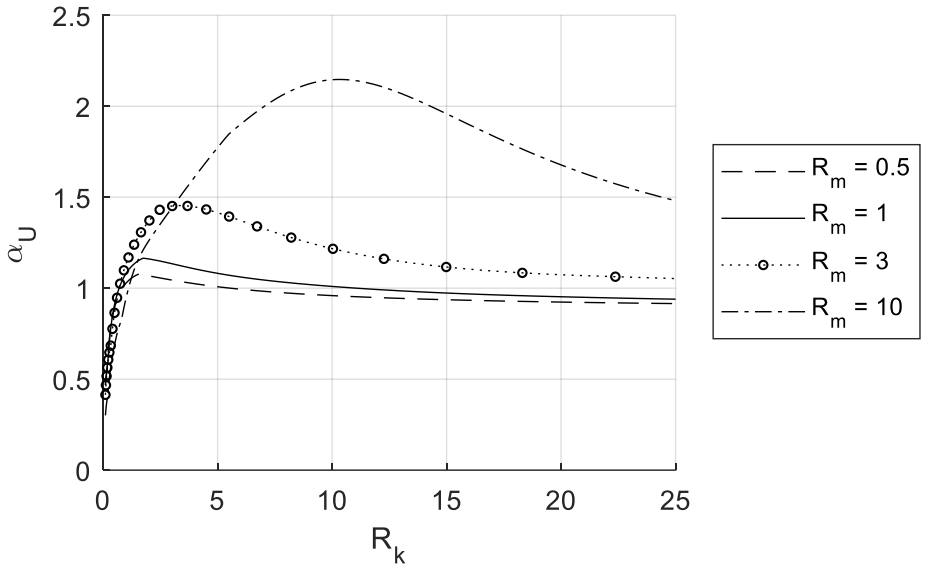

Figure 3.3: Effect of R_m and R_k on amplification factor α_U

Effect of upper structure period T_U and $S_a(T)$

Typically, an increase in T_U and an increase in the slope of $S_a(T)$ (as described by $S_a(0.2)/S_a(0.5)$ or $S_a(0.2)/S_a(5.0)$) can be expected to lead to a decrease in α_U, as in Figure 3.4. However, this is not always the case. The effect of T_U and $S_a(T)$ on α_U varies based on the relative values of modal periods and the relative slope of $S_a(T)$ (e.g. as gauged by $S_a(0.2)/S_a(0.5)$ or $S_a(0.2)/S_a(5.0)$). The modal periods will generally be such that $0 < T_2 \leq T_U \leq T_1$ as discussed in Appendix A (where T_1 and T_2 are the first two periods of the full MDOF model). The stiffer lower structure means that the period of the full structure will be longer than T_U. Considering this, the following observations can be made:

1. Where T_U and T_1 are both in the constant acceleration region (i.e. typically ≤ 0.2 s), $S_a(T_1)/S_a(T_U) = 1$ and α_U is at its maximum. As is the case in Figure 3.4, $T_U \leq 0.2$ seconds

alone does not necessarily imply this is the case – as T_U increases, T_1 eventually falls into the next segment of $S_a(T)$ (0.2 s ≤ T ≤ 0.5 s), at which point $S_a(T_1)/S_a(T_U) < 1$. In Figure 3.4, this occurs when $T_U \approx 0.1$ seconds, but this varies based on the input parameters.

2. At extremely long periods, ($T \rightarrow 10$ s) $S_a(T_1)/S_a(T_U) \rightarrow 1$ as the spectral curve flattens. Structures with such a period are outside the scope of this study, and so the effect on α_U is irrelevant. In any event, $S_a(T)$ is low enough for such structures that the effect of $S_a(T_1)/S_a(T_U) \rightarrow 1$ on α_U for large T is likely not of concern.

3. For intermediate periods, the spectral acceleration $S_a(T)$ is monotonically decreasing and so it is tempting to assume that α_U always decreases. This is not the case. As both $S_a(T_U)$ and $S_a(T_1)$ are piecewise linear, the shape of $S_a(T_1)/S_a(T_U)$ varies based on whether T_U and T_1 lie on the same or different segments of $S_a(T)$, and based on the slope of the spectrum. As further discussed in Appendix B, this results in a relationship for $S_a(T_1)/S_a(T_U)$ which transitions between downward-sloping segments in which T_1 and T_U lie in the same segment of $S_a(T)$, and upward-sloping segments caused by the transition of period T_1 (which is longer than T_U) to the subsequent segment of $S_a(T)$. It is therefore not sufficient to use the ratio of periods to gauge how α_U changes - $S_a(T_1)/S_a(T_U)$ itself should be evaluated.

Figure 3.4 demonstrates the variable nature of this behaviour by comparing five locations with widely different spectra – from top to bottom: Vancouver, Halifax, Wrigley (NWT), Montreal, and Toronto. As annotated in the figure, each has a different value of $S_a(0.2)/S_a(0.5)$ and thus a different slope for the initial descending portion of the spectrum. It is clear that compared to Figure 3.5, the relationship is less specific as a function of T_U and more variable as a function of $S_a(T)$ – not only as a function of the initial slope $S_a(0.2)/S_a(0.5)$ but also by the values of the other values as evidenced by the differences in overall shape between the different locations. Figure 3.5 is from Yuan (2016) and based on the ASCE 7 spectrum, and Figure 3.4 is constructed to provide a clear parallel between the two spectra. In general, while the NBCC curve depends on $S_a(T)$ and has no well-defined endpoints, the ASCE curve transitions cleanly between a maximum and minimum at the well-defined points $T_U/T_S = 1$ and $T_U/T_S = T_U/T_1$ (= 0.56 in Figure 3.5), where T_s is analogous to 0.2 seconds in the NBCC and defines the start of the descending portion in the ASCE.

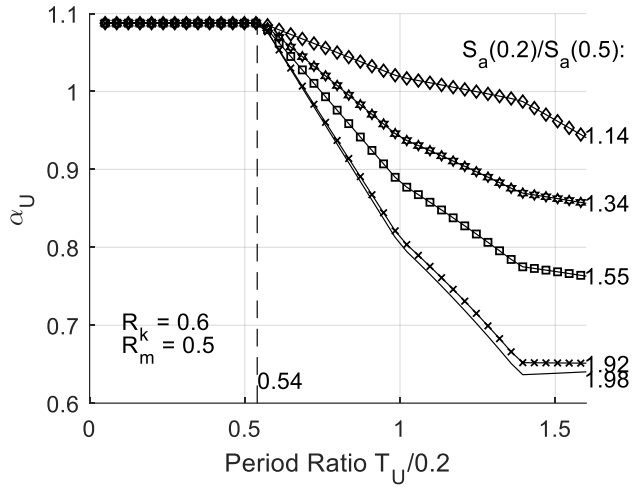

Figure 3.4: Effect of period ratio T_U/0.2 on α_U (NBCC)

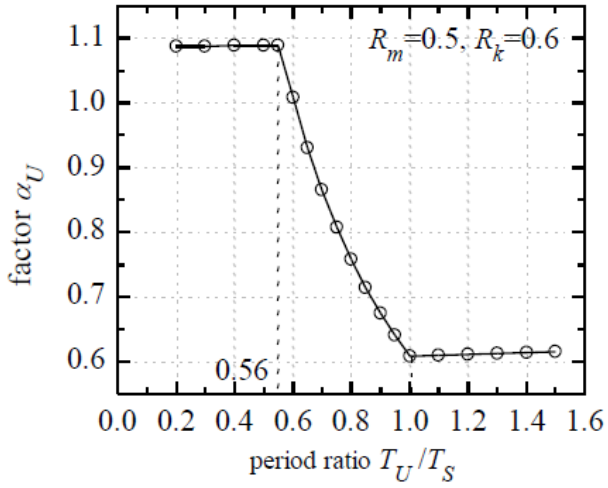

Figure 3.5: Effect of period ratio T_U/T_S on α_U (ASCE), (Yuan, 2016)

3.3.3 Analytical results based on the MDOF model

Yuan (2016) develops the relationship for α_U in terms of the 2DOF model and subsequently investigates the results in the context of their scope to confirm that the results are adequate for direct application to the MDOF model. Yuan (2016) concludes that:

1. For $R_k < R_{kU2}$, the simplified 2DOF model may underestimate α_U, and thus the MDOF model should be used.

2. For $R_k > R_{kU3}$, the simplified 2DOF model is adequate to estimate α_U, given minor modifications to ensure α_U is not underestimated.

3. Otherwise, the simplified 2DOF model is accurate.

As will be seen in the forthcoming section, R_{kU2} and R_{kU3} are used to approximate the bounds of R_k associated with the maximum response α_U. It can then be inferred that between these bounds that the 2DOF model best approximates the MDOF model, and this efficacy diminishes further from this region.

However, an alternative approach is taken in the current study. Whereas Yuan (2016) is based fundamentally on the 2DOF model with modifications to ensure that the results are conservative for the MDOF model, the current study focuses on the MDOF model, leveraging the previous observations and parameter survey. For application to the MDOF model, α_U in the MDOF model is most important, and this can only be confirmed by computation of the MDOF results. The procedure used in the current study to verify the R_k-α_U relationship is as follows:

1. For each input variable (N_U, N_L, r_m, r_k, T_{singU}, $S_a(T)$), a linearly-spaced vector is generated between the upper and lower bound of each variable defined in the scope as in Section 1.3.2. In the case of $S_a(T)$, values are taken from the Geological Survey of Canada Open File 7893 (Halchuk et al., 2015). The Open File provides seismic hazard values for all of Canada in a 10 km grid, including at the 2%/50 years risk level specified by NBCC 2015, For input, several dozen linearly spaced rows are selected from the data file. It is not of concern that certain $S_a(T)$ curves are selected over others – as defined in Equation (3.5), α_U is based on the relative values of $S_a(T)$, not on absolute values. Linearly spaced rows from the dataset provide geographically well-spaced locations and varied spectral shapes (by proxy, varied $S_a(0.2)/S_a(0.5)$).

2. Each of these input vectors is combined to obtain every permutation of N_U, N_L, r_m, r_k, T_{singU}, and location selected from the open file (i.e. $S_a(T)$ curve), and invalid combinations (e.g. $N_U + N_L > 12$) are removed from the set based on the relationship being investigated. This includes omitting scenarios where $m_L < m_U$ and $k_L < k_U$ since these correspond to $r_m < 1$ and $r_k < 1$. In general, this results in several million different combinations for investigation.

3. α_U and other outputs are computed for every permutation generated in the prior step.

While the approach is more computationally intensive than that used by Yuan, it allows for the computation of only MDOF results based on inputs within the scope, rather than trying to post-process the 2DOF results. Given that the volume of inputs is larger than the previous study and conforms to the scope, it is also possible to elaborate on variation in the MDOF model.

3.3.4 Proposed equations to evaluate shear-force-amplification factor α_U

The premise of the proposed Equations (3.21) to (3.33) is to convert the MDOF model to a simplified 2DOF one and then evaluate α_U based on these generalized parameters. Nevertheless, the intent is not to determine α_U corresponding to the 2DOF model – because higher mode effects are prevalent, the proposed equations must encapsulate these higher modes. Instead, the intent is that α_U be interpreted as a conservative overestimate of the α_U associated with the MDOF model, rather than the 2DOF model. The 2DOF model truncates the effects of the 3rd and higher modes, which may significantly alter the response – for any MDOF value of α_U, the corresponding 2DOF value of α_U may be either larger or smaller based on the effect of the 3rd and higher modes. The premise, then, of incorporating the 2DOF model is as a generalized language to describe the relationships between the variables of otherwise disparate MDOF models. In any event, α_U magnifies the value of the upper structure base shear, and thus a larger value is more conservative. As alluded to in Section 3.3.2, α_U can be determined as a function of R_k, R_m and $S_a(T_1)/S_a(T_U)$ via the following empirical equations, The rationale for the provided factors R_k and α_U are discussed in Section 3.3.5 and elaborated on in more detail in Appendix C.

The overall equation for upper structure amplification factor α_U

$$\alpha_U = \begin{cases} \alpha_{U1}\left(\dfrac{R_k}{R_{kU1}}\right)^{x_1} C_{U1} \le \alpha_{Umax} & R_{kU1} \le R_k < R_{kU2} \\ \alpha_{Umax} & R_{kU2} \le R_k \le R_{kU3} \\ \alpha_{Umax}\left(\dfrac{R_k}{R_{kU3}}\right)^{x_2} & R_{kU3} < R_k < R_{kU2stg} \\ \alpha_{U2stg} & R_{kU2stg} \le R_k \end{cases} \tag{3.21}$$

General coefficients and exponents

$$x_1 = \frac{ln\,(\alpha_{Umax}/\alpha_{U1})}{ln\,(R_{kU2}/R_{kU1})} \tag{3.22}$$

$$x_2 = \frac{ln\left(\alpha_{U2stg}/\alpha_{Umax}\right)}{ln\left(R_{kU2stg}/R_{kU3}\right)} \tag{3.23}$$

$$C_{U1} = -\frac{2}{5}\left(\frac{R_k - R_{kU1}}{R_{kU1} - R_{kU2}}\right)^2 - \frac{2}{5}\left(\frac{R_k - R_{kU1}}{R_{kU1} - R_{kU2}}\right) + 1 \tag{3.24}$$

Critical overall stiffness ratios R_k:

$$R_{kU1} = f(N_U, N_L, r_m) \tag{3.25}$$

$$R_{kU2} = R_m + 1 \tag{3.26}$$

$$R_{kU3} = \begin{cases} 4.13R_m + 2 & R_m \leq 0.8 \\ -0.26R_m + 5.52 & 0.8 < R_m < 2 \\ R_m + 3 & R_m \geq 2 \end{cases} \tag{3.27}$$

$$R_{kU2stg} = 10R_m \geq 10 \tag{3.28}$$

Amplification factor α_{U1} associated with critical stiffness ratio R_{kU1}:

$$\alpha_{U1} = A_{U1}e^{\left(B_{U1}\frac{S_a(T_1)}{S_a(T_U)}\right)} \tag{3.29}$$

$$S_a(T_1) \approx S_a\left(\frac{T_U}{\sqrt{1 - \phi_{L1}(R_{kU1}, R_m)}}\right) \tag{3.30}$$

Amplification factor α_{Umax} associated with critical stiffness ratios R_{kU2} and R_{kU3}:

$$\alpha_{Umax} = A_{max}e^{\left(B_{max}\frac{S_a(T_1)}{S_a(T_U)}\right)} \tag{3.31}$$

$$S_a(T_1) \approx S_a\left(\frac{T_U}{\sqrt{1 - \phi_{L1}(R_{kU2}, R_m)}}\right) \tag{3.32}$$

Amplification factor α_{U2stg} associated with critical stiffness ratio R_{kU2stg}:

$$\alpha_{U2stg} = \begin{cases} 1 + \frac{R_m}{8} & R_m < 2 \\ 1.25 & R_m \geq 2 \end{cases} \tag{3.33}$$

where R_{kU1}, A_{U1}, B_{U1}, A_{max}, and B_{max} are given in Appendix E. Each table should be interpolated for intermediate values of r_m. It is expected that φ_{L1} and T_U are evaluated according to Equations (A.13) and (3.14), T_1 based on Equation (A.13) and T_U, and $S_a(T_1)$ and $S_a(T_U)$ evaluated using the NBCC

2015 spectrum rather than the exponential or power approximations given by Yuan (2016) (e.g. the EXP-2 approximation given in Appendix D). The parameters in the previous equations are calibrated so that the equations conservatively predict the base shears acting on the upper structure of the MDOF model.

3.3.5 The rationale for proposed equations to evaluate upper structure base shear amplification factor α_U

The intent of the equations to evaluate α_U is to find a solution to the design criterion given by Equation (3.9). Based on Section 3.3.2, α_U is a function of the overall mass and stiffness ratios (R_m and R_k) and the spectral acceleration associated with the first period of the upper structure, $S_a(T_U)$. It is assumed that k_U, the storey stiffness of the upper structure, is the design variable. All other design parameters are assumed to be known a priori or otherwise derived.

The idealized relationship between R_k and α_U is adopted similarly to Yuan (2016), as illustrated in Figure 3.6. This relationship, represented by Equation (3.21), is divided into four regions based on three sets of critical values:

1. R_{kU1} and α_{U1} describe the lower bound on the stiffness ratio and amplification factor which are within the scope of the thesis based on the design requirement given by Equation (3.9). As discussed in Appendix C, R_{kU1} delimits the boundary of R_k beyond which the maximum interstorey drift is at the base of the upper structure, and is defined empirically as a function of r_m, N_L, and N_U. Rather than an assumed mode shape as used in the previous formulation, the new proposal features interpolation via a table, similarly to how α_{U11} and α_{U12} are described in Yuan (2016).

   α_{U1} is the α_U value corresponding to R_{kU1} and is significantly changed from the previous formulation. In the original formulation (Equations (C.18) to (C.20)), α_{U1} varies between a minimum and maximum value as a power function of $S_a(T_1)/S_a(T_U)$ (T_U/T_S for the ASCE formulation), with the empirically-derived maximum and minimum values being tabulated as a function of N_U, N_L and r_m. However, on account of the difficulty of defining the lower bound analogously to the original ASCE formulation, given that $S_a(T_1)/S_a(T_U)$ is not directly related to T_U/T_1 in NBCC 2015, Equations (3.29) and (3.30) redefine α_{U1} in terms of an exponential function so that the precise definition of endpoints is not required. $S_a(T_1)$ is defined similarly to the original formulation, except that T_1 is now defined relative to the

2DOF model directly rather than the ambiguously-derived value given by Yuan (2016). Besides this, the proposed form is more intuitive – it is immediately understandable how a simple exponential function changes based on $S_a(T_1)/S_a(T_U)$.

2. R_{kU2}, R_{kU3} and α_{Umax} describe the region for which $\alpha_U = \alpha_{Umax}$. R_{kU2} and R_{kU3} are given by Equations (3.26) and (3.27), identically to Yuan (2016). Considering that they are significantly based on the 2DOF parameter survey rather than purely empirical, they are considered sufficiently accurate. Meanwhile, α_{Umax} is redefined to the exponential form given by Equation (3.32), just like α_{U1}. The rationale is the same – it is easier to define the fit parameters for the exponential curve than the endpoints. On some occasions, α_{Umax} will be less than α_{U2stg}. In this case, no modification should be applied – this simply means that the approximated α_U increases as a function of R_k beyond R_{kU3}.

3. R_{kU2stg} and α_{U2stg} are related to the two-stage procedure given by ASCE 7, and a number of changes have been applied to clarify and improve the definitions. R_{kU2stg} is the stiffness ratio associated with the two-stage procedure, beyond which it is expected that the two-stage procedure is applicable, and beyond which α_U generally maintains a constant value. The definition has been revised slightly to be simpler by consolidating the results of previous research by Yuan & Xu (2016) and Chen & Ni (2020). Likewise, the proposed definition consolidates the ambiguously named R_{kU2stg} and R_{k2stg} defined by Yuan (2016). In Yuan (2016), R_{kU2stg} approximately indicates R_k beyond which α_U is approximately constant (in their words, approximately unity), whereas R_{k2stg} demarcates the two-stage procedure's applicability. These definitions are quite different for the ASCE formulation given by Yuan (2016), but nigh-identical for the NBCC formulation, and thus for the current application they have been consolidated. There is not an apparent need for the two variables to be separate, particularly in light of their near-identical definition in the Yuan (2016) NBCC formulation, and so they have been consolidated. α_{U2stg} is similar to the previous formulation, except recalibrated for the expanded scope and restricted only to values of variables that are within the scope. For example, the previous definition of α_{U2stg}, Equation (C.26), is said to apply to $R_m > 3$ despite that no value of R_k within the scope satisfies $R_k > R_{kU2stg}$ for $R_m > 3$.

   However, despite its name, R_{kU2stg} does not indicate that the ASCE 7 two-stage procedure can be used – the two-stage procedure corresponds to $\alpha_U \approx 1$. Instead, R_{kU2stg}

indicates that the behaviour is analogous but not equivalent to that assumed by the two-stage procedure. To be conservative, either the proposed procedure for multistorey upper structures (Chapter 4.5) or the Yuan (2016) two-stage procedure (Appendix F) should be used.

Despite these changes to the definitions of the critical values of R_k and α_U, the idealized form of the relationship given by Equation (3.21) remains similar to that of Equation (D.1) (the form given by Yuan (2016)) and is divided into 4 regions:

1. For $R_{kU1} \leq R_k < R_{kU2}$, α_U is interpolated between α_{U1} (at R_{kU1}) and α_{Unax} (at R_{kU2}) using a power function. If $R_{kU2} < R_{kU1}$, this region does not apply. Compared to Yuan (2016), the R_k-α_U relationship given by Equation (3.21) features an additional coefficient C_{U1}. C_{U1}, defined by Equation (3.24), varies quadratically between R_{kU1} and R_{kU2} and applies a slight increase of up to 10% at the midpoint of R_{kU1} and R_{kU2} (i.e. $C_{U1} = 1$ at R_{kU1} and R_{kU2}, and increases quadratically to 1.1 at the midpoint of the segment). This increase diminishes towards the endpoints and is applied to ensure that the approximated α_U conservatively estimates the α_U obtained from the linear modal response spectrum analysis. For closely-spaced endpoints, this may sometimes result in $\alpha_U > \alpha_{Umax}$, and so the predicted α_U is limited to α_{Umax}. C_{U1} is necessary so that the values are not underestimated given the new values of R_{kU1}, R_{kU2}, α_{U1} and α_{Umax} – the exponent x_1 does not produce a sufficient curvature alone to prevent α_U from being underestimated at the midpoint. If C_{U1} is omitted, α_U may be underestimated by as much as 5%.

2. For $R_{kU2} \leq R_k \leq R_{kU3}$, it is assumed that $\alpha_U = \alpha_{Umax}$. The only difference from before it the changed definition of α_{Umax}, which is now defined as an exponential function of $S_a(T_U)/S_a(T_L)$ rather than a power function.

3. For $R_{kU3} < R_k < R_{kU2stg}$, α_U is interpolated between α_{Umax} (at R_{kU3}) and α_{U2stg} (at R_{kU2stg}) using a power function.

4. For $R_{kU2stg} < R_k$, it is assumed that $\alpha_U = \alpha_{U2stg}$. The formulation for α_{U2stg} is aggregated from any results for R_k larger than R_{kU2stg}. Beyond this point, it is also assumed that the two-stage procedure proposed by Yuan (2016) is applicable. This procedure appears in Appendix F.

For any of the above regions, R_{kU1} is the minimum value of R_k – only values such that $R_k \geq R_{kU1}$ are within the scope of the current study, and the R_k-α_U distribution should be truncated accordingly.

Specifically, where $R_{kU2} \leq R_{kU1}$, the critical points are according to the values of α_{Umax}, R_{kU2}, R_{kU2stg} etc., rather than α_{U1} and R_{kU1}. α_{U1} and R_{kU1} only defines the minimum R_k.

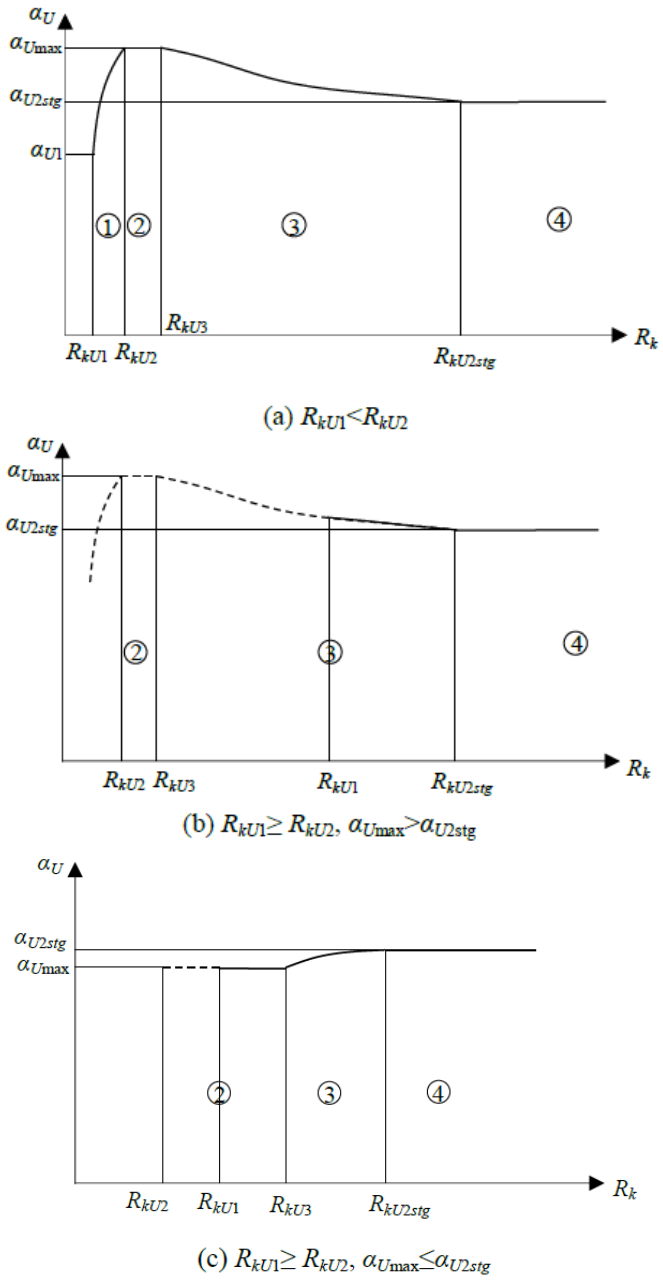

Figure 3.6: Idealized R_k-α_U relationship (Yuan, 2016)

In general, the proposed α_U increases in value for larger values of r_m (R_m) and $S_a(T_1)/S_a(T_U)$.

3.4 Error of the proposed R_k-α_U relationship

To evaluate the effectiveness of the proposed approach, α_U is evaluated according to both the proposed and previous (Yuan, 2016) approaches for a range of valid inputs within the scope (i.e. r_m, r_k, N_U, N_L, T_{singU}, $S_a(T)$) and compared to the corresponding values of α_U evaluated based on the modal response spectrum method, MDOF model and the CQC combination rule. This section summarizes several aspects of the results, namely: 1) the comparison of the overall effectiveness of the proposed and previous approaches insofar as estimating α_U and 2) the evaluation of proposed procedure's error based on the proposed and previous scope, and based on the combination of storeys being used. Both the previous scope (where $N_U+N_L \leq 10$ and $1 \leq r_m \leq 3$) and the proposed scope (where $N_U+N_L \leq 12$ and $1 \leq r_m \leq 5$) are considered, on account of the previous approach being calibrated for and applicable to only the previous scope.

However, Yuan (2016) provides four alternative schemes to evaluate $S_a(T_1)/S_a(T_U)$ for their NBCC 2010-based method. These schemes approximate NBCC 2010's $S_a(T)$ such that $S_a(T_1)/S_a(T_U)$ corresponds to a ratio of periods as it does in ASCE 7. This being the case, the approximated relationships can be directly substituted into the ASCE 7 procedure as the relationships are defined analogously. Yuan (2016) provides approximations based on both power functions (referred to as PWR-1 and PWR-2) and exponential functions (referred to as EXP-1 and EXP-2) and recommends that the exponential EXP-2 formulation be used for best performance. Therefore, of the four, only the EXP-2 form given in Appendix D is used to evaluate $S_a(T_1)/S_a(T_U)$ here. Despite this, the EXP-2 transformation is not strictly necessary. It is possible to evaluate $S_a(T_1)/S_a(T_U)$ directly via the definition of $S_a(T)$ given by NBCC 2015. This renders it impossible to establish a direct correspondence between $S_a(T_1)/S_a(T_U)$ and a ratio of periods but requires no additional variables, ensures that $S_a(T)$ is defined familiarly to Canadian designers and uses the newer NBCC 2015 spectral shape.

In fewer words, three approximations for α_U are compared to the value of α_U calculated from the MDOF model:

1. The proposed approach - α_U is evaluated according to Equations (3.21) to (3.33), (A.13) and (3.14) as indicated by Section 3.3.4. Values of A_{U1}, B_{U1}, A_{Umax}, B_{Umax} and R_{kU1} are evaluated according to Appendix E.

2. The Yuan (2016) approach - α_U is evaluated according to Equations (D.1) to (D.17), where α_{U1}, α_{Umax} and R_{kU2stg} are evaluated by their NBCC formulation i.e. Equations (D.15) to (D.17). Values of α_{U12} and α_{Umax2} are given in Table D.1 and Table D.3. In this case, $S_a(T)$ is numerically evaluated based on its NBCC 2015 definition rather than using the EXP-2 approximation.
3. The EXP-2 approach is the same as the Yuan (2016) approach, except that $S_a(T)$ is evaluated according to Equations (D.20) to (D.23). To define the fit parameters, the NBCC 2015 values are used.

For each of these comparisons, the error is defined as follows:

$$Error\ (\%) = \frac{\left(\alpha_{U,approx} - \alpha_{U,MRS}\right)}{\alpha_{U,MRS}} \times 100 \tag{3.34}$$

where $\alpha_{U,approx.}$ and $\alpha_{U,MRS}$ refer to the approximated and MRS-derived values of the amplification factor α_U. $\alpha_{U,approx.}$ corresponds to the approach being used – in the case of the proposed approach, it is defined by Section 3.3.4, i.e. according to Equations (3.21) to (3.33), (A.13) and (3.14) as previously described. Conversely, $\alpha_{U,MRS}$ is the value of α_U derived according to the MRS analysis of the MDOF model. Positive error values indicate that the approximation overestimates the MRS-derived value, whereas negative error values indicate an underestimate.

For these purposes, the MRS-derived value of α_U is considered the correct value which $\alpha_{U,approx.}$ attempts to conservatively approximate. But $\alpha_{U,MRS}$ is itself an approximation, albeit a better one than $\alpha_{U,approx.}$, for several reasons. First, like M_v in NBCC 2015, $\alpha_{U,MRS}$ is strictly applicable only for the linear response – as noted by Humar & Rahgozar (2000), M_v increases monotonically with both the period and ductility. It is not clear how this relates to α_U, but to establish an inelastic α_U with any sort of generality would be a herculean undertaking. Secondly, α_U is based on $S_a(T)$ and modal analysis rather than time history analysis – thus, rather than encapsulating any specific earthquake record, α_U represents the NBCC's consensus as to a conservative spectrum at a given site. The third aspect is the assumption that the upper structure and lower structure are each uniform and have uniformly distributed mass and stiffness – the observed value of α_U will increase or decrease based on the impact of non-uniformity on the distribution of the effective mass of the structure. In general, however, α_U is based on similar simplifications as those already tolerated by the NBCC for M_v.

Figure 3.7 illustrated the comparison between the MRS-derived values versus a) the proposed method and the Yuan (2016) scope, b) the proposed method and the expanded scope, c) the Yuan (2016) value of α_U, without the EXP-2 approximation being adopted, and d) the Yuan (2016) value of α_U, including the EXP-2 approximation. In all of the subplots, the results are generally conservative, with only a modest difference between each plot. There are some differences – the Yuan (2016) approximation exhibits a small gap between the 1:1 line and the data points for $\alpha_U \geq 2$, which indicates a slightly more conservative approximation in that range. The shape of the lower end of the distribution is subtly different as well – the proposed approach shows a larger variance for $\alpha_U \leq 1$. Finally, for the expanded scope there is a modest underestimate around $\alpha_U = 1.25$. Given the comparison between a) and b), this can be attributed to the expanded scope – structures with rm > 3 and N_U+N_L > 10.

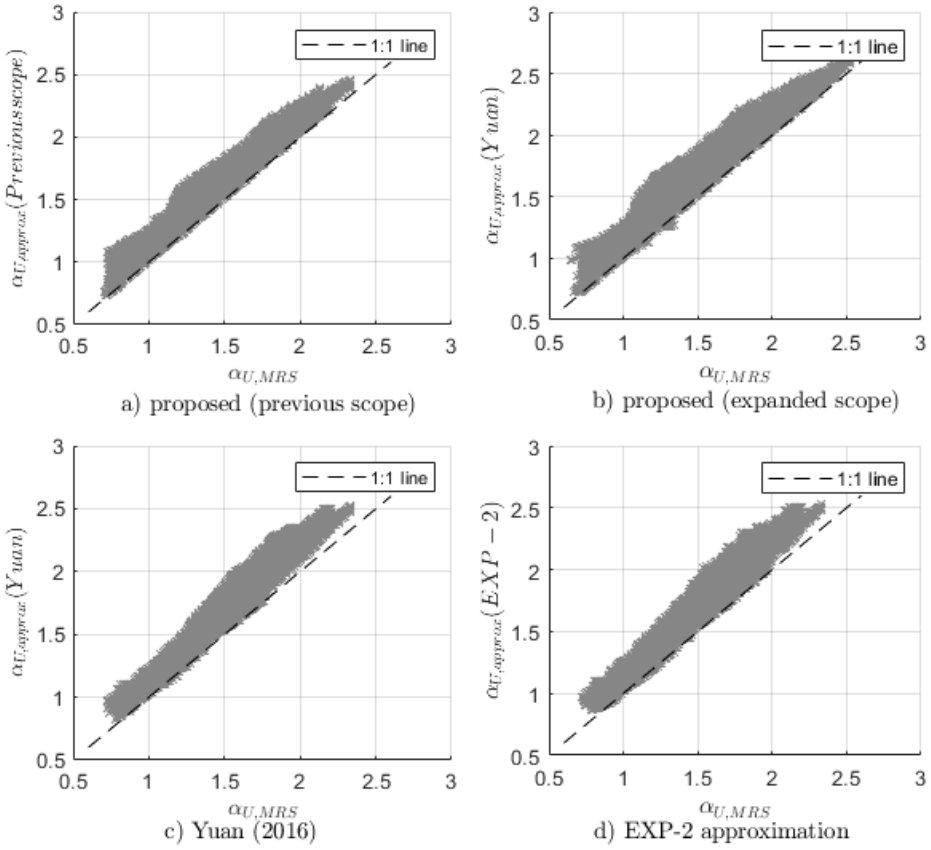

Figure 3.7: α_U – MRS value versus approximated value (Yuan, 2016)

However, while Figure 3.7 indicates where values might be over/underestimated relative to the MRS-derived values, it does not indicate the density of those values. Given that there are a larger number of combinations (≈ 8 million) of input values that are evaluated compared to Yuan (2016), it is not ideal to only investigate whether or not the values are conservative, it is also meaningful to investigate the density of the distribution of those values. It is not reasonable to expect that the results are equally distributed throughout the area illustrated in Figure 3.7, after all – for example, the error could be normally distributed about some median error value. Figure 3.8 provides four histograms of the error for the different regions of R_k for each of the three approaches for the previous scope. The y-axis of each is normalized to approximate the probability distribution function (PDF). Based on Figure 3.8, it can be observed that:

1. The error is generally lower for the proposed approach, except for $R_{kU3} \leq R_k \leq R_{kU2stg}$, for which the proposed and previous approaches perform equally well. The proposed approach works equally well regardless of R_k.
2. The error is identical for Yuan (2016), regardless of whether $S_a(T)$ is approximated using the EXP-2 approximation or if the value is calculated directly using the NBCC 2015 spectrum.

Figure 3.9 consolidates each of the subplots of Figure 3.8, and it is clear from Figure 3.9 that the proposed approximation performs better than the previous formulation. Both formulations produce errors that are approximately normally distributed about their medians, with very few values in the vicinity of the maximum and minimum values reported in Table 3.2.

An analogous comparison to Figure 3.8 and Figure 3.9 is made in Figure 3.10 and Figure 3.11, comparing instead the error of the proposed approach for the previous and expanded scope. In general, there is little observable difference between the two results aside from the absolute maximum and minimum extents noted in Table 3.2. The shape of the distribution is largely unchanged based on the change in scope, and the median changes marginally.

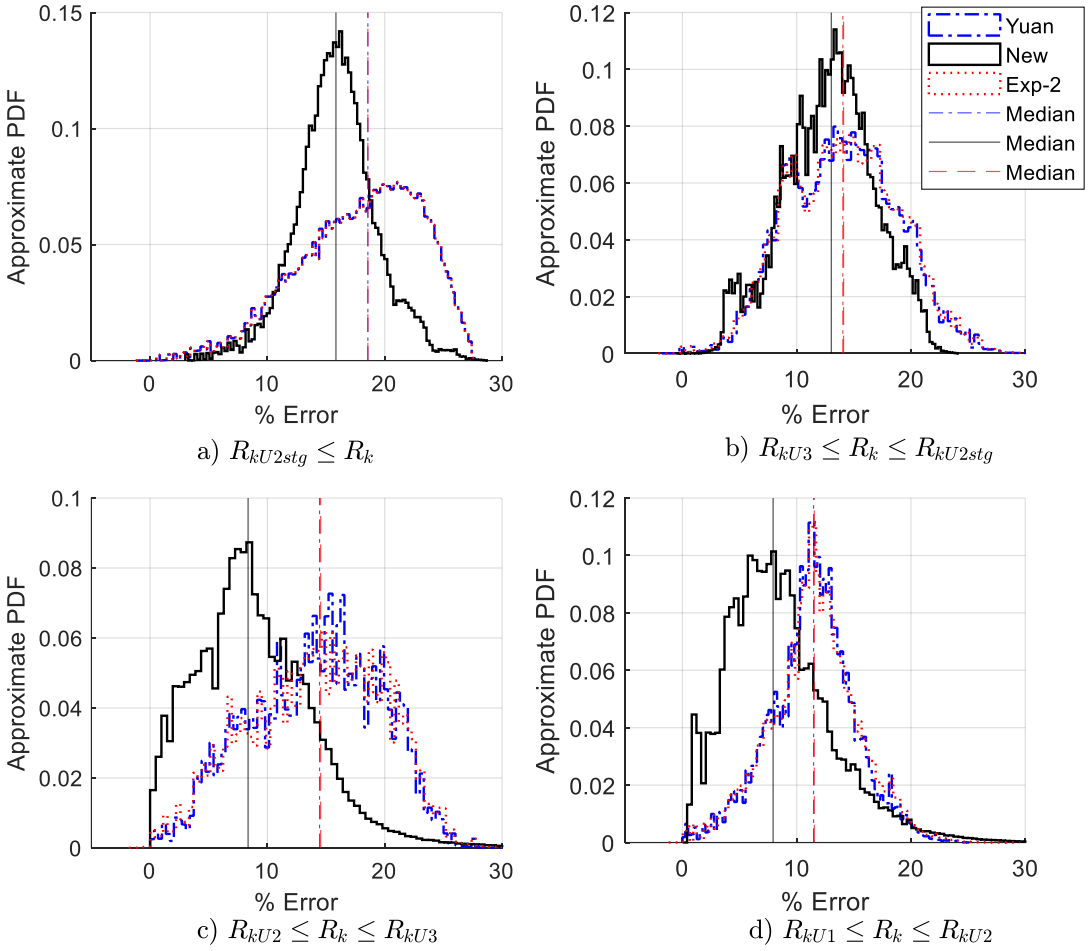

Figure 3.8: Comparison of error as a function of R_k - Proposed versus Yuan (2016), previous scope

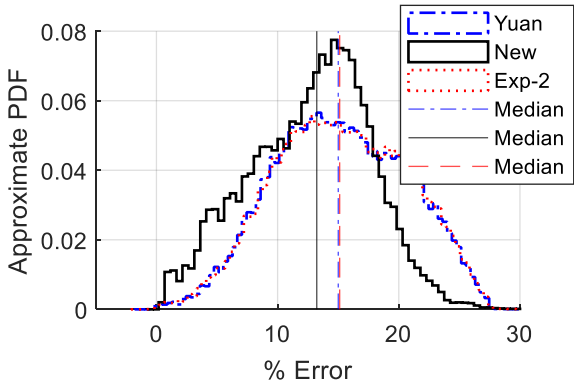

Figure 3.9: Comparison of error - Proposed versus Yuan (2016), previous scope

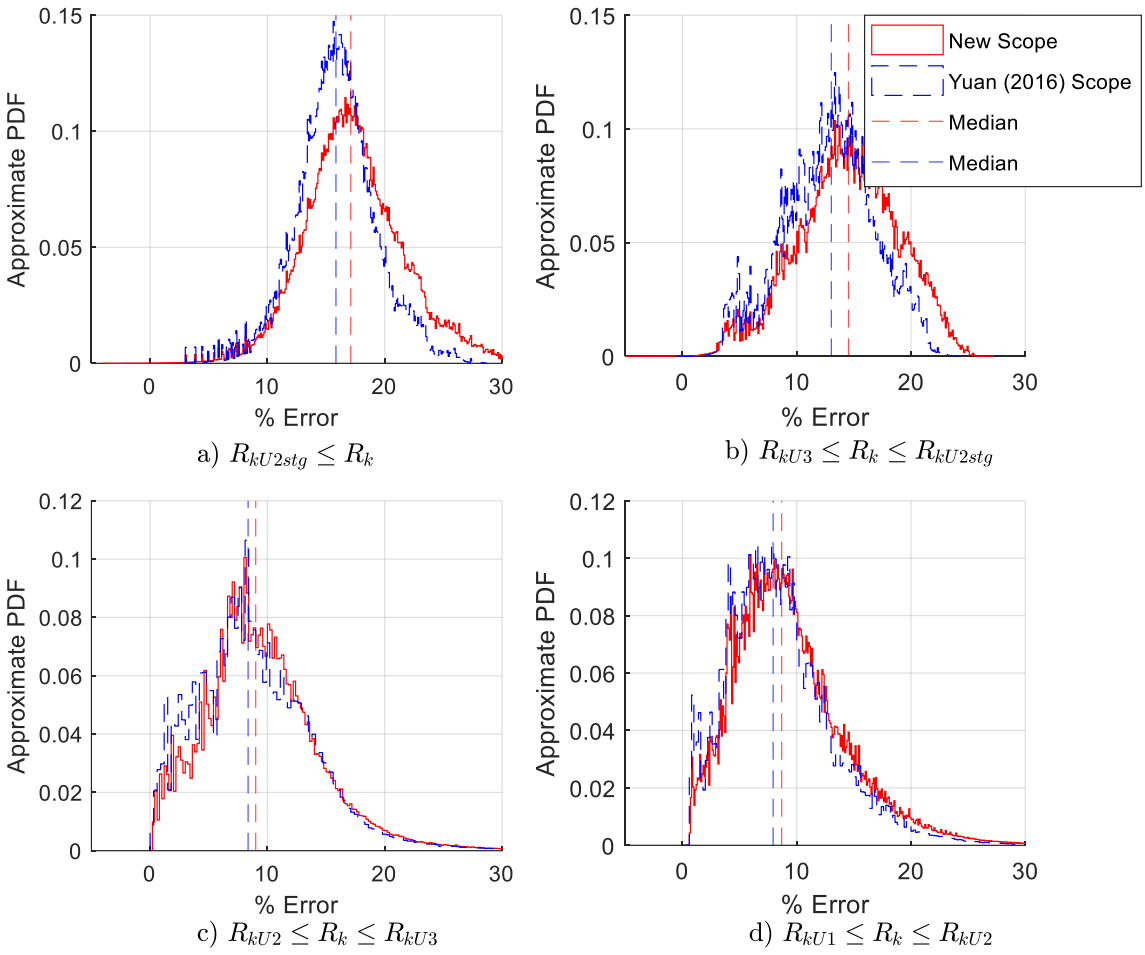

Figure 3.10: Comparison of error as a function of R_k - Proposed, previous versus expanded scope

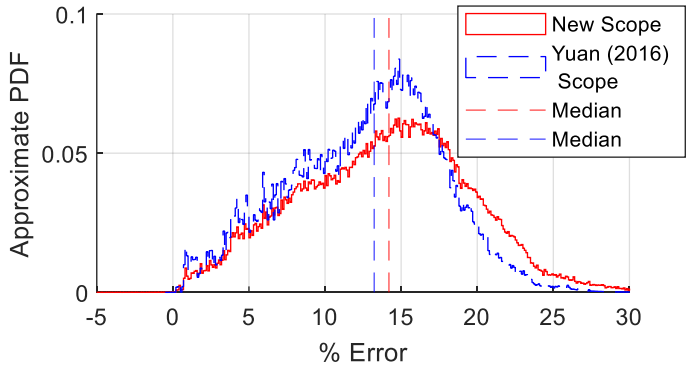

Figure 3.11: Comparison of error – Proposed, previous versus expanded scope

To further summarize the ≈ 8 million combinations of input values are evaluated, summary statistics are useful. Table 3.2 provides the minimum, median and maximum values for each formulation as well as the 1st and 99th percentile values. Negative values indicate underestimates and positive values indicate overestimates of the MRS-derived α_U value for the MDOF model. For the previous scope, the proposed approach provides overall better accuracy than that of Yuan (2016) evaluated by either the EXP-2 approximation or directly via the NBCC 2015 spectrum. While the maximum error is slightly larger for the proposed approach, the rest of the summary statistics perform better, with a larger minimum error and smaller median error. For the larger, expanded scope, the proposed formulation performs slightly more poorly, albeit with a slightly larger maximum and minimum error. The reason that the extremes of the error values (the maximum and minimum) are worse for the expanded scope is simple. The expanded scope permits a larger overall mass ratio due to both the increase in the storey-mass ratio and in the number of storeys, both of which are associated with higher amplification. While this means that the minimum/maximum error is more severe, it is only markedly worse for a very small proportion of the inputs. Namely, those associated with the most severe irregularities. These are uncommon. In general, a larger degree of irregularity imposes a more significant amplification. However, given the limitations of approximating the dynamic response, this is adequate.

Table 3.2: Comparison of α_U approximation error

	Minimum	1st Percentile	Median	99th Percentile	Maximum
Proposed	-0.42%	1.36%	13.23%	23.35%	48.25%
Yuan (2016)	-1.78%	3.44%	15.00%	26.09%	36.66%
Exp-2 (Yuan, 2016)	-1.93%	3.25%	15.12%	26.12%	36.66%
Proposed (expanded scope)	-5.50%	1.84%	14.20%	27.00%	60.17%

Note: negative error indicates an underestimate of α_U, positive error indicates an overestimate

One final useful comparison is on the maximum and minimum error as a function of the number of storeys, as is done in Table 3.3 and Table 3.4 for the previous scope, and Table 3.5 and Table 3.6 for the expanded scope. In general, the maximum error is larger for larger values of $N_U + N_L$ (i.e. taller

structures with more storeys), and for structures where the upper and lower structures are comparatively equal in height, and for the newer expanded scope relative to the previous one. The largest underestimates correspond to $N_U > N_L$, particularly where the number of storeys in the upper structure is much larger. Speculatively, structures with a relatively equal number of storeys between the lower and upper structures perform worst for the error as neither structure fully dominates the vibration response. An upper structure with lower storey stiffness and mass but an equal period to the lower structure could be subject to significant interaction effects causing large amplification of the base shear.

Table 3.3: Minimum error for α_U - Proposed, $N_U+N_L \leq 10$, $r_m \leq 3$

N_U \ N_L	1	2	3	4	5	6	7	8	9
1	0.2%	0.4%	0.7%	0.7%	0.7%	0.7%	0.8%	0.9%	1.2%
2	2.5%	2.4%	2.3%	1.2%	1.2%	1.0%	2.2%	0.2%	N/A
3	2.4%	2.2%	3.2%	2.4%	2.4%	1.6%	1.8%	N/A	N/A
4	2.0%	3.2%	4.4%	3.9%	3.4%	0.5%	N/A	N/A	N/A
5	3.4%	2.7%	3.1%	-0.4%	3.8%	N/A	N/A	N/A	N/A
6	4.0%	4.2%	4.1%	3.7%	N/A	N/A	N/A	N/A	N/A
7	5.3%	6.4%	5.1%	N/A	N/A	N/A	N/A	N/A	N/A
8	6.1%	6.8%	N/A	N/A	N/A	N/A	N/A	N/A	N/A
9	6.4%	N/A	N/A	N/A	N/A	N/A	N/A	N/A	N/A

Note: negative values (indicated by grey shading) indicate an underestimate. Where no negative values are shown, the value of α_U is always overestimated (conservative).

Table 3.4: Maximum error for α_U - Proposed, $N_U+N_L \leq 10$, $r_m \leq 3$

N_U \ N_L	1	2	3	4	5	6	7	8	9
1	15.1%	14.8%	14.7%	14.8%	20.1%	26.7%	31.3%	31.9%	32.5%
2	19.0%	30.5%	29.9%	27.2%	26.9%	24.6%	23.9%	24.0%	N/A
3	18.7%	23.6%	43.2%	36.3%	34.7%	32.4%	31.6%	N/A	N/A
4	19.1%	23.9%	36.4%	47.7%	39.4%	40.8%	N/A	N/A	N/A
5	19.5%	24.1%	30.2%	41.5%	48.3%	N/A	N/A	N/A	N/A
6	19.8%	24.0%	26.9%	34.2%	N/A	N/A	N/A	N/A	N/A
7	20.0%	23.9%	26.8%	N/A	N/A	N/A	N/A	N/A	N/A
8	20.3%	23.8%	N/A	N/A	N/A	N/A	N/A	N/A	N/A
9	20.4%	N/A	N/A	N/A	N/A	N/A	N/A	N/A	N/A

Table 3.5: Minimum error for α_U – Proposed, expanded scope

N_U \ N_L	1	2	3	4	5	6	7	8	9	10	11
1	0.2%	0.4%	0.7%	0.7%	0.7%	0.7%	0.8%	0.9%	0.5%	0.4%	0.7%
2	2.5%	1.7%	1.0%	0.8%	0.8%	1.0%	1.7%	0.2%	2.3%	0.8%	N/A
3	2.4%	2.2%	2.4%	0.5%	1.2%	1.2%	1.6%	1.5%	0.8%	N/A	N/A
4	2.0%	3.1%	1.9%	3.0%	2.1%	0.5%	0.5%	0.9%	N/A	N/A	N/A
5	3.1%	2.1%	-5.5%	-0.9%	3.5%	3.0%	2.0%	N/A	N/A	N/A	N/A
6	4.0%	2.8%	-1.7%	-5.3%	-0.8%	3.5%	N/A	N/A	N/A	N/A	N/A
7	4.7%	3.8%	1.9%	-4.0%	-3.6%	N/A	N/A	N/A	N/A	N/A	N/A
8	5.4%	4.6%	3.6%	-1.2%	N/A	N/A	N/A	N/A	N/A	N/A	N/A
9	5.5%	3.5%	0.9%	N/A	N/A	N/A	N/A	N/A	N/A	N/A	N/A
10	-0.8%	-4.0%	N/A	N/A	N/A	N/A	N/A	N/A	N/A	N/A	N/A
11	-0.2%	N/A	N/A	N/A	N/A	N/A	N/A	N/A	N/A	N/A	N/A

Note: negative values (indicated by grey shading) indicate an underestimate. Where no negative values are shown, the value of α_U is always overestimated (conservative).

Table 3.6: Maximum error for α_U – Proposed, expanded scope

N_U \ N_L	1	2	3	4	5	6	7	8	9	10	11
1	16.1%	14.8%	14.7%	18.4%	23.4%	27.6%	31.3%	31.9%	32.5%	31.3%	26.5%
2	21.8%	30.5%	29.9%	27.2%	26.9%	24.6%	25.5%	31.6%	36.0%	38.3%	N/A
3	24.3%	23.6%	43.2%	36.3%	34.7%	32.4%	31.6%	30.2%	29.3%	N/A	N/A
4	24.0%	27.9%	36.4%	47.7%	39.4%	40.8%	38.9%	34.8%	N/A	N/A	N/A
5	23.6%	30.9%	30.2%	41.5%	48.3%	39.1%	42.9%	N/A	N/A	N/A	N/A
6	23.6%	30.2%	31.1%	34.2%	45.1%	60.2%	N/A	N/A	N/A	N/A	N/A
7	23.4%	29.7%	32.4%	36.1%	51.4%	N/A	N/A	N/A	N/A	N/A	N/A
8	23.3%	29.2%	33.4%	36.2%	N/A	N/A	N/A	N/A	N/A	N/A	N/A
9	23.1%	28.7%	32.8%	N/A	N/A	N/A	N/A	N/A	N/A	N/A	N/A
10	23.1%	28.3%	N/A	N/A	N/A	N/A	N/A	N/A	N/A	N/A	N/A
11	23.0%	N/A	N/A	N/A	N/A	N/A	N/A	N/A	N/A	N/A	N/A

3.5 Revised formulation for design stiffness k_U

Given the approximation for the stiffness-amplification relationship (R_k-α_U) characterized by Equation (3.21), the next step is to transform the relationship into one for k_U and k_L for design purposes. More specifically, the R_k-α_U relationship is transformed into an R_k-k_U relationship, in which k_U is dependent on the remaining variables, and eventually into a k_U-k_L relationship that defines the feasible stiffness region for the design of upper and lower structures. As an initial step in the

transformation, Equation (3.9) is rearranged to develop an inequality of k_U, into which Equation (3.21) is then substituted:

$$k_U \geq \frac{\alpha_U m_U N_U S_a(T_U) g}{\Delta_{Ulim}} \tag{3.35}$$

$$k_U \geq \frac{m_U N_U g S_a(T_U)}{\Delta_{Ulim}} \begin{cases} \alpha_{U1}\left(\frac{R_k}{R_{kU1}}\right)^{x_1} C_{U1} \leq \alpha_{Umax} & R_{kU1} \leq R_k < R_{kU2} \\ \alpha_{Umax} & R_{kU2} \leq R_k \leq R_{kU3} \\ \alpha_{Umax}\left(\frac{R_k}{R_{kU3}}\right)^{x_2} & R_{kU3} < R_k < R_{kU2stg} \\ \alpha_{U2stg} & R_{kU2stg} \leq R_k \end{cases} \tag{3.36}$$

where $S_a(T_U)$ corresponds to the piecewise linear spectral acceleration curve specified by NBCC 2015, evaluated at period T_U, i.e. (NRCC, 2015a):

$$S_a(T_U) = \begin{cases} max(S_a(0.2), S_a(0.5)) & T_U \leq 0.2 \\ S_a(0.5) & \begin{cases} 0.2 < T_U \leq 0.5 \\ S_a(0.5) \geq S_a(0.2) \end{cases} \\ S_a(0.2) + \frac{S_a(0.5) - S_a(0.2)}{0.3}(T_U - 0.2) & \begin{cases} 0.2 < T_U \leq 0.5 \\ S_a(0.5) < S_a(0.2) \end{cases} \\ S_a(0.5) + \frac{S_a(1.0) - S_a(0.5)}{0.5}(T_U - 0.5) & 0.5 < T_U \leq 1.0 \\ S_a(1.0) + \frac{S_a(2.0) - S_a(1.0)}{1.0}(T_U - 1.0) & 1.0 < T_U \leq 2.0 \\ S_a(2.0) + \frac{S_a(5.0) - S_a(2.0)}{3.0}(T_U - 2.0) & 2.0 < T_U \leq 5.0 \\ S_a(5.0) + \frac{S_a(10.0) - S_a(5.0)}{5.0}(T_U - 5.0) & 5.0 < T_U \leq 10.0 \\ S_a(10.0) & 10.0 < T_U \end{cases} \tag{3.37}$$

Equation (3.36) specifies a minimum k_U at any given value of R_k. However, R_k is not known a priori on account of being a function of k_U and k_L, and so a solution for k_U via Equation (3.36) would require further assumptions on R_k or k_L. Instead, the intended approach is to develop a solution on k_U which in turn imposes requirements on R_k and k_L.

Per Section 3.2, the design criterion given by Equation (3.9) can be interpreted as the balance between the expected amplification of the upper structure base shear due to higher mode effects and the expected resistance to said amplification, characterized by the stiffness, mass and interstorey drift limit. In essence, some amplification α_U of the base shear V_{Ub} is expected and is resisted by the other term of the inequality. This expected amplification is characterized as a function of R_m, R_k and $S_a(T)$

according to the assumed R_k-α_U relationship (Equations (3.21) to (3.33)). The same relationship applies to k_U via Equation (3.36) – for each of the critical values of the amplification factor α_U, there is a minimum value of the upper storey stiffness k_U below which the storey drift limit given by Δ_{Ulim} is exceeded. In other words, below which the amplification resistance provided by k_U is exceeded. Therefore, three scenarios can be established based on the value of k_U:

1. If k_U is above a certain threshold, $k_{U,unconditional}$, the resisting α_U always lies above or on the R_k-α_U curve. Thus, for such k_U, all values of R_k within the domain of the R_k-α_U curve are valid.
2. If k_U is below a certain threshold, $k_{U,required}$, the resisting α_U always lies below the R_k-α_U curve. Thus, for such k_U, all values of R_k within the domain of the R_k-α_U curve are invalid. $k_{U,required}$ is, therefore, the absolute minimum value of k_U.
3. If k_U lies between $k_{U,required}$ and $k_{U,unconditional}$, so long as the resisting α_U lies above or on the R_k-α_U curve a solution exists. This is only true for some subset of R_k, and so k_L will be constrained by the value of k_U.

Considering the form of the R_k-α_U curve, $k_{U,required}$ and $k_{U,unconditional}$ (formerly k_{Umin} and k_{Umax}) correspond to the minimum and maximum values of α_U on the curve. These can be fully described using only the values of α_U at the critical values R_{kU1}, R_{kU2}, R_{kU3} and R_{kU2stg}. Therefore:

$$k_{U,required} = \begin{cases} min(k_{U1}, k_{Umax}, k_{U2stg}) & R_{kU1} < R_{kU2} \\ min(k_{Umax}, k_{U2stg}) & R_{kU2} \leq R_{kU1} \end{cases} \tag{3.38}$$

$$k_{U,unconditional} = \begin{cases} max(k_{U1}, k_{Umax}, k_{U2stg}) & R_{kU1} < R_{kU2} \\ max(k_{Umax}, k_{U2stg}) & R_{kU2} \leq R_{kU1} \end{cases} \tag{3.39}$$

where

$$k_{U1} = \frac{\alpha_{U1} m_U N_U g}{\Delta_{Ulim}} S_a(T_U) \tag{3.40}$$

$$k_{Umax} = \frac{\alpha_{Umax} m_U N_U g}{\Delta_{Ulim}} S_a(T_U) \tag{3.41}$$

$$k_{U2stg} = \frac{\alpha_{U2stg} m_U N_U g}{\Delta_{Ulim}} S_a(T_U) \tag{3.42}$$

To proceed further and determine the valid ranges of k_L and k_U, each of Equations (3.40) to (3.42) must be solved for k_{U1}, k_{Umax} and k_{U2stg} using the critical values of α_U and $S_a(T_1)$ per Equations (3.25)

to (3.33), as applicable. Unfortunately, the determination of the critical values of k_U via Equations (3.40) to (3.42) is possible only by numerical solution, on account of both k_U and $S_a(T_U)$ appearing in each equation. T_U, as given by Equation (3.14), is a function of k_U, and thus both sides are a function of k_U. The nature of the NBCC 2015 spectrum precludes a concise, closed-form solution, and so this numerical solution is inevitably required.

To equate this to the physical system, the relationship for stiffness is obtained by mapping the R_k-α_U curve to stiffness via the given by Equation (3.9) – for each value of R_k and α_U (itself a function of R_m, R_k and $S_a(T)$), there is a corresponding value of k_U for which the interstorey drift criterion is exactly satisfied. For any lower or higher value of k_U, assuming that the system changes accordingly so that R_k and α_U do not change, the interstorey drift between the bottom storey of the upper structure and the top storey of the lower structure increases or decreases. In the former case, this is problematic, since it implies that the NBCC-specified interstorey drift limit is exceeded. As with the R_k-α_U curve given in Section 3.3.4, the corresponding mapping to k_U is defined completely by the critical values R_{kU1}, R_{kU2}, R_{kU3} and R_{kU2stg} and α_{U1}, α_{Umax} and α_{U2stg}, thus k_{U1}, k_{Umax} and $k_{U2stg.}$ But in the proposed approach the selection of k_U takes place before R_k is finalized – accordingly, $k_{U,unconditional}$ and $k_{U,required}$ indicate the maximum and minimum values of k_U. If k_U is less than $k_{U,required}$, the interstorey drift criterion is not satisfied for any possible combination of R_k and α_U (i.e. R_m, R_k and $S_a(T)$) – this stiffness is therefore required. Meanwhile, if k_U is greater than $k_{U,unconditional}$, the interstorey drift criterion is always satisfied. In between, the satisfaction of the criterion depends on the selection of R_k (k_L), considering that all else is constant. The physical relationship regarding k_U is therefore entirely related to the relative satisfaction, or not, of the interstorey drift criterion.

It may be unclear why 1) α_{U1} and thus k_{U1} might not be applicable and 2) why, while there are R_{kU2} and R_{kU3}, that only k_{Umax} is used. This relates to the definition of the R_k-α_U relationship defined in Section 3.3.4. α_{U1} is only applicable if $R_{kU1} < R_{kU2}$, otherwise α_{U1} is not required, and R_{kU1} is used only as a lower bound on R_k. Consequently, k_{U1} is applicable only if α_{U1} is. Meanwhile, R_{kU2} and R_{kU3} both relate to the same value α_{Umax}, and thus the same k_{Umax}. They only come into play when defining the permissible range of R_k (k_L) once k_U has been specified. In her solution for the critical k_U, Yuan (2016) proceeds as described in Appendix D.4 by using an exponential approximation (EXP-2) of the NBCC 2010 spectrum. Her approach is similar up until the derivation of Equation (3.36), at which point they make several substitutions and fully expand the equations. Namely, she substitutes the NBCC 2010 spectrum with a piecewise exponential (EXP-2) approximation, substitute their approximation for α_U

and fully expand the resulting relationship for each of the critical stiffnesses k_{U1}, k_{Umax} and k_{U2stg}, which they refer to instead as $k_{\alpha U1}$, $k_{\alpha Umax}$ and $k_{\alpha U2stg}$. The result is a set of three piecewise equations for each critical stiffness value, each of which contains up to eight separate terms. One of these equations is transcendental and requires a numerical solution according to a pre-generated table of values.

These equations require additional parameters – to define the EXP-2 fit: τ, A and T'_s, and to define the remainder of the solution: b_i and y_i. The fit parameters τ, A and T'_s are defined by Equations (D.21) to (D.23) based on the NBCC 2010 spectral acceleration curve $S_a(T)$. Specifically, for the EXP-2 approximation, the midpoint of each linear segment of the NBCC 2010 spectrum (e.g. $S_a(0.35)$, $S_a(0.75)$) is used to define the parameters. Each is recursive, so for larger values of T multiple values of τ, A and T'_s must be calculated. Meanwhile, the critical values of k_U are defined by Equations (D.24) to (3.31), and by two sets of parameters y_i and b_i in conjunction with the EXP-2 fit parameters. The parameters y_i and b_i are not given a physical meaning by Yuan (2016) and are defined by Table D.4 and Equations (D.32) to (D.34), respectively.

To solve these equations, the following procedure is necessary:

1. For each piece of the equation for each critical k_U, it is necessary to solve a separate transcendental equation, Equation (D.31), for numerical parameter y_i.
2. To solve for each y_i, it is necessary to determine the associated coefficient b_i, which is uniquely defined for each piece of each piecewise equation for k_U by Equations (D.32) to (D.34).
3. Having calculated intermediate parameters b_i and y_i for each piece, it is necessary to solve for the bounds to each piece of the equation for each critical k_U. These bounds are expressed in terms of stiffness, transformed from the periods used to express the EXP-2 approximation to NBCC 2010, and three further equations define the bounds' values.
4. Having calculated the bounds for each piecewise equation, the result of the piecewise equation must be calculated for each piece.
5. Given each piecewise equation, the resulting critical k_U corresponds to the piece of the piecewise equation that lies within the bounds that define that specific piece of the piecewise equation. In other words, if one piece evaluates to some constant x and the bounds are $x - 1 <$

$x < x + 1$, then the function value is x. Yuan (2016) provides no remedy for multiple solutions.

Given the approach taken by Yuan (2016), the resulting equations are sprawling, onerous to calculate and not clearly nor immediately related to the prior steps in the derivation (e.g. Equation (3.36)). This poses additional problems:

1. The substitutions and derivation are complex and prone to error – inconsistencies in the definition of piecewise elements between analogous rows are present in her formulations, including in the definition of the EXP-2 coefficients, which do not match the values used in the original MATLAB code.
2. The formulation is lengthy – at standard font size, it requires more than 3 pages to list all the pieces of the piecewise equation, without commentary.
3. The piecewise definition of the EXP-2 approximation is recursively defined – for a period of e.g. 4 seconds, all parameters for all previous segments for smaller periods must be calculated.
4. The formulation imposes many novel parameters not familiar to Canadian designers - not only the fit parameters for the EXP-2 fit (τ, A, T'_s) but also the numerical solution parameters b_i and y_i.
5. Parameters b_i and y_i correspond to no clear physical interpretation, and the transcendental equation may have multiple solutions. No guideline is given for interpreting which is which, aside from pre-specified values. This lends itself to errors – designers are forced to take the calculated value of b_i and y_i at face value without any supporting intuition.
6. The formulation is defined only for NBCC 2010, and the EXP-2 fit would need to be extended to the new spectrum used in NBCC 2015.

Instead, the proposed approach uses the NBCC 2015 spectrum given by Equation (3.37) and the newly-proposed definition of the R_k-α_U curve given by Equations (3.25) to (3.33) to provide a new, updated and more intuitive solution, either graphically or analytically (i.e. purely numerical). Rather than perform substitutions and manipulations, the revised premise is to solve Equations (3.40) to (3.42) directly as a function of k_U. After all, if the solution is ultimately numerical, there is no clear

benefit to introducing many new parameters and expanding the equation simply to arrive at an impossible to parse set of equations.

For an analytical solution, Equations (3.40) to (3.42) can be expanded and represented with each term of the equation being represented as a function of k_U. For example, by substituting the definition of α_{U1}, Equation (3.40) can be expanded to the form $k_U = f(k_U)$:

$$k_{U1} = \frac{m_U N_U g}{\Delta_{Ulim}} \left(A_{U1} e^{\left(B_{U1} \frac{S_a(T_1)}{S_a(T_U)} \right)} \right) S_a(T_U) \tag{3.43}$$

As T_U (and thus, T_1) are defined by Equations (3.14) and (3.30) as functions of k_U, a nonlinear solver can be used to find the solution for k_U directly. Numerous options exist, including MATLAB and Microsoft Excel's solver tool. Nonetheless, care should be taken, as the form of Equations (3.40) to (3.42) may lead to multiple solutions, on account of the fact they are non-smooth. This non-smoothness arises from the piecewise nature of $S_a(T)$. To avoid missing a larger second solution, the initial value of the solver input should be taken as a sufficiently large value (e.g. 10^{20} N/m) so that the largest possible value is found, and care should be taken to find the largest solution. The largest of all solutions for each critical k_U should be considered the correct one, as this poses the most restrictive requirement on the stiffness and storey drift.

It can also be advantageous to solve the solution to Equations (3.40) to (3.42) graphically, given that they can be represented in the form $k_U = f(k_U)$, since $T_U = f(k_U)$ and $T_1 = f(T_U)$. Given that Equations (3.40) to (3.42) are functions of only k_U, and because their output is itself k_U. any valid solution will occur when the input k_U is equal to the output of $k_U = f(k_U)$. Consequently, this can be plotted in two dimensions, with the input k_U on the x-axis and the output $k_U = f(k_U)$ on the y-axis. Valid solutions occur where the line $k_U = k_U$, lying at 45 degrees to either axis, intersects the curve $k_U = f(k_U)$. This concept is illustrated schematically in Figure 3.12 b) – each of Equations (3.40) to (3.42) correspond to one of the black lines, which plots $k_U = f(k_U)$ relative to the red line $k_U = k_U$. Valid solutions are illustrated at the intersections of the red and black lines by a red circle, and it is these values that correspond to the numerical solutions to each of k_{U1}, k_{Umax} and k_{U2stg}. It is readily apparent from a graphical solution whether multiple solutions exist, unlike an analytical solution. This solution can also be plotted in terms of T_U, as in Figure 3.12 a).

Whether solved numerically or graphically, the ultimate goal is to calculate each critical k_U so that $k_{U,unconditional}$ and $k_{U,required}$ are established according to Equations (3.38) and (3.39). Depending on the

relative values of R_{kU1}, R_{kU2}, R_{kU3} and R_{kU2stg}, there may be either two or three critical k_U to consider, as (e.g.) if $R_{kU1} > R_{kU3}$, values of $R_k < R_{KU1}$ (including R_{kU3}) are not applicable and therefore not included. Regardless, once $k_{U,unconditional}$ and $k_{U,required}$ are established the full set of limits on k_U and k_L can be defined by rearranging Equation (3.36) for k_L and by applying the limitations imposed by the scope.

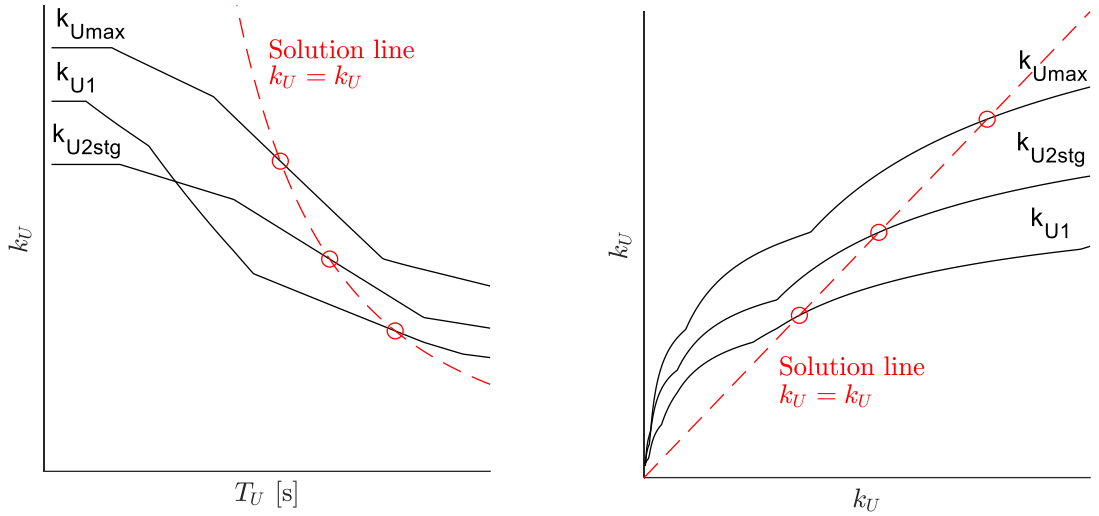

Figure 3.12: Schematic representation of the graphical solution for k_U

Note: the relative position of the lines corresponding to k_{U1}, k_{Umax} and k_{U2stg} in Figure 3.12 varies based on relative values of α_{U1}, α_{Umax} and α_{U2stg}

The constraints on k_L following the selection of k_U depend on the values of $k_{U,required}$ and $k_{U,unconditional}$ relative to a given k_U. More specifically, the three cases discussed mentioned earlier are relevant:

1. If $k_U < k_{U,required}$, no valid solutions of k_L exist for the selected k_U – k_U must be increased to at least $k_{U,required}$
2. If $k_U \geq k_{U,unconditional}$, any k_L is valid, subject to the scope of the study.
3. If $k_{U,required} \leq k_U < k_{U,unconditional}$, it is required that the selected point (R_k, k_U) lies above the R_k-k_U line corresponding to the design criterion. Therefore k_L is limited based on the values of the R_k-k_U line described by Equations (3.40) to (3.42) (for critical k_U) and Chapter 3.3.4 (for critical R_k).

Namely, if $k_{U,required} \leq k_U < k_{U,unconditional}$, the following conditions apply based on the value of R_k. They are derived directly from the transformation of Equation (3.36).

1. If $R_{kU1} < R_{kU2}$, either of the following is valid:

$$k_L \leq k_U R_{kU1} \left(\frac{N_U}{N_L}\right) \left(\frac{\bar{\omega}_{1U}}{\bar{\omega}_{1L}}\right)^2 \left(\frac{\min(\alpha_{Ulim}, \alpha_{Umax})}{1.1\alpha_{U1}}\right)^{\frac{1}{x_1}} \tag{3.44}$$

$$k_L \geq k_U R_{kU3} \left(\frac{N_U}{N_L}\right) \left(\frac{\bar{\omega}_{1U}}{\bar{\omega}_{1L}}\right)^2 \left(\frac{\alpha_{Ulim}}{\alpha_{Umax}}\right)^{\frac{1}{x_2}} \tag{3.45}$$

   In Equation (3.44), C_{U1} is taken as its maximum value of 1.1. C_{U1} is a function of R_k, and thus to use its definition in the derivation of Equation (3.44) would make the equation nonlinear with respect to k_L. Instead, by using $C_{U1} = 1.1$ the expression is much simpler and conservative since larger C_{U1} corresponds to a larger estimate of α_U. If C_{U1} is evaluated numerically rather than taken as 1.1, the restriction on k_L will be slightly less restrictive than that predicted by Equation (3.44), corresponding to a larger feasible region.

2. If $R_{kU2} \leq R_{kU1}$ and $\alpha_{Umax} > \alpha_{U2stg}$:

$$k_L \geq k_U R_{kU3} \left(\frac{N_U}{N_L}\right) \left(\frac{\bar{\omega}_{1U}}{\bar{\omega}_{1L}}\right)^2 \left(\frac{\alpha_{Ulim}}{\alpha_{Umax}}\right)^{\frac{1}{x_2}} \tag{3.46}$$

3. If $R_{kU2} \leq R_{kU1}$ and $\alpha_{Umax} \leq \alpha_{U2stg}$

$$k_L \leq k_U R_{kU3} \left(\frac{N_U}{N_L}\right) \left(\frac{\bar{\omega}_{1U}}{\bar{\omega}_{1L}}\right)^2 \left(\frac{\alpha_{Ulim}}{\alpha_{Umax}}\right)^{\frac{1}{x_2}} \tag{3.47}$$

where:

$$\alpha_{Ulim} = \frac{k_U \Delta_{Ulim}}{m_U N_U g S_a(T_U)} \tag{3.48}$$

Additionally, k_U and k_L are subject to the following constraints inherited from the scope:

1. The single-storey periods (T_{singU} and T_{singL}) of the upper and lower structures must be less than or equal to 0.31 seconds (Equation (3.49) and (3.50)). As discussed in Chapter 1.3.2, the limits on T_{singU} and T_{singL} are imposed so that they are less than or equal to the most flexible code-specified period approximation for a 3.3-metre storey height.

2. The storey stiffness ratio should be between 1 and 20, inclusive, and if $1 < r_{kU1}$, r_k should also be larger than or equal to r_{kU1} (Equation (3.51)).

$$k_U \geq m_U \left(\frac{2\pi}{0.31}\right)^2 \tag{3.49}$$

$$k_L \geq m_L \left(\frac{2\pi}{0.31}\right)^2 \tag{3.50}$$

$$\max(r_{kU1} k_U, k_U) \leq k_L \leq 20 k_U \tag{3.51}$$

In combination, Equations (3.35) to (3.51) are the set of equations that describe the set of valid solutions of k_U and k_L (equivalently, R_k). By solving these equations, it is possible to identify valid values of k_U and the associated valid range of k_L. While this can be as simple as confirming whether a given combination is valid, it can also be used to optimize the design for the minimum required stiffness k_U associated with the minimum amplification α_U. Of course, care should be taken when using the minimum k_U value or one which lies along the boundary which delineates the feasible and infeasible regions, as subtle changes or inaccuracies to the stiffness could increase the expected α_U and thus required stiffness. The curve is selected to be conservative but is nonetheless a theoretical estimate of a practical characteristic.

Practical application aside, it can be difficult to parse the logic of Equations (3.35) to (3.51) to interpret the procedure intuitively, even once the critical values of k_U (k_{U1}, k_{Umax}, k_{U2stg}) are determined. Fortunately, it is possible to relate the Equations (3.35) to (3.51) graphically to the R_k-α_U curve from which they are derived, as in Figure 3.13. Any combination of k_U and k_L can be mapped to the R_k-α_U curve via the design criterion (Equation (3.9)) in combination with the definitions of the R_k and α_U. Specifically, the right-hand side of Equation (3.9) corresponds to a provided value of α_U which may or may not exceed the approximated value of the R_k-α_U curve – if this value corresponding to k_U is larger than the value of the R_k-α_U curve, Equation (3.9) is satisfied. As before, this is akin to a provided resistance being greater than an expected amplification response. In this context, the R_k-α_U space is divided graphically into four distinct regions based on the value of k_U and k_L:

1. The critical points of the R_k-α_U curve (i.e. R_{kU1}, R_{kU2}, α_{U1}, etc.) correspond directly to k_{U1}, k_{Umax} and k_{U2stg}. Regions above the line are possibly feasible, whereas regions below the line are always infeasible. Combinations of k_U and R_k are considered feasible if they satisfy the design criterion given by Equation (3.9) as well as the scope described by Section 1.3.2.

2. The left and right bounds on R_k are defined using the most restrictive of $r_k \geq 1$, $r_k \leq 20$ and $r_k \geq r_{kUI}$. Values that lie outside this range are considered out-of-scope, corresponding to the grey region of the figure.

3. The green region which is greater than or equal to all points on the R_k-α_U curve corresponds to the condition $k_U \geq k_{U,unconditional}$. Regardless of what the value of k_L is, the value of the right-hand side of Equation (3.9) will be adequate so long as it is larger than the largest α_U and therefore also lies in the green region.

4. The blue region corresponds to combinations of k_U and k_L which are feasible, but only while the combination of k_U and k_L lie above the R_k-α_U curve. If k_L or k_U changes and the point (R_k, α_U) moves into the red or grey regions, the combination is no longer considered adequate. The bottom of this region corresponds to $k_U = k_{U,required}$, and Equations (3.44) to (3.48) are applied to ensure that the considered values of k_U and k_L lie above the R_k-α_U curve.

5. The single-storey periods T_{singU} and T_{singL} also apply a floor on k_U and k_L (and consequently R_k), but this is not necessarily obvious in the R_k-α_U domain.

Note that, in general throughout this thesis, red regions indicate that the interstorey drift limit is not satisfied but that each variable is within this study's scope, and grey out-of-scope regions indicate that at least one variable is outside the scope, but not necessarily that the interstorey drift limit is exceeded. Thus, points within the grey region may satisfy the interstorey drift limit. However, the out-of-scope data is associated with, for example, a storey count larger than the limit of 12, a longer single-storey period (*TsingU*/*TsingL*) than 0.31 seconds, or a mass or stiffness ratio that is either too high or too low. In the case of the stiffness ratio, if the stiffness ratio $r_k < 1$, $r_k < r_{kUI}$, or $20 < r_k$, the structure is out-of-scope. With respect to structures with a large difference in stiffness that might otherwise be analyzed with the two-stage procedure, this method is applicable so long as the stiffness ratio, mass ratio and other parts are in the limits set out in the scope. Nonetheless, a structure that is out-of-scope may be a practical design, it just cannot be analyzed by this thesis – this includes structures with an extreme setback, such that e.g. $20 < r_k$.

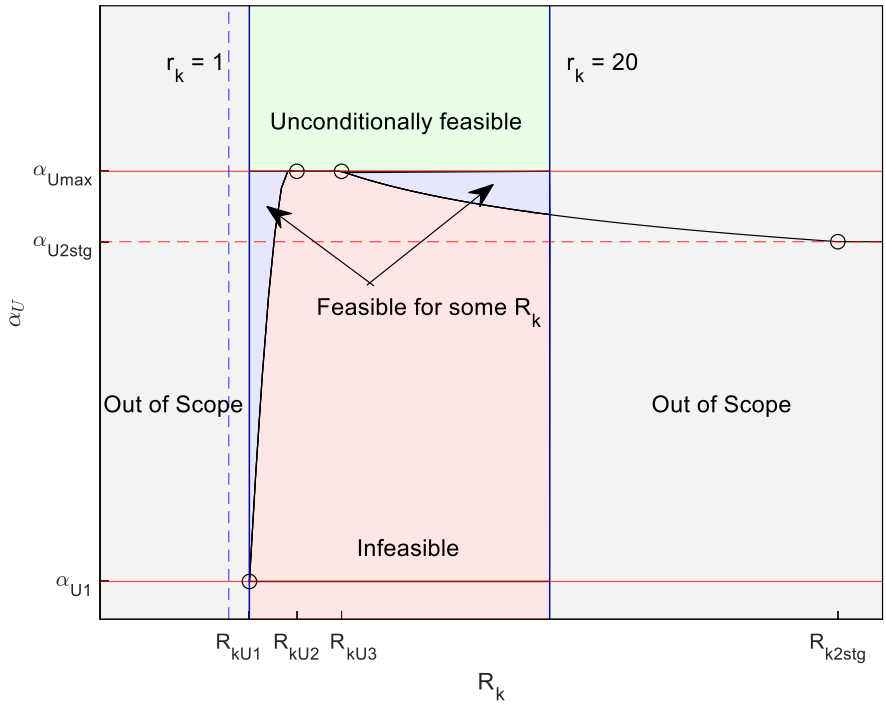

Figure 3.13: Graphical Illustration of Bounds on Design Stiffness k_U in terms of R_k and α_U

Now, while the relationship between k_U and k_L can be discussed in the context of the R_k-α_U curve, the relationships given in Equations (3.38), (3.39), and (3.44) to (3.51) (i.e. $k_{U,required}$, $k_{U,unconditional}$, and the limits imposed by the R_k-α_U curve and scope) can also be used to map the problem directly in terms of k_U and k_L. For example, in Figure 3.14, which is related to Figure 3.13. If the relationships, excluding those which correspond to $k_{U,required} \leq k_U < k_{U,unconditional}$ (Equations (3.44) to (3.48)) are plotted for the same scenario as Figure 3.13, the resulting plot resembles a linear programming problem – each of the conditions constrains k_U and k_L with an upper or lower bound, and the resulting area is the region of valid combinations. In the case of Figure 3.14, the black lines are imposed by the need to keep the single-storey periods T_{singU} and T_{singL} within the scope, the red lines correspond to $k_{U,required}$ and $k_{U,unconditional}$, and the blue lines correspond to the upper and lower bounds on the storey stiffness ratio r_k imposed by the scope of the study. The magenta lines characterize the conditions on k_L imposed via k_U, R_k and Equations (3.44) to (3.48) – one is marked with upwards triangles, indicating that values above the line are valid, and the other is marked with downwards triangles, indicating that values below the line are valid. As in Equations (3.44) to (3.48), the satisfaction of one requirement, not both, is sufficient. In this case, the scope restricts the valid ranges of k_U and k_L, but this may not always be the case.

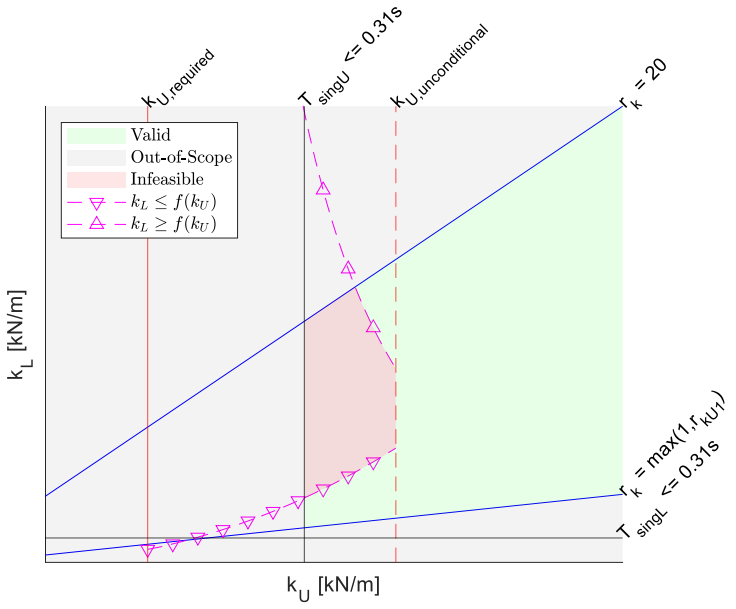

Figure 3.14: Sample graphical illustration of the feasible range of stiffness k_U and k_L

3.6 Summary of R_k-α_U relationship and procedure to evaluate upper structure stiffness k_U

The amplification factor α_U, analogous to M_v used in NBCC 2015, quantifies the increase in higher-mode effects on the base shear of the upper structure of a structure with a stiff-and-massive lower structure and a less stiff, less strong upper structure. It is, in general, a function of the overall stiffness and mass ratios R_k and R_m and the spectral acceleration $S_a(T)$ and modal periods T_U, T_L, T_1, T_2, etc. α_U is approximated as a function of $S_a(T)$, R_m and R_k at four critical values of the stiffness ratio: R_{kU1}, corresponding to the minimum stiffness ratio such that the base of the upper structure experiences the structure's largest interstorey drift, R_{kU2} and R_{kU3}, which correspond to the maximum amplification ratio, and R_{kU2stg}, which corresponds to the ASCE 7 two-stage requirement and to an effective plateau beyond which α_U is generally constant.

By enforcing the code-specified interstorey drift limit on the base of the upper structure, a design criterion is established which sets a limit on α_U as a function of the upper structure stiffness k_U. By transforming this relationship and substituting the proposed approximation for α_U, a limit on k_U is established corresponding to the critical values of the proposed R_k-α_U curve. This limit must be evaluated numerically for each critical point. Eschewing the transformations and piecewise exponential spectral approximation used by Yuan (2016), it is proposed that the critical values of k_U

be numerically evaluated directly from their proposed definitions using either a nonlinear solver or by using a graphical solution.

The resulting critical values of k_U are used in conjunction with limitations imposed by the scope and are substituted into the relationship between k_U and R_k. These relationships are used to impose limitations on k_L and k_U, classifying values of k_U into the three classifications based on the design criterion – 1) where k_L is unrestricted, 2) where limitations on R_k constrain k_L and 3) where no value of k_L in combination with the selected k_U produces a feasible design. The design problem, which can be displayed graphically, is intended to aid the preselection of k_U and k_L statically so that the structure can tolerate the expected amplification without exceeding drift limits. Given an objective function to assign some weighting to k_U and k_L, the solution could be used as the basis for a nonlinear programming problem. Conceivably, it could be specified that it is preferable to reinforce the upper structure rather than the lower one, for example. Such a nonlinear programming problem would aim to find the most preferred combination of k_U and k_L, subject to the constraints imposed by the equations given in Chapter 3.5.

Consequently, the procedure to determine k_U is as follows:

1. Select based on the structural configuration: m_U, m_L, N_U, N_L, $S_a(T)$
2. Evaluate $\bar{\omega}_{1L}$ and $\bar{\omega}_{1U}$ from Table 3.1, corresponding to $N = N_L$ and $N = N_U$
3. Calculate r_m and R_m based on Equations (3.16) and (3.18)
4. Determine R_{kU1}, R_{kU2}, R_{kU3} and R_{kU2stg} according to Equations (3.25) to (3.28) and Appendix E, as well as A_{U1}, B_{U1}, A_{Umax}, and B_{Umax} from Appendix E.
5. Solve for the critical values of k_U. If any equation produces multiple solutions, choose the largest k_U corresponding to a solution.
    a. Solve for k_{U1} numerically based on: k_{U1} - Equation (3.40), $S_a(T_U)$ - Equation (3.37), α_{U1} - Equation (3.29), $S_a(T_1)$ – Equation (3.30), φ_{L1} – Equation (A.13), and A_{U1} and B_{U1}
    b. If $R_{kU1} \leq R_{kU3}$, solve for k_{Umax} numerically based on: k_{Umax} – Equation (3.41), $S_a(T_U)$ - Equation (3.37), α_{Umax} – Equation (3.31), $S_a(T_1)$ – Equation (3.32), φ_{L1} – Equation (A.13), and A_{Umax} and B_{Umax}

c. Solve for k_{U2stg} numerically based on: k_{U2stg} – Equation (3.42), $S_a(T_U)$ - Equation (3.37), and α_{U2stg} - Equation (3.33)

6. Evaluate $k_{U,required}$ and $k_{U,unconditional}$ based on Equations (3.38) and (3.39) using k_{U1}, k_{Umax} and k_{U2stg}
7. Select a value of k_U, not less than dictated by $k_{U,required}$ and Equation (3.49)
8. Select a value of k_L. If $k_{U,required} \leq k_U < k_{U,unconditional,}$ then one of the following conditions a) to d) applies:
    a. If $R_{kU1} < R_{kU2}$, k_L must satisfy either Equation (3.44) or (3.45)
    b. If both $R_{kU2} \leq R_{kU1}$ and $\alpha_{Umax} > \alpha_{U2stg}$, k_L must satisfy Equation (3.46)
    c. If both $R_{kU2} \leq R_{kU1}$ and $\alpha_{Umax} \leq \alpha_{U2stg}$, k_L must satisfy Equation (3.47)
    d. Otherwise, if $k_{U,unconditional} \leq k_U$, k_L is not subject to the limits specified by items a) to c)
9. In addition, the selected k_L and k_U must satisfy Equations (3.49) to (3.51). The parameter r_{kU1} is determined from Equation (3.19) in combination with the predetermined value of R_{kU1}.

Following the selection of k_U and k_L satisfying the design criterion, an initial framing layout can be determined, and with which the interstorey drifts ratios, storey shears and overturning moments, and any other applicable requirements should be checked to ensure that the structure meets the requirements of NBCC 2015.

3.7 Design examples

To demonstrate the proposed procedure to evaluate the critical stiffnesses k_U, two examples are provided. Each is a hypothetical structure with a vertical combination of framing systems, in which the assumed masses and stiffness provide a basis for the design. Detailed design is not provided – the intent is to provide an approximately realistic example for the proposed method rather than a fully realized design. The examples are as follows:

1. A six-storey structure with a three-storey upper structure and a three-storey lower structure, in St. Catharines, Ontario. This example is evaluated only for the proposed procedure.

2. Having the same properties as Example 5-1 from Yuan (2016), a nine-storey structure having a six-storey lower structure and a three-storey upper structure located in Vancouver, the critical stiffnesses k_U is assessed in three cases:

    a. according to the proposed procedure and NBCC 2015 spectrum

    b. according to the proposed procedure and NBCC 2015 spectrum, considering the 2.61 amplification recommended by Yuan (2016)

    c. A comparison of the EXP-2 approximation to the NBCC 2010 $S_a(T)$ relationship proposed by Yuan (2016) and direct numerical calculation of $S_a(T)$

For simplicity, the same combination of SFRS is considered in each example – a reinforced concrete moment-resisting frame for the lower structure, per CSA A23.3-19 (2019), and a cold-formed steel frame with oriented strand board (OSB) sheathed shear walls, per AISI S400-15 (2015). Specifically, the masses are assumed based on a specified dead load, and stiffnesses are based on an assumed unit stiffness. However, the two examples differ insofar as the estimation of the stiffnesses and the storey plan size. The first example is new and features a constant 25-metre by 25-metre floor plan in which the columns (for the lower structure) are arranged at five-metre increments, and in which the stiffness of the upper structure is estimated according to the rationale provided in Appendix G. Conversely, Example 3-2 is based on Example 5-1 appearing in Yuan (2016) and features a four-by-four grid of columns spaced at 6.1 metres centre-to-centre. Furthermore, while the new example uses a stiffness estimated from AISI S400-15 (2015), Yuan (2016) adopts a value of stiffness directly inferred from physical testing performed by Branston (2004).

3.7.1 Example 3-1

In this example, a sample structure located in St. Catharines, Ontario is evaluated according to the new proposed procedure to demonstrate how to calculate the feasible distribution of k_U and k_L. The SFRS of the lower structure is a reinforced concrete moment-resisting frame, and the SFRS of the upper structure is a CFS frame having OSB-sheathed shear walls. Each of the lower and upper structures is three storeys in height - $N_U = N_L = 3$ – and subject to the spectral accelerations specified by Table 3.7.

Table 3.7: NBCC 2015 spectral acceleration for St. Catharines, Ontario (NRCC, 2015a)

$S_a(0.2)$	$S_a(0.5)$	$S_a(1.0)$	$S_a(2.0)$	$S_a(5.0)$	$S_a(10.0)$
0.319	0.155	0.071	0.032	0.0076	0.0028

Both the lower structure and upper structure are set on a 25 metre by 25 metre floor plan, in which the columns or shear walls (as applicable) are arranged uniformly. In the lower structure, it is assumed that the columns are 500 mm by 500 mm in dimension and constructed from standard-density concrete having a 35 MPa compressive strength. The according assumed stiffness is 3.08×10^4 kN/m stiffness per column – the final requirements on stiffness are expressed in terms of this unit stiffness. As discussed in Appendix G, the assumed unit stiffness of the CFS shear walls is 1640 kN/m/m. It is assumed that the interstorey height is 3 metres.

The specified dead loads applied to each storey of the upper and lower structures are 3 kPa and 9 kPa, respectively, and thus the upper and lower structures' storey masses are 191000 kg and 573980 kg, respectively. The critical properties are summarized in Table 3.8 as follows:

Table 3.8: Input characteristics of Example 3-1

Parameter	Value	Parameter	Value
m_U	191000 kg	m_L	573980 kg
N_U	3	N_L	3
r_m	3	Δ_{Ulim} (2.5%)	0.075 m

For the newly proposed method, the first step in the procedure is to establish the critical stiffness ratios R_{kU1}, R_{kU2}, R_{kU3} and R_{kU2stg}, as well as to establish the values of A_{U1}, B_{U1}, A_{Umax} and B_{Umax}. Using Equation (3.18) to evaluate R_m, Equations (3.25) to (3.28) to evaluate R_{kU1}, R_{kU2}, R_{kU3} and R_{kU2stg}, and Appendix E to define R_{kU1}, A_{U1}, B_{U1}, A_{Umax}, and B_{Umax}, the key parameters are given in Table 3.9:

Table 3.9: Example 3-1 critical intermediate parameters

Parameter	Value	Parameter	Value
R_m	3.00		
R_{kU1}	2.28	R_{kU3}	6.00
R_{kU2}	4.00	R_{kU2stg}	30.00
A_{U1}	0.465	A_{Umax}	0.499
B_{U1}	1.163	B_{Umax}	1.117

Using the above properties, the solution of Equations (3.40) to (3.42), for k_{Umax}, k_{U2stg} and k_{U1} are plotted in Figure 3.20. As illustrated, the solutions of k_{Umax}, k_{U2stg} and k_{U1} are 3.20×10^2 kN/m, 2.62×10^2 kN/m and 3.12×10^2 kN/m, and so $k_{U,required}$ and $k_{U,unconditional}$ are 2.62×10^2 kN/m and 3.20×10^2 kN/m. In this case, the minimum stiffnesses based on the R_k-α_U formulation are quite low, corresponding to $T_U > 10$ seconds on account of the values of the input parameter given in Table 3.8. This can be attributed to the relatively low value of $S_a(T_U)$ – per Equations (3.40) to (3.42), the critical values of k_U are heavily dependent on the intensity of $S_a(T_U)$. Without the 2.61 scaling factor applied by Yuan (2016), it is significantly more likely that the required stiffnesses are controlled by the scope. Specifically, the critical stiffness values specified by Equations (3.38) to (3.42) are an approximately linear function of $S_a(T_U)$, whereas the limits imposed by the scope, Equations (3.49) to (3.51), are constant as a function of $S_a(T_U)$. Therefore, if $S_a(T_U)$ is small, it is more likely that Equations (3.49) to (3.51) will govern the requirements on k_U and k_L, whereas if $S_a(T_U)$ is increased it is more likely that the critical stiffness values specified by Equations (3.38) to (3.42) will be larger than those imposed by Equations (3.49) to (3.51). By scaling the entire spectrum by a factor of 2.61, it is more likely that the latter case is true, and that the limitations imposed by the scope, Equations (3.49) to (3.51), are less significant. Now, α_U, not only (e.g.) k_{U1} is a function of $S_a(T)$, and so it would be reasonable to expect that k_{U1} is not linear for $S_a(T)$. However, α_U is not a function of $S_a(T)$ but of ratios of $S_a(T)$. A constant scaling of $S_a(T)$ will not change α_U. This factor is explained to some extent in Example 3-2, but overall changes the spectral accelerations to match a higher hazard level than the default.

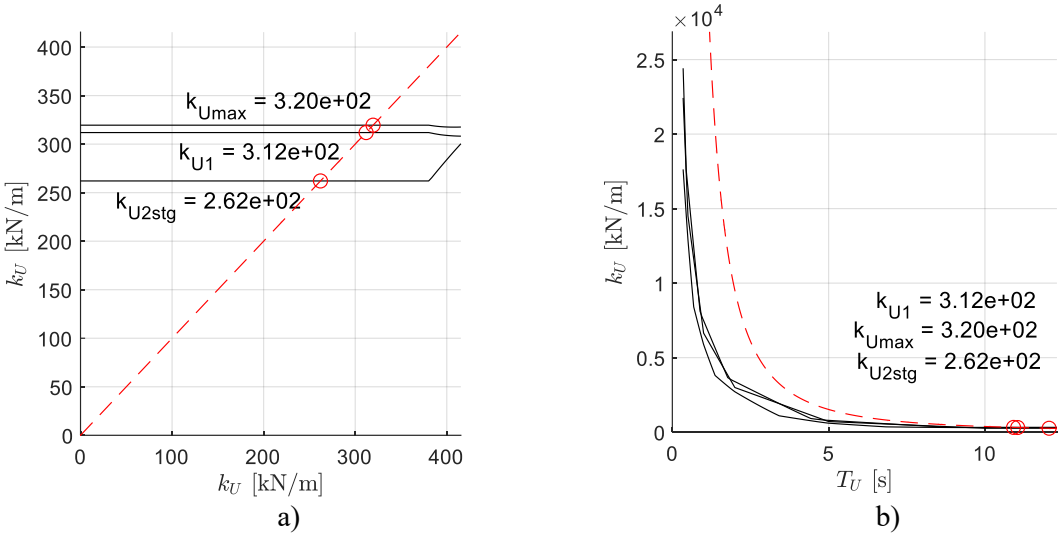

Figure 3.15: Graphical solution for critical stiffnesses k_U

The remaining restrictions on the range of k_U and k_L are: 1) based on the scope according to Equations (3.49) to (3.51), and 2) based on $k_{U,required}$ and $k_{U,unconditional}$, according to Equations (3.44) to (3.48). In this case, Equations (3.49) to (3.51) are evaluated as follows:

$$k_U \geq m_U \left(\frac{2\pi}{0.31}\right)^2 = 7.85(10^4)\ kN/m \tag{3.52}$$

$$k_L \geq m_L \left(\frac{2\pi}{0.31}\right)^2 = 2.35(10^5)\ kN/m \tag{3.53}$$

$$\max(r_{kU1}k_U, k_U) = 2.28k_U \leq k_L \leq 20k_U \tag{3.54}$$

In combination with $k_{U,required}$ and $k_{U,unconditional}$, the upper bound on T_{singU} significantly constricts k_U such that the correct minimum value of k_U is 7.85×10^4 kN/m rather than 2.62×10^2 kN/m. As for Equations (3.44) to (3.48), the value of k_L is a function of both k_U and α_{Ulim}, itself a function of k_U on account of $S_a(T_U)$. These limits on k_L therefore cannot be so simply expressed in terms of k_U and should instead be evaluated over the range of $k_{U,required}$ to $k_{U,unconditional}$ to establish the overall curve. In this case, $R_{kU1} < R_{kU2}$ and so either Equation (3.44) or (3.45) can be satisfied. It can be hard to parse these equations, and so they can be interpreted graphically as in Figure 3.20, similarly to Figure 3.14.

In the case of Figure 3.20, the structural configuration places such small limits on k_U as a result of α_U such that the limits on the periods T_{singU} and T_{singL} govern the lower bound on the two stiffnesses by several orders of magnitude. Expressed instead in terms of the equivalent number of columns or length of shear wall, Figure 3.19 can be transformed into Figure 3.22.

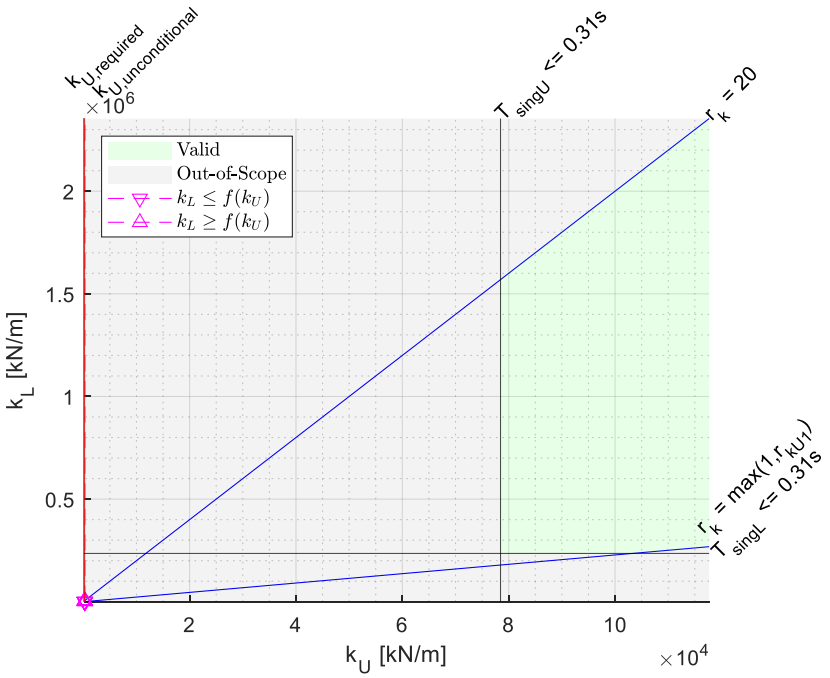

Figure 3.16: Graphical illustration of bounds on design stiffness k_U in terms of k_U and k_L

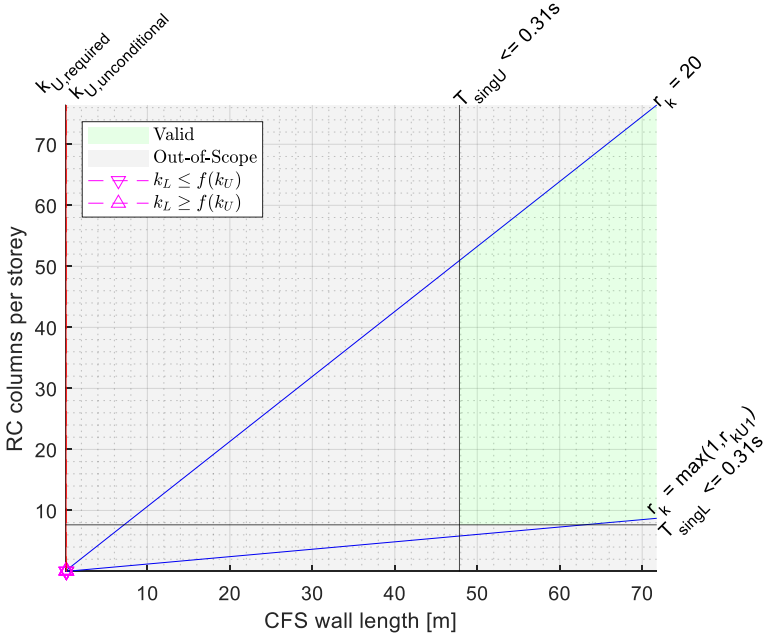

Figure 3.17: Graphical illustration of bounds on design stiffness k_U in terms of system properties

In both Figure 3.16 and Figure 3.17, the minimum value of k_U is strictly limited by the requirements on T_{singU}, given that $S_a(T)$ is relatively small and thus the value of k_U,unconditional is much smaller than the value of k_U associated with T_{singU}. For example, the lines $k_L \leq f(k_U)$ and $k_L \geq f(k_U)$ are not clearly visible in Figure 3.15 and 3.16 because $k_{U,required}$ and $k_{U,unconditional}$ are of much smaller magnitude than the limit for T_{singU}. If instead the spectral curve for Victoria, British Columbia is used per Table 3.10, $k_{U1} = 7.45\times10^4$ kN/m, $k_{Umax} = 1.15\times10^5$ kN/m and $k_{U2stg} = 7.45\times10^4$ kN/m. In this case, the critical stiffnesses (k_{U1}, k_{Umax}, k_{U2stg}) and thus $k_{U,required}$ and $k_{U,unconditional}$ are of an equal or larger magnitude to the scope-imposed limitations and thus more prominent in the feasible stiffness distribution, as illustrated by Figure 3.18. Correspondingly, the restrictions on R_k impose limitations on k_L in the case of Victoria. The specific importance of each of the limitations depends on the degree of irregularity as well as the spectral acceleration.

Table 3.10: NBCC 2015 spectral acceleration for Victoria, British Columbia (NRCC, 2015a)

$S_a(0.2)$	$S_a(0.5)$	$S_a(1.0)$	$S_a(2.0)$	$S_a(5.0)$	$S_a(10.0)$
1.30	1.16	0.676	0.399	0.125	0.044

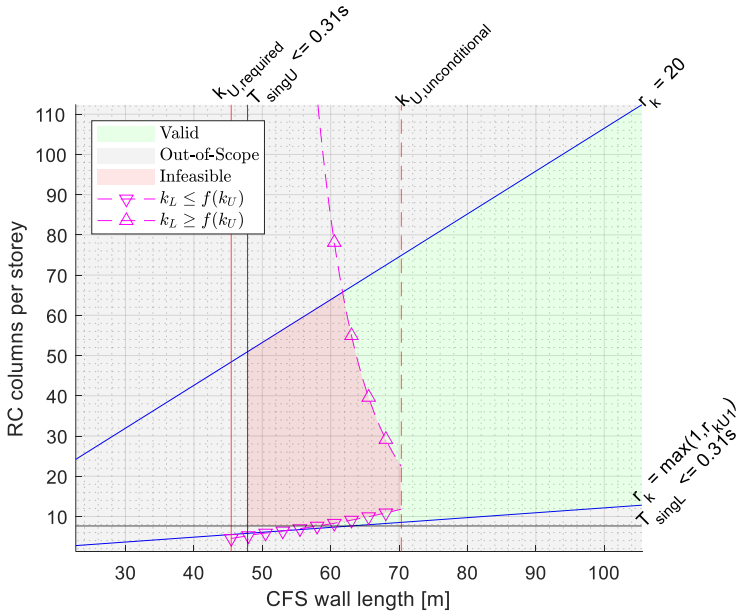

Figure 3.18: Graphical illustration of bounds on design stiffness k_U in terms of system properties – Victoria, BC

Finally, to briefly examine the effect of $C_{U1} = 1.1$ on Equation (3.44) corresponding to Figure 3.18 (Victoria, BC), consider the limit if $k_U = 1.12\times10^5$ kN/m (68 metres of shear wall) and $k_L = 3.08\times10^5$

kN/m (10 times the assumed column stiffness). If evaluated using these stiffnesses, C_{UI} = 1.08 and therefore:

$$k_L \leq k_U(2.28)\left(\frac{\min(1.38,1.38)}{1.08 \times 1.02}\right)^{\frac{1}{0.53}} = 3.49k_U \tag{3.55}$$

Compare this to if C_{UI} = 1.1:

$$k_L \leq k_U(2.28)\left(\frac{\min(1.38,1.38)}{1.1 \times 1.02}\right)^{\frac{1}{0.53}} = 3.37k_U \tag{3.56}$$

Thus, depending on the value of R_k corresponding to any given combination of k_U and k_L, the maximum value dictated by Equation (3.44) is slightly smaller if C_{UI} is taken as 1.1 for defining the limit. In this case, $\alpha_{Ulim} \approx 1.38$ – all this indicates is that for $\alpha_U > 1.38$ the interstorey drift limit is not satisfied. However, note that the specific values given are applicable only in the vicinity of the chosen k_U and k_L, given that these values influence α_U and α_{Ulim}. Nonetheless, assuming C_{UI} = 1.1 imposes a slightly more restrictive limit than if calculated for specific values of k_U and k_L.

3.7.2 Example 3-2

For the second example, Example 5-1 from Yuan (2016) is re-examined to provide a comparison between the previous and proposed NBCC-based methods. As appearing also in Yuan (2016) Example 3-1, the structure is a nine-storey building consisting of a six-storey reinforced concrete lower structure and a three-storey cold-formed steel upper structure. Specifically, the lower structure is a moment-resisting frame (MRF) supported by a four-by-four square grid of columns arranged as in Figure 3.19. The lateral forces in the CFS frame are resisted by oriented strand board (OSB) sheathed shear walls. Each column of the MRF is assumed to be 600 mm by 600 mm in cross-section, with E = 30000 MPa and $f_c^{'}$ = 30 MPa, thus providing a stiffness of $k_L = 5.41 \times 10^4$ kN/m per column. This value is calculated according to FEMA 356 (2000) recommendations for the effective moment of inertia as opposed to the Canadian standard (i.e. CSA SA23.3) but is nonetheless used for both the ASCE 7-based and NBCC 2010-based examples provided in Yuan (2016). Besides this, the CFS shear wall strengths are not calculated. Instead, Yuan (2016) assumes that the wall's elastic stiffness is 3836 kN/m per metre of wall length and refers to experimental data published by Branston (2004). Yuan (2016) provides no context on the wall configuration, indicating only that a double-sided 11 mm OSB configuration is used, but details given by Branston (2004) indicate that the tested specimens are 1220 x 2440 mm in size and use 11 mm OSB according to CSA O325 (Canadian

Standards Association, 1992) alongside back-to-back 362S162-43 CFS chord studs with F_y = 230 MPa (33 ksi) (Clark Dietrich, 2017). It is not immediately clear that the 3836 kN/m per metre value is provided by Branston (2004) – the provided values are doubled to estimate the effect of the second sheet of OSB. This assumption is only valid if it is assumed that the local failure of the end studs does not control the strength of the wall. Compare this to the value calculated in Appendix G via AISI S400-15 (2015) of 1634 kN/m/m for the same configuration. Nonetheless, for consistency's sake the 3836 kN/m/m value is used in this example.

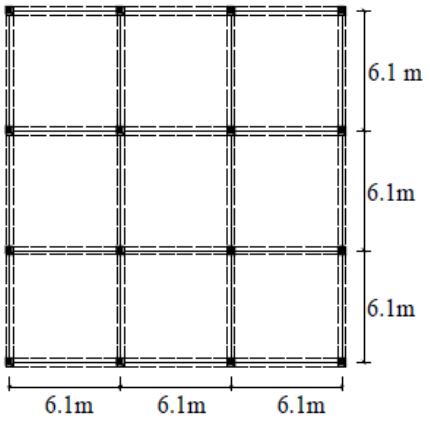

Figure 3.19: Floor plan of the lower RC structure (Yuan, 2016)

These stiffnesses being assumed, the mass is based on an assumed dead lead applied to each storey – 2.87 kPa for the upper structure, and 6.55 kPa for the lower structure. The corresponding masses are 96113 kg for each storey of the upper structure, and 219352 kg for each storey of the lower structure. The interstorey heights are assumed to be 3.06 metres. These key inputs are summarized in Table 3.11.

Table 3.11: Input characteristics of Example 3-2

Parameter	Value	Parameter	Value
m_U	96113 kg	m_L	219352 kg
N_U	3	N_L	6
r_m	2.28	Δ_{Ulim} (2%)	0.0612 m

The last remaining key parameter is the spectral acceleration, which varies based on the assumptions being made. As used in the original example in Yuan (2016), it is assumed that the structure is located on Class C soil in Vancouver:

Table 3.12: NBCC 2010 spectral acceleration for Vancouver (Yuan, 2016)

	$S_a(0.2)$	$S_a(0.5)$	$S_a(1.0)$	$S_a(2.0)$
NBCC 2010	0.940	0.640	0.330	0.170
Yuan (2016)	2.453	1.670	0.861	0.444

However, as indicated in Table 3.12, Yuan (2016) does not use the values of the NBCC 2010 spectral values as-is and instead applies a 2.61 multiplier to uniformly scale the spectrum. This multiplier, which they apply to both their ASCE and NBCC-derived examples, is based on an interpretation of the inherent hazard level in ASCE 7. According to FEMA P-695 (FEMA, 2009a), the mean collapse probability of buildings designed for ASCE 7-10 (2010) is 10% under the maximum considered earthquake (MCE). ASCE 7-10 specifies that the design acceleration to be used is the median demand rather than the MCE. Thus, Yuan argues, the design acceleration must be scaled by a factor of 2.61 to ensure that the non-exceedance probability of a storey drift larger than the storey drift limit Δ_{Ulim} is 90%. It is unclear whether this scaling is appropriate or necessary, particularly when applied to NBCC 2015, for which the seismic hazard is defined differently than ASCE 7. While the modern incarnations of both codes use the mean hazard values to determine design spectral accelerations, the commentary to NBCC 2015 notes that direct comparison of the hazard level considered by the two codes is both inconsistent and difficult to quantify, owing to significant methodological differences between the codes (NRCC, 2015b). It is therefore unclear whether the specific value or even the use of such a scaling factor is required. Such a determination requires further study and is outside the scope of the current study. Except for comparing results to those calculated by Yuan (2016), the spectral accelerations are used as-is.

Another complication regarding the spectral accelerations is the differences between NBCC 2015 and NBCC 2010. Modelling changes have changed the values of $S_a(T)$ in some locations between NBCC 2010 and 2015, and so the spectral acceleration applied at identical locations varies between the two versions. To provide an analogous location, the Vancouver City Hall spectrum is adopted for calculations involving NBCC 2015:

Table 3.13: NBCC 2015 spectral acceleration for Vancouver City Hall (NRCC, 2015a)

$S_a(0.2)$	$S_a(0.5)$	$S_a(1.0)$	$S_a(2.0)$	$S_a(5.0)$	$S_a(10.0)$
0.848	0.751	0.425	0.257	0.080	0.029

Given the differences between the proposed and Yuan (2016) formulations, there are therefore three relevant calculations to be made as part of this example:

1. The calculation of design stiffnesses for the newly proposed method, using the default NBCC 2015 spectral values provided by Table 3.13
2. The calculation of design stiffnesses for the newly proposed method, using the default NBCC 2010 spectral values, scaled by a factor of 2.61 as used by Yuan (2016)
3. The calculation of design stiffnesses for the Yuan (2016) method using the NBCC 2010 values given by Table 3.12, to compare the direct numerical solution of k_U to that using the EXP-2 approximation given in Appendix D.

Case a) – Newly proposed method

For the newly proposed method, the first step in the procedure is to establish the critical stiffness ratios R_{kU1}, R_{kU2}, R_{kU3} and R_{kU2stg}, as well as to establish the values of A_{U1}, B_{U1}, A_{Umax} and B_{Umax}. Using Equation (3.18) to evaluate R_m, Equations (3.25) to (3.28) to evaluate R_{kU1}, R_{kU2}, R_{kU3} and R_{kU2stg}, and Appendix E to define R_{kU1}, A_{U1}, B_{U1}, A_{Umax}, and B_{Umax}, the key parameters are given in Table 3.14:

Table 3.14: Critical intermediate parameters

Parameter	Value	Parameter	Value
R_m	4.56		
R_{kU1}	1.83	R_{kU3}	7.56
R_{kU2}	5.56	R_{kU2stg}	45.60
A_{U1}	0.488	A_{Umax}	0.591
B_{U1}	1.129	B_{Umax}	1.072

Using the above properties, the solution of Equations (3.40) to (3.42), for k_{Umax}, k_{U2stg} and k_{U1} are plotted in Figure 3.20. As illustrated, the solutions of k_{Umax}, k_{U2stg} and k_{U1} are 4.95×10^4 kN/m,

3.38×10^4 kN/m and 2.24×10^4 kN/m, and so $k_{U,required}$ and $k_{U,unconditional}$ are 2.24×10^4 kN/m and 4.95×10^4 kN/m.

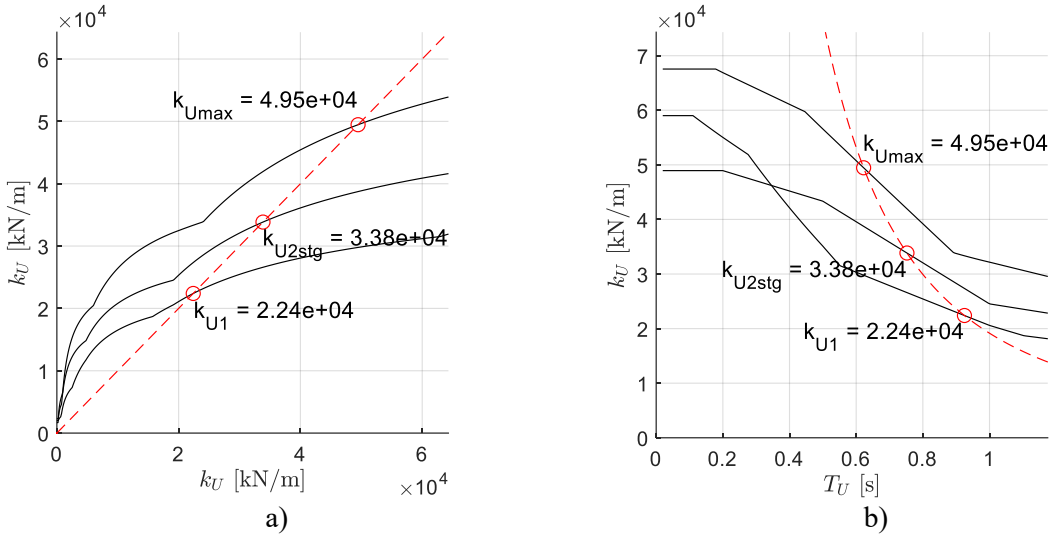

Figure 3.20: Graphical solution for critical stiffnesses k_U

Having established $k_{U,required}$ and $k_{U,unconditional}$, only two considerations remain: restricting the range of k_U and k_L based on the scope according to Equations (3.49) to (3.51), and where $k_{U,required}$ and $k_{U,unconditional}$, restricting k_L according to Equations (3.44) to (3.48). In this case, Equations (3.49) to (3.51) are evaluated as follows:

$$k_U \geq m_U \left(\frac{2\pi}{0.31}\right)^2 = 3.98(10^4)\ kN/m \tag{3.57}$$

$$k_L \geq m_L \left(\frac{2\pi}{0.31}\right)^2 = 9.00(10^4)\ kN/m \tag{3.58}$$

$$\max(r_{kU1} k_U, k_U) = 3.11 k_U \leq k_L \leq 20 k_U \tag{3.59}$$

In combination with $k_{U,required}$ and $k_{U,unconditional}$, the upper bound on T_{singU} constricts k_U such that the correct minimum value of k_U is 3.98×10^4 kN/m rather than 2.24×10^4 kN/m. As for Equations (3.44) to (3.48), the value of k_L is a function of both k_U and α_{Ulim}, itself a function of k_U on account of $S_a(T_U)$. These limits on k_L therefore cannot be so simply expressed in terms of k_U and should instead be evaluated over the range of $k_{U,required}$ to $k_{U,unconditional}$ to establish the overall curve. In this case, $R_{kU1} < R_{kU2}$ and so either Equation (3.44) or (3.45) can be satisfied. It can be hard to parse these equations, and so they can be interpreted graphically as in Figure 3.21, similarly to Figure 3.14.

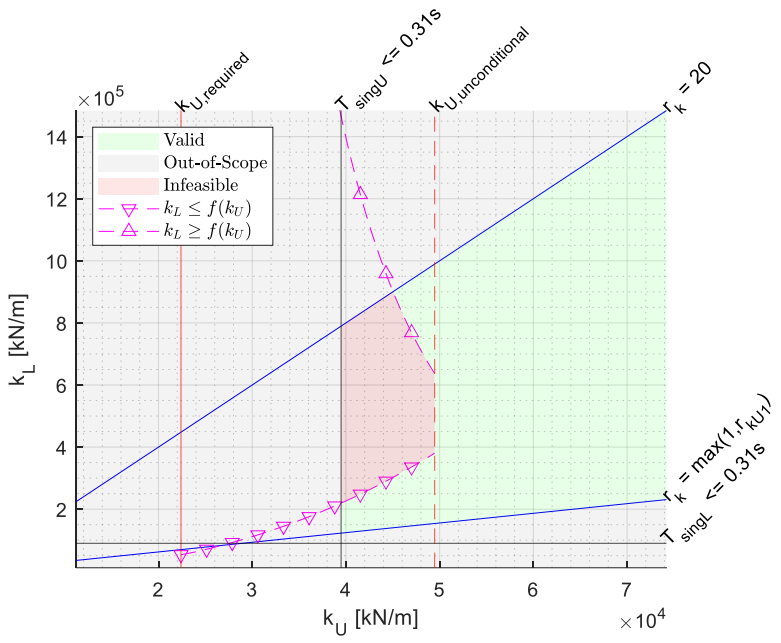

Figure 3.21: Graphical illustration of bounds on design stiffness k_U in terms of k_U and k_L

In Figure 3.21, the green area is that which corresponds to a permissible combination of k_U and k_L. For $k_{U,unconditional} \leq k_U$, combinations are valid so long as k_U and k_L are within the bounds of the scope – namely, between the blue lines which represent Equation (3.51) and the limitations on the storey stiffness ratio r_k, and above the black lines which correspond to the bounds on single-storey periods T_{singU} and T_{singL} (Equations (3.49) to (3.50)). For $k_{U,required} \leq k_U < k_{U,unconditional}$, the same limits apply in combination with Equations (3.44) to (3.48). In this case, $R_{kU1} < R_{kU2}$, and so both $k_U \geq f(k_U)$ corresponding to Equation (3.45), and $k_U \leq f(k_U)$ corresponding to Equation (3.44) apply. Only one of Equations (3.44) and (3.45) must be satisfied – these two limits correspond to the two regions illustrated in Figure 3.21. If the same assumed unit stiffnesses of 5.41×10^4 kN/m per column of the concrete structure and 3836 kN/m per unit length of the CFS frame/OSB shear wall system are adopted, the k_U and k_L axes of Figure 3.21 can be normalized so that they are defined in terms of the required length of shear wall and the number of columns per storey, respectively. If normalized using these properties, Figure 3.21 can be transformed into Figure 3.22.

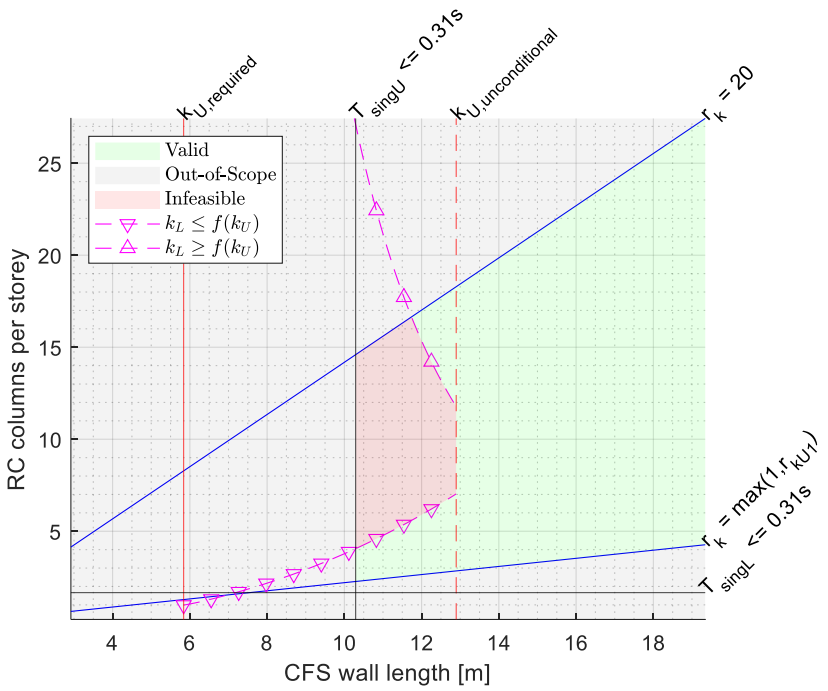

Figure 3.22: Graphical illustration of bounds on design stiffness k_U in terms of system properties

To give a specific example, consider if twelve metres of the shear wall are provided and five columns are provided per storey of the upper and lower structure, respectively. In practical terms, this does not imply that only five columns are used, only that the stiffness equivalent to five columns is provided. To suit the intended column arrangement, a larger number of less stiff columns could be used. Considering the assumed unit stiffness of 3836 kN/m/m for the shear wall and 5.41×10^4 kN/m per column for the moment-resisting frame, the corresponding stiffnesses are $k_U = 4.60\times10^4$ kN/m and $k_L = 2.71\times10^5$ kN/m. Therefore, $r_k = 5.88$, $R_k = 3.45$, $T_U = 0.65$ s and $\alpha_U = 1.41$ according to the proposed approximation given in Section 3.3.4. Considering the design criterion given by Equation (3.9):

$$\alpha_U = 1.41 \leq \frac{k_U \Delta_{\text{Ulim}}}{m_U N_U g S_a(T_U)} = \frac{\left(4.60 \times \frac{10^7 N}{m}\right)(0.0612\text{m})}{(96113kg)(3)\left(9.81\frac{N}{kg}\right)(0.656)} = 1.52 \qquad (3.60)$$

Given these inputs, the expected amplification is $\alpha_U = 1.41$, and the quotient on the right-hand side representing the maximum acceptable value of α_U is 1.52, so the design criterion is satisfied, and the design is feasible (at least insofar as $kU - k_L$ must also be checked if $k_U < k_{U,unconditional}$). This is

consistent with Figure 3.22 – the minimum k_U corresponds to a 10.5-metre shear wall length (approximately) – the assumed wall is 14% longer and stiffer, and the design criterion is satisfied by an extra 8%. The MRS-derived value of α_U is 1.19, and so the estimate is conservative. Now, because the selected k_U is less than $k_{U,unconditional}$, it is also necessary to confirm that the selection of k_L (equivalently, R_k) is valid, but per Figure 3.22 this requirement does not govern, so this calculation is omitted.

To consider a second configuration, if the shear wall is instead fourteen metres in length, the resulting stiffness $k_U = 5.37\times10^4$ kN/m. Assuming that the lower structure is unchanged, the new properties are $r_k = 5.05$, $Rk = 2.96$, $T_U = 0.60$ s and $\alpha_U = 1.30$ (versus the MRS-derived value of 1.14). The same calculation can be performed for the design criterion:

$$\alpha_U = 1.30 \leq \frac{k_U \Delta_{\mathrm{Ulim}}}{m_U N_U g S_a(T_U)} = \frac{\left(5.37 \times \frac{10^7 N}{m}\right)(0.0612\mathrm{m})}{(96113kg)(3)\left(9.81\frac{N}{kg}\right)(0.688)} = 1.69 \qquad (3.61)$$

As the stiffness ratio R_k has changed, so has the value of α_U. In this case, the margin between the provided resistance and the expected amplification is larger on account of the larger distance from the minimum k_U indicated in Figure 3.22. Likewise, k_U is greater than $k_{U,unconditional}$, and so k_L does not need to be checked, so long as r_k is between max(1, r_{kU1}) and 20. In fact, because k_U is greater than $k_{U,unconditional}$, it is reasonable to expect that the value of 1.69 is larger than any value of α_U on the R_k-α_U curve. Indeed, in this case, $\alpha_{U1} = 0.96$, $\alpha_{Umax} = 1.60$, and $\alpha_{U2stg} = 1.25$.

Case b) – Newly proposed method with 2.61x spectrum magnification

Following the same procedure as for case a), but for applying a 2.61 modification factor as done by Yuan (2016), the previous calculation can be repeated using the NBCC 2010 spectrum. The critical stiffness values are summarized in Table 3.15. Compared to Yuan (2016), the values are generally slightly lower but of similar magnitude. Given the variation between the definitions of α_U, it is reasonably expected that the values will be different, but their similarity suggests that the revised formulation performs adequately despite its simplifications. The values are most different for k_{U1} – this difference can be attributed to the changed form of R_{kU1}, which in some cases has significantly changed versus Yuan (2016). Other than that, some differences can be attributed to solving the numerical problem directly using $S_a(T)$ rather than the EXP-2 approximation.

Table 3.15: Comparison of critical stiffness values – Proposed versus Yuan (2016)

	Proposed	Yuan (2016)
k_{U1}	7.17×10^4 kN/m	1.21×10^5 kN/m
k_{Umax}	1.55×10^5 kN/m	1.79×10^5 kN/m
k_{U2stg}	1.08×10^5 kN/m	9.14×10^4 kN/m
$k_{U,required}$	7.17×10^4 kN/m	9.14×10^4 kN/m
$k_{U,unconditional}$	1.55×10^5 kN/m	1.79×10^5 kN/m

The resulting plot of the k_U-k_L relationship, normalized according to the assumed stiffness of each column and metre of the shear wall, is plotted in Figure 3.23 for both the newly proposed method and for the previous method (as illustrated by Yuan (2016)). For comparison, the dashed black lines superimposed on Figure 3.23a) indicate the extents of Figure 3.23b). It is immediately clear from this comparison that the scope of results illustrated varies between the two plots. Part of this is on account of physical limits applied by Yuan (2016) – whereas plot a) is scaled to suit the annotations being used and so that each of the limits defined in the formulation is clearly visible, Figure 3.23 b) is cut off at a value of 16 on the y-axis, i.e. the number of columns in the assumed frame. Correspondingly, the area illustrated by Yuan (2016) is not the theoretical one given by the formulation for k_U and k_L, but is truncated based on assumed practical limits on the two variables. The new plot instead shows the full theoretical space without restriction due to preconceived practical limits. This is ultimately up to the designer, as the number of columns and shear wall length (e.g.) are only proxies for the actual stiffness afforded by the specific systems – a larger column or stiffer shear wall would provide a larger unit stiffness. To plot the full theoretical space better illustrates where each of the limits is relative to each other – this is ambiguous in Yuan (2016).

Also significantly varying between Figure 3.23 a) and b) is the lower bound corresponding to $r_k = \max(r_{kU1},1)$. The value of R_{kU1} has changed from 2.59 in Yuan (2016) to 1.83 in the new proposal, and thus the slope of the lower bound on the scope is approximately only 70% of that corresponding to the previous definition. Likewise, the upper bound for shear wall lengths of < 37.21 m (presumably corresponding to $r_k = 20$) is significantly different between the Yuan (2016) plot and the new one. Yuan (2016) does not clearly distinguish what requirement imposes this upper bound. As it does not appear to correspond to $r_k = 20$, it is speculatively different from the new proposed plot on account of

the revised stiffness-amplification formulation and the abandonment of the EXP-2 approximation in the new proposed formulation.

Compared instead to Figure 3.22, Figure 3.23a) is of similar shape, with two key differences. The increased spectrum from Figure 3.22 to Figure 3.23a) has predictably shifted the lower bound on k_U and k_L (i.e. the shear wall length and the number of columns) upwards, as larger spectral accelerations reduce the limit on α_U characterized by Equation (3.9). At the same time, the lower bound on k_L for $k_U \leq k_{U,unconditional}$ has shifted due to the changed values of $S_a(T)$, and thus the value of k_L is restricted in Figure 3.23a) beyond those restrictions imposed by $k_{U,required}$ and r_k.

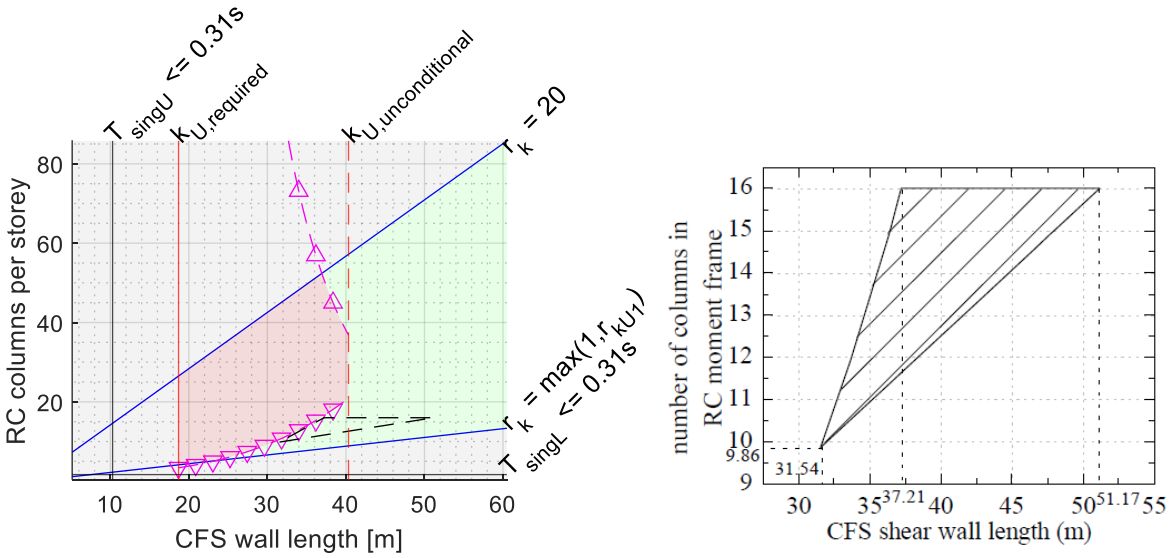

a) Newly proposed b) Appearing in Yuan (2016)

Figure 3.23: Graphical illustration of bounds on design stiffness k_U in terms of system properties

Case c) – Comparison of Yuan (2016) method – EXP-2 approximation of $S_a(T)$ versus direct numerical evaluation of $S_a(T)$

The final element of investigation for Example 3-2 is the aspect of the EXP-2 (exponential) approximation – is it necessary? Yuan (2016) argues that the EXP-2 approximation is necessary to determine the solution of each critical k_U numerically, rather than solving the problem by numerical solution of the k_U via the assumed definitions directly. Instead, the current study proposes to simply solve the provided functions (e.g. $S_a(T_U)$) numerically without transformation via the EXP-2

approximation. In other words, the solution for k_U can be found without the EXP-2 approximation via commonplace nonlinear solvers. Given that the EXP-2 approximation is calibrated only for the NBCC 2010 spectrum, the following procedure uses the NBCC 2010 spectrum with the 2.61 multiplier applied (Table 3.12). The Yuan (2016) formulation for α_U and the EXP-2 approximation are given in Appendix D.

As before, the input parameters m_U, N_U, etc. are given in Table 3.8. Using these input values, the values of R_{kU1}, R_{kU2}, R_{kU3} and R_{kU2stg} can be determined via Equations (D.11) to (D.14), and the counterpart values of r_k can be defined via Equation (3.19). The values of $\bar{\omega}_{1L}$ and $\bar{\omega}_{1U}$ are unchanged and are defined using Table 3.1. Thus, the values of R_k and r_k are:

Table 3.16: Critical stiffness ratio values – Yuan (2016)

Parameter	Value	Parameter	Value
r_{kU1}	4.41	R_{kU1}	2.59
r_{kU2}	9.47	R_{kU2}	5.56
r_{kU3}	12.88	R_{kU3}	7.56
r_{kU2stg}	81.44	R_{kU2stg}	47.79

Having defined the critical stiffness ratios, the corresponding key values of α_U can be determined via Equation (D.15) for α_{U1}, Equation (D.16) for α_{Umax}, and Equation (D.10) for α_{U2stg}. The solution for α_{U1} requires values α_{U11}, α_{U12} and x_3, and the solution for α_{Umax} requires values α_{Umax1}, α_{Umax2} and x_4.

The values of α_{U12} and α_{U12} are interpolated from Yuan (2016) Table 3.1, and α_{Umax1} and α_{Umax2} are interpolated from Yuan (2016) Table 5.1. These tables are provided in Appendix D. For other combinations of N_U, N_L and r_m, the values should be taken from Yuan (2016). The exponents x_3 and x_4, meanwhile, are defined by Equations (D.5) and (D.7). The values of these parameters used by Yuan (2016) are listed in Table 3.17. Also important are the fit parameters which define the EXP-2 approximation to the NBCC spectral acceleration curve. These equations are given incorrectly in Yuan (2016) – the corrected forms are given by Equations (D.21) to (D.23), and the correct values are given in Table 3.18.

Table 3.17: Critical values of α_U – Yuan (2016)

Parameter	Value	Parameter	Value
α_{U11}	1.169	α_{U12}	1.702
α_{Umax1}	1.661	α_{Umax2}	1.976
x_3	-0.850	x_4	-1.005
α_{U2stg}	1.100		

Table 3.18: EXP-2 fit parameters – Yuan (2016)

Parameter	Value	Parameter	Value
τ_1	-1.266	A_1	3.211
τ_2	-1.192	A_2	3.095
τ_3	-0.729	A_3	1.949
τ_4	-0.309	A_4	0.840
T_s'	0.213 s		

Having established the fit parameters, three different approaches are used to determine the stiffnesses k_{U1}, k_{Umax}, and k_{U2stg} corresponding to the Yuan (2016) formulation for α_U given by Equations (D.1) to (D.17). Given that this is for the NBCC formulation, α_{U1}, α_{Umax} and R_{kU2stg} are evaluated according to Equations (D.15), (D.16) and (D.17) instead of Equations (D.4), (D.6), (D.8), (D.9) and (D.14), which apply only to the ASCE formulation. The first approach is that given by Yuan (2016) – the fit parameters for the EXP-2 approximation are used to evaluate Equations (D.24) to (D.34), and the equations are solved using the tabulated values of y_i provided in Table D.4. Of the pieces of each piecewise equation, the correct one is which the result lies within the bounds related to that result. The second approach substitutes $S_a(T_U)$ with the EXP-2 approximation for $S_a(T_U)$ and evaluates the proper value of each k_U numerically as a function of k_U rather than using the fully expanded expressions given by Equations (D.24) to (D.34). This is possible because Equations (3.40) to (3.42) are derived from the design criterion regardless of the assumed form of α_U – the right-hand side of the functions can be numerically evaluated based on the relevant value of $S_a(T_U)$ and α_U directly, rather than by the transformations which produce the form provided by Yuan (2016). The

third approach is like the second, except that $S_a(T_U)$ is evaluated directly based on the definition given by NBCC 2010 rather than the EXP-2 approximation. The numerical results of these three analyses are provided in Table 3.19, and the corresponding graphical solution appears in Figure 3.24.

Table 3.19: Critical k_U as evaluated by different methods

Scenario	k_{aU1} [10^5 kN/m]	k_{aUmax} [10^5 kN/m]	k_{aU2stg} [10^5 kN/m]
Yuan (2016)	1.21	1.79	0.91
EXP-2	1.21	1.76	0.91
NBCC 2010	1.21	1.76	0.90

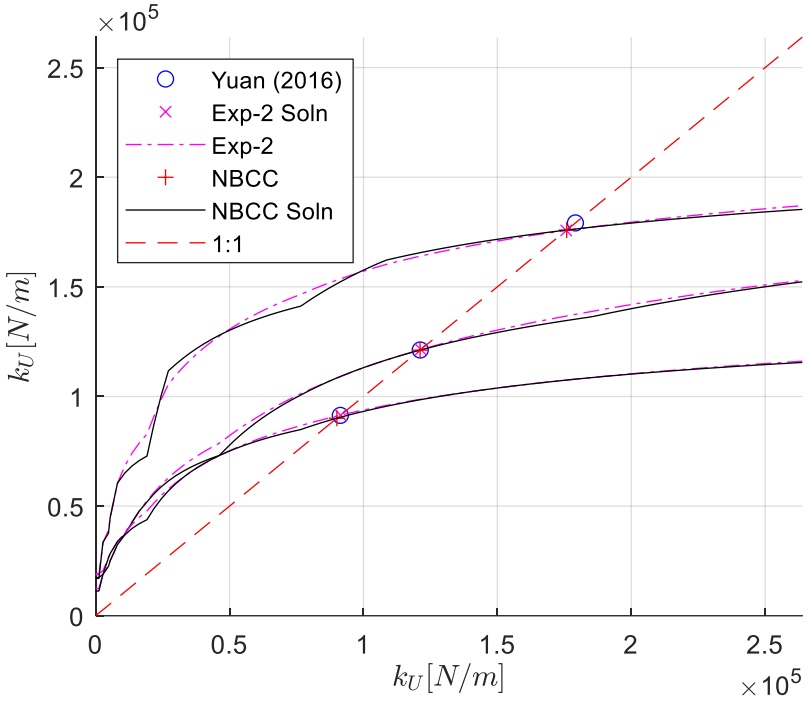

Figure 3.24: Graphical solution for critical stiffnesses k_U

Based on Table 3.19 and Figure 3.24, it is clear that the numerical solution of the critical values k_U can be done without the substitutions proposed by Yuan (2016). Specifically, while the EXP-2 formulation provides a smoother relationship between the input and output values of k_U for Equations (3.40) to (3.42), it provides no clear advantage over directly solving based on the code-specified form of $S_a(T)$. The form given by Yuan (2016) requires that a numerical solution takes place in addition to

several cumbersome substitutions and transformations – it is, therefore, advantageous to simply solve the relationships as-is rather than use the Yuan (2016) transformations.

3.8 Conclusions

This chapter presents two key elements of the newly-proposed design approach – the approximation for the amplification factor α_U and the base shear of the upper structure, and the permissible storey stiffnesses that satisfy the NBCC 2015 interstorey drift requirement. The method applies to a wide variety of mid-rise structures with a vertical combination of framing systems and explicitly characterizes the impact of the mass and stiffness irregularity unlike both ASCE 7-10/16 (2010, 2017) and NBCC 2010/2015 (NRCC, 2010, 2015c). Much of the derivational framework underlying those methods proposed by Yuan & Xu is preserved; however, many changes have been made to the methods to streamline their execution and expand their scope.

First and foremost, the newly proposed method is based on NBCC 2015, not ASCE 7 or NBCC 2010. Accordingly, the exponential and power approximations to the NBCC 2010 spectrum proposed by Yuan (2016) are abandoned and replaced by a direct numerical or graphical solution using the NBCC 2015 spectrum. Concurrently, the scope of the methods is also expanded to apply to up to twelve storeys as opposed to only ten, and the maximum storey mass ratio is now five as opposed to three. The scope vis-à-vis the stiffness ratio or the single-storey period is unchanged.

As before, R_m, R_k and $S_a(T)$ are the primary variables defining the approximation of α_U, and the following conclusions apply:

1. The overall mass and stiffness ratios R_m and R_k are introduced along with the 2DOF model to characterize the relative importance of the upper and lower structures. R_m and $R_k = 1$ do not correspond to regularity in the traditional sense – they are a function of the storey count and reflect instead the relative mass and stiffness of the two structures.

2. As R_k increases from below one, α_U generally first increases towards a global maximum at some value of R_k between R_{kU2} and R_{kU3}. Following this maximum, α_U typically decreases as R_k continues to increase towards R_{kU2stg}, beyond which it maintains a constant value, typically modestly larger than one. In theoretical terms, α_U approaches zero as R_k approaches zero, and one as R_k approaches infinity, but in more practical terms, α_U is often at least one. The maximum practical value of α_U for structures within the scope will not generally be larger than 2.5-2.75 or so.

3. The proposed approximation for α_U mirrors that of Yuan (2016) and is based on four critical stiffness ratios R_k and three critical stiffness values α_U. Many of the definitions are changed to facilitate their use with NBCC 2015. Nonetheless, the proposed approximation of α_U demonstrates improved performance compared to the Yuan (2016) definition, both by direct numerical solution and by the EXP-2 approximation. For the Yuan (2016) scope, the newly-proposed approximation typically overestimates α_U by 1% to 24% (median: 13%), compared to 3% to 26% (median: 15%) for the Yuan (2016) procedure. For the expanded scope, the error is typically between 2% and 27%. In rare scenarios within the expanded scope, α_U may be underestimated by 5% or overestimated by 60%.
4. Both a graphical and a numerical solution are proposed to be used to determine feasible stiffness distributions. The EXP-2 and other approximations of $S_a(T)$ proposed by Yuan (2016) are abandoned in favour of a direct solution, resulting in a streamlined and more concise formulation.
5. The proposed approach to determine feasible stiffness distributions is demonstrated in two examples, the latter of which also considers the methods proposed by Yuan (2016).

Despite the proposed approach, some aspects need to be clarified by future research. The effect of stiffness variation on α_U should be investigated, as should the appropriateness of the 2.61 modifier that Yuan (2016) suggests should be applied to spectral accelerations. These are the main two points, in addition to a nonlinear investigation, but expanding the scope is another possibility for future work.

Chapter 4
Equivalent Static Loads on Vertically Irregular Structures

4.1 Introduction

This chapter concerns the determination of equivalent static loads on a mid-rise structure with a vertical combination of framing systems. Both ASCE 7 and NBCC 2015 do not capture the effect of vertical irregularity, and so two methods are proposed following a discussion of the NBCC 2015 equivalent static force procedure:

1. A method applicable to appendage structures (one-storey upper structure) is proposed based on an analogous method proposed by Yuan (2016). The proposed method is defined for the expanded scope and does not include the stiffness ratio requirement previously adopted by Yuan (2016).
2. A more general method applicable to structures having a multistorey upper structure is proposed, incorporating elements from both NBCC 2015 (NRCC, 2015c) and ASCE 7-16 (2017). This method extends the concept of α_U to the top storey of α_U to the top storey of the upper structure and modifies the upper structure's force distribution accordingly.

Two examples are given to demonstrate the newly proposed methods. The two-stage procedure proposed by Yuan (2016), is given in Appendix F for comparison.

4.2 The NBCC 2015 Equivalent Static Force Procedure

Notwithstanding that modal response spectrum analysis (or other dynamic analysis) is recommended by NBCC 2015 for mid-rise irregular structures, linear elastic static analysis continues to have a place in the design of such structures. Part of this role is mandated by NBCC 2015 itself, for the minimum dynamic base shear is set to be a fixed percentage of the base shear determined by the Equivalent Static Force Procedure (ESFP) (NRCC, 2015c). This percentage varies based on whether the structure is regular or irregular – if irregular, the dynamic base shear must be at least that predicted by the ESFP, and if regular 80% of the ESFP base shear is the minimum. Therefore, even for structures for which the higher modes may counteract the first mode, the static estimate is used as a conservative baseline. Thus, the static response via the ESFP is an inescapable element of NBCC 2015's dynamic analysis, even if only insofar as the base shear. Per NBCC 2015, the static base shear V is evaluated according to the following form:

$$V = \frac{S_a(T_1)M_v I_E W}{R_d R_o} \tag{4.1}$$

where $S_a(T_1)$ is the spectral acceleration acting at the first mode period T_1, M_V is the higher mode factor defined in Equation (3.2), I_E is the importance factor (= 1 for most structures), W is the total structural weight, and R_d and R_o are the inelastic modification factors for ductility and overstrength, respectively. Now, strictly speaking, $S_a(T_1)$ is replaced by $S(T_a)$ in NBCC 2015, but this study neglects the effect of the site soil conditions, and thus $S_a(T_1)$ is used instead. Likewise, T_1 is used in place of T_a. T_a is the preferred nomenclature used by NBCC 2015. The maximum limits on T_a specified by the NBCC are not enforced.

For reference elsewhere, the values of M_v given by NBCC 2015 corresponding to the *other systems* archetype (the most severe/general) are provided in Table 4.1, subject to some caveats. Firstly, $S(0.2)/S(5.0)$ and T_a, the nomenclature used by NBCC 2015, are swapped with $S_a(0.2)/S_a(5.0)$ and T (T_1, T_U, etc) – because it is assumed that the soil is class C and because the theoretical rather than code-specified empirical periods are used, these substitutions match what is used in this thesis. Furthermore, per NBCC 2015, M_v is to be interpolated for $S_a(0.2)/S_a(5.0)$ and T. However, for the period, the product $S(T)M_v$ is to be interpolated rather than only M_v. Finally, the values for $T \geq 5$ seconds are taken as equal to those for 2.0 seconds based on NBCC 2015 – ideally, the NBCC itself should be consulted for periods longer than 2.0 seconds to ensure that the correct values are being used.

Table 4.1: NBCC 2015 higher mode factor M_v – Other Systems (NRCC, 2015c)

$S_a(0.2)/S_a(5.0)$	$T \leq 0.5$	$T = 1.0$	$T = 2.0$	$T \geq 5.0$
5	1	1	1	1
20	1	1	1.18	1.18
40	1	1.19	1.75	1.75
65	1	1.55	2.25	2.25

Note that V as defined by Equation (4.1) alone is not the static base shear – the NBCC's ESFP specifies a lower and/or upper bound based on the structural system and other requirements. The most general of these requirements applies to moment-resisting frames, braced frames and other systems

not otherwise classified by NBCC 2015, and defines a minimum base shear based on the spectral value at 2 seconds:

$$V \geq \frac{S_a(2.0)M_v I_E W}{R_d R_o} \tag{4.2}$$

The above is henceforth referred to as the code-specified minimum base shear and is the most stringent of the requirements on V imposed by the NBCC. There is a different, lower requirement based on *S(4.0)* for walls, coupled walls, and wall-frame systems, and a further relaxed requirement for certain structures, but Equation (4.2) is the most severe and generally applicable.

In general, this is the extent of the ESFP – except for the design base shear, the remainder of the analysis should be done dynamically. For some structures, however, the ESFP applies. Namely, if any of the following are true, then the ESFP is considered appropriate for the full analysis:

1. $I_E F_a S_a(0.2) < 0.35$, ($I_E F_a = 1$ for/ the current study, i.e. site class C, normal importance), or:
2. The structure is regular, less than 60 metres in height, and has $T_1 < 2$ seconds in both orthogonal axes, or:
3. The structure has specific types of irregularity (including vertical stiffness, mass and geometric irregularity), is less than 20 metres in height and has $T_1 < 0.5$ seconds in both orthogonal axes

Notwithstanding the ambiguous nature of the irregularity limits as discussed in Chapter 2, the general premise of these limitations is sound. An increase in the height, degree of irregularity or the fundamental period is associated with a more complex and nuanced dynamic analysis, and so in general it is reasonable to apply dynamic analysis for taller, more flexible and more irregular structures. On the other hand, designers will inevitably refer to the storey shears determined from the ESFP as a baseline for any dynamic analysis. Dynamic analysis is inherently variable on account of the assumptions vis-à-vis stiffness, mass and other system properties, and therefore it can be helpful to compare the assumed static response to that predicted by dynamic analysis.

The default NBCC 2015 (NRCC, 2015c) force distribution used by the ESFP is defined by Equation (4.3) and consists of two components :

1. To account for higher mode effects, a portion of the base shear V is applied to the top storey as the top storey shear F_t. F_t does not change the total shear, but increases the top storey shear for

longer periods to account for higher mode effects. It is defined by Equation (4.4) as a function of the first mode period T_1.

2. The remaining shear, V - F_t, is applied at each storey x as storey force F_x according to the product of storey weight W_x and storey height (from the ground level) h_x, normalized by the sum of the weight W_i and height h_i for all n storeys in the structure.

$$F_x = (V - F_t)\frac{W_x h_x}{\sum_{i=1}^{n} W_i h_i} \tag{4.3}$$

$$F_t = \begin{cases} 0 & T_1 \leq 0.7 \\ 0.07 T_1 V & 0.7 < T_1 < 3.6 \\ 0.25V & 3.6 \leq T_1 \end{cases} \tag{4.4}$$

The form of Equation (4.3) is traditional for North American building codes and standards and appears similarly in both ASCE 7 (2010, 2017), FEMA P-695 (2009a), and elsewhere. It appears in NBCC-related documents as far back as Ward (1966) and is largely unchanged but for the addition of F_t and changes to V. In any case, the key assumptions of Equation (4.4) are that the first mode shape is linear, and thus that the storey forces increase proportionally to their height, and that the total mass, rather than the effective mass acting in the first mode, is used (NRCC, 2015c, NRCC, 2015b). This simplification generally results in an underestimation of higher-mode effects and an overestimation of the first-mode effective masses and performs best for relatively short, stiff and regular structures (Humar & Mahgoub, 2003; Rosenblueth et al., 1980). For longer periods, the NBCC's top storey shear, inherited from UBC 1997 (ICBO, 1997), attempts to counteract increased higher mode effects. To address the same problem, ASCE 7 (2017) applies an exponent to the storey heights instead.

Regardless, the goal of such methods is not to exactly match the expected force distribution but is to conservatively approximate the envelope of such effects (NRCC, 2015b; Rosenblueth et al., 1980). The commentary to the NBCC provides little detail on the extent of the overestimate expected from static analysis compared to dynamic analysis. What then, is the expected performance of the NBCC 2015 ESFP applied to regular structures, to which it presumably performs best? The following subsection addresses this, for it is meaningless to propose a new static method without an understanding of the inherent margins in the currently accepted NBCC 2015 ESFP. The comparison of the NBCC 2015 ESFP for irregular structures is made in forthcoming sections alongside the newly proposed methods.

4.2.1 Regular structures

Insofar as irregularity of stiffness and mass, podium structures designed according to NBCC 2015 (NRCC, 2015c) are considered to be regular if the stiffness of each of the upper storeys is no less than 80% than those in the lower structure, and if the mass of each storey of the lower structure is no more than 150% of those in the upper structure, i.e. $r_k \leq 1.25$ and $r_m \leq 1.5$. That is, assuming each of the lower and upper structures is uniform. The NBCC compares adjacent storeys and so strictly speaking a larger maximum mass and stiffness ratio is possibly considered regular if adjacent storeys satisfy the prescribed limits – this storey-by-storey variation is common in realistic structures. This aside, a regular structure can be analyzed by the ESFP if it is less than 60 metres tall and has a first mode period of 2 seconds or less, or if the spectral acceleration is sufficiently low. For this study, the total height will never exceed 60 metres, and I_E and F_a are both assumed to be unity, and so the ESFP applies to a regular structure if $T_1 < 2$ seconds or if $S_a(0.2) < 0.35$.

As for the performance of regular structures meeting these criteria, the NBCC 2015 commentary implies no range of error. To determine such a range, results corresponding to the ESFP and modal response spectrum methods are computed for $1 \leq r_k \leq 1.25$ and $1 \leq r_m \leq 1.5$ (assuming the upper and lower structures are uniform), with all other variables varied according to the scope of the current study. This is subject to two caveats. First, the assumed range on r_k is assumed to override $R_k \geq R_{kU1}$, as $R_k \geq R_{kU1}$ is not generally true for regular structures. Secondly, the period used to calculate the results for the ESFP is the theoretical period rather than that dictated by NBCC 2015, to ensure that it is consistent with the computed modal response spectrum results. However, the code-specified minimum base shear given in Equation (4.2) is still applied, as is the top storey shear given by Equation (4.4).

Considering each combination of variables as a separate structure, Figure 4.1 summarizes the most severe overestimate across all the storeys for each. As before, a negative value indicates that the NBCC distribution underestimates the MRS results and a positive value corresponds to an overestimate. But for these regular structures the NBCC is always conservative – as apparent in Table 4.2, the NBCC generally overestimates the regular structure's storey shears by at least 5% for the selected regular structures. There are therefore only ever overestimates.

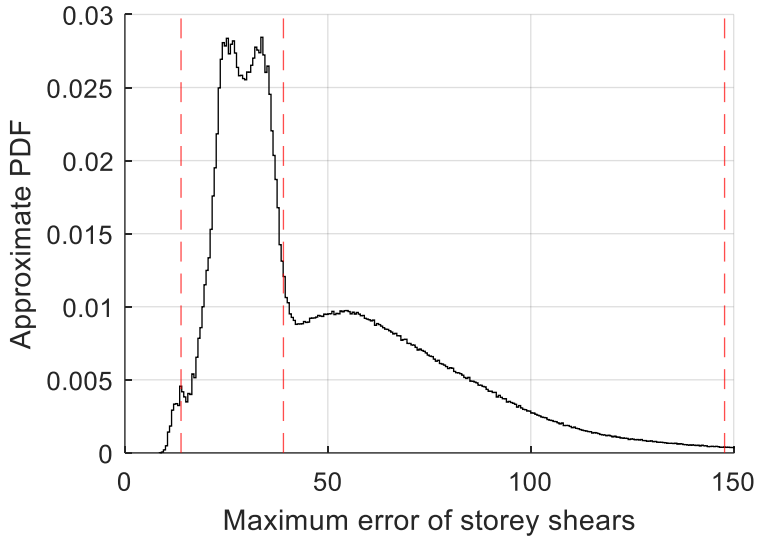

Figure 4.1: Maximum overestimate associated with NBCC 2015 ESFP

Specifically, considering each set of inputs as representing a different structure, Figure 4.1 illustrates the maximum error across all the storeys of that structure, evaluated as:

$$Error = \max\left(\frac{\mathrm{V_{approx}} - \mathrm{V_{MRS}}}{\mathrm{V_{MRS}}} \times 100\right) \tag{4.5}$$

where V_{approx} is the value of the storey shear at a given storey estimated by the NBCC 2015 ESFP, and V_{MRS} is the storey shear estimated by the MDOF model and MRS analysis. This is evaluated at each storey, and the maximum value of all the storeys is the value summarized in Figure 4.1.

Categorically, the NBCC does not underestimate the storey shears as applied to regular mid-rise structures. Most typically, the NBCC overestimates storey shears by at least 10-15%. This much is expected, given the overestimation of first-mode effective masses and the predominance of first-mode effects for regular structures. However, as evident from Figure 4.1, this conservatism does not imply that the distribution is accurate. The red lines on Figure 4.1 indicate the 1st percentile, median and 99th percentile values of the overestimate for the approximately three million different combinations that appear in Figure 4.1. While the method is modestly conservative much of the time, under some circumstances the ESFP predicts storey shears as much as an additional 150% above the value predicted via MRS analysis. This is particularly true of taller structures, and generally is worst at the base shear of the structure, but altogether implies that the NBCC is content with a potentially large overestimate of the storey shears if it is conservative. In more specific terms, the results as a function

of N_U and N_L are summarized in Table 4.2 and Table 4.3. Note that these tables and the preceding figures do not incorporate any storey-wise variation of properties, only variation between the upper and lower structures enumerated by N_U and N_L.

It is not unreasonable to expect that the mismatch between the NBCC ESFP and the MRS analysis results is largest for structures that are tall (i.e. larger $N_U + N_L$) - particularly at the base of the structure - for three reasons. First, the NBCC ESFP intentionally overestimates the actual effective modal mass attributed to the first mode by using the full mass of the structure rather than the effective mass (NRCC, 2015c; Rosenblueth et al., 1980). Rosenbluth et al. (1980) assert that the first mode mass is typically 60-80% of the total mass, and thus the default base shear is much larger than that predicted for regular structures via MRS analysis. Accordingly, the NBCC permits that a base shear as low as 80% of the static value may be used as the base shear for dynamic analysis of regular structures. Furthermore, taller structures have longer periods than shorter ones, and thus the top storey shear and the higher mode factor M_v are increased relative to a structure having fewer storeys but identical storey properties. These factors are introduced to account for higher-mode effects at the top of the structure that might cause shears in the upper storeys to be underestimated, but they also increase the storey shear throughout the structure – particularly for M_v, which magnifies the total base shear. Finally, on a related note, the effects of higher modes are more significant in taller structures, especially the second mode. Considering a typical mode shape for the second mode of a uniform structure, it is often the case that the second mode increases the storey shears in the top storeys and reduces the total shears nearer to the base of the structure relative to the first mode shears – numerous examples are provided by Chopra (2012). But the ESFP assumes a first-mode response, thus neglecting the reduction that the second mode may provide to the base shear. The result is a distribution that is consistently conservative for regular structures but nonetheless may be quite conservative at the base of the structure.

Table 4.2: Minimum overestimate for shear – NBCC 2015 ESFP, regular structure

N_U \ N_L	1	2	3	4	5	6	7	8	9	10	11
1	3.7%	7.1%	8.6%	9.3%	9.1%	9.3%	9.2%	9.3%	9.9%	10.2%	10.2%
2	7.9%	9.1%	9.0%	8.8%	9.0%	8.9%	8.7%	8.7%	8.5%	9.1%	N/A
3	9.4%	8.9%	9.0%	8.9%	9.3%	8.9%	8.7%	8.6%	8.6%	N/A	N/A
4	9.4%	8.6%	8.5%	9.0%	8.7%	8.6%	8.7%	9.2%	N/A	N/A	N/A
5	10.2%	9.2%	8.6%	8.3%	8.3%	8.5%	9.1%	N/A	N/A	N/A	N/A
6	10.1%	8.5%	9.4%	9.5%	8.3%	8.9%	N/A	N/A	N/A	N/A	N/A
7	10.7%	9.5%	9.3%	9.7%	8.6%	N/A	N/A	N/A	N/A	N/A	N/A
8	10.4%	9.6%	9.7%	8.3%	N/A	N/A	N/A	N/A	N/A	N/A	N/A
9	10.4%	10.1%	10.3%	N/A	N/A	N/A	N/A	N/A	N/A	N/A	N/A
10	10.9%	10.9%	N/A	N/A	N/A	N/A	N/A	N/A	N/A	N/A	N/A
11	11.8%	N/A	N/A	N/A	N/A	N/A	N/A	N/A	N/A	N/A	N/A

Table 4.3: Maximum overestimate for shear – NBCC 2015 ESFP, regular structure

N_U \ N_L	1	2	3	4	5	6	7	8	9	10	11
1	17.7%	34.4%	50.0%	65.8%	85.7%	101.5%	119.2%	158.5%	209.4%	267.9%	338.8%
2	31.1%	47.7%	62.0%	80.2%	94.1%	108.7%	138.0%	183.7%	235.9%	298.9%	N/A
3	42.5%	59.6%	78.9%	93.3%	107.9%	129.9%	172.8%	222.0%	281.6%	N/A	N/A
4	58.2%	72.9%	89.1%	105.2%	123.4%	162.6%	210.0%	266.9%	N/A	N/A	N/A
5	67.8%	83.4%	99.7%	118.5%	152.4%	198.9%	253.4%	N/A	N/A	N/A	N/A
6	78.7%	94.9%	117.6%	141.4%	187.3%	240.2%	N/A	N/A	N/A	N/A	N/A
7	91.9%	115.0%	139.3%	175.6%	225.6%	N/A	N/A	N/A	N/A	N/A	N/A
8	110.8%	136.8%	162.8%	212.0%	N/A	N/A	N/A	N/A	N/A	N/A	N/A
9	132.2%	151.5%	197.3%	N/A	N/A	N/A	N/A	N/A	N/A	N/A	N/A
10	147.0%	183.2%	N/A	N/A	N/A	N/A	N/A	N/A	N/A	N/A	N/A
11	177.7%	N/A	N/A	N/A	N/A	N/A	N/A	N/A	N/A	N/A	N/A

Considering Table 4.2, the minimum error is generally 10% or so, regardless of the number of storeys, and so the NBCC ESFP is effective at providing a conservative estimate of the storey shears, even for structures where $T_1 > 2$ s. Conversely, Table 4.3 indicates that the maximum error is most severe for taller structures. This effect only modestly varies as a function of N_U and N_L – the tolerable irregularities for a structure to remain regular only modestly change the maximum and minimum error. For practical purposes, the maximum error is generally smaller than that given by Table 4.3 (as is clear from Figure 4.1 b)), for Table 4.3 represents only the most severe case for each N_U and N_L. Nonetheless, this maximum error can be attributed to several factors. For example, severely high overestimates can be partially attributed to the imposition of the strictest possible code minimum

shear per Equation (4.2) and the conservatism inherent in the higher mode factor M_v. For small periods in particular, M_v intentionally overestimates the effects of higher modes on regular structure (Humar & Mahgoub, 2003; NRCC, 2015b)

Most important is the period T_1. The fundamental period is associated throughout the ESFP via M_v, F_t, $S_a(T)$ and elsewhere, and thus has a significant impact on the value of the error. Specifically, constraining T_1 to 2 seconds as done by the NBCC for use of ESFP does not significantly change the distribution of Figure 4.1 nor the values of the minimum error (Table 4.2), but lowers the maximum value of the error (Table 4.3). If $T_1 < 2$ seconds is enforced, the maximum error is as much as 100% lower for some combinations, albeit only where the scope limitation of $T_{singU} \leq 0.31$ seconds permits $T_1 \geq 2$ seconds to be possible. The values associated with this restriction are given in Table 4.4.

Table 4.4: Maximum error for Shear – NBCC 2015 ESFP, regular structure, $T_1 < 2$ s

N_U \ N_L	1	2	3	4	5	6	7	8	9	10	11
1	17.7%	34.4%	50.0%	65.8%	85.7%	101.5%	119.2%	131.8%	144.4%	158.7%	171.4%
2	31.1%	47.7%	62.0%	80.2%	94.1%	108.7%	125.1%	138.2%	149.5%	162.7%	N/A
3	42.5%	59.6%	78.9%	93.3%	107.9%	122.4%	133.7%	145.1%	158.7%	N/A	N/A
4	58.2%	72.9%	89.1%	105.2%	119.8%	127.6%	142.0%	155.4%	N/A	N/A	N/A
5	67.8%	83.4%	99.7%	118.5%	125.8%	136.0%	149.5%	N/A	N/A	N/A	N/A
6	78.7%	94.9%	117.6%	129.3%	133.0%	147.0%	N/A	N/A	N/A	N/A	N/A
7	91.9%	115.0%	132.4%	131.3%	141.0%	N/A	N/A	N/A	N/A	N/A	N/A
8	110.8%	130.6%	133.6%	136.0%	N/A	N/A	N/A	N/A	N/A	N/A	N/A
9	126.7%	129.8%	133.3%	N/A	N/A	N/A	N/A	N/A	N/A	N/A	N/A
10	122.4%	131.3%	N/A	N/A	N/A	N/A	N/A	N/A	N/A	N/A	N/A
11	123.9%	N/A	N/A	N/A	N/A	N/A	N/A	N/A	N/A	N/A	N/A

In general, both the maximum and minimum error values increase as both T_1 and $S_a(0.2)/S_a(5.0)$ increase, as suggested by M_v and the NBCC 2015 commentary.

Altogether, the NBCC 2015 ESFP is therefore typically effective and conservative at estimating the force distribution of regular structures, albeit at times severely overestimating some storey shears. This is true regardless of the number of storeys, although the maximum error increases as the number of storeys (i.e. the height) of the structure increases, the period lengthens, of the ratio $S_a(0.2)/S_a(5.0)$ increases. The consideration or omission of the code minimum shear or the limit $T_1 < 2$ changes the maximum value of the error but does not change the overarching distribution of error given in Figure 4.1 appreciably for the structures considered.

4.3 Using α_U to estimate the upper base shear on an irregular structure

Recalling Equation (3.4), α_U explicitly relates the first mode shear at the base of the upper structure, $m_U N_U g S_a(T_U)$ to the higher mode shear at the base of the upper structure, V_{Ub}. It follows, therefore, that if a conservative approximation for α_U is established based on the MDOF value of α_U, that this conservative approximation can be used in reverse to estimate the base shear V_{Ub} acting on the upper structure independently of that at the base of the lower structure, in the same manner as M_v is applied in NBCC 2015 If the first mode shear is scaled by α_U and the error relative to the modal response spectrum results are calculated for each combination of inputs in the scope, the resulting distribution of error is that of Figure 4.2.

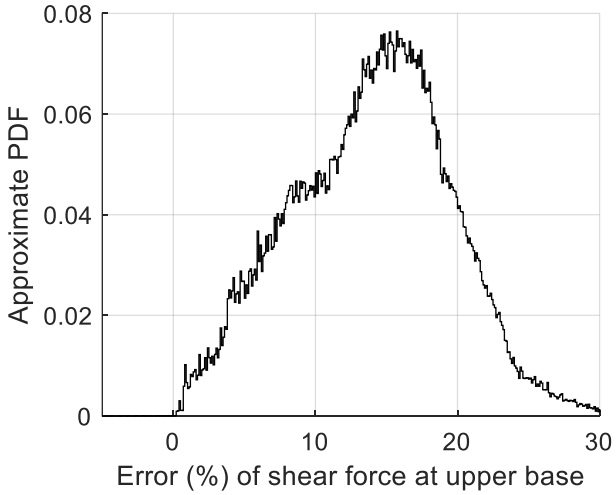

Figure 4.2: Error at base of upper structure using α_U to scale the first-mode shear

Figure 4.2 is essentially identical to the part of Figure 3.11 corresponding to the expanded scope. As α_U specifically relates $m_U N_U g S_a(T_U)$ to V_{Ub}, the error between the estimate of α_U and the α_U calculated from the MDOF model via MRS is by definition equivalent to the error between $m_U N_U g S_a(T_U)$ and V_{Ub}. α_U therefore can be used to well-approximate the base shear considering higher mode effects.

4.4 Appendage structures

It is generally understood that structures having a relatively lightweight appendage structure ($N_U = 1$) atop a much stiffer and more massive lower structure behave largely as a more regular structure does. This is recognized by NBCC 2015 (NRCC, 2015c) and other codes, which typically provide

exceptions for lightweight roof structures and penthouses. After all, one significant concern for irregular structures is the shifting of effective modal mass from the first to higher modes, complicating the analysis and causing higher-than-expected loads in the upper structure. Given that such appendage structures generally constitute only a modest proportion of the mass for a lightweight appendage storey, their effect on the effective modal masses is itself minor. As articulated by Yuan (2016), the premise of such an assumption is that the lower structure can be treated as an independent structure dominated in the first mode.

This does not, however, imply that the ESFP given by NBCC 2015 (NRCC, 2015c) can be immediately applied. Past research suggests that appendage structures are prone to larger-than-expected shears in the appendage which may cause larger damage than elsewhere in the structure (Blume et al., 1960; Penzien & Chopra, 1965; Skinner et al., 1965). This effect is based on the relative stiffness and mass of the appendage and lower structures and is referred to as a *whipping effect* by some authors. This effect was observed by Sexton & Keith (1965) in the aftermath of the 1960 Chile and 1964 Anchorage earthquakes - they note that some appendages failed despite only minor damage to the supporting structures. This amplification of the base shears of the appendage is captured by α_U, and Yuan (2016) proposes that the base shear of the appendage structure be evaluated by Equation (3.7), i.e. that the upper structure's first mode base shear should be scaled by α_U.

4.4.1 The Yuan (2016) modified equivalent lateral force method

These observations are the basis of the modified equivalent lateral load method proposed by Yuan (2016). In this method, it is assumed that the lightweight appendage has minimal effect on the lower structure, and thus the base shear of the lower structure, V_{Lb}, can be evaluated according to the ASCE 7 equivalent lateral load method, i.e. according to the first mode response of the structure:

$$V_{Lb} = (\mathrm{M_L} + \mathrm{M_U})\mathrm{S_a}(\mathrm{T_1}) \tag{4.6}$$

Except for the appendage, which is evaluated using α_U and Equation (3.7), the storey forces F_x are evaluated conventionally based on the static load distribution assumed by ASCE 7 (2010, 2017), using $V = V_{Lb}$ as the base shear:

$$F_x = V\frac{W_x h_x^k}{\sum_{i=1}^{n} W_i h_i^k} \tag{4.7}$$

The ASCE 7 force distribution is identical to that given by NBCC 2015 in Equation (4.3), except that there is no top storey force F_t. Instead, ASCE 7 specifies an exponent k which modifies the

assumed mode shape according to the period to account for higher modes. This exponent is defined by Equation (4.7):

$$k = \begin{cases} 1 & T_1 \leq 0.5 \\ 1 + \dfrac{2-1}{(2.5-0.5)}(T_1 - 0.5) & 0.5 < T_1 < 2.5 \\ 2 & 2.5 \leq T_1 \end{cases} \tag{4.8}$$

As applied to NBCC 2010 rather than ASCE 7, the Yuan (2016) procedure is identical, except that the base shear and force distribution are evaluated according to their NBCC counterparts. Namely, Equations (4.3) and (4.4) for the force distribution, and the default NBCC 2010 $S_a(T)$. However, Yuan (2016) suggests $M_v = 0$, given that higher mode effects are expected to be small. The resulting force distributions are therefore defined by Equation (4.9) for ASCE 7, and Equation (4.10) for NBCC 2010:

$$F_x = \begin{cases} \alpha_U M_U \mathrm{S_a(T_U)} & x = N_U + N_L \\ V_{Lb} \dfrac{W_x h_x^k}{\sum_{i=1}^{n} W_i h_i^k} & x \leq N_L \end{cases} \tag{4.9}$$

$$F_x = \begin{cases} \alpha_U M_U \mathrm{S_a(T_U)} & x = N_U + N_L \\ (V_{Lb} - F_t) \dfrac{W_x h_x}{\sum_{i=1}^{n} W_i h_i} + F_t & x = N_L \\ (V_{Lb} - F_t) \dfrac{W_x h_x}{\sum_{i=1}^{n} W_i h_i} & x \leq N_L \end{cases} \tag{4.10}$$

However, the modified equivalent lateral force procedure proposed by Yuan (2016) is not permitted to be applied to any appendage structure – it is assumed to apply only for values of the overall stiffness ratio such that $R_k \leq R_{kb1}$. R_{kb1} is the overall stiffness at which the effective modal mass associated with the first mode is equal to 90% of the total structural mass, and is defined as follows:

$$R_{kb1} = \begin{cases} 0.386R_m + 1.1 & 1 \leq R_m \leq 2 \\ 0.65R_m + 0.58 & R_m > 2 \end{cases} \tag{4.11}$$

The threshold of 90% of the total mass is commonly used in dynamic analyses to demonstrate that the number of considered modes is adequate to represent the structural response. Yuan (2016) derives the limit of R_{kb1} by identifying the R_k associated with the ratio of the effective modal mass in the first mode M_1^* to the total mass $M_U + M_L$. These parameters are defined according to Equations (A.16), (3.10) and (3.12).

4.4.2 Newly proposed method to evaluate appendage structures

However, the procedure proposed by Yuan (2016) has room for improvement. It is expected that the upper structure's base shear is well-approximated by α_U and Equation (3.7) and that the lower structure is well-approximated by the NBCC 2015 ESFP. Presupposing then that the top and bottom storey shears are well-approximated, the restriction on R_{kb1} is unnecessarily strict – so long as the assumed loads are conservative, there is no need to enforce that 90% of the total mass is effective in the first mode. The 90% threshold itself is somewhat suspect according to some researchers (Dhileep et al., 2019), and therefore the proposed method eschews R_{kb1} as a requirement for appendage structures.

Notwithstanding R_{kb1}, the procedure is similar to that proposed by Yuan (2016). The upper base shear is evaluated via Equation (3.7), as before, and the lower base shear is evaluated according to the code-specified first-mode base shear. Despite this, the new assumed definition of the lower base shear is slightly different than that of Yuan (2016). Yuan (2016) assumes that the base shear of the lower structure is evaluated by the first mode response of the full structure without higher-mode effects. Instead, the newly proposed procedure assumes that the lower structure and upper structure are to be evaluated separately and combined in a manner more like that of the two-stage procedure. Namely, it is assumed that V_{Lb} is instead defined as:

$$V_{Lb} = \alpha_U M_U g \mathrm{S_a}(\mathrm{T_U}) + M_v M_L g S_a(T_L) = V_{Ub} + M_v M_L g S_a(T_L) \tag{4.12}$$

The first term of Equation (4.12) corresponds to the base shear of the upper structure as defined by α_U and Equation (3.7), and the second term corresponds to the first mode response of the lower structure only. Unlike Yuan (2016), the lower structure incorporates the higher mode factor M_v and is evaluated at its period T_L rather than the period of the combined upper and lower structure, T_1. As T_L is less than T_1, this slightly increases the associated spectral value, but this change will generally be small owing to the minor contribution of the upper structure. For consistency with NBCC 2015, it is assumed that the contribution corresponding to the lower structure, $M_v M_L S_a(T_L)$ is not less than the code-specified minimum base shear dictated by Equation (4.2).

Equation (4.12) is based on a different philosophy than the base shear given by Equation (4.6). Yuan (2016) assumes that the upper and lower structures act as a larger whole, with the upper base shear being corrected via α_U but the structure otherwise acting according to the equivalent static force procedure. Meanwhile, the new proposal is more akin to the two-stage procedure, in which the two

structures are analyzed independently. It is not true that the upper structure is independent of the lower structure, but because α_U well-approximates the shear on the upper structure it can be separated from the lower structure and applied as a top storey shear. For the lower structure, because the upper structure has only a minor contribution, it can be applied after the evaluation of the lower structure alone analogously to F_t. This rearrangement is a contrivance that nonetheless allows the contributions of the lower and upper structures to be distinguished. Whereas Yuan (2016) treats the upper and lower structure as two parts of a whole, the proposed method assumes that the appendage's base shear is additive to, rather than part of, the lower base shear. This is strictly a matter of interpretation – the Yuan (2016) approach to define the lower base shear is likely equally effective.

Considering this alternative paradigm, the storey forces are distributed differently than in Yuan (2016). Unlike Yuan (2016), the entire mass of the upper structure is assumed to be applied as a top storey shear (i.e. the first term of Equation (4.12)). Only $M_v M_L S_a(T_L)$, the portion associated with the lower structure, is distributed according to the standard distribution specified by Equation (4.3). It is assumed that the top storey shear F_t is replaced by the base shear applied to the lower structure, and therefore the storey force distribution is:

$$F_x = \begin{cases} V_{Ub} & x = N_U + N_L \\ [M_v M_L g S_a(T_L)] \dfrac{W_x h_x}{\sum_{i=1}^{n} W_i h_i} & x \leq N_L \end{cases} \tag{4.13}$$

Where F_x indicates the x-th storey counted from the bottom. Note that for this study, each storey height is assumed to be identical, and each storey of the lower structure is assumed to have identical mass. To be exceedingly clear, the corresponding shear distribution is:

$$V_x = \begin{cases} V_{Ub} & x = N_U + N_L \\ [M_v M_L g S_a(T_L)] \dfrac{\sum_{i=x}^{n} W_i h_i}{\sum_{i=1}^{n} W_i h_i} + V_{Ub} & x \leq N_L \end{cases} \tag{4.14}$$

4.4.3 Efficacy of the newly proposed method to evaluate appendage structures

To evaluate the proposed method, it is compared with two analogous methods (three methods are compared):

1. The proposed approach is articulated by Equation (4.13). The contribution $M_v M_L S_a(T_L)$ from the lower structure is not less than the minimum code-specified base shear.

2. The proposed method, using M_v evaluated at T_U rather than α_U at the base of the upper structure, to demonstrate that M_v is inadequate to capture the amplification of the top storey.
3. The default NBCC distribution, evaluated at period T_1 obtained from the MDOF eigenvalue analysis. The default top storey shear and code minimum base shear are enforced.

As elsewhere, the results are calculated for a variety of values for each input parameter in the same manner as Section 3.4, but only for $N_U = 1$. Considering first the upper appendage structure alone, as in Figure 4.3, it is apparent that neither M_v applied to the upper structure nor the default ESFP adequately account for the higher mode effects in the upper structure. Using M_v to scale the first mode shear of the appendage structure is particularly problematic, and underestimates the MRS shear. Conversely, using α_U to characterize the appendage shear is relatively accurate, with a median overestimate of 10%. Considering instead the maximum and minimum error, using α_U to evaluate the appendage produces error values between -0.7% (underestimate) and 30% (overestimate).

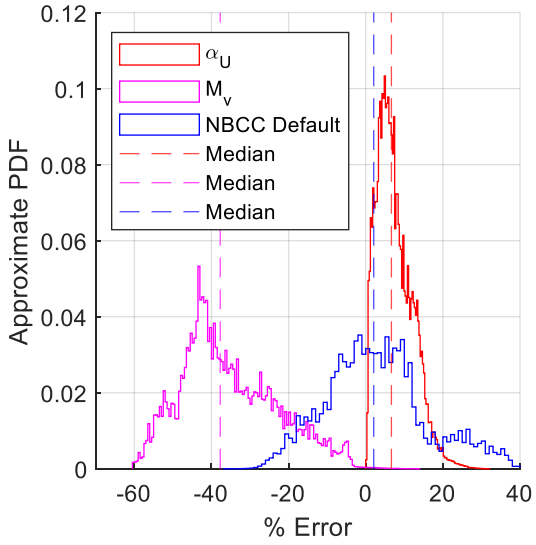

Figure 4.3: Error at base of the upper structure for appendage structure

If the largest underestimates and overestimates across each structure are considered as in Figure 4.4, the relative success of the method (including the lower structure) can be inferred. Based on the similarity between Figure 4.4 a) and Figure 4.3, it is clear that the upper structure is where the error is generally at its minimum and thus the largest underestimates occur. The same conclusions can therefore be made as in Figure 4.3 insofar as the adequacy of each method at preventing the underestimation of shears in the appendage structure. Meanwhile, Figure 4.4 b) indicates that each

method produces generally modest overestimations of the storey shears in the worst-case scenario. These overestimates are 10% higher for the median structure via the proposed method versus the others. This is likely due to an increase in the base shear of the lower structure due to the increased top storey shear - the base of the lower structure is where the largest overestimates generally appear. However, because the newly proposed method is better at controlling the minimum error (i.e. the underestimate) at the upper structure, it is an effective alternative to the default NBCC method. Despite the removal of the R_{kb1} requirement compared to Yuan (2016), the error is not excessively increased.

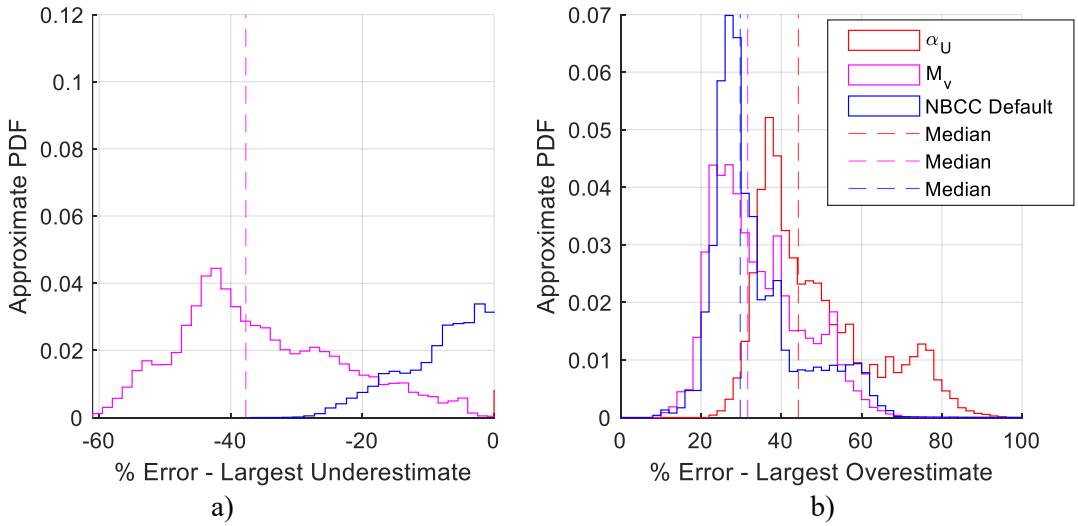

Figure 4.4: Error for appendage structure

Based on Figure 4.3 and Figure 4.4, the proposed method is therefore adequate at conservatively addressing the underestimate of the error at the appendage which is inherent in the default force distribution used by NBCC 2015. In exchange, the newly proposed procedure generally increases the overestimate of storey shears in the lower structure, but only by about 10% on a median basis.

4.5 Newly proposed method

Whereas the method provided in the previous section is applicable only to one-storey upper structures, this proposed method applies to a wider array of structures. The method involves both elements of the NBCC and ASCE 7 equivalent static methods – the base shears are evaluated (roughly) according to the NBCC, and the force distribution is modified by an exponent similarly to ASCE 7. Specifically:

1. The upper structure base shear is defined by α_U (Chapter 3).
2. The top storey shear is defined by α_{Utop}, analogously to α_U (Chapter 4.5.1).
3. The force distribution is selected so that the top storey and upper structure base shears are consistent with α_U and α_{Utop}. No NBCC-specified top storey shear is applied (Chapter 4.5.3).
4. The base shear of the lower structure is the sum of the upper structure's base shear and the inertial force associated with the mass of the lower structure. The lower structure component is distributed through the lower structure, and the upper base shear is applied as a top storey shear to the lower structure, replacing the NBCC-specified top storey shear (Chapter 4.5.4).

4.5.1 Top storey higher mode amplification factor α_{Utop}

The storey-wise distribution of force on irregular structures is not constant and varies not only as a function of the period e.g. T_1 and the degree of irregularity e.g. R_m and R_k but also based on the storey of the structure being considered. This much is acknowledged by both building codes such as NBCC 2015 (NRCC, 2015c) and ASCE 7 (2017) and by researchers e.g. Yuan & Xu (Yuan, 2016; Yuan & Xu, 2016). The higher mode amplification factor, α_U, is based on this premise and characterizes the changing impact of higher-mode effects at the base of the upper structure on account of stiffness and mass irregularity. Predicting the effect of higher modes on the force distribution is, therefore, necessary to approximate it with any degree of accuracy for irregular structures. Insofar as the base shear of the upper structure, α_U adequately captures this effect.

Unfortunately, while α_U is performative at the base of the upper structure (and consequently the top of the lower structure), it does not address the top storey shear. Both NBCC 2015 (NRCC, 2015c) and ASCE 7 (2017) acknowledge that the top storey is the most vulnerable to being underestimated by traditional static approaches and provide some means of increasing the shear at the top storey. The NBCC does so via the top storey shear F_t of Equation (4.4), and ASCE 7 does so via the exponent k of Equation (4.7). Each has a different effect on the shear distribution - F_t uniformly increases each of the storey shears by a set amount, and k modifies the assumed distribution of forces such that the storey forces increase more aggressively towards the top of the structure compared to the default distribution.

However, neither of these approaches captures the effect of irregularity, given that they are concerned only with the fundamental period of the structure T_1. Regular structures are indeed sensitive to the fundamental period, but the variation of stiffness and mass present in irregular

structures further modifies this relationship based on the extent of the irregularity. Despite this, both NBCC 2015 (NRCC, 2015c) and ASCE 7 (2017) use an identical force distribution for all structures having an identical fundamental period, irrespective of any irregularity. This is problematic for attaining accurate force distributions on irregular structures, as both the top storey shears and the shape of the force distribution change as a function of the irregularity. Both F_t and k are predicated on certain assumptions regarding the behaviour of structures which may misestimate the top storey shear.

Therefore, it is advantageous to have an effective estimate for the top storey shear. The storey shears vary more or less smoothly between the top and base shears, and if both the top and bottom shears are known, the remaining shears can be estimated. Towards this end, the top storey higher mode amplification factor, α_{Utop}, is defined analogously to the theoretical definition of α_U:

$$\alpha_{Utop} = \frac{V_{Utop}}{m_U g S_a(T_{singU})} \tag{4.15}$$

where V_{Utop} is the top storey shear predicted by the modal response spectrum analysis. Similar to α_U which is defined for the N_U-storey upper structure, α_{Utop} is defined for the top storey alone. Accordingly, the period T_U is replaced with T_{singU}, the mass is that of a single storey, m_U, and the top storey shear alone, V_{Utop}, is of concern. In this way, the higher-mode effect on the top storey of the upper structure can be quantified in the same way as that of the lower structure.

Based on an empirical investigation, the upper bound on α_{Utop} is approximately linear as a function of the ratio $S_a(T_1)/S_a(0.2)$, i.e. the ratio of the structure's first mode spectral acceleration to the maximum value. In general, the value of α_{Utop} increases as $S_a(T_1)$ approaches $S_a(0.2)$, and thus, the higher mode effects in the top storey increase as the period shortens. The proposed formulation for α_{Utop} is, therefore:

$$\alpha_{Utop} = A_{top}\left(\frac{S_a(T_1)}{S_a(0.2)}\right) + B_{top} \tag{4.16}$$

A_{top} and B_{top} are fit parameters calibrated such that α_{Utop} is a conservative overestimate of the values of α_{Utop} calculated from the MDOF model, just like α_U. Specifically, the parameters A_{top} and B_{top} apply only to configurations that satisfy the scope set out in Section 1.3.2, e.g. $\max(r_{kU1}, 1) \leq r_k \leq 20$. Much like A_{U1} and B_{U1}, these values are tabulated as a function of N_U, N_L and r_m, and appear in Table 4.5 and Table 4.6. That is not to say that A_{top} and B_{top} are only a function of the mass ratio and number of

storeys. As with $A_{Ul,}$ $B_{Ul,}$ A_{max} and B_{max}, the stiffness ratio R_k and single-storey period T_{singU} are implicitly embodied by T_1, which is defined by Equations (3.14) and (A.13), i.e. T_1 is defined via φ_{L1} and T_U. These values are tabulated to achieve reasonable accuracy. For $r_m = 4$, $N_U = 2$, and $N_L = 6$, the proposed α_{Utop} is plotted against the calculated results in Figure 4.5.

Table 4.5: Values of A_{top}

		r_m							r_m					
N_U	N_L	1	2	3	4	5	N_U	N_L	1	2	3	4	5
2	1	0.89	0.88	0.86	0.89	0.90	5	2	1.06	1.00	0.96	0.95	0.97
2	2	0.89	0.88	0.95	1.04	1.10	5	3	1.02	0.99	1.04	1.11	1.18
2	3	0.91	1.05	1.16	1.37	1.61	5	4	1.01	1.07	1.19	1.31	1.43
2	4	1.00	1.28	1.49	1.79	1.93	5	5	1.03	1.18	1.35	1.49	1.62
2	5	1.12	1.41	1.76	1.90	1.95	5	6	1.08	1.29	1.49	1.65	1.82
2	6	1.24	1.60	1.79	1.82	1.74	5	7	1.14	1.39	1.61	1.80	2.01
2	7	1.35	1.68	1.74	1.66	1.57	6	1	1.09	1.07	1.05	1.04	1.02
2	8	1.43	1.68	1.62	1.51	1.42	6	2	1.07	1.02	0.98	0.96	0.96
2	9	1.44	1.61	1.51	1.41	1.34	6	3	1.04	0.99	1.02	1.07	1.14
2	10	1.48	1.54	1.41	1.31	1.25	6	4	1.02	1.05	1.15	1.24	1.34
3	1	1.01	0.99	0.97	0.97	0.95	6	5	1.03	1.14	1.29	1.41	1.52
3	2	0.99	0.95	0.96	1.00	1.07	6	6	1.07	1.24	1.41	1.55	1.68
3	3	0.98	1.02	1.15	1.28	1.40	7	1	1.11	1.09	1.07	1.05	1.03
3	4	1.00	1.18	1.39	1.54	1.74	7	2	1.09	1.03	0.99	0.97	0.97
3	5	1.07	1.34	1.55	1.80	2.02	7	3	1.06	1.00	1.02	1.05	1.10
3	6	1.16	1.49	1.75	1.99	2.13	7	4	1.03	1.04	1.12	1.20	1.28
3	7	1.25	1.58	1.88	2.04	2.07	7	5	1.03	1.12	1.25	1.35	1.45
3	8	1.33	1.69	1.92	1.98	1.94	8	1	1.12	1.10	1.08	1.06	1.04
3	9	1.39	1.75	1.90	1.86	1.78	8	2	1.10	1.04	1.00	0.97	0.97
4	1	1.06	1.03	1.01	1.00	0.97	8	3	1.07	1.00	1.01	1.03	1.07
4	2	1.03	0.98	0.96	0.97	1.01	8	4	1.04	1.03	1.10	1.17	1.24
4	3	1.00	1.00	1.08	1.17	1.29	9	1	1.12	1.11	1.08	1.07	1.05
4	4	1.00	1.11	1.27	1.41	1.54	9	2	1.10	1.05	1.01	0.98	0.97
4	5	1.04	1.24	1.45	1.61	1.79	9	3	1.07	1.01	1.01	1.02	1.06
4	6	1.11	1.37	1.60	1.80	2.00	10	1	1.13	1.11	1.09	1.08	1.06
4	7	1.18	1.48	1.72	1.96	2.14	10	2	1.11	1.06	1.02	0.99	0.97
4	8	1.25	1.58	1.84	2.06	2.19	11	1	1.13	1.12	1.10	1.09	1.07
5	1	1.08	1.06	1.03	1.02	1.00							

Note: Table 4.5 is to be interpolated for intermediate values of r_m.

Table 4.6: Values of B_{top}

		r_m							r_m				
N_U	N_L	1	2	3	4	5	N_U	N_L	1	2	3	4	5
2	1	0.40	0.54	0.67	0.74	0.84	5	2	0.39	0.58	0.70	0.78	0.84
2	2	0.52	0.72	0.85	0.92	1.02	5	3	0.49	0.69	0.78	0.86	0.94
2	3	0.61	0.73	0.85	0.86	0.85	5	4	0.56	0.73	0.84	0.87	0.74
2	4	0.64	0.68	0.77	0.78	0.86	5	5	0.62	0.76	0.76	0.63	0.68
2	5	0.63	0.70	0.75	0.85	0.89	5	6	0.64	0.74	0.57	0.62	0.65
2	6	0.58	0.69	0.81	0.85	0.81	5	7	0.65	0.61	0.55	0.61	0.62
2	7	0.57	0.72	0.81	0.76	0.70	6	1	0.28	0.39	0.47	0.55	0.60
2	8	0.58	0.73	0.75	0.70	0.67	6	2	0.36	0.54	0.66	0.75	0.81
2	9	0.62	0.74	0.69	0.66	0.65	6	3	0.45	0.65	0.76	0.81	0.87
2	10	0.62	0.70	0.67	0.67	0.76	6	4	0.52	0.72	0.76	0.85	0.90
3	1	0.33	0.48	0.59	0.67	0.75	6	5	0.58	0.69	0.79	0.78	0.67
3	2	0.45	0.67	0.81	0.91	0.97	6	6	0.62	0.71	0.71	0.59	0.64
3	3	0.56	0.78	0.87	0.77	0.82	7	1	0.26	0.37	0.44	0.51	0.56
3	4	0.63	0.78	0.65	0.71	0.70	7	2	0.34	0.51	0.61	0.70	0.77
3	5	0.68	0.62	0.64	0.65	0.67	7	3	0.43	0.61	0.72	0.80	0.85
3	6	0.68	0.55	0.61	0.66	0.74	7	4	0.49	0.67	0.75	0.83	0.89
3	7	0.61	0.56	0.63	0.73	0.83	7	5	0.54	0.70	0.77	0.85	0.85
3	8	0.55	0.57	0.69	0.79	0.79	8	1	0.26	0.36	0.43	0.49	0.54
3	9	0.52	0.60	0.74	0.78	0.73	8	2	0.34	0.49	0.59	0.68	0.74
4	1	0.30	0.45	0.54	0.62	0.69	8	3	0.41	0.58	0.68	0.76	0.83
4	2	0.42	0.62	0.75	0.86	0.94	8	4	0.48	0.64	0.75	0.80	0.87
4	3	0.52	0.73	0.86	0.96	0.90	9	1	0.27	0.36	0.43	0.48	0.53
4	4	0.59	0.80	0.84	0.68	0.73	9	2	0.33	0.48	0.57	0.65	0.72
4	5	0.64	0.79	0.61	0.64	0.67	9	3	0.40	0.57	0.67	0.75	0.81
4	6	0.68	0.63	0.57	0.61	0.63	10	1	0.26	0.34	0.41	0.46	0.51
4	7	0.69	0.52	0.58	0.60	0.65	10	2	0.32	0.45	0.55	0.63	0.70
4	8	0.63	0.51	0.57	0.63	0.74	11	1	0.25	0.33	0.39	0.44	0.49
5	1	0.29	0.42	0.51	0.57	0.63							

Note: Table 4.6 is to be interpolated for intermediate values of r_m.

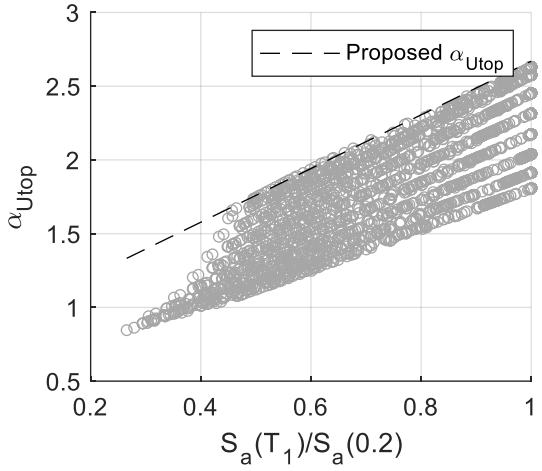

Figure 4.5: α_{Utop} versus calculated results for $N_U = 2$, $N_L = 6$ and $r_m = 4$

4.5.2 Error associated with α_{Utop}

The use of α_{Utop} to estimate the response of the top storey is predicated on the assumption that Equation (4.16) adequately predicts the MRS-derived value corresponding to Equation (4.15). Fortunately, as apparent from Figure 4.6, Equation (4.16) provides an effective estimate of α_{Utop}. The error of Equation (4.16) is generally between 0% and 40%, with a median of 10%. It is therefore concluded that α_{Utop} is adequate for determining the top storey shear.

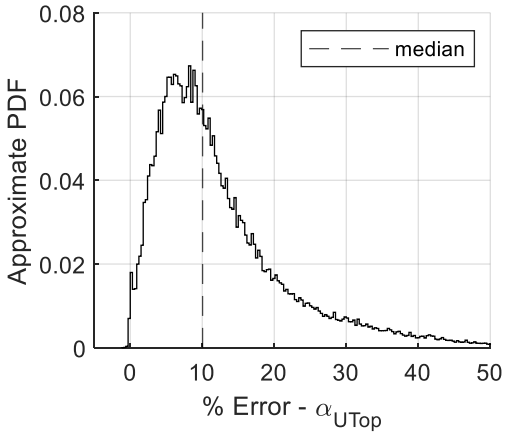

Figure 4.6: Error of proposed approximation of α_{Utop}

4.5.3 Evaluating loads on the upper structure via α_U and α_{Utop}

Considering each of the equivalent static force procedures proposed by the NBCC (NRCC, 2010, 2015c), ASCE 7 (2010, 2017) and Yuan & Xu (Yuan, 2016; Yuan & Xu, 2016), each method's shear distribution (including the ASCE 7 and Yuan & Xu two-stage procedures) requires three elements to determine the distribution of forces on any given segment:

1. The base shear
2. An assumed force distribution
3. A modification to the response that increases the storey shears in the upper storeys to account for higher mode effects

This seems a trivial conclusion, but each method does so by different means. In the NBCC, the force distribution is assumed to be a constant shape – the top storey shear is added where the base shear is not adequate by itself. In the ASCE, there is no additional top storey shear – instead, the force distribution is changed by the exponent k such that the top storey shear is conservative. This is also true of the two-stage procedure – the intent is that the base shear of the upper structure plus the expected response of the lower structure's top storey is conservative. Likewise, in their two-stage (Yuan, 2016; Yuan & Xu, 2016) and modified ELF (Yuan, 2016) methods, Yuan & Xu either scale the top storey shear via α_U or apply an additional top storey shear as a function of the irregularity. The convention of these methods is to assume a force distribution and a base shear and then apply adjustments to the top storey shear to ensure that the method is conservative.

However, if α_{Utop} and α_U are used to estimate the shear at the top and bottom of the upper structure, the procedure can be reversed. Each value of the exponent k used by ASCE 7, as in Equations (4.7) and (4.8), corresponds to a top storey shear which is some proportion of the upper base shear. If this ratio between the top and upper base shears is evaluated using α_{Utop} and α_U, the k (and thus the force distribution) matching these endpoints can be determined using α_{Utop} and α_U rather than by presupposing some value arbitrarily.

In other words, if the base shear V_{Ub} and the top storey shear V_{Utop} of the upper structure are defined as:

$$V_{Ub} = \alpha_U M_U g S_a(T_U) \tag{4.17}$$

$$V_{Utop} = \alpha_{Utop} m_U g S_a(T_{singU}) \tag{4.18}$$

then the corresponding value of the exponent, k, is evaluated based on Equation (4.19):

$$solve\ for\ k\text{:}\ \frac{(W_x h_x^k)_{x=N_U}}{\sum_{i=1}^{n=N_U} W_i h_i^k} = \frac{V_{Utop}}{V_{Ub}} \tag{4.19}$$

Note: in Equation (4.19) the heights are evaluated beginning at the base of the upper structure.

The left-hand side of Equation (4.19) corresponds to the top storey of the force distribution given by ASCE 7 in Equation (4.7). The desired value of the exponent k is that which produces a distribution matching V_{Ub} at the base and V_{Utop} at the top, given that V_{Ub} is the base shear of the upper structure. V_{Ub} is automatically the total base shear given by Equation (4.7), and so k is selected based on the requirement that the top storey value of the ASCE 7 distribution (i.e. at $x = N_U$) is the same proportion of the top storey shear as V_{Utop}, the proposed estimate of the top storey shear.

However, based on the input values (i.e. r_m, r_k, N_U, N_L, T_{singU}, $S_a(T)$), the solution of k via Equation (4.19) may produce unreasonably large or small values. For example, where V_{Utop} is a significant portion of V_{Ub}, the k for which Equation (4.19) is satisfied may be much larger than otherwise. A large value of k may cause the lower storeys of the upper structure to be significantly overestimated, and a small value of k may cause some underestimation of the storey immediately below the top storey. For practical purposes, it is assumed that k lies between 0.5 and 3.0, as specified by Equation (4.20). These limits are selected based on the following rationale – the lower bound of 0.5 is applied to ensure that the upper storey shears are not excessively diminished where V_{Utop} is small, and the upper bound of 3 is applied so that the lower storeys of the upper structure are not excessively overestimated just to suit the top storey. A value of 0.5 indicates that the height of each storey has a significantly diminished effect and thus the forces are distributed more evenly through the height, and a value of 3.0 indicates that much more force is concentrated at the uppermost storeys.

$$0.5 \leq k \leq 3.0 \tag{4.20}$$

Compared to the definition of k given by ASCE 7 and Equation (4.8), the limits in Equation (4.20) correspond to a relaxed lower bound and a larger upper bound. The relaxed lower bound indicates that the irregularity may sometimes decrease the top storey forces relative to the assumed distribution of NBCC 2015/ASCE 7, and the larger upper bound indicates that potentially much larger upper storey forces than expected are sometimes warranted. This lower bound is less stringent than that

dictated by either ASCE 7 or NBCC 2015 – designers who wish to be even more conservative can apply a lower bound of 1.0, corresponding to the NBCC's default distribution, if desired.

Given k and V_{Ub}, the storey forces on the upper structure are evaluated for the upper structure as though it is fixed at its base (where $i = 1$ at the base of the upper structure):

$$F_{x,upper} = (V_{Ub})\frac{W_x h_x^k}{\sum_{i=1}^{n=N_U} W_i h_i^k} \tag{4.21}$$

where $F_{x,upper}$ here concerns only the upper structure. Therefore, the storey shear distribution for the upper structure, $V_{x,upper}$ is:

$$V_{x,upper} = (V_{Ub})\frac{\sum_{i=x}^{n=N_U} W_i h_i^k}{\sum_{i=1}^{n=N_U} W_i h_i^k} \geq V_{Utop} \tag{4.22}$$

It is assumed that the storey shears are greater than the value of V_{Utop} - this may not be the case if $k = 3$.

If the calculated value of $k \geq 3.0$ ($k = 3.0$ is the upper bound), the storey shear at all storeys is increased by 50% of the top storey shear:

$$if\ k = 3.0, V_{x,upper} = (V_{Ub})\frac{\sum_{i=x}^{n=N_U} W_i h_i^k}{\sum_{i=1}^{n=N_U} W_i h_i^k} + 0.5V_{Utop} \leq V_{Ub} \tag{4.23}$$

This surcharge for $k = 3.0$ is to account for the truncation of larger values of k. There is no issue with selecting a larger value of k – this increases the shears in the upper storeys without reducing those in the lower storeys. However, the truncation of value values of k via the upper bound of 3.0 leads to some limited circumstances where the top storey shear is underestimated. Therefore, where $k = 3.0$, a minimum storey shear must be applied to ensure that the top storey is not underestimated despite the upper bound on the exponent. However, there is no need to increase the storey shears beyond the calculated value of V_{Ub}.

4.5.4 Evaluating loads on the lower structure:

Like the formulation for appendage structures set out in Section 4.4.2, it is assumed that the lower structure behaves approximately as a regular structure fixed at its base with the upper structure loads being applied as an additional top storey shear. Similarly, then, the base shear of the lower structure,

V_{Lb}, is assumed to be the superposition of the upper structure's base shear and a base shear associated with the lower structure:

$$V_{Lb} = V_{Ub} + M_v M_L S_a[\min(T_1, 0.75)] \tag{4.24}$$

As in Equation (4.12), V_{Lb} has two parts. The first part, V_{Ub}, corresponds to Equation (4.17) and is the shear force contributed from the base of the upper structure. It is treated as an additional top storey shear and thus is applied at the top of the lower structure. The second portion, $M_v M_L S_a[\min(T_1, 0.75)]$, corresponds to the lower structure and is somewhat different than that dictated in Equation (4.12). In Equation (4.12), it is recommended that the period of the lower structure, T_L, be used as a conservative period. This is acceptable if somewhat over-conservative because T_L and T_1 are relatively close for an appendage structure and the influence of the relatively small irregularity is small on the lower structure. Meanwhile, for other structures, especially where N_L is small, T_L is sometimes much, much smaller than T_1 and using it instead is excessively conservative. Therefore, for the more general case, it is recommended that T_1 is used with the caveat that T_1 be not more than 0.75 seconds for evaluation of $S_a(T)$. Under certain circumstances, large irregularities may cause a much larger base shear than predicted for the given first-mode period T_1 for large values of T_1 within the scope. This upper bound on T_1 is applied to ensure that the base shear is conservatively estimated even for cases where the irregularity is large. Note also that $M_v M_L S_a(\min(T_1, 0.75))$ should be larger than the code-specified base shear given by Equation (4.2), and that M_v should be evaluated according to the selected value of T_1. T_1 can be approximated from T_U as a function of R_m and R_k using Equation (A.13).

Assuming that the portion $M_v M_L S_a(\min(T_1, 0.75))$ (i.e. $V_{Lb} - V_{Ub}$) associated with the lower structure is distributed according to the NBCC distribution with V_{Ub} applied at the top storey, the storey shears in the lower structure are evaluated as:

$$F_{x,lower} = \begin{cases} [V_{Lb} - V_{Ub}]\dfrac{W_x h_x}{\sum_{i=1}^{n=N_L} W_i h_i} + V_{Ub} & x = N_L \\ [V_{Lb} - V_{Ub}]\dfrac{W_x h_x}{\sum_{i=1}^{n=N_L} W_i h_i} & x < N_L \end{cases} \tag{4.25}$$

The corresponding shear distribution across the lower structure is, therefore:

$$V_{x,lower} = \begin{cases} [V_{Lb} - V_{Ub}] \dfrac{(W_x h_x)_{x=N_L}}{\sum_{i=1}^{n=N_L} W_i h_i} + V_{Ub} & x = N_L \\ [V_{Lb} - V_{Ub}] \dfrac{\sum_{i=x}^{n=N_L} W_i h_i}{\sum_{i=1}^{n=N_L} W_i h_i} + V_{Ub} & x < N_L \end{cases} \quad (4.26)$$

where $i = 1$ at the first storey.

In summary, the proposed shear distribution is:

$$V_x = \begin{cases} (V_{Ub}) \dfrac{\sum_{j=x}^{n=N_U} W_j h_j^k}{\sum_{j=1}^{n=N_U} W_j h_j^k} \leq V_{Ub} & x > N_L \\ [V_{Lb} - V_{Ub}] \dfrac{\sum_{i=x}^{n=N_L} W_i h_i}{\sum_{i=1}^{n=N_L} W_i h_i} + V_{Ub} & x \leq N_L \end{cases} \quad (4.27)$$

where the heights h_j for the distribution of forces in the upper structure are measured from the base of the upper structure rather than the base of the overall structure, and where the storey shears in the upper structure are not larger than V_{Ub}, but at minimum V_{Utop}.

4.5.5 Error of proposed procedure

To evaluate the relative performance of the newly proposed method, the error between the proposed method and the modal response spectrum results are calculated for linearly-spaced inputs for each of T_{singU}, r_m, r_k, N_U, N_L and $S_a(T)$ (in the manner of Section 3.3.3) and compared to the corresponding storey shear predicted by the default NBCC 2015 ESFP. The calculations comprise approximately 7.3 million different combinations of variables within the scope, after having been pre-processed to remove out-of-scope combinations. This includes omitting scenarios where $m_L < m_U$ and $k_L < k_U$ since these correspond to $r_m < 1$ and $r_k < 1$.

Figure 4.7 a) to c) depicts the relative error for the top storey, the base of the upper structure and the base of the lower structure for both the proposed method and the NBCC. Based on Figure 4.7 a) and b), the estimates provided by α_U and α_{Utop} provide a better estimate of the MRS base shear compared to the NBCC. The error at the top storey and the base of the upper structure by the proposed method is better on both a median and minimum basis than that given by the NBCC and demonstrates a smaller variance. Whereas the NBCC exhibits at times a 20% underestimate (-20% error) of the top and upper base shears, the newly proposed method does not underestimate either. Strictly speaking, the NBCC ESFP distribution does not apply to most irregular structures; however,

there is no alternative in the NBCC for irregular structures, and thus the ESFP distribution is considered to be the default assumption to be compared to. Overall:

1. The median overestimate at the top storey is 10% by the newly proposed method, and generally not more than 40%. Any underestimates are negligible.
2. The median overestimate for the upper base shear is approximately 15% for the newly proposed method, and generally not more than 30%. The estimates are conservative.

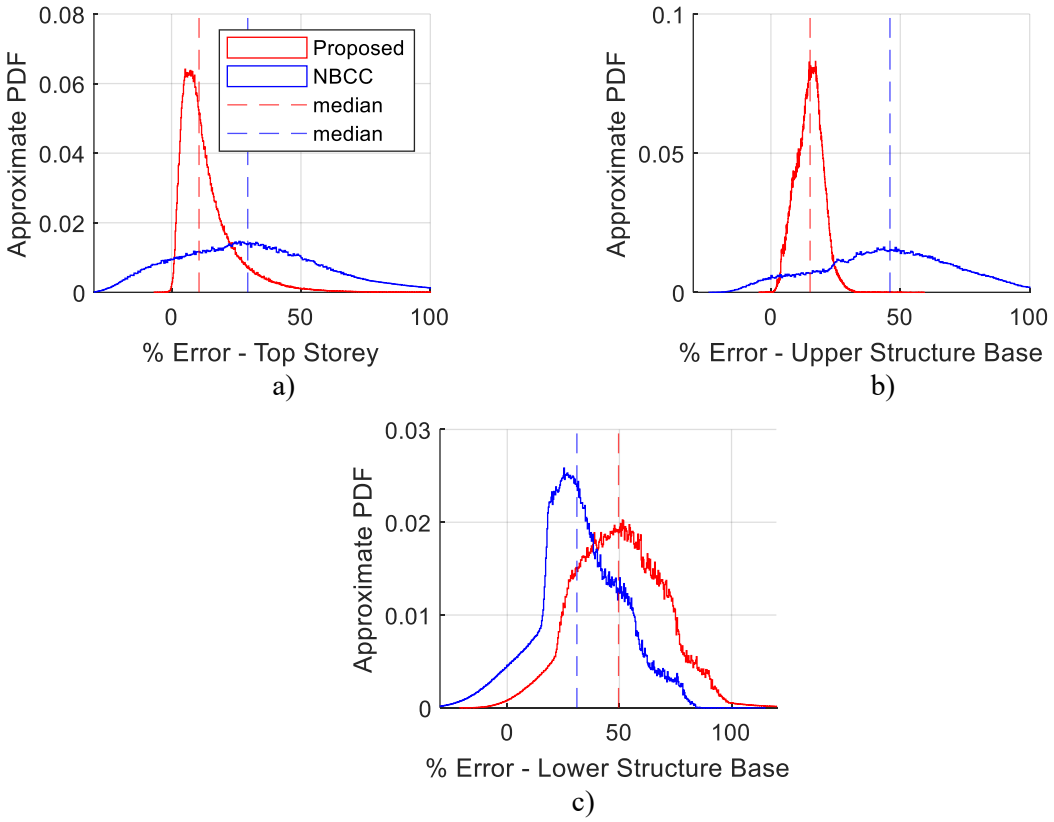

Figure 4.7: Error for the proposed method and NBCC – specific locations

Meanwhile, per Figure 4.7 c), the newly-proposed method appears to more conservative on average but better at a minimum than the NBCC at predicting the lower structure's base shear. Whereas the NBCC has a median overestimate of 40% for the overall base shear, the newly proposed method has a median overestimate of 75%. In exchange, the newly proposed method does not underestimate the lower structure's base shear.

Considering each of the upper and lower structures, the lower bound of the error is usually governed by the top storey for the upper structure and the bottom storey of the lower structure, for

which the proposed method most closely predicts the shear. It is because of this that the period T_1 must be capped to ensure a minimum base shear for the full structure, or else the lower base shear would be underestimated. Meanwhile, the largest overestimate in the upper structure is generally amidst the upper storeys given that the top and bottom storeys are generally well-approximated. This is less clear for the lower structure and generally depends on how effective the base shear and the assumed force distribution represent the lower structure. This is more variable than the selected values for the upper structure and should be further studied.

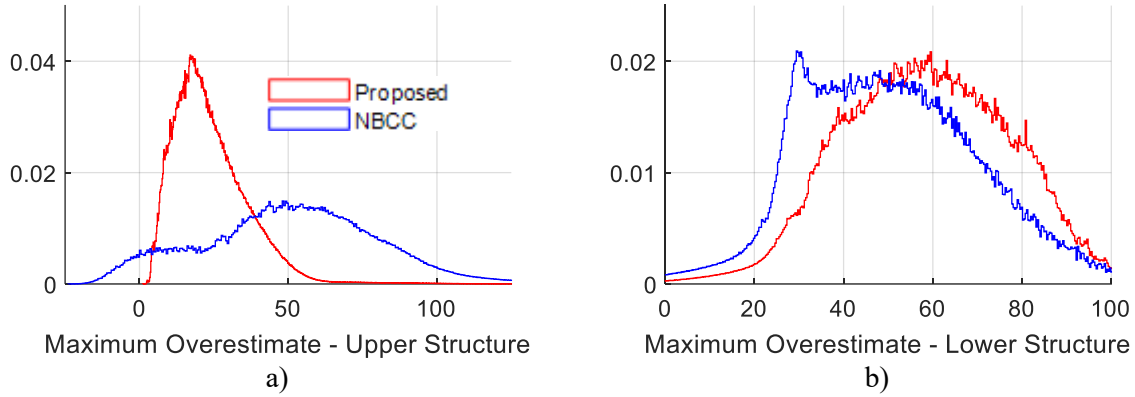

Figure 4.8: Worst-case overestimate for the proposed method and NBCC

4.5.6 Error considering non-uniform storey stiffness of the upper structure

In the forthgoing analysis, it is assumed that the storey stiffness of the upper structure, k_U, is constant, and thus that the upper structure is entirely uniform. For practical reasons, this may be unrealistic – a more appropriate assumption is that the storey stiffness gradually decreases towards the top of the upper structure, on account of the accumulation of forces towards the base of the upper structure. Any change in the stiffness matrix of the structure changes the dynamic response, and therefore it is prudent to investigate whether this effect changes the accuracy of the proposed method.

To evaluate the effects of a gradual reduction of stiffness in the upper structure, four different constant reductions of storey stiffness are considered as illustrated in Figure 4.9. The uniform structure is modified in each case by applying a constant, stepping reduction through the height of the structure such that the storey stiffness of the base is always k_U. Each case is associated with a stiffness reduction factor – 1 indicates a uniform structure in which all stiffnesses are identical, 1.10 indicates that the base storey stiffness is 10% larger than the stiffness of the storey above, 1.20 corresponds to 20% larger, and so on. This is repeated throughout the height of the upper structure for each

subsequent storey. Therefore, if the base of the upper structure is 1.25 times the stiffness of the 2nd storey of the upper structure, it will be $(1.25)^2 = 1.56$ times the stiffness of the 3rd storey, $(1.25)^3 = 1.95$ times the stiffness of the 4th storey and so on (equivalently, the storey stiffnesses are k_U, $0.8k_U$, $0.64k_U$, etc.). This modification is approximately based on the stiffness regularity threshold of NBCC 2015 listed in Table 2.1**Error! Reference source not found.**, which specifies that the stiffness of any storey must be at least 70% that of an adjacent storey, or 80% of the average of the three storeys above or below. Technically, a stiffness distribution of k_U, $0.8k_U$, $0.64k_U$, etc. exceeds the 80% three-storey average limit set out by the NBCC, but for simplicity only the storey-to-storey variation is considered.

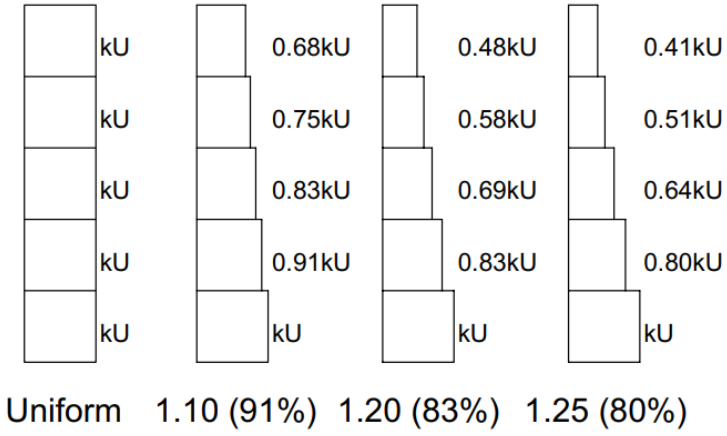

Figure 4.9: Variation of storey stiffness in the upper structure (N_U = 5)

As before, the response is first calculated for a variety of values of N_U, N_L, r_m, r_k, T_{singU}, and $S_a(T)$, assuming that the lower structure is uniform with constant storey stiffness k_L and the upper structure is uniform with constant storey stiffness k_U. This is considered the base case, and the corresponding load distributions for the modal response spectrum and the newly proposed method are calculated. Next, the stiffness distribution is modified for each of the distributions illustrated in Figure 4.9, and the MRS results are recalculated given the new stiffness matrix. For each stiffness distribution, the error is calculated between the proposed force distribution associated with the base case and its period T_1, and the MRS force distribution associated with the modified stiffness matrix. The corresponding error is therefore between the proposed force distribution assuming a uniform structure and the MRS results for each modified stiffness distribution. The proposed force distribution is not recalculated for the modified stiffness distributions – it is based on the uniform case.

Considering again the error at the top of the upper structure, the base of the upper structure and the base of the full structure, the error for each of the arrangements illustrated in Figure 4.9 is plotted in Figure 4.10 a) to d). It is apparent from Figure 4.10 that the method is still applicable for a non-uniform variation of stiffness. However, the error is not precisely the same. Per Figure 4.10 a), the top storey shear is prone to additional underestimation of up to 10% given a variation of the stiffness, and so the top storey force should be increased by 5-10% to ensure that the top storey shear is not underestimated. Moving onto Figure 4.10 b), there is no apparent increase in the underestimate at the base of the upper structure. Instead, the median overestimate increases significantly from 15% to 30% for the most severe stiffness variation. This indicates that the upper structure experiences larger overestimates of the storey shears in the upper structure if the stiffness varies but remains conservative but for some of the uppermost storeys. Figure 4.10 c) indicates that the lower structure's base shear is largely unchanged despite the variation of shears in the upper structure. A more severe stiffness reduction in the uppermost storeys modestly increases the median and maximum overestimates but otherwise does not significantly change the adequacy of the proposed method. Finally, Figure 4.10 d) considers the largest underestimate for each combination across all storeys. The distribution is similar to Figure 4.10 a), as expected – the worst underestimates are generally at the top storey. In general, the largest underestimate is 10% for the most severe stiffness variation, and this underestimate diminishes for a more uniform upper structure.

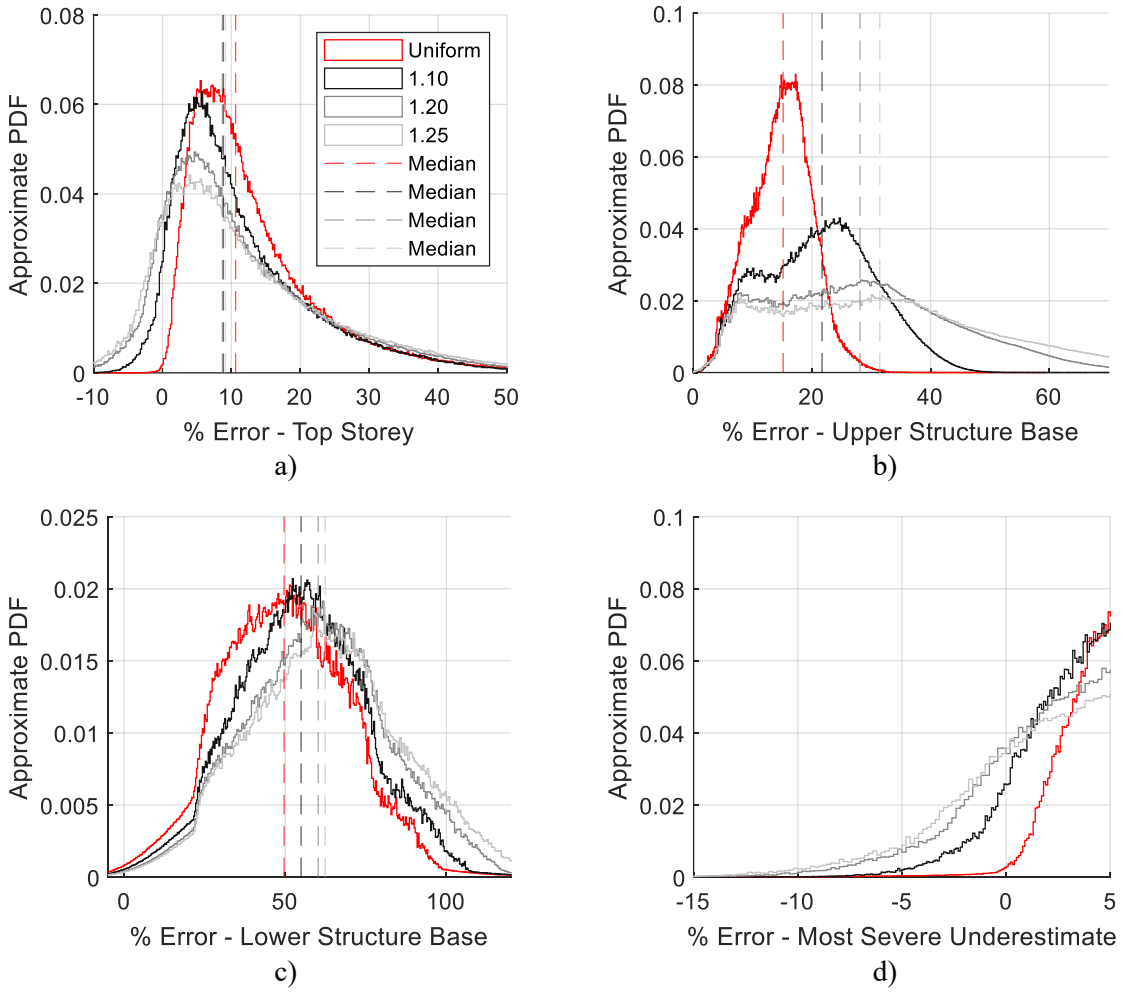

Figure 4.10: Error for proposed method considering upper structure with stiffness variation

4.6 Design Procedure

For either method proposed to evaluate the lateral loads defined by the current study, the first step is to define the input parameters and α_U. Therefore, the following steps are taken irrespective of the number of storeys:

1. Based on the selected building configuration, identify the value of each of these parameters: m_U, k_U, m_L, k_L, N_U, N_L, $S_a(T)$
2. Evaluate $\bar{\omega}_{1L}$ and $\bar{\omega}_{1U}$ from Table 3.1, corresponding to $N = N_L$ and $N = N_U$
3. Calculate r_m, r_k, R_m and R_k based on Equations (3.16) to (3.19)

4. Determine R_{kU1}, R_{kU2}, R_{kU3} and R_{kU2stg} according to Equations (3.25) to (3.28) and Appendix E, as well as A_{U1}, B_{U1}, A_{Umax}, and B_{Umax} from Appendix E. If $R_k \geq R_{kU2stg}$, it is possible to use the two-stage procedure detailed in Appendix F, subject the conditions listed in that appendix.

5. Evaluate α_{U1} according to Equations (3.29) and (3.30) (if applicable, i.e. $R_{kU1} < R_{kU2}$), α_{Umax} according to Equations (3.31) and (3.32) and α_{U2stg} according to Equation (3.33). $S_a(T_U)$ is evaluated according to Equation (3.37) and φ_{L1} according to Equation (A.13). As with the definition of α_U given in Chapter 3, if $R_{kU1} \geq R_{kU2}$, α_U does not require α_{U1} to be calculated, only α_{U2stg} and α_{Umax} are required. In such a case, R_{kU1} is only used as a lower bound on R_k, i.e. it is required that $R_{kU1} \leq R_k$.

6. Evaluate α_U according to Equations (3.21) to (3.24). Recall that R_k must be larger than R_{kU1}. If α_U is larger than desired, repeat steps 1-6 with a modified set of properties. Note that the estimate of α_U will never be greater than the maximum of α_{U1}, α_{U2stg} and α_{Umax}, nor less than the minimum. If a lower value is desired, dynamic analysis (e.g. MRS analysis) can be used.

7. Evaluate V_{Ub} according to Equation (3.7). It should not be less than Equation (4.2).

Having established α_U, the procedure diverges based on whether the upper structure is an appendage, i.e. $N_U = 1$ or not. If the upper structure is an appendage, Chapter 4.4.2 applies. Otherwise, Chapter 4.5 applies. Steps 8 onwards differ depending on the structure being considered – evaluate the loads according to the relevant list.

Appendage Structure ($N_U = 1$):

8. Evaluate T_L according to Equation (3.15), and the corresponding M_v based on Table 4.1. Note that for interpolation for T, the product $M_v S_a(T_L)$ should be interpolated rather than M_v only, per NBCC 2015.

9. Evaluate V_{Lb} according to Equation (4.12), but not less than Equation (4.2)

10. Evaluate the storey forces via Equation (4.13), or the storey shears via Equation (4.14)

Structures that are not appendage structures ($N_U > 1$):

8. Evaluate T_1 using Equation (A.13) and the value of T_U already calculated. Evaluate the corresponding M_v based on Table 4.1. Note that for interpolation for T, the product $M_v S_a(T_1)$ should be interpolated rather than M_v only, per NBCC 2015.

9. Determine $S_a(T_1)$, and determine A_{top} and B_{top} from Table 4.5 and Table 4.6.

10. Determine α_{Utop} according to Equation (4.16), and then V_{Utop} according to Equation (4.18). T_{singU} is defined by Equation (3.14).
11. Solve for k via Equation (4.19). The value should not be less than 0.5 or more than 3.0, as specified by Equation (4.20).
12. Define the upper structure storey forces $F_{x,upper}$ according to Equation (4.21). Equivalently, the storey shears $V_{x,upper}$ are defined by Equation (4.22).
13. If the exponent calculated in step 11 is equal to or greater than 3, an additional surcharge must be applied, as defined by Equation (4.23). The storey shears do not need to be larger than the upper base shear V_{Ub}, but should not be less than V_{Utop}
14. Evaluate the lower structure's base shear V_{Lb} using Equation (4.24).
15. Define the lower structure storey forces F_x according to Equation (4.25). Equivalently, the storey shears V_x are defined by Equation (4.26).
16. Finally, to address the possibility that the upper structure's storey shears are not underestimated considering stiffness variation as discussed in Section 4.5.6, increase the storey shears in the upper structure by 10%. They do not need to be larger than V_{Ub}

4.7 Design examples

To demonstrate the efficacy of the two proposed approaches, four examples are given, two for each of the proposed methods. Each example is set up to provide an approximately realistic demonstration of the methods (albeit without detailing e.g. reinforcement), with stiffnesses determined using the methodology described in Appendix G and according to CSA A23.3-19 (2019) (for concrete) and AISI S400-15 (2015) (for cold-formed steel shear walls). Each consists of an N_U-storey OSB-sheathed CFS shear wall frame atop an N_L-storey RC moment-resisting frame. The provided examples are:

1. A ten-storey structure with a one-storey upper structure in Montreal, evaluated using the method for appendages.
2. A twelve-storey structure with a one-storey upper structure, in Vancouver, evaluated using the method for appendages.

3. An eight-storey structure having a four-storey upper and lower structure, in St. Catharines, Ontario, evaluated using the proposed method.
4. A nine-storey structure having a three-storey lower structure and a six-storey upper structure in Montreal is evaluated using the proposed method. The structure exceeds the two-stage limit and so is also compared using the Yuan (2016) two-stage method described in Appendix F.

Note that none of the above examples are specifically selected to be a worst-case scenario for the applicability of the NBCC, but are instead selected to demonstrate a variety of different configurations. The NBCC generally performs worst when the mass ratio and stiffness ratio are as large as possible, but $r_m = 5$ and $r_k = 20$ are rare in practical structures. The proposed methods may be over-conservative in some cases to accommodate these extreme cases, but fine-tuning these methods is for a future study. Strictly speaking, the NBCC ESFP distribution does not apply to most irregular structures; however, there is no alternative in the NBCC for irregular structures, and thus the ESFP distribution is considered to be the default assumption for comparison. In the absence of an alternative, designers will likely use the NBCC ESFP distribution in order to provide a baseline for dynamic analysis results, thus, even if it is not strictly applicable the NBCC-specified force distribution is considered the default assumption. Therefore, the example calculations include an NBCC calculation. These calculations include: 1) the base shear V, limited by the NBCC-specified minimum shear specified for *other systems* (i.e. not otherwise classified), 2) the default top storey shear F_t, and 3) the default higher mode factor M_v, and 4) the default assumed force distribution. It is assumed that each structure is of normal importance ($I_E = 1$), on soil class C (no soil modification), and no inelastic modification is applied ($R_d R_o = 1$). Some factors are kept constant between the examples for simplicity's sake – it is assumed in each case, for example, that the floor dimensions are a constant 25 metre by 25 metre square, on which either the shear walls or the moment-resisting frame columns (as applicable) are symmetrically and uniformly arranged.

4.7.1 Example 4-1

To demonstrate the proposed procedure for appendage structures, a ten-storey structure placed at Montreal (City Hall) is selected. The corresponding spectral values are as follows:

Table 4.7: NBCC 2015 spectral acceleration for Montreal City Hall (NRCC, 2015a)

$S_a(0.2)$	$S_a(0.5)$	$S_a(1.0)$	$S_a(2.0)$	$S_a(5.0)$	$S_a(10.0)$
0 595	0.311	0.148	0.068	0.018	0.0062

As for the structure itself, it is assumed that the one-storey upper (appendage) structure experiences a 3 kPa specified dead load over a 25 metre by 25 metre floor plan, thus: $m_U = 1.91\times10^5$ kg. It is assumed that 75 metres of the shear wall are provided at a unit stiffness of 1640 kN/m/m, and thus $k_U = 1.23 \times 10^5$ kN/m and $T_{singU} = 0.25$ seconds. Meanwhile, the lower structure is assumed to be a nine-storey reinforced concrete moment-resisting frame over the same 25 metre by 25 metre dimensions. The frame consists of a five-by-five square grid of columns that are 600 mm by 600 mm in dimension which have a compressive strength of 40 MPa, an elastic modulus of approximately 28460 MPa and a stiffness of 6.83×10^4 kN/m per column. Therefore, $k_L = 1.71 \times 10^6$ kN/m and $r_k = 13.90$. It is assumed that $r_m = 2.40$ and thus $m_L = 4.58\times10^5$ kg and $T_{singL} = 0.10$ s. The assumed interstorey height is 3 metres.

Following the procedure given by Section 4.6, the relevant values are: $R_m = 21.60$, $R_k = 3.41$, $R_{kU1} = 2.76$, $R_{kU2} = 22.60$, $\alpha_{U1} = 1.14$, $\alpha_{Umax} = 2.99$, and finally, $\alpha_U = 1.28$. R_k lies between R_{kU1} and R_{kU2}, and so the other critical values of R_k and α_U are irrelevant. Using m_U, T_{singU} and α_U, V_{Ub} is found to be 1.31×10^3 kN. For the lower structure component, $M_v S_a(T_L) = 0.27$, and the base shear is 1.11×10^4 kN. In combination with the shear contributed from the upper structure, the final base shear is 1.24×10^4 kN. The final force distribution, with the upper structure acting as a top storey force on the lower structure, is illustrated alongside both the modal response spectrum and default NBCC distributions in Figure 4.11.

As expected, the proposed method is not necessary for the lower structure for structures having an appendage – the default NBCC distribution well-represents the loads on the lower structure. Indeed, the proposed procedure modestly worsens the accuracy of the loads on the lower structure. The proposed method explicitly separates the lower and appendage structures' loads despite this to thoroughly separate the calculations for the upper and lower structures' contributions. Where the NBCC does not perform well is at the top storey with the top-storey shear being underestimated by 20%. As discussed elsewhere, M_v and the default force distribution are inadequate to predict the top-storey shear, and instead, α_U should be used. As R_{kb1} is 14.62 per Equation (4.11) and the Yuan (2016) method would also be applicable. The two methods are quite similar; in any event, it can be said that the proposed method performs better than the default NBCC ESFP at predicting the storey loads such

that the estimate is consistently conservative, despite a significant difference in stiffness and mass on a storey-by-storey basis between the appendage and lower structures.

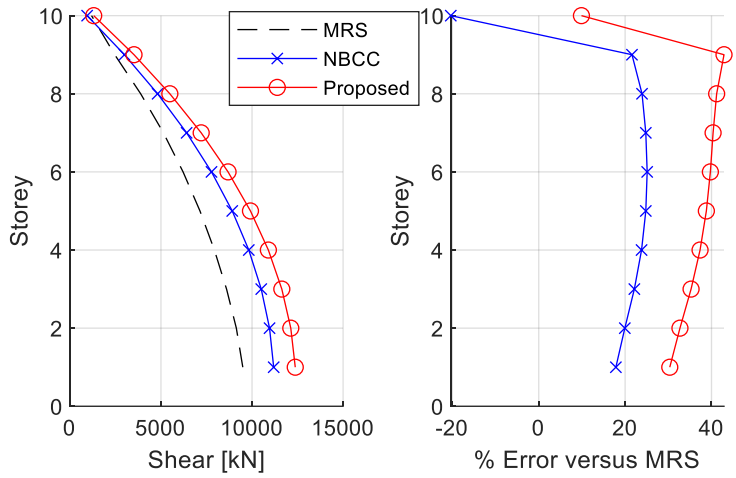

Figure 4.11: Example 4-1 force distribution and error

4.7.2 Example 4-2

As a second example, consider the same structure as Example 4-1, but at Vancouver City Hall and with an eleven-storey lower structure rather than a nine-storey one. The Vancouver City Hall spectrum values appear in Table 3.13. In this case, the same storey masses and stiffnesses are adopted, and following the same procedure as Example 4-1: $R_m = 26.40$, $R_k = 2.85$, $R_{kU1} = 2.74$, $R_{kU2} = 27.40$, $\alpha_{U1} = 1.42$, $\alpha_{Umax} = 3.29$, and finally, $\alpha_U = 1.42$. The assumed interstorey height is 3 m.

Like Example 4-1, the proposed method is much better at predicting the top storey shear of the upper structure than the NBCC despite a significant degree of irregularity. However, unlike Example 4-1, the NBCC does not underestimate the top storey force – instead, the NBCC overestimates it by 60%, compared to only a marginal overestimate by the proposed method.

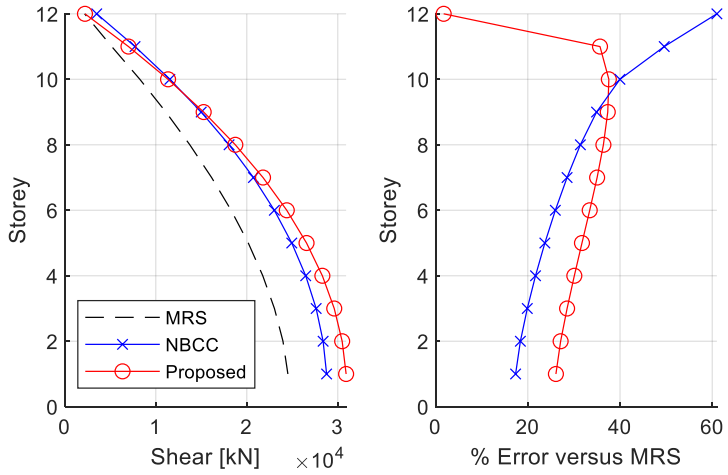

Figure 4.12: Example 4-2 force distribution and error

4.7.3 Example 4-3

For Example 4-3, consider a structure having a four-storey lower structure and a four-storey upper structure ($N_U = N_L = 4$) and having the same storey properties for the upper structure ($m_U = 1.91\times10^5$ kg, $k_U = 1.23 \times 10^5$ kN/m). This structure is assumed to be constructed in St. Catharines, Ontario using the values given in Table 3.7. It is assumed that $r_m = 3.10$ and $r_k = 5.87$, corresponding to $m_L = 5.92\times10^5$ kg, and $k_L = 7.23 \times 10^5$ kN/m and to the same five-by-five grid of columns, each 500 mm by 500 mm in dimension having a compressive strength of 30 MPa, an elastic modulus of approximately 24975 MPa and a stiffness of 2.89×10^4 kN/m per column. Therefore: $R_m = 3.10$, $R_k = 7.14$, $R_{kU1} = 2.29$, $R_{kU2} = 4.10$, $R_{kU3} = 6.10$, $\alpha_{Umax} = 1.35$, and finally, $\alpha_U = 1.35$. However, because the upper structure is more than a single storey, so the method applicable to appendage structures does not apply – the more general method described by Chapter 4.5 must be used. Thus, it is necessary to also calculate α_{Utop} and the exponent k.

Per Equation (3.14) and then Equation (A.13), $T_U = 1.04$ seconds and $T_l = 1.07$ seconds (and thus, A_{top} and B_{top} are evaluated from Table 4.5 and Table 4.6 as 1.28 and 0.82, and thus per Equation (4.16) $\alpha_{Utop} = 1.20$. Therefore:

$$V_{Ub} = (1.35)(7.64 \times 10^6 kg)(9.8N/kg)(0.118) = 1.19 \times 10^3 kN \quad (4.28)$$

$$V_{Utop} = (1.20)(1.91 \times 10^5 \text{kg})(9.8N/kg)(0.292) = 6.54 \times 10^2 kN \quad (4.29)$$

$$\frac{(1.91 \times 10^5 \text{kg})(N_U \times 3m)^k}{\sum_{i=1}^{n=N_U}[(1.91 \times 10^5 \text{kg})(i \times 3m)^k]} = \frac{6.54 \times 10^2 kN}{1.19 \times 10^3 kN} \rightarrow k = 2.12 \tag{4.30}$$

The storey shears for the upper structure are defined using Equation (4.22):

$$V_{x,upper} = (V_{Ub}) \frac{\sum_{i=x}^{n=N_U} W_i h_i^k}{\sum_{i=1}^{n=N_U} W_i h_i^k} \tag{4.31}$$

The loads on the lower structure are evaluated according to Equation (4.24) and Equation (4.26):

$$V_{Lb} = 1.19 \times 10^3 kN + 0.121(9.8N/kg)(4 \times 5.92 \times 10^5 kg) = 4.00 \times 10^3 kN \tag{4.32}$$

The calculation of the loads according to Equation (4.27) is tabulated in Table 4.8, and the results are plotted alongside the MRS and NBCC results in Figure 4.14.

Table 4.8: Calculation of proposed force distribution

Storey	$(V_{Ub}) \frac{\sum_{i=x}^{n=N_U} W_i h_i^k}{\sum_{i=1}^{n=N_U} W_i h_i^k}$	$[V_{Lb} - V_{Ub}] \frac{\sum_{i=x}^{n=N_L} W_i h_i}{\sum_{i=1}^{n=N_L} W_i h_i}$	V_x
8	$7.20 \times 10^2 kN$		$7.20 \times 10^2 kN$
7	$1.11 \times 10^3 kN$		$1.11 \times 10^3 kN$
6	$1.16 \times 10^3 kN$		$1.16 \times 10^3 kN$
5	$1.19 \times 10^3 kN$		$1.19 \times 10^3 kN$
4		$1.21 \times 10^3 kN$	$2.40 \times 10^3 kN$
3		$2.01 \times 10^3 kN$	$3.20 \times 10^3 kN$
2		$2.54 \times 10^3 kN$	$3.73 \times 10^3 kN$
1		$2.81 \times 10^3 kN$	$4.00 \times 10^3 kN$

For Figure 4.13, the proposed method adequately predicts the force distribution on the structure, albeit not consistently better than the NBCC. In this example, the NBCC generally performs better in the lower structure whereas the proposed method performs better in the upper structure. The reason for the overestimate in the lower structure is that T_1 = 1.07 seconds but is limited to 0.75 seconds for the calculation of the base shear for the proposed method. This is necessary to ensure that the method is generally conservative – see Example 4-4 for an example where the NBCC method underpredicts the base shear.

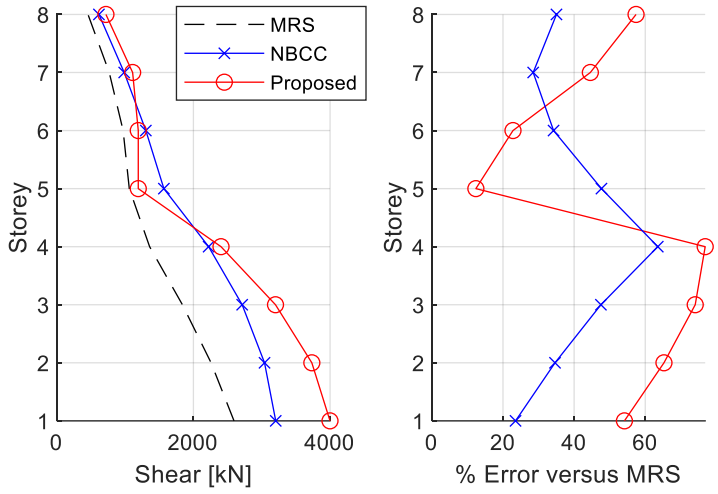

Figure 4.13: Example 4-3 force distribution and error

4.7.4 Example 4-4

For Example 4-4, consider the same parameters as Example 4-1 ($m_U = 1.91\times10^5$ kg, $k_U = 1.23 \times 10^5$ kN/m, $m_L = 4.58\times10^5$ kg , $k_L = 1.71 \times 10^6$ kN/m), except that the upper structure is now six storeys tall and the lower structure is three storeys tall – $N_U = 6$, $N_L = 3$. As before, the key variables are therefore: $R_m = 1.20$, $R_k = 23.69$, $R_{kU1} = 2.85$, $R_{kU2stg} = 12.00$, $\alpha_{U2stg} = 1.15$, and finally, $\alpha_U = 1.15$. However, because the upper structure is more than a single storey, so the method applicable to appendage structures does not apply – the more general method described by Chapter 4.5 must be used. Thus, it is necessary to also calculate α_{Utop} and the exponent k.

Per Equation (3.14) and then Equation (A.13), $T_U = 1.04$ seconds and $T_l = 1.07$ seconds (and thus, Atop and B_{top} are evaluated from Table 4.5 and Table 4.6 as 1.00 and 0.69, and thus per Equation (4.16) $\alpha_{Utop} = 0.93$. Therefore:

$$V_{Ub} = (1.15)(1.15 \times 10^6 kg)(9.8N/kg)(0.145) = 1.87 \times 10^3 kN \tag{4.33}$$

$$V_{Utop} = (0.93)(1.91 \times 10^5 \text{kg})(9.8N/kg)(0.548) = 9.57 \times 10^2 kN \tag{4.34}$$

$$\frac{(1.91 \times 10^5 \text{kg})(N_U \times 3m)^k}{\sum_{i=1}^{n=N_U}[(1.91 \times 10^5 \text{kg})(i \times 3m)^k]} = \frac{9.57 \times 10^2 kN}{1.87 \times 10^3 kN} \rightarrow k = 3.25 \tag{4.35}$$

The exact value of the exponent k satisfying Equation (4.19) is 3.25. Since it is assumed that k is no larger than 3, Equation (4.23) applies:

$$V_{x,upper} = (V_{Ub})\frac{\sum_{i=x}^{n=N_U} W_i h_i^k}{\sum_{i=1}^{n=N_U} W_i h_i^k} + 0.5V_{Utop} \leq V_{Ub} \tag{4.36}$$

The loads on the lower structure are evaluated according to Equation (4.24) and Equation (4.26):

$$V_{Lb} = 1.87 \times 10^3 kN + 0.239(9.8N/kg)(3 \times 4.58 \times 10^5 kg) = 5.09 \times 10^3 kN \tag{4.37}$$

The calculation of the loads according to Equation (4.27) is tabulated in Table 4.9.

Table 4.9: Calculation of proposed force distribution

Storey	$(V_{Ub})\frac{\sum_{i=x}^{n=N_U} W_i h_i^k}{\sum_{i=1}^{n=N_U} W_i h_i^k}$	$V_{x,upper}$	$[V_{Lb} - V_{Ub}]\frac{\sum_{i=x}^{n=N_L} W_i h_i}{\sum_{i=1}^{n=N_L} W_i h_i}$	V_x
9	$1.1 \times 9.57 \times 10^2 kN$	$1.1 \times 1.42 \times 10^3 kN$		$1.56 \times 10^3 kN$
8	$1.49 \times 10^3 kN$	$1.87 \times 10^3 kN$		$1.87 \times 10^3 kN$
7	$1.72 \times 10^3 kN$	$1.87 \times 10^3 kN$		$1.87 \times 10^3 kN$
6	$1.84 \times 10^3 kN$	$1.87 \times 10^3 kN$		$1.87 \times 10^3 kN$
5	$1.87 \times 10^3 kN$	$1.87 \times 10^3 kN$		$1.87 \times 10^3 kN$
4	$1.87 \times 10^3 kN$	$1.87 \times 10^3 kN$		$1.87 \times 10^3 kN$
3			$1.69 \times 10^3 kN$	$3.57 \times 10^3 kN$
2			$2.71 \times 10^3 kN$	$4.58 \times 10^3 kN$
1			$3.22 \times 10^3 kN$	$5.09 \times 10^3 kN$

However, because $R_k > R_{kU2stg}$ (equivalently, R_{k2stg} per Yuan (2016)), the two-stage procedure given by Appendix F is applicable, albeit without the 2.61 multiplier that Yuan specifies should be applied to the spectral acceleration (this multiplier is described in Example 3-2 and not used otherwise). For comparative purposes, the Yuan (2016) two-stage calculation is performed here, but rather than using the NBCC 2010 values or EXP-2 approximation, the NBCC 2015 spectral values are used for brevity's sake and to ensure that the same values are being used for each method. Strictly speaking, the Yuan (2016) two-stage method is applicable only for ASCE 7-10 and NBCC 2010, but the spectral accelerations required by NBCC 2010 and 2015 are different, and so the 2015 values are used for each calculation in this example so that the results are consistent Per Table F.1, Table F.2 and Equations (F.6) and (F.7), γ_{reg} is evaluated as:

$$\gamma_{reg} = 0.05 \tag{4.38}$$

$N_U = 6$, $T_L = 0.23$ seconds and $T_U = 1.04$ seconds, therefore $(T_U/T_L)_{CRT1} < (T_U/T_L) = 4.44 < (T_U/T_L)_{CRT2}$, $\eta_{min} = \eta_{min2} = 0.62$ and $(T_U/T_S)_{CRT} = 1.24 \leq S_a(T_L)/S_a(T_U) = 3.88 \leq T_U/T_L$. Therefore, η_{intr} is calculated according to the second term of Equation (F.9) as 0.65. α_{U2stg} per Equation (D.10) is 1.1. Thus, per Equations (F.1) and (F.4):

$$V_{Ub} = (1.1)(1.15 \times 10^6 kg)(9.8N/kg)(0.145) = 1.80 \times 10^3 kN \tag{4.39}$$

$$F_t = (0.05 + [1 - 0.65])V_{Ub} = 7.20 \times 10^2 kN \tag{4.40}$$

Figure 4.4 depicts the response predicted by the newly proposed method, the Yuan (2016) two-stage method and the default NBCC distribution side-by-side. Both the newly proposed method and the Yuan (2016) two-stage method represent the forces in the upper structure well, especially at the base of the structure where α_U is defined. At the top storey, the Yuan (2016) method performs better, but this is expected – its method is explicitly tailored to the two-stage scenario, as opposed to the newly-proposed method which is intended to be more general. By comparison, the NBCC demonstrates a much larger error at the base of the upper structure compared to either of the other methods. At the top storey, the NBCC is approximately correct, but this is likely circumstantial based on the selected inputs. It cannot be generally said that the NBCC is effective at predicting the loads in the upper structure – as demonstrated by Example 4-2.

Insofar as the lower structure, the response varies widely based on how the base shear is calculated. In the newly proposed method, the lower base shear is based on the absolute sum of the upper structure base shear with the inertia of the lower structure evaluated at T_I, whereas the Yuan (2016) method uses T_L instead and combines the upper and lower structure responses using the SRSS method. As T_L is much smaller than T_I, Yuan (2016) predicts a larger base shear for the lower structure. By using T_I instead of T_L, the proposed method generally predicts a lower shear. The $T_I \leq$ 0.75 seconds requirement is imposed to ensure that this does not cause the lower base shear to be underestimated as it is by the NBCC in this example. This sometimes causes the base shear to be excessively conservative via the proposed method – this is an area for further investigation.

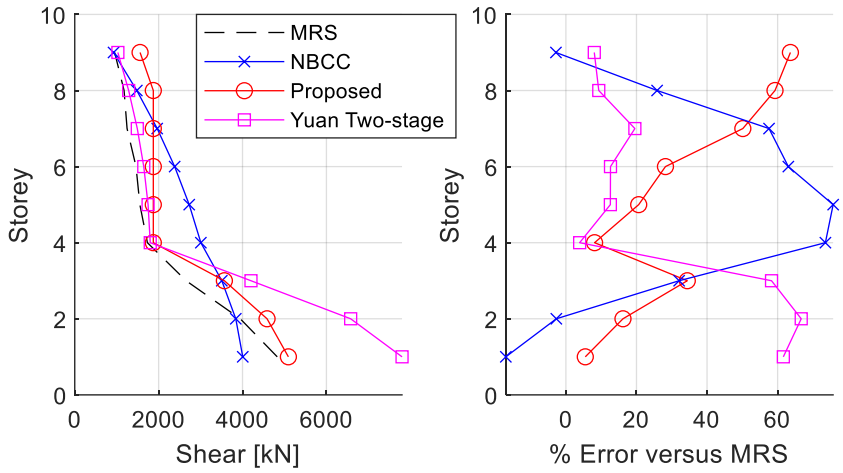

Figure 4.14: Example 4-4 force distribution and error

4.8 Conclusions

In this chapter, three major aspects are discussed: 1) the NBCC 2015 ESFP and its adequacy as applied to regular structure, 2) a method to address appendage structures (one-storey upper structure), and 3) a more general method intended to conservatively estimate loads on structures with a multi-storey upper structure. The key conclusions, divided according to these categories, are as follows:

1. The NBCC 2015 ESFP is based on a set of assumptions primarily oriented around regular structures. For mid-rise regular structures, it is generally conservative. Nevertheless, while the error associated with the NBCC 2015 ESFP is typically small, the MRS-derived storey shears associated with some configurations may be overestimated by 100% or more, especially at the base of the lower structure. The NBCC is primarily concerned with conservatism and simplicity but does not incorporate any systematic means of addressing irregular structures. This last aspect is also true of ASCE 7 in general.

2. For structures having a one-storey upper structure, the upper structure is a relatively small portion of the mass, and thus its impact on the lower structure is relatively small. Conversely, the lower structure's presence significantly amplifies the upper structure's response. The premise of the proposed method is that the upper base shear is scaled by α_U and the lower structure shears are adapted from the typical ESFP. In contrast to Yuan (2016), the proposed method proposes that the requirement R_{kb1} is not necessary and that the period of the lower structure rather than the full structure should be used to analyze the lower structure. The

proposed method does not underestimate the appendage's shear force but is modestly more conservative in its estimates of the lower structures' storey shears.

3. For structures having an upper structure of more than one storey in height, a more general method is proposed to assess the distribution of storey shears. In recognition that the top storey shear force is prone to underestimation by the NBCC ESFP, the concept of α_U is extended to the top storey to estimate the top storey force. Rather than assuming a force distribution, the force distribution of ASCE 7 is adopted and modified to suit the endpoints defined by α_U and α_{Utop}. This defines the upper structure, and the lower structure is defined similarly to the appendage method, albeit using the full structure's period in place of that of the lower structure. To account for the potential that this is unconservative at the base of the lower structure, T_1 is limited to a fixed value. Whereas the NBCC is prone to underestimating the storey shears throughout the structure, the proposed method is conservative and performs particularly well in the upper structure. The median error at the top storey and the base of the upper structure is approximately 10% and 20%, respectively via the proposed method. However, the base shears of the lower structure are generally at least 25% larger than that predicted by the modal response spectrum analysis on account of the constraints, including those applied to T_1. A future study should investigate improvements to the overall base shear of the lower structure, specifically to replace the fixed limit on T_1 currently adopted.

   As an addendum to the investigation of the method applicable to structures having a multi-storey upper structure, a brief investigation considers the storey-by-storey variation of stiffness in the upper structure. A decrease in stiffness from the base to the top of the upper structure modestly affects the adequacy of the proposed method insofar as predicting the storey shears. Considering this variation, the top storey shear may be underestimated by up to 10%, whereas the estimates remain conservative at the base of the upper and lower structures. For a future study, this investigation should be extended to the lower structure and incorporate changes to prevent the underestimation of shears under more realistic distributions of stiffness. To address this potential underestimation, each storey in the upper structure is increased by 10%, but not in excess of the upper base shear.

A total of four examples, two for each of the proposed methods, compare the proposed methods to the NBCC 2015 ESFP. Each features an OSB-sheathed CFS shear wall frame as the seismic-force resisting system of the upper structure, and a reinforced concrete moment-resisting frame for the

lower structure. The stiffnesses and masses are selected to approximate a realistic pre-design example based on the relevant building and material codes. In one example the Yuan (2016) two-stage method is also compared alongside the NBCC and one of the newly proposed methods. In either case, the proposed methods conservatively estimate the storey shears, particularly in the upper structure.

More generally, future work should consider the proposed methods alongside the two-stage procedure given by Yuan (2016) in more detail. Each method advantages and disadvantages, and it may be possible to better suit the methods to specific applications. In addition, Yuan (2016) specifies that all spectral accelerations be multiplied by 2.61. The rationale for this is discussed in Example 3-2, but it is not used in the Chapter 4 examples, pending further investigation of its relevance as applied to the NBCC.

Chapter 5
Conclusions and Recommendations

5.1 Summary

Ultimately, the investigation conducted in the current study addresses the same concerns as Yuan (2016) except for damping irregularity. Namely, for mid-rise structures having a stiff, massive lower structure, and a less stiff, less massive upper structure, two aspects are considered: 1) a procedure to define feasible distributions of design stiffnesses based on an approximation of higher-mode effects on the upper base shear, as a function of the irregularity of the structure, and 2) the estimation of the equivalent static load distribution on such structures. Chapters 3 and 4 of this thesis concerns these two aspects – Chapter 3 concerns the stiffness distribution and expected higher-mode amplification effects, and Chapter 4 concerns the approximation of the equivalent static loads.

Chapter 3 concerns two main elements, which in combination define the feasible stiffness distributions. Using the code-specified interstorey drift limit, the stiffness of the upper structure is directly related to the higher-mode amplification of shear at the upper structure. Analogously to the NBCC's higher mode factor M_v, α_U quantifies this amplification as a function of the mass and stiffness irregularity and is approximated via the overall mass ratio R_m, the overall stiffness ratio R_k and the spectral acceleration $S_a(T)$. Using α_U and the storey drift, a limit state analogue is defined – to satisfy the interstorey drift limit for a given structure, the storey stiffness of the upper structure must provide adequate resistance against the amplification quantified by α_U. In this way, the stiffness of the upper structure is said to provide resistance to the loading represented by α_U. Thus, combinations of upper and lower structure storey stiffnesses satisfying both this requirement and the scope are said to be feasible. The latter half of Chapter 3 concerns how to solve for these feasible stiffnesses, including two examples.

Meanwhile, Chapter 4 concerns the approximation of equivalent static loads on vertically irregular structures. It begins with a discussion of the NBCC 2015 Equivalent Static Force Procedure (ESFP) and its application to regular structures and proposes two approaches to evaluate the loads on vertically irregular structures – one applicable to a single-storey (appendage) upper structure, and another applicable to a multistorey upper structure. Whereas the ESFP does not always provide conservative estimates for the storey shears, particularly in the upper structure, the proposed methods

are consistently conservative. Four examples, two for each method, are used to demonstrate the proposed methods.

5.2 Conclusions

Overall, the key conclusions for Chapter 3 are:

1. The observed behaviour vis-à-vis R_k is the same as in Yuan: a) for a lower structure which is much less stiff than the upper structure, its behaviour approaches that of a damper, counteracting the effects of the upper structure, b) for a lower structure which is much stiffer than the upper structure, the upper structure acts as though attached to a rigid base, and c) for more practical ranges of relative stiffness and mass, the lower structure and upper structure may interact – the resulting amplification is potentially greater than or less than unity, representing a decrease or increase in the upper structure's base shear, respectively. The values of R_m and $S_a(T)$ heavily influence which of these three conditions are applicable. In general, larger values of R_m increase the influence of the lower structure on the upper one and therefore correspond to a larger amplification factor α_U, particularly where R_m and R_k are approximately equal – equivalently, where the fundamental periods of the upper and lower structure are closely-spaced.

2. The value of α_U indicates the effect that higher mode effects have on the upper structure's base shear: a) $\alpha_U < 1$ indicates that higher mode effects decrease the expected upper structure base shear and is associated especially with the upper structure being much stiffer than the lower structure overall (i.e. the damper case above), and b) $\alpha_U > 1$ indicates that the higher mode effects amplify the base shear and is associated with closely-spaced periods between the upper and lower structure. Meanwhile, a very stiff lower structure is associated with a relatively constant α_U - Yuan (2016) interprets this as $\alpha_U \approx 1$. More specifically, α_U in this region can be as large as 1.25. The proposed formulation modestly improves on the accuracy of the previous formulation and expands the scope – within the expanded scope, α_U is generally overestimated by 2% to 27% by the proposed method.

3. This α_U directly relates the storey drift at the base of the upper structure to the upper structure storey stiffness k_U. In conjunction with the overall stiffness ratio R_k, this relationship is used to characterize those combinations of stiffness that satisfy the scope of the study and the code-specified interstorey drift requirement. The derivation uses the NBCC 2015 spectrum to solve

the relationships directly rather than using the transformed NBCC spectrum adopted by Yuan (2016). While this can still be done numerically, a graphical solution is also proposed for the critical values of k_U.

4. The existing examples and calculations are defined using the linear response, and thus $R_dR_o = 1$. Correspondingly, the proposed methods, including α_U, are independent of R_dR_o. For practical application, designers may adopt the smallest R_dR_o of the two seismic force-resisting systems that are used, consistent with NBCC 2015 recommendations.

Much of Chapter 3 is similar to Yuan (2016). Consequently, the high-level details of α_U and the procedure to define feasible stiffness distributions are mostly identical. The main differences are in the form rather than the substance of the formulation – to better suit the NBCC 2015, the critical values of R_k and α_U are updated, and the feasible stiffnesses distributions feature a more direct (albeit still numerical) solution.

The following chapter, Chapter 4, proposes two procedures to determine the storey shears on a mid-rise structure with a combination of framing systems:

1. The first method applies only to structures with a one-storey upper structure (appendage). In the method, the appendage's base shear is amplified using α_U to account for higher-mode effects due to irregularity, and the lower structure's base shear is defined similarly to the NBCC base shear. The loads on the lower structure are defined according to the standard NBCC static procedure, albeit with the upper structure's base shear replacing the code-specified top storey shear F_t.

2. The second method applies to structures having a multistorey upper structure. The α_U concept is extended to the top storey to define α_{Utop}, and using α_{Utop} and α_U the higher-mode top storey and upper structure base shears are defined. The force distribution on the upper structure is chosen to suit these endpoints. For the lower structure, the default NBCC distribution is used, albeit with the upper structure base shear replacing the code-specified top storey shear F_t. An additional limit on the period of the full structure is applied to ensure that the base shear of the lower structure is conservative. The method is still largely conservative if the upper structure is considered to have some degree of stiffness variation – however, a modest increase of 5-10% to the top storey loads is appropriate to prevent underestimation in this more realistic scenario.

Therefore, a 10% increase is applied to the storey shears of all storeys in the upper structure. These adjusted shears do not need to be larger than the upper base shear.

3. Unlike the default equivalent static procedure specified by NBCC 2015, neither method considers the entire structure in one piece. Instead, both methods bear a passing resemblance to the ASCE 7 two-stage procedure – the upper structure and lower structure are analyzed separately and reassembled, with the upper structure's base shear being applied to the top of the lower structure.
4. The existing examples and calculations are defined using the linear response, and thus R_dR_o = 1. Correspondingly, the proposed methods are independent of R_dR_o. For practical application, designers may adopt the smallest R_dR_o of the two seismic force-resisting systems that are used, consistent with NBCC 2015 recommendations.

In general, α_U is an appropriate measure of irregularity and is useful in defining both appropriate stiffness distributions and equivalent static loads on the base of the upper structure. The proposed methods defined using α_U are generally conservative and applicable to a wide array of structures. The proposed methods have been updated to cover a larger scope than those proposed by Yuan & Xu (Xu & Yuan, 2015; Yuan, 2016; Yuan & Xu, 2016, 2014) and have been updated to reflect NBCC 2015.

5.3 Recommendations

Much like the existing National Building Code of Canada, the current study relies on a mix of linear dynamic modal response spectrum analysis and linear static analysis, rather than nonlinear and/or time history analysis, besides a limited nonlinear time history analysis investigation performed by Yuan (2016). Nonlinear analysis, especially for complex systems such as mid-rise structures with a vertical combination of framing systems, is difficult and time-consuming to perform, difficult to interpret, and difficult to generalize. Thus, codes often rely on a mix of linear elastic analysis and engineering judgment, in part because they wish to be both general and simple-to-use. It is inevitable that some of these simplifications must be made for a non-iterative, static method. Unfortunately, focusing exclusively on the linear modal response spectrum is somewhat myopic – nonlinear and time history analysis can reveal trends that are not evident in a simpler analysis.

Insofar as nonlinear analysis:

1. Research should investigate the inelastic modification factors R_dR_o (NBCC) and R (ASCE) for combined framing systems. The existing research is piecemeal and not generalizable, and sometimes the values given in the codes themselves for individual systems are somewhat arbitrary or reliant on engineering judgment (FEMA, 2009b). The treatment between codes is likewise inconsistent – NBCC 2015 specifies that the lowest of the two systems should be used, whereas ASCE 7's two-stage procedure sometimes allows a mix of values to be used. The risks and expected performance should be made clear by the design codes, and research should be undertaken the evaluate the effective R_dR_o of combined framing systems.
2. A more comprehensive set of nonlinear time history analyses should be undertaken to assess the effectiveness of α_U and the other parameters and procedures introduced in this study. In particular, previous research has identified that the effect of closely-spaced periods of the upper and lower structures, or of the structure and the seismic excitation, may not be well-captured by linear modal response spectrum or static analyses. Studies have also identified the risk of damage concentration in the vicinity of the irregularity – this must be evaluated.

Aside from the issue of nonlinear behaviour, there remain limitations on the linear analysis. Further research could expand the scope to which these methods apply, or investigate such issues such as equivalent damping, flexible diaphragms, torsion or soil conditions other than Class C. More fundamentally, several outstanding issues remain for the method proposed in this thesis, namely:

1. The definitions of α_U and the procedure to derive feasible stiffnesses proposed in Chapter 3 should be extended so that it applies for $R_k < R_{kU1}$. This limitation is imposed to ensure that the largest interstorey drift occurs at the base of the upper structure, but it is reasonable to expect that a more regular structure is less vulnerable. The current procedure is unable to analyze regular structures.
2. Yuan (2016) suggests that spectral accelerations should be multiplied by 2.61 to ensure a certain level of seismic hazard. It is unclear whether this is necessary for the NBCC spectrum given its methodological differences from ASCE 7, and so this matter should be investigated.
3. The investigation of the variation of stiffness should be extended to the lower structure. The current study considers only the upper structure having variation of stiffness.
4. In general, the methods proposed to determine the loads in this thesis, as well as the Yuan (2016) two-stage method, have different approaches and therefore may be better suited if

calibrated to specific ranges of R_k. This notwithstanding, the newly proposed method for multistorey upper structures relies heavily on rules-of-thumb and approximate limits on specific variables. Further investigation should improve these approximations, particularly applied to the base of the lower structure. Likewise, the 10% surcharge applied to the upper structure to account for stiffness variation should be further improved.

5. The current study applies only to NBCC 2015. Given that revisions to both the NBCC and the US National Earthquake Hazard Reduction Program (NEHRP) recommendations (which inform ASCE 7) are imminent, the newly-proposed methods and those proposed by Yuan & Xu (Xu & Yuan, 2015; Yuan, 2016; Yuan & Xu, 2016, 2014) should be re-examined in the context of the new provisions. In particular, NBCC 2020 will be incorporating new ground-motion prediction models which may change the spectral acceleration relationships in some regions (Adams et al., 2019).

References

Adams, J., Allen, T., Halchuk, S., & Kolaj, M. (2019). Canada's 6th Generation Seismic Hazard Model, as Prepared for the 2020 National Building Code of Canada. *The 12th Canadian Conference on Earthquake Engineering*.

Aghdam, A. Y., & Tariverdilo, S. (2012). A numerical criterion to detect vertical stiffness irregularity. *Advances in Structural Engineering*, *15*(1), 31–39. https://doi.org/10.1260/1369-4332.15.1.31

Al-Ali, A. A. K. (1998). *Effects of vertical irregularities on seismic behavior of building structures*. Standford University.

Al-Ali, A. A. K., & Krawinkler, H. (1998). *Effects of vertical irregularities on seismic behavior of building structures* (Issue 130). https://purl.stanford.edu/qh189ph3062

Allen, D., & Wills, R. (2017, March). Specifying cold-formed steel to meet project goals. *The Construction Specifier*. https://www.constructionspecifier.com/specifying-cold-formed-steel-to-meet-project-goals/

Allen, M., Chung, N. C., Tran, A., & Zepeda, D. (2013). Two stage analysis: Implementation challenges. *Structures Congress 2013*, 2192–2202. https://doi.org/10.1061/9780784412848.192

American Iron and Steel Institute (AISI). (2015). *AISI S400-15: North American Standard for Seismic Design of Cold-Formed Steel Structural Systems*.

American Society of Civil Engineers (ASCE). (2010). *ASCE 7-10: Minimum design loads and associated criteria for buildings and other structures*.

ASCE. (2017). *ASCE 7-16: Minimum design loads and associated criteria for buildings and other structures*.

American Wood Council (AWC). (2017). *NDS: National Design Specification for wood construction: 2018 Edition*. American Wood Council.

AWC. (2018). *Manual for engineered wood construction: 2018 Edition* (1st ed.). American Wood Council.

Anagnostopoulou, V. V., Volakos, E. K., & Zeris, C. A. (2015). Objective evaluation of the q factor of irregular RC buildings designed according to EC8 - Design and analyses procedures. *COMPDYN 2015 - 5th ECCOMAS Thematic Conference on Computational Methods in Structural Dynamics and Earthquake Engineering*, *May*, 1040–1053. https://doi.org/10.7712/120115.3449.1617

Aranda, G. R. (1984). Ductility demands for R/C frames irreagular in elevation. *8th World Conference on Earthquake Engineering*.

Bhosale, A. S., Davis, R., & Sarkar, P. (2017). Vertical Irregularity of Buildings: Regularity Index versus Seismic Risk. *ASCE-ASME Journal of Risk and Uncertainty in Engineering Systems, Part A: Civil Engineering*, *3*(3), 1–10. https://doi.org/10.1061/AJRUA6.0000900

Bhosale, A. S., Davis, R., & Sarkar, P. (2018a). New Seismic Vulnerability Index for Vertically Irregular Buildings. *ASCE-ASME Journal of Risk and Uncertainty in Engineering Systems, Part A: Civil Engineering*, *4*(3), 1–8. https://doi.org/10.1061/AJRUA6.0000973

Bhosale, A. S., Davis, R., & Sarkar, P. (2018b). Seismic Safety of Vertically Irregular Buildings: Performance of Existing Indicators. *Journal of Architectural Engineering*, *24*(3), 1–9. https://doi.org/10.1061/(ASCE)AE.1943-5568.0000319

Blume, J. A., Knox, M. T., & Lindskog, E. (1960). Appendix C: Report on setbacks. In *Recommended lateral force requirements and commentary 1st edition*. Structural Engineers Association of California.

Branston, A. E. (2004). *Development of a Design Methodology for Steel Frame/Wood Panel Shear Walls*.

Canadian Commission on Building and Fire Codes. (2018). *National Building Code 2015 - Proposed Change 1205: Revision to requirement for structures with large gravity-induced lateral demand*.

Canadian Standards Association. (1992). *CSA O325: Construction Sheathing*.

Cassis, J. H., & Cornejo, E. (1996). Influence of Vertical Irregularities in The Response of Earthquake Resistant Structures. In *11th World Conference on Earthquake Engineering* (Issue

No:1102).

Chen, Z., & Ni, C. (2020). Criterion for Applying Two-Step Analysis Procedure to Seismic Design of Wood-Frame Buildings on Concrete Podium. *Journal of Structural Engineering*, *146*(1).

Cheung, V. W. T., & Tso, W. K. (1987). Lateral load analysis for buildings with setback. *Journal of Structural Engineering*, *113*(2), 209–227.

Chintanapakdee, C., & Chopra, A. K. (2004). Seismic response of vertically Irregular frames: Response history and modal pushover analyses. *Journal of Structural Engineering*, *130*(8), 1177–1185. https://doi.org/10.1061/(ASCE)0733-9445(2004)130:8(1177)

Chopra, A. K. (2012). *Dynamics of structures: Theory and applications to earthquake engineering* (4th ed.). Prentice Hall.

Chopra, A. K. (2020). Modal combination rules in response spectrum analysis: Early history. *Earthquake Engineering and Structural Dynamics*, *July*, 1–10. https://doi.org/10.1002/eqe.3333

Clark Dietrich. (2017). *Cold-formed structural framing products: Technical design guide*.

Cruz, E. F., & Cominetti, S. (1996). Influence of irregularities in height and different design criteria on the inelastic response of building models. *11th World Conference on Earthquake Engineering*.

CSA Group. (2019). *CSA A23.3:19 Design of concrete structures*.

Das, S., & Nau, J. M. (2003). Seismic Design Aspects of Vertically Irregular Reinforced Concrete Buildings. *Earthquake Spectra*, *19*(3), 455–477. https://doi.org/10.1193/1.1595650

De Stefano, M., & Pintucchi, B. (2008). A review of research on seismic behaviour of irregular building structures since 2002. *Bulletin of Earthquake Engineering*, *6*(2), 285–308. https://doi.org/10.1007/s10518-007-9052-3

Dhileep, M., Arumairaj, P. D., & Hemalatha, G. (2019). A dynamic correction for the seismic analysis of structures. *Innovative Infrastructure Solutions*, *4*(23). https://doi.org/10.1007/s41062-019-0205-4

Dolce, M. (1988). Nonlinear response of buildings vs. vertical regularity requirements of seismic codes: a parametric study. *9th World Conference on Earthquake Engineering*.

Duan, X. N., & Chandler, A. M. (1995). Seismic Torsional Response and Design Procedures. *Earthquake Engineering & Structural Dynamics*, *24*, 761–777.

Elnashai, A. S., & Soliman, M. M. (1995). Effect of Building Configuration on Seismic Response Parameters. *Third International Conference on Recent Advances in Geotechnical Earthquake Engineering and Soil Dynamics*.

European Committee for Standardization. (2004). Part 1: General rules, seismic actions and rules for buildings. In *EN 1998-1:2004: Eurocode 8: Design of structures for earthquake resistance*.

Fajfar, P. (2018). Analysis in seismic provisions for buildings: past, present and future: The fifth Prof. Nicholas Ambraseys lecture. *Bulletin of Earthquake Engineering*, *16*(7), 2567–2608. https://doi.org/10.1007/s10518-017-0290-8

Fanaie, N., & Shamlou, S. O. (2012). Studying seismic behavior of mixed structures in height. *15th World Conference on Earthquake Engineering, Lisbon Portugal*.

Fanaie, N., & Shamlou, S. O. (2015). Response modification factor of mixed structures. *Steel and Composite Structures*, *19*(6), 1449–1466. https://doi.org/10.12989/scs.2015.19.6.1449

Federal Emergency Management Agency (FEMA). (2000). *FEMA 356: Prestandard and commentary for the seismic rehabilitation of buildings*.

FEMA. (2009a). *FEMA P-695: Quantification of building seismic performance factors*.

FEMA. (2009b). *FEMA P-750: NEHRP recommended seismic provisions for new buildings and other structures*.

Fragiadakis, M., Vamvatsikos, D., & Papdrakakis, M. (2006). Evaluation of the influence of vertical irregularities on the seismic performance of a nine-storey steel frame. *Earthquake Engineering & Structural Dynamics*, *35*, 1489–1509.

Guo, S., He, M., & Ni, C. (2014). Seismic analysis of hybrid multi-story light wood frames in China.

2014 World Conference on Timber Engineering.

Habibi, A., Vahed, M., & Asadi, K. (2018). Evaluation of Seismic performance of RC setback frames. *Structural Engineering and Mechanics*, *66*(5), 609–619. https://doi.org/10.12989/sem.2018.66.5.609

Halchuk, S., Adams, J., & Allen, T. I. (2015). *Geological Survey of Canada Open File 7893: Fifth generation seismic hazard maps of Canada: Maps and grid values to be used with the 2015 National Building Code of Canada*. National Resources Canada. https://doi.org/10.4095/297378

Head, M., Dennis, S., Muthukumar, S., Nielson, B., & Mackie, K. (2014). Nonlinear Analysis in Modern Earthquake Engineering Practice. *Structure Magazine*, *March*, 16–20.

Hoesly, N. (2019). *Cost-Effective Mid-Rise Podium Construction*. Niskian & Associates Web Site. https://www.nishkian.com/cost-effective-mid-rise-podium-construction/

Huang, W., Qian, J., Zhou, Z., & Fu, Q. (2015). An approach to equivalent damping ratio of vertically mixed structures based on response error minimization. *Soil Dynamics and Earthquake Engineering*, *72*, 119–128. https://doi.org/10.1016/j.soildyn.2015.02.008

Humar, J., & Mahgoub, M. A. (2003). Determination of seismic design forces by equivalent static load method. *Canadian Journal of Civil Engineering*, *30*(2), 287–307. https://doi.org/10.1139/l02-067

Humar, J., & Rahgozar, M. A. (2000). Application of uniform hazard spectra in seismic design of multistorey buildings. *Canadian Journal of Civil Engineering*, *27*(3), 563–580. https://doi.org/10.1139/l99-045

Humar, J., & Wright, E. W. (1977). Earthquake response of steel-framed multistorey buildings with set-backs. *Earthquake Engineering & Structural Dynamics*, *5*(1), 15–39. https://doi.org/10.1002/eqe.4290050103

International Code Council (ICC). (2015). *2015 International Building Code*.

International Conference of Building Officials (ICBO). (1988). *Uniform building code*.

ICBO. (1997). Volume 2: Structural engineering design provisions. In *1997 Uniform Building Code* (p. 300).

Jain, S. K., & Sharma, R. (1988). Dynamic response of a setback building with a flexible floor diaphragm. *Proceedings of Ninth World Conference on Earthquake Engineering*.

Jharveri, D. P. (1967). *Earthquake forces in tall buildings with setbacks*. University of Michigan.

Karavasilis, T. L., Bazeos, N., & Beskos, D. E. (2008a). Estimation of seismic inelastic deformation demands in plane steel MRF with vertical mass irregularities. *Engineering Structures*, *30*, 3265–3275. https://doi.org/10.1016/j.engstruct.2008.05.005

Karavasilis, T. L., Bazeos, N., & Beskos, D. E. (2008b). Seismic response of plane steel MRF with setbacks: Estimation of inelastic deformation demands. *Journal of Constructional Steel Research*, *64*, 644–654. https://doi.org/10.1016/j.jcsr.2007.12.002

Krawinkler, H. (2006). Importance of good nonlinear analysis. *Structural Design of Tall and Special Buildings*, *15*(5), 515–531. https://doi.org/10.1002/tal.379

Le-Trung, K., Lee, K., Lee, J., & Lee, D. H. (2012). Evaluation of seismic behaviour of steel special moment frame buildings with vertical irregularities. *The Structural Design of Tall and Special Buildings*, *21*, 215–232.

Lin, J. L., Tsaur, C. C., & Tsai, K. C. (2019). Two-degree-of-freedom modal response history analysis of buildings with specific vertical irregularities. *Engineering Structures*, *184*(December 2018), 505–523. https://doi.org/10.1016/j.engstruct.2019.01.106

Liu, H., Van De Lindt, J. W., & Pryor, S. (2008). Seismic Performance Assessment of a Seven-Story Wood-Steel Hybrid Building. *14th World Conference on Earthquake Engineering*. www.engr.colostate.edu/NEESWood/sapwood

Louisiana Pacific. (2012). *OSB sheathing specification - APA rated Sheathing & structural 1 sheathing*.

Lu, Z., Li, J., & Zhou, Y. (2018). Shaking table test and numerical simulation on a vertical hybrid structure under seismic excitation. *Structural Design of Tall and Special Buildings*, *27*.

https://doi.org/10.1002/tal.1497

Magliulo, G., Capozzi, V., & Ramasco, R. (2012). Seismic performance of R/C frames with overstrength discontinuities in elevation. *Bulletin of Earthquake Engineering*, *10*, 679–694. https://doi.org/10.1007/s10518-011-9316-9

Magliulo, G., Ramasco, R., & Realfonzo, R. (2002). A critical review of seismic code provisions for vertically irregular frames. *Proceedings of the Third European Workshop on the Seismic Behavior of Irregular and Complex Structures*.

Magliulo, G., Ramasco, R., & Realfonzo, R. (2004). Seismic Vulnerability of R/C Frames with Strength Irregularity in Elevation. *13th World Conference on Earthquake Engineering*.

Maley, T. J., Sullivann, T. J., & Pampanin, S. (2012). Issues with the seismic design of mixed MRF Systems. *15th World Conference on Earthquake Engineering (15WCEE)*.

Mazzolani, F. M., & Piluso, V. (1996). *Theory and design of seismic resistant steel frames*. SPON Press.

Meskouris, K., Butenweg, C., Hinzen, K.-G., & Höffer, R. (2019). *Structural Dynamics with Applications in Earthquake and Wind Engineering* (2nd ed.). Springer. https://doi.org/10.1007/978-3-662-57550-5

Moehle, J. P., & Alarcon, L. F. (1986). Seismic analysis methods for irregular buildings. *Journal of Structural Engineering*, *112*(1), 35–52.

Moehle, J. P., & Sozen, M. A. (1980). *Experiments to study earthquake response of R/C structures with stiffness interruptions*.

Montazeri, S. M., Khaledi, F., & Kheyroddin, A. (2012). A Study on Steel Moment Resisting Frames with Setbacks: Dynamic properties. *15th World Conference on Earthquake Engineering*.

National Research Council of Canada (NRCC). (1971). *National building code of Canada 1970*.

NRCC. (2010). *National Building Code of Canada 2010*.

NRCC. (2015a). Appendix C: Climatic and seismic information for building design in Canada. In *National Building Code of Canada 2015 Volume 1*.

NRCC. (2015b). Commentary J: Design for seismic effects. In *Structural Commentaries User's Guide - NBC 2015: Part 4 of Division B*. National Research Council of Canada.

NRCC. (2015c). *National Building Code of Canada 2015*. National Research Council of Canada.

Newmark, N. M., & Hall, W. J. (1982). *Earthquake Spectra and Design*. Earthquake Engineering Research Institute.

Ni, C., Popovski, M., Wang, J. B., & Karacabeyli, E. (2016). Advanced topics in seismic analysis and design of mid-rise wood-frame structures. *WCTE 2016 - World Conference on Timber Engineering*, 5311–5319.

Nitterhouse Concrete Products. (2019). *Podium Structures*. Nitterhouse Concrete Products Web Site. https://nitterhouseconcrete.com/precast/podium-structures/

Osman, A. (2002). Seismic response of steel frames with symmetric setback. *7th US National Conference on Earthquake Engineering*.

Papageorgiou, A. V., & Gantes, C. J. (2010). Equivalent modal damping ratios for concrete/steel mixed structures. *Computers and Structures*, *88*, 1124–1136. https://doi.org/10.1016/j.compstruc.2010.06.014

Pekau, O. A., & Green, R. (1974). Inelastic structures with set-backs. *5th World Conference on Earthquake Engineering*. http://www.iitk.ac.in/nicee/wcee/fifth_conf_Rome/

Penzien, J., & Chopra, A. K. (1965). Earthquake response of appendage on a multi-storey building. *3rd World Conference on Earthquake Engineering*. http://www.iitk.ac.in/nicee/wcee/third_conf_NewZealand/

Pinto, D., & Costa, A. (1993). Influence of vertical irregularities on seismic response of buildings. *Sextas Jornadas Chilenas de Sismología e Ingeniería Antisismica*.

Pirizadeh, M., & Shakib, H. (2013). Probabilistic seismic performance evaluation of non-geometric

vertically irregular steel buildings. *Journal of Constructional Steel Research*, *82*, 88–98. https://doi.org/10.1016/j.jcsr.2012.12.012

Pnevmatikos, N. G., Papagiannopoulos, G. A., & Papavasileiou, G. S. (2019). Fragility curves for mixed concrete/steel frames subjected to seismic excitation. *Soil Dynamics and Earthquake Engineering*, *116*, 709–713. https://doi.org/10.1016/j.soildyn.2018.09.037

Podesto, L. (2017). *Strategies And Trends For Mid-Rise Construction In Wood*. Whole Building Design Guide: A Program of the National Institute of Building Sciences. https://www.wbdg.org/resources/strategies-trends-mid-rise-construction-with-wood

Qian, J., Zhou, Z., & Huang, W. (2015). Investigation on the modal strain energy for dynamic analysis of steel-concrete vertically mixed structures. *Journal of Asian Architecture and Building Engineering*, *14*(3), 671–678. https://doi.org/10.3130/jaabe.14.671

Romao, X., Costa, A., & Delgado, R. (2004). Seismic behavior of reinforced concrete frames with setbacks. *13th World Conference on Earthquake Engineering*.

Rosenblueth, E., Chopra, A. K., Newmark, N. M., Esteva, L., de Buen, O., Park, R., Paulay, T., Priestley, M. J. N., Whitman, R. V., Bielak, J., Goldberg, A., & Rukos, E. A. (1980). *Design of Earthquake Resistant Structures* (E. Rosenblueth (ed.)). Pentech Press.

Roy, R., & Mahato, S. (2013). Equivalent lateral force method for buildings with setback: Adequacy in elastic range. *Earthquake and Structures*, *4*(6), 685–710. https://doi.org/10.12989/eas.2013.4.6.685

Sadashiva, V. K., MacRae, G. A., & Deam, B. L. (2012). Seismic response of structures with coupled vertical stiffness-strength irregularities. *Earthquake Engineering & Structural Dynamics2*, *41*, 119–138.

Sarkar, P., Prasad, A. M., & Menon, D. (2010). Vertical geometric irregularity in stepped building frames. *Engineering Structures*, *32*(8), 2175–2182. https://doi.org/10.1016/j.engstruct.2010.03.020

Seismology Committee Structural Engineers Association of California (SEAOC). (1960).

Recommended lateral force requirements and commentary (1st ed.).

SEAOC. (1988). *Recommended lateral force requirements and tentative commentary* (5th ed.).

SEAOC. (1996). *Recommended lateral force requirements and commentary* (6th ed.). Structural Engineers Association of California.

SEAOC. (1999). *Recommended Lateral Force Requirements and Commentary* (7th ed.).

SEAOC. (2015). *2015 IBC SEAOC Structural/Seismic design manual, Volume 1*. ICC/SEAOC.

SEAOC. (2019). *SEAOC Blue Book: Seismic design recommendations 2019*.

Sexton, H. J., & Keith, E. J. (1965). Discussion of "Earthquake response on appendage of a multi-story building." *3rd World Conference on Earthquake Engineering*.

Shahrooz, B. M., & Moehle, J. P. (1990). Seismic response and design of setback buildings. *Journal of Structural Engineering*, *116*(5), 1423–1439. https://doi.org/10.1061/(ASCE)0733-9445(1990)116:5(1423)

Shibata, H., Sato, H., & Shigeta, T. (1965). Aseismic design of machine structure. *3rd World Conference on Earthquake Engineering*.

Skinner, R. I., Skilton, D. W. C., & Laws, D. A. (1965). Unbalanced buildings, and buildings with light towers, under earthquake forces. *3rd World Conference on Earthquake Engineering*. https://www.nicee.org/wcee/search3.php

Sobaih, M., Hindi, A., & Al-Noury, S. (1988). Nonlinear seismic analysis of setback reinforced concrete frames. *9th World Conference on Earthquake Engineering*.

Soni, D. P., & Mistry, B. B. (2006). Qualitative review of seismic response of vertically irregular building frames. *ISET Journal of Earthquake Technology*, *43*(4), 121–132.

Standards Australia. (2007). *AS1170.4 - Structural design actions part 4: Earthquake actions in Australia*.

Tena-Colunga, A. (2004). Review of the Soft First Story Irregularity Condition of Buildings for

Seismic Design. *The Open Civil Engineering Journal*, *4*, 1–15. https://doi.org/10.2174/1874149501004010000l

Tena-Colunga, A., & Hernández-García, D. A. (2020). Peak seismic demands on soft and weak stories models designed for required code nominal strength. *Soil Dynamics and Earthquake Engineering*, *129*. https://doi.org/10.1016/j.soildyn.2019.05.037

Terzic, V., Schoettler, M. J., Restrepo, J. I., & Mahin, S. A. (2015). *Concrete column blind prediction contest 2010: outcomes and observations*.

Teshigawara, M. (2012). Preliminary reconnaissance report of the 2011 Tohoku-Chiho Taiheiyo-Oki Earthquake. Appendix A: Outline of earthquake provisions in the Japanese building codes. In *Geotechnical, Geological and Earthquake Engineering* (Vol. 23). https://doi.org/10.1007/978-4-431-54097-7

Think Wood. (2019). *Light Frame Construction*. https://www.thinkwood.com/products-and-systems/light-frame-construction

Thornburg, D. W., & Henry, J. R. (2015). *2015 International Building Code Illustrated Handbook*. McGraw Hill.

Tremblay, R., Merzouq, S., Izvernari, C., & Alexieva, K. (2005). Application of the equivalent static force procedure for the seismic design of multistorey buildings with vertical mass irregularity. *Canadian Journal of Civil Engineering*, *32*(3), 561–568. https://doi.org/10.1139/L05-007

Tremblay, R., & Poncet, L. (2005). Seismic performance of concentrically braced steel frames in multistory buildings with mass irregularity. *Journal of Structural Engineering*, *131*(9), 1363–1375. https://doi.org/10.1061/(ASCE)0733-9445(2005)131:9(1363)

Valmundsson, E. V., & Nau, J. M. (1997). Seismic Response Of Building Frames With Vertical Structural Irregularities. *Journal of Structural Engineering*, *123*(1), 30–41. https://doi.org/https://doi.org/10.1061/(ASCE)0733-9445(1997)123:1(30)

Varadharajan, S., Sehgal, V. K., & Saini, B. (2013). Determination of inelastic seismic demands of RC moment resisting setback frames. *Archives of Civil and Mechanical Engineering*, *13*(3),

370–393. https://doi.org/10.1016/j.acme.2013.02.006

Varadharajan, S., Sehgal, V. K., & Saini, B. (2014). Seismic behavior of multistory RC building frames with vertical setback irregularity. *The Structural Design of Tall and Special Buildings*, *23*, 1345–1380.

Ward, H. S. (1966). *Earthquake load provisions of the National Building Code of Canada*. National Research Council of Canada Division of Building Research. https://doi.org/https://doi.org/10.4224/20358645

Warr, R. (2019). Reaching Higher with Cold-Formed Steel Framing for Podium Structures. *Structure Magazine*.

Weller, R. (2005). *Earthquake actions in Australia — Worked examples to AS 1170.4*. https://aees.org.au/wp-content/uploads/2013/11/24-Weller.pdf

Wong, C. M., & Tso, W. K. (1994). Seismic loading for buildings with setbacks. *Canadian Journal of Civil Engineering*, *21*(5), 863–871. https://doi.org/10.1139/l94-092

Wood, S. L. (1986). *Experiments to study the earthquake response of reinforced concrete frames with setbacks*. University of Illinois.

Wood, S. L. (1992). Seismic response-of R/C frames with irregular profiles. *Journal of Structural Engineering*, *118*(2), 545–566. https://doi.org/10.1061/(ASCE)0733-9445(1992)118:2(545)

Xiong, H., NI, C., Lu, X., & Jia, G. (2015). Shake Table Tests on 3-Storey Wood Hybrid Structures. *Proceedings of the 10th World Conference on Timber Engineering*.

Xu, L., & Yuan, X. L. (2015). A simplified seismic design approach for mid-rise buildings with vertical combination of framing systems. *Engineering Structures*, *99*, 568–581. https://doi.org/10.1016/j.engstruct.2015.05.019

Yuan, X. L. (2016). *A simplified seismic design approach for mid-rise buildings with vertical combination of framing systems*. University of Waterloo.

Yuan, X. L., & Xu, L. (2016). An improved two-stage seismic analysis procedure for mid-rise

buildings with vertical combination of cold-formed steel and concrete framing. *International Specialty Conference on Cold-Formed Steel Structures*, 853–867.

Yuan, X. L., & Xu, L. (2014). Simplified seismic design for mid-rise buildings with vertical combination of cold-formed steel and concrete framing. *International Specialty Conference on Cold-Formed Steel Structure*, 617–631.

Appendix A

Modal Response Spectrum Analysis to Evaluate α_U of Simplified 2DOF Model

As in Yuan (2016) and Chopra (2012), the governing ordinary differential equation (ODE) for an MDOF lumped-mass system is:

$$\boldsymbol{M}\ddot{\boldsymbol{x}}(t) + \boldsymbol{C}\dot{\boldsymbol{x}}(t) + \boldsymbol{K}\boldsymbol{x}(t) = \boldsymbol{F}(\boldsymbol{t}) \tag{A.1}$$

where $\boldsymbol{M}$, $\mathbf{C}$, and $\boldsymbol{K}$ are the mass, damping and stiffness matrices associated with the structure, $\boldsymbol{F}$ is the forcing vector, and $\boldsymbol{x}$, $\dot{\boldsymbol{x}}$, and $\ddot{\boldsymbol{x}}$, represent the displacement, velocity and acceleration co-ordinates. For a 2DOF system fixed at its base and separated into upper and lower degrees of freedom (denoted by U and L respectively), the matrices are constructed as follows:

$$\boldsymbol{M} = \begin{bmatrix} M_L & 0 \\ 0 & M_U \end{bmatrix} \tag{A.2}$$

$$\boldsymbol{K} = \begin{bmatrix} K_U + K_L & -K_U \\ -K_U & K_U \end{bmatrix} \tag{A.3}$$

$$\boldsymbol{C} = \begin{bmatrix} C_U + C_L & -C_U \\ -C_U & C_U \end{bmatrix} \tag{A.4}$$

From the ODE (Equation (A.1)), the eigenvalue problem for free vibration of the 2DOF system is defined as:

$$\omega_n^2 \boldsymbol{M}\Phi = \boldsymbol{K}\Phi \tag{A.5}$$

$$\therefore det|\boldsymbol{K} - \omega_n^2\boldsymbol{M}| = 0 \tag{A.6}$$

$$(K_L + K_U - \omega_n^2 M_L)(K_U - \omega_n^2 M_U) - K_U^2 = 0 \tag{A.7}$$

where the eigenvalues ω_n and eigenvectors $\boldsymbol{\Phi}$ correspond to the circular frequencies and mode shapes of the system. Each column of $\boldsymbol{\Phi}$ (ϕ_n), corresponds to the n-th mode shape of the structure. Using Equations (3.18) and (3.19) to express K_L and M_L in terms of K_U and M_U, the first and second mode periods of the 2DOF model, as well as the period of the SDOF upper structure are obtained:

$$\omega^2 = \frac{M_U K_U (R_m + R_k + 1) \pm \sqrt{M_U^2 K_U^2 (R_m + R_k + 1)^2 - 4R_m R_k M_U^2 K_U^2}}{2R_m M_U^2} \tag{A.8}$$

$$T_1 = \sqrt{\frac{M_U}{K_U}\left[\frac{8\pi^2 R_m}{R_m + R_k + 1 - \sqrt{(R_m - R_k - 1)^2 + 4R_m}}\right]} \tag{A.9}$$

$$T_2 = \sqrt{\frac{M_U}{K_U}\left[\frac{8\pi^2 R_m}{R_m + R_k + 1 + \sqrt{(R_m - R_k - 1)^2 + 4R_m}}\right]} \tag{A.10}$$

Using the definitions of T_U, T_1 and T_2 from Equations (3.14), (A.9) and (A.10), the mode shapes can likewise be expressed in terms of M_U, K_U, T_U, T_1 and T_2:

$$[-K_U]\phi_L + [K_U - \omega_n^2 M_U]\phi_U = 0 \tag{A.11}$$

$$\begin{aligned}\phi_L &= \frac{K_U - \omega_n^2 M_U}{K_U}\phi_U \\ &= \left(1 - \frac{M_U}{K_U}\frac{K_U}{M_U}\left[\frac{R_m + R_k + 1 \pm \sqrt{(R_m + R_k + 1)^2 - 4R_m R_k}}{2R_m}\right]\right)\phi_U\end{aligned} \tag{A.12}$$

$$\phi_1 = \begin{Bmatrix}\phi_{L1}\\ \phi_{U1}\end{Bmatrix} = \begin{Bmatrix}\frac{1}{2}\left(\frac{R_m - R_k - 1 + \sqrt{(R_m - R_k - 1)^2 + 4R_m}}{R_m}\right)\\ 1\end{Bmatrix} = \begin{Bmatrix}1 - \left(\frac{T_U}{T_1}\right)^2\\ 1\end{Bmatrix} \tag{A.13}$$

$$\phi_2 = \begin{Bmatrix}\phi_{L2}\\ \phi_{U2}\end{Bmatrix} = \begin{Bmatrix}\frac{1}{2}\left(\frac{R_m - R_k - 1 - \sqrt{(R_m - R_k - 1)^2 + 4R_m}}{R_m}\right)\\ 1\end{Bmatrix} = \begin{Bmatrix}1 - \left(\frac{T_U}{T_2}\right)^2\\ 1\end{Bmatrix} \tag{A.14}$$

The effect of the 2DOF masses in each mode can be characterized by the *n*-th mode effective mass M_n^*. Chopra (2012) defines the quantities as:

$$M_n^* = \frac{\left(\sum_{j=1}^{N} m_j \phi_{jn}\right)^2}{\left(\sum_{j=1}^{N} m_j {\phi_{jn}}^2\right)} \tag{A.15}$$

where N is the number of degrees of freedom of the structure, and ϕ_{jn} is the *n*-th mode shape value at the *j*-th DOF. With some manipulation and by using the definition of R_m given by Equation (3.18), the effective modal masses for the first two modes can be defined:

$$M_1^* = M_{U1}^* + M_{L1}^* = \frac{R_m\phi_{L1} + 1}{R_m\phi_{L1}^2 + 1}M_U + \frac{R_m\phi_{L1}^2 + \phi_{L1}}{R_m\phi_{L1}^2 + 1}M_L \tag{A.16}$$

$$M_2^* = (M_U + M_L) - M_1^* = M_{U2}^* + M_{L2}^* \tag{A.17}$$

where M_{jn}^* is the effective mass of the *j*-th DOF in the *n*-th mode, and where the notation M_1^* is used rather than M_{b1}^* as is used in Yuan (2016) to denote the effective mass of the full structure in the first mode (likewise, M_2^* for the second mode). As is the case in Yuan (2016), the contributions associated with the upper and lower masses M_U and M_L can be isolated to determine the effective mass associated with each of the upper and lower structure:

$$M_{U1}^{*} = \frac{R_m \phi_{L1} + 1}{R_m \phi_{L1}^2 + 1} M_U \tag{A.18}$$

$$M_{U2}^{*} = M_U - M_{U1}^{*} \tag{A.19}$$

$$M_{L1}^{*} = \frac{R_m \phi_{L1}^2 + \phi_{L1}}{R_m \phi_{L1}^2 + 1} M_L \tag{A.20}$$

$$M_{L2}^{*} = M_L - M_{L1}^{*} \tag{A.21}$$

Yuan (2016) also normalizes the effective modal masses by the mass of the relevant DOFs. The so-called normalized effective modal masses, denoted by omitting the asterisk, are:

$$M_{U1} = \frac{R_m \phi_{L1} + 1}{R_m \phi_{L1}^2 + 1} \tag{A.22}$$

$$M_{U2} = 1 - M_{U1} \tag{A.23}$$

$$M_{L1} = \frac{R_m \phi_{L1}^2 + \phi_{L1}}{R_m \phi_{L1}^2 + 1} \tag{A.24}$$

$$M_{L2} = 1 - M_{L1} \tag{A.25}$$

$$M_1 = M_{U1} + M_{L1} \tag{A.26}$$

$$M_2 = 1 - M_1 \tag{A.27}$$

Using the effective modal masses M_{U1}^{*} and M_{U2}^{*} above in conjunction with α_U expressed in its complete quadratic combination (CQC) form via Equations (3.5) and (3.6), α_U and the base shear V_{Ub} are expressed in the 2DOF model as :

$$V_{Ub} = \sqrt{(M_{U1}^{*})^2 [g S_a(T_1)]^2 + (M_{U2}^{*})^2 [g S_a(T_2)]^2 + \rho_{12} g^2 \left(M_{U1}^{*} S_a(T_1)\right)\left(M_{U2}^{*} S_a(T_2)\right)} \tag{A.28}$$

$$\alpha_U = \sqrt{(M_{U1})^2 \left[\frac{S_a(T_1)}{S_a(T_U)}\right]^2 + (M_{U2})^2 \left[\frac{S_a(T_2)}{S_a(T_U)}\right]^2 + \rho_{12} \left(M_{U1} \frac{S_a(T_1)}{S_a(T_U)}\right)\left(M_{U2} \frac{S_a(T_2)}{S_a(T_U)}\right)} \tag{A.29}$$

By omitting the modal interaction terms associated with ρ, the square-root-sum-of-squares (SRSS) combination can also be defined for α_U:

$$\alpha_U = \sqrt{(M_{U1})^2 \left[\frac{S_a(T_1)}{S_a(T_U)}\right]^2 + (M_{U2})^2 \left[\frac{S_a(T_2)}{S_a(T_U)}\right]^2} \tag{A.30}$$

However, while Equation (A.30) may occasionally be representative, interaction effects are significant and so Equation (A.29) should be used.

Appendix B

Analytical Study on α_U

B.1 Introduction

In Section 3.3.2, the typical behaviour for several variables' influence on α_U is summarized. This Appendix is intended to further develop this parameter survey. Inevitably, much of the following is similar to that of Xu & Yuan (2015) and Yuan (2016) owing to the similarities between the two models. Despite this, it is necessary to reiterate this information for ready access throughout the thesis text. Where possible the original content is supplemented with additional commentary and insights specific to NBCC 2015.

B.2 Effect of overall stiffness ratio R_k and overall mass ratio R_m on α_U

As with Xu & Yuan (2015) and Yuan (2016) and per Equation (A.29), α_U is chiefly subject to the variables M_{U1}, M_{U2}, $S_a(T_1)/S_a(T_U)$ and ρ, and thus R_m and R_k. The influence of R_k on each of these variables is therefore essential to articulate how α_U changes as a function of R_k. However, Equation (A.29) is based on the 2DOF model and therefore ignores the third and higher modes. Consequently, the following conclusions based on the 2DOF model indicate the general trend but may obscure variation hidden by truncating higher modes. Note that frequent reference is made to a line $R_k = R_m + 1$ in the following plots. The line $R_k = R_m + 1$ is used frequently in Xu & Yuan (2015) and Yuan (2016) and so to avoid unnecessarily changing the previous formulation it is kept the same. Ultimately, $R_k = R_m + 1$ are adequate for the degree of specificity of the proposed method, and rather than expend great effort fixing the line to some other value it is preserved for simplicity and consistency.

B.2.1 Effects of R_k and R_m on φ_{L1}

Yuan (2016) provides that the derivatives of φ_{L1} with respect to R_k, where φ_{L1} is defined by Equation (A.13), is:

$$\frac{d\phi_{L1}}{dR_k} = \frac{-\sqrt{(R_m - R_k - 1)^2 + 4R_m} - (R_m - R_k - 1)}{2R_m\sqrt{(R_m - R_k - 1)^2 + 4R_m}} \tag{B.1}$$

Likewise, the derivative for R_m can be derived, but in a form complex enough that a plot is more intuitive. Figure B.1 illustrates the change of φ_{L1} with respect to R_k (a) and R_m (b).

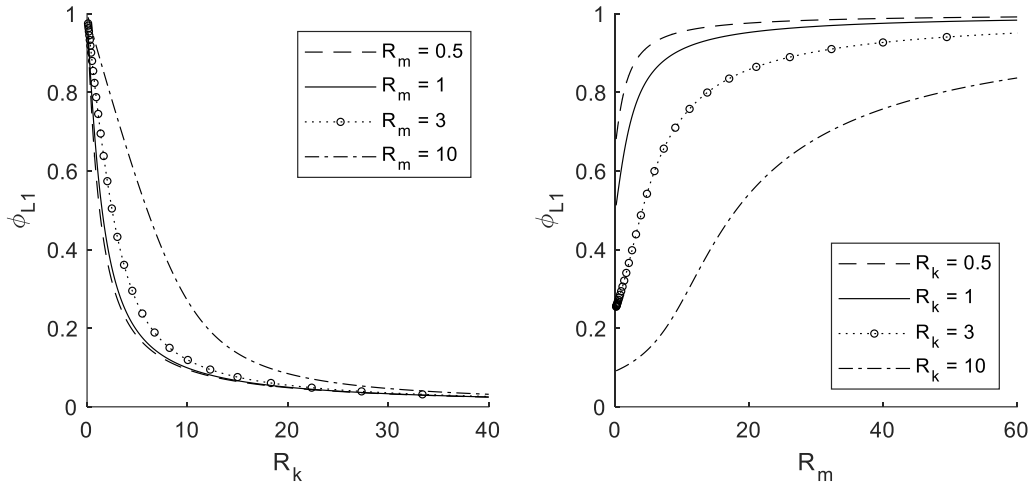

a) b)

Figure B.1: Variation of φ_{L1} as a function of R_k and R_m

It is observed that φ_{L1} increases as R_m increases and decreases as R_k increases, assuming that only one of the two is varied at a time. While in general φ_{L1} is bounded between 0 and 1, an increase in R_k will generally cause φ_{L1} to decrease from 1 quickly and then asymptotically approach 0 as R_k further increases. Likewise, for practical values of R_k, an increase in R_m will cause φ_{L1} to increase from some minimum and proceed asymptotically towards 1.

B.2.2 Effects of R_k and R_m on φ_{L2}

The second mode shape of the lower structure, φ_{L2}, is also relevant as it is related to T_2/T_U via Equation (A.14). While φ_{L1} is bounded between zero and one given that the first mode shape values increase towards the maximum (normalized to one in this case) from the base towards the top, φ_{L2} may take any negative value so long as it is consistent with the upper structure's second mode shape value, which is normalized to a value of one. Consequently, φ_{L2} may hypothetically take any negative value based on the value of R_m and R_k. In this case, it is apparent in Figure B.2 that φ_{L2} is comparatively small in magnitude for small R_k and large R_m, and increases greatly in magnitude for an increase in R_k or a decrease of R_m. For extremely small values of R_k or large values of R_m, φ_{L2} trends towards zero. This is indicative of the full effective mass being concentrated in the first mode and occurs as the upper structure becomes either relatively rigid (small R_k) such that it acts as a rigid body or relatively massive (small R_m) relative to the lower structure such that the upper structure's inertia is dominant. By Equation (A.13), it can also be understood that as R_k increases or R_m decreases, φ_{L2} increases in magnitude, and therefore the magnitude of T_U/T_2 increases.

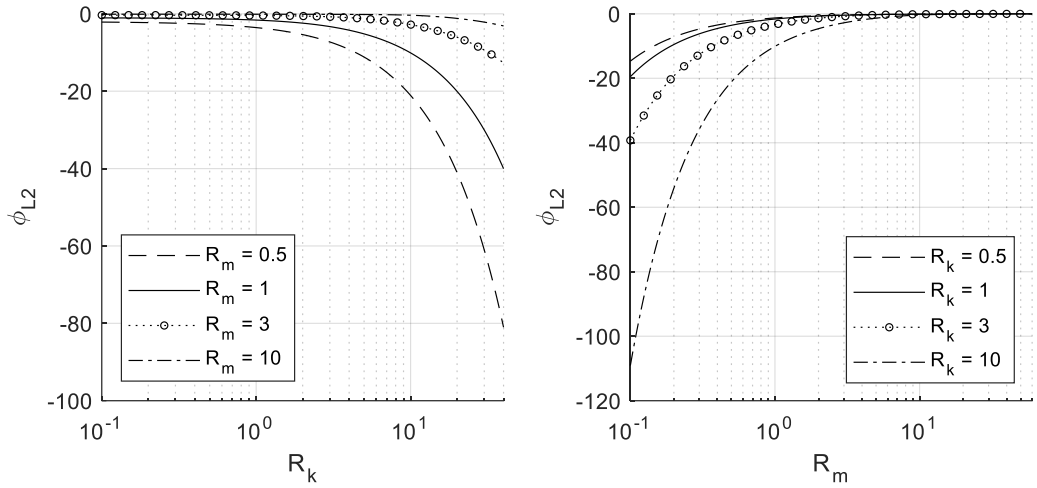

Figure B.2: Variation of φ_{L2} as a function of R_k and R_m

B.2.3 Effects of R_k and R_m on M_{U1} and M_{U2}

Based on the definition of M_{U1} provided by Equation (A.21), Xu & Yuan (2015) and Yuan (2016) provide the first derivative of M_{U1} as a function of R_k:

$$\frac{d\mathrm{M}_{U1}}{d\phi_{L1}} = \frac{-R_m(R_m\phi_{L1}^2 + 2\phi_{L1} - 1)}{(R_m\phi_{L1}^2 + 1)^2} \tag{B.2}$$

Combining the above expression with that of Equation (D.19), they state that M_{U1} reaches its maximum at $R_k = R_m + 1$, which can be easily verified by calculating the R_k-M_{U1} curve for different values of R_m, and identifying the co-ordinate (R_k, R_m) associated with the maximum. They further provide that where $R_k = R_m + 1$, the maximum M_{U1} is:

$$M_{U1,max} = \frac{R_m\sqrt{1+R_m}}{\left(\sqrt{1+R_m} - 1\right)^2 + R_m} \tag{B.3}$$

However, Equations (B.2) and (B.3) do not lend themselves to an intuitive understanding. Figure B.3 illustrates how M_{U1} and M_{U2} change as a function of R_m and R_k. Compared to the mathematical representation, the trends are obvious in three dimensions, namely:

1. M_{U1} is largest when the distance from the line $R_k = R_m + 1$ is the smallest. Correspondingly, the effective mass of co-ordinates (R_m, R_k) farther from the line is smaller, and trends towards unity at the extremes. The rate of change is most pronounced near the line $R_k = R_m + 1$, and the slope flattens as R_k or R_m approach 0.

2. The absolute value of M_{U2} is largest when M_{U1} is largest and follows the same trend as M_{U1}. Nevertheless, while this is true of the 2DOF model on account of how M_{U1} and M_{U2} are defined this is only approximately true of the MDOF model, in which the definitions are slightly different and where higher modes may either decrease or increase the overall response.

3. As M_{U1} approaches unity, M_{U2} necessarily approaches 0, and in relative terms M_{U2} is negative-valued.

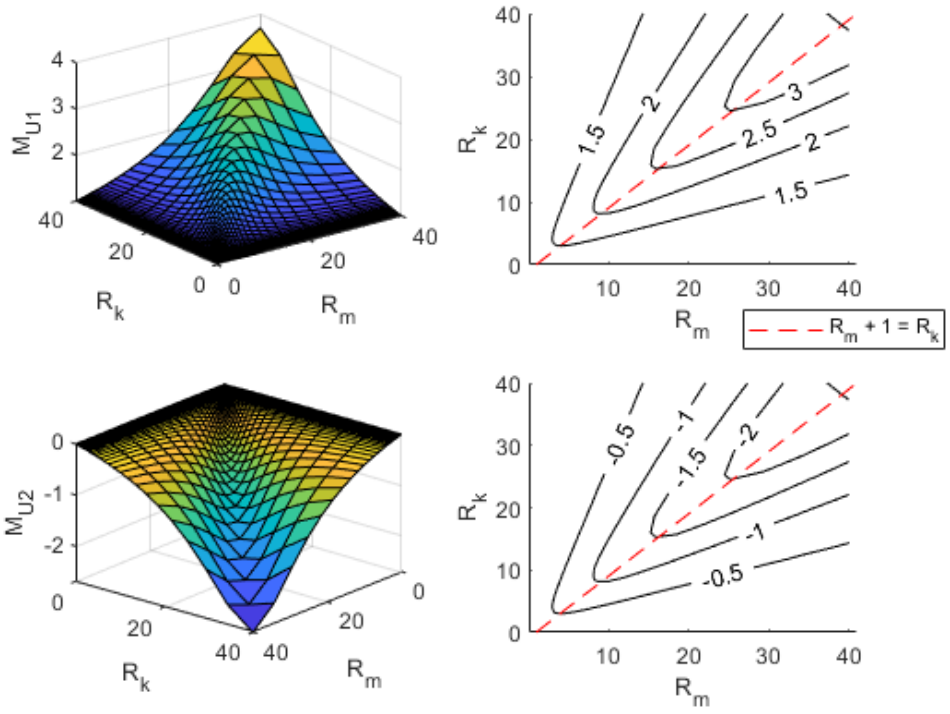

Figure B.3: Variation of M_{U1} and M_{U2} as a function of R_k and R_m

Note that the axes of the upper left (M_{U1}) and lower left plots (M_{U2}) are swapped in direction. This is done to emphasize the shape of M_{U2} which would otherwise be obscured.

B.2.4 Effect of R_k and R_m on periods T_U, T_1, T_2, and spectral ratios $S_a(T_1)/S_a(T_U)$ and $S_a(T_2)/S_a(T_U)$

As expressed in Equations (A.29) and (A.30), the period of the upper structure (T_U) and the first two periods of the full structure (T_1 and T_2) are related to the amplification factor α_U owing to the relationship between these periods and the corresponding spectral values $S_a(T_U)$, $S_a(T_1)$ and $S_a(T_2)$. In Yuan (2016), ASCE 7 permits ratios of these values to be directly related to the periods themselves

on account of the shape of the ASCE 7 spectrum, which facilitates a very concise and simple definition of $S_a(T_1)/S_a(T_U)$ and $S_a(T_2)/S_a(T_U)$. As alleged in Section 3.3.2, this association is not as clear in the NBCC as in the ASCE formulation provided by Yuan (2016), owing largely to the differences between the NBCC and ASCE 7 spectra. To reiterate the key statements of Yuan (2016) and Section 3.3.2 (concerning $S_a(T_1)/S_a(T_U)$):

1. Where both T_1 and T_U as calculated using the 2DOF approximation lie within the constant acceleration region (i.e. ≤ 0.2 seconds for most locations in NBCC 2015, or, equivalently: $(T_U/T_S) \leq (T_U/T_1)$ per Yuan (2016), α_U takes its maximum value and is constant as a function of T_U. So long as both periods are in the constant acceleration range, this applies equally to both the NBCC and ASCE spectra.

2. As T_U and T_1 grow beyond 0.2 seconds, α_U changes as the spectral acceleration curve $S_a(T)$ descends with an increase in T_U and T_1. Using the ASCE spectrum, the ratio $S_a(T_1)/S_a(T_U)$ in this region can be described with only T_U and T_1, such that $S_a(T_1)/S_a(T_U)$ monotonically decreases. This is possible because $S_a(T)$ in the so-called constant velocity region is a linear function of $1/T$, and so $S_a(T_1)/S_a(T_U)$ is directly a function of T_U/T_1. Conversely, the NBCC spectrum is more indirect: $S_a(T)$ is a piecewise linear function of T, and so $S_a(T_1)/S_a(T_U)$ fluctuates in slope when T_1 and T_U lie in different segments. As a consequence, $S_a(T_1)/S_a(T_U)$ often decreases but is punctuated by regions of local increase.

3. At long periods, the distinction remains. In the ASCE spectrum, $S_a(T)$ for long periods is a linear function of $1/T^2$ and consequently continues decreasing ad infinitum, while for NBCC 2015 $S_a(T) = S_a(10.0)$ for all periods beyond 10 seconds. Thus, while $S_a(T_1)/S_a(T_U)$ does not significantly increase at longer periods for ASCE 7, it returns to one for the NBCC where both T_1 and T_U exceed 10 seconds. Long periods ($T > 10$ seconds) are not of importance in this study, but what this implies is that $S_a(T_1)/S_a(T_U)$ neither consistently decreases nor increases for the NBCC spectrum. In approximate terms, the NBCC 2015 spectrum leads to $S_a(T_1)/S_a(T_U)$ having an approximately U-shaped form – equal to one at the extremes, some intermediate minimum, and multiple intermediate changes between downward-sloping and upward-sloping segments as the two periods transition between segments of the $S_a(T)$ curve.

Figure B.4 depicts the relationship between α_U and $S_a(T_1)/S_a(T_U)$ as calculated according to the NBCC 2015 spectrum for an assumed ratio of T_1 and T_U. Showing three locations (Toronto, Halifax and Vancouver) side-by-side, it is evident that α_U matches the shape of the $S_a(T_1)/S_a(T_U)$ distribution. α_U

and $S_a(T_1)/S_a(T_U)$ change slope at T_U values matching the critical T-values which define the NBCC 2015 spectrum (0.2, 0.5, 1.0 seconds, etc.), and the critical T-values multiplied by the ratio of T_U/T_1 (0.2 T_U/T_1, 0.5 T_U/T_1 seconds, etc.). Moving left to right, these points mark where either T_1 or T_U transition to the next segment of the NBCC spectrum. The trend is not uniformly downward and depends both on the periods and on the shape of the spectral acceleration curve $S_a(T)$. Unlike the ASCE formulation given by Yuan (2016), $S_a(T_1)/S_a(T_U)$ cannot be replaced by T_1/T_U or some other combination of periods – it must be evaluated directly.

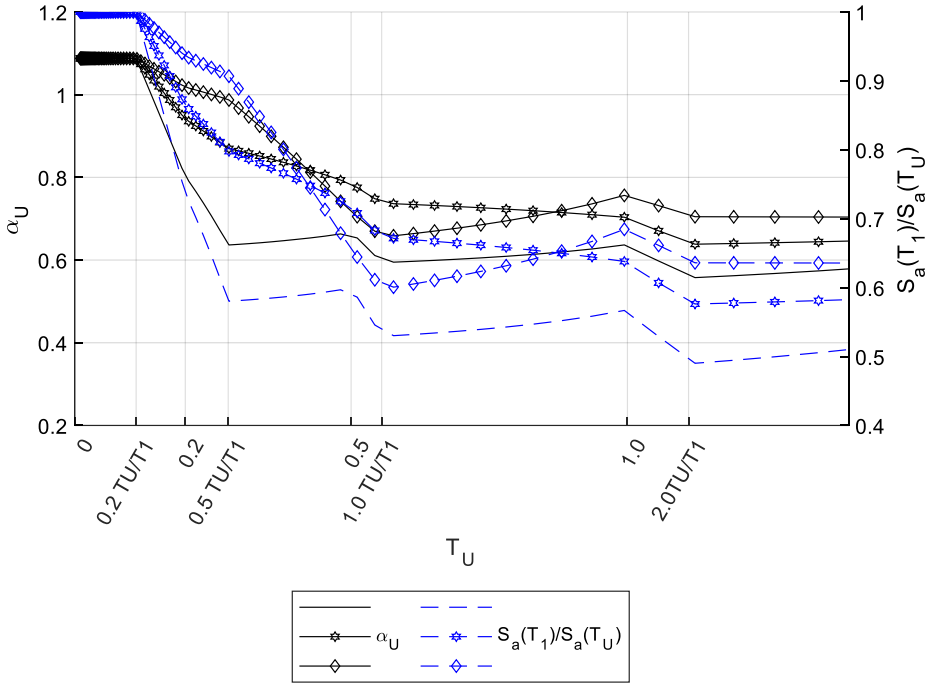

Figure B.4: Variation of α_U relative to $S_a(T_1)/S_a(T_U)$

Thus, T_1 and T_2 must be evaluated. Generically, they can be considered as more inputs to the model, but this is unhelpful. Instead, the same approach as Yuan (2016) is used – T_1 and T_U are related to R_m and R_k via φ_{L1} and Equation (A.13), and so therefore for any arbitrary R_m and R_k, $S_a(T_1)$ can be approximated. In a similar manner, Equation (A.14) relates T_2 and T_U.

From the conclusions of Section B.2.1, it is known that φ_{L1} increases as R_m increases and decreases as R_k increases, but the relationships of Equations (A.13) and (A.14) are not immediately obvious as they apply to R_k and R_m. With some manipulation of Equations (A.13) and (A.14), the following relationships can be derived between T_1, T_2 and T_U:

$$\sqrt{1-\phi_{L1}} = \frac{T_U}{T_1} \tag{B.4}$$

$$\sqrt{1-\phi_{L2}} = \frac{T_U}{T_2} \tag{B.5}$$

Using these functions to estimate and plot the ratios T_U/T_1 and T_U/T_2 as a function of R_m and R_k in Figure B.5, it is easily recognized that the plots featuring T_U/T_1 mirror Figure B.1. Evidently, a decrease in φ_{L1} increases T_U/T_1, and as before this is associated with either an increase in R_k or a decrease in R_m. However, because the relationship is of the square root of $1 - \varphi_{L1}$ rather than φ_{L1} itself, the characteristics of T_U/T_1 are distinct. As T_U/T_2 is nigh-identically defined, it is of identical shape but inverted in orientation. This can be attributed to the fact that generally $T_2 \leq T_U \leq T_1$, and so well-separated T_1 and T_U produce a ratio of less than 1, whereas T_2 is less than T_U and therefore an equal absolute distance (in seconds) apart to that of T_1 and T_U will result in a ratio larger than 1.

The first observation to be made is that an increase in R_k or a decrease in R_m will result in an increase in the value of T_U/T_1 and of T_U/T_2, such that T_U/T_1 tends towards zero and T_U/T_2 tends towards infinity. These endpoints are bounded in a practical sense because of limitations on the relative stiffnesses and masses of the upper and lower structures (and accordingly, of the upper structure and the whole), and on how well the 2DOF model approximates the MDOF periods (setting aside the altogether different problem of estimating periods on realistic structures). Let it suffice to say that none of the structures in the current scope will have any of T_1, T_2, or T_U which are of excessively small magnitude compared to the others.

The remaining key takeaway is what Figure B.5 implies about the relative distance between T_1 and T_U and between T_2 and T_U. For example, T_U/T_1 increases as R_k increases (albeit at a slower rate with higher R_m), which implies that the influence of the first mode on the upper structure becomes relatively more significant, consistent with the trend of M_{U1} observed in Figure B.3. Meanwhile, the same change of R_k causes an increase in the ratio between T_U/T_2. Considering that T_U is generally between T_2 and T_1, this implies that as R_k increases, T_U moves farther and farther away from the second mode until the theoretical limit at which it vibrates only in the first mode. While the details are elaborated further in developing R_{kU2stg} in Section C.2.3, there is a relationship between Figure B.5 and the $R_k \geq 10$ and $T_1/T_U \leq 1.1$ limits which delineate the two-stage procedure in ASCE 7 (2010, 2017). A parallel can also be drawn between Figure B.5 and the logic given by Yuan & Xu (2016) and Yuan (2016), in which the two-stage assumption is characterized by $T_1 \approx T_U$ while $T_2 \approx T_L$.

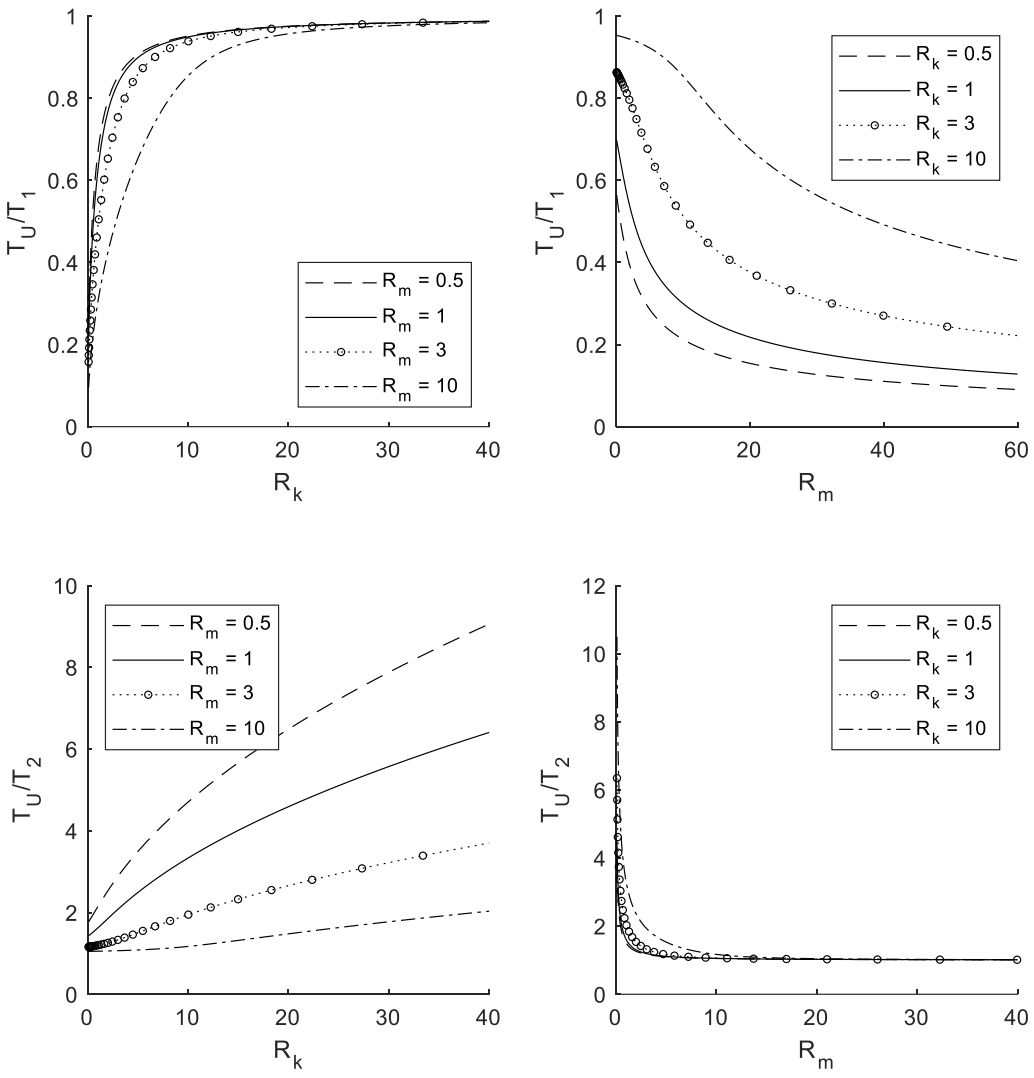

Figure B.5: Variation of T_U/T_1 and T_U/T_2 relative to R_k and R_m

Having characterized T_1/T_U and T_2/T_U, it is desirable to describe $S_a(T_1)/S_a(T_U)$ in terms of R_k and R_m. Figure B.6 depicts the variation of $S_a(T_1)/S_a(T_U)$ relative to R_k in the same fashion as illustrated in Yuan (2016). As expected the relationship is similar despite some small variation in the shape of the plotted curves - $S_a(T_1)/S_a(T_U)$ increases as R_k does, and attains a value of unity beyond approximately $R_k = R_m + 1$.

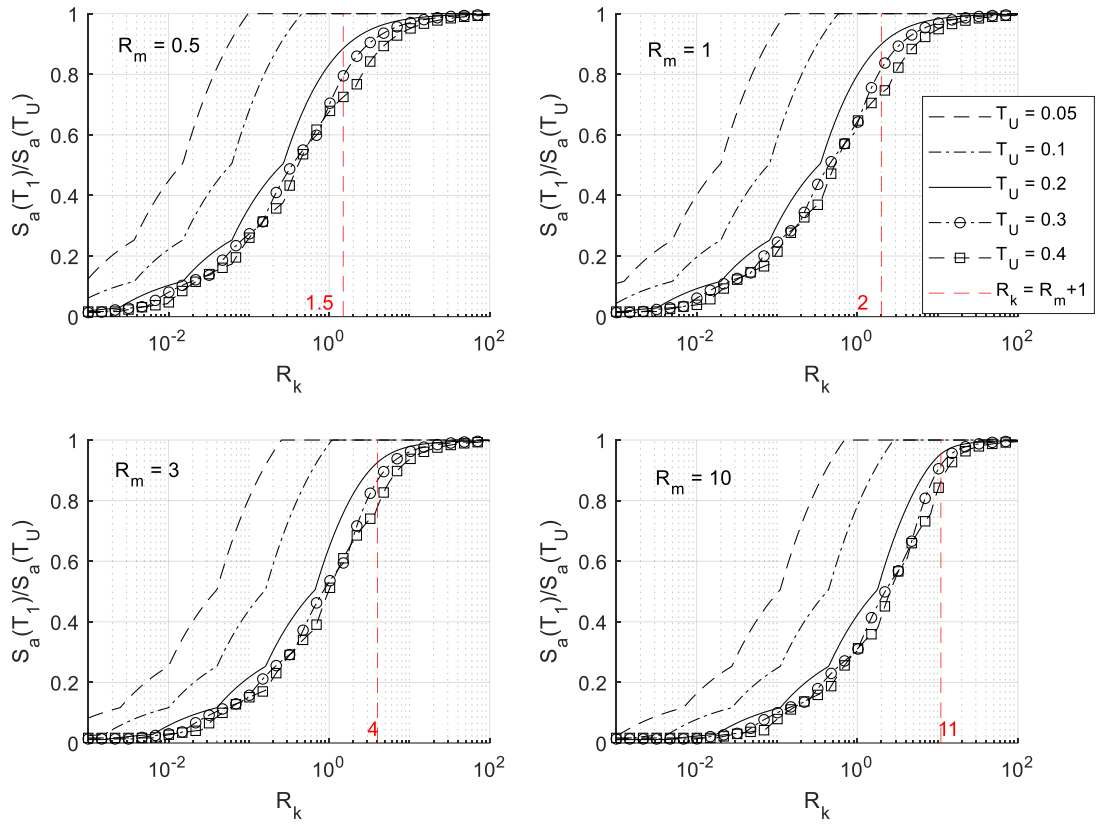

Figure B.6: Variation of $S_a(T_1)/S_a(T_U)$ relative to R_k and R_m

The relationship for $S_a(T_2)/S_a(T_U)$ is slightly different and is plotted in Figure B.7. Unlike $S_a(T_1)/S_a(T_U)$, $S_a(T_2)/S_a(T_U)$ is always unity for $T_U \leq 0.2$ seconds because of $T_2 \leq T_U$ and thus $S_a(T_2) = S_a(T_U)$. For $T_U > 0.2$ seconds, $S_a(T_2)/S_a(T_U)$ increases with R_k until it reaches its peak value. Unlike $S_a(T_1)/S_a(T_U)$, this does not correspond as clearly to $R_k = R_m + 1$. As $S_a(T_2)/S_a(T_U)$ also appears in Equation (A.29), this necessarily entails that the (R_k, R_m) co-ordinate associated with the maximum value of α_U is not a single value but instead a range of possible values. The selection of approximations for these points is considered in Appendix C.

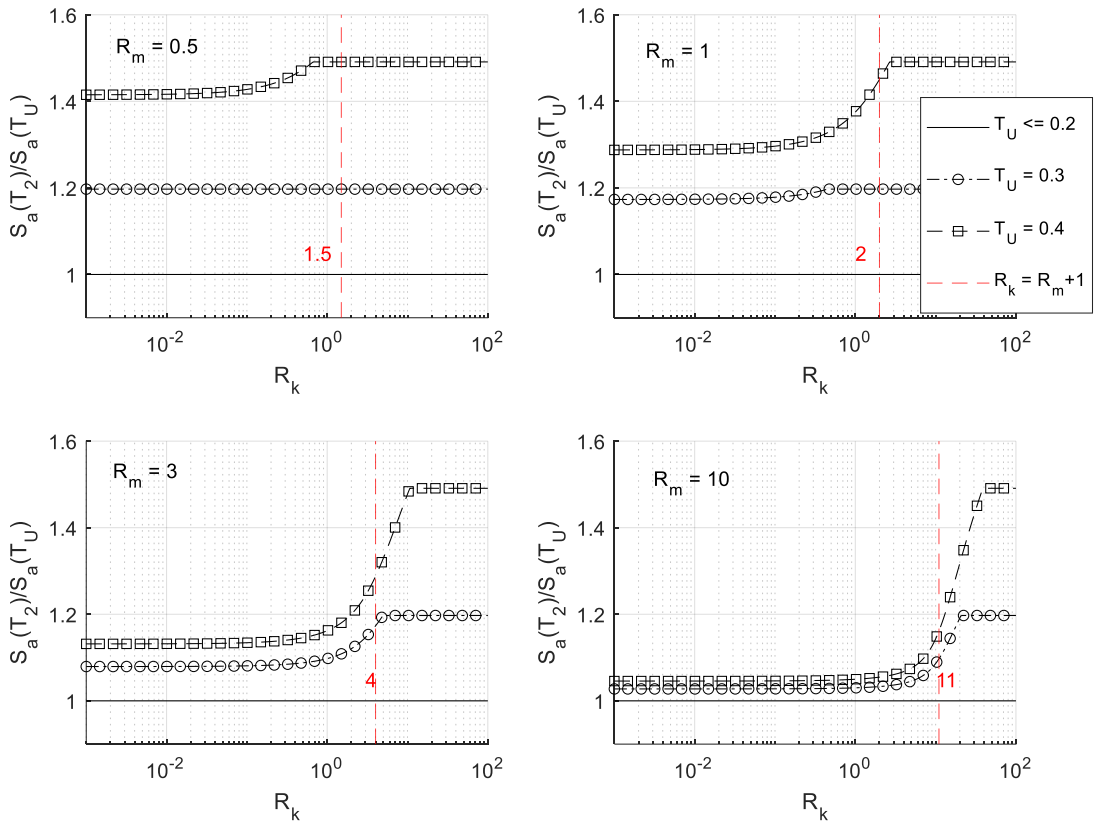

Figure B.7: Variation of $S_a(T_2)/S_a(T_U)$ relative to R_k and R_m

B.2.5 Effect of R_k and R_m on T_2/T_1 and ρ

Having established the effect of R_k and R_m on the first mode shape, on the effective modal masses and the periods and associated spectral values, all that remains is to articulate the effect of R_k and R_m on ρ, the correlation coefficient which differentiates the CQC combination method from that of the SRSS combination method. If ρ is insubstantial, this implies that the modes are well-separated and thus the SRSS method is adequate, whereas if ρ is not negligible this implies that the contributions predicted by the SRSS method may significantly differ from those of the CQC method on account of modal interactions being neglected. ρ as defined by Equation (3.9) is itself a function only of ζ, and T_2/T_1 (in the 2DOF model). ζ is assumed to be 5% in all modes in this study, consistent with the definition of $S_a(T)$ given by NBCC 2015 (NRCC, 2015c), and so therefore ρ is a function only of T_2/T_1, which themselves are expressed only as functions of R_m and R_k according to Equations (A.9) and (A.10). Using Equations (A.9) and (A.10), T_2/T_1 may be defined as (Yuan, 2016):

$$\frac{T_2}{T_1} = \sqrt{\frac{R_m + R_k + 1 - \sqrt{(R_m - R_k - 1)^2 + 4R_m}}{R_m + R_k + 1 + \sqrt{(R_m - R_k - 1)^2 + 4R_m}}} = \sqrt{\frac{1 - \phi_{L1}}{1 + \frac{1}{R_m \phi_{L1}}}} \quad \text{(B.6)}$$

If Equation (B.6) is plotted as a function for R_k and R_m as in Figure B.8, the conclusions are similar to those for M_{U1} given in Section B.2.2, except that the curvature with respect to R_k and R_m is inverted. The following observations can be made based on Figure B.8:

1. As identified by Yuan (2016) and similarly to M_{U1} (Section B.2.2), T_2/T_1 is the largest along the line $R_k = R_m + 1$. As the distance from the line increases, the value of T_2/T_1 decreases at an accelerating rate as the distance from the line increases.

2. For R_m or R_k approaching zero, T_2/T_1 approaches zero, and as $R_k = R_m + 1$ approaches infinity T_2/T_1 approaches one.

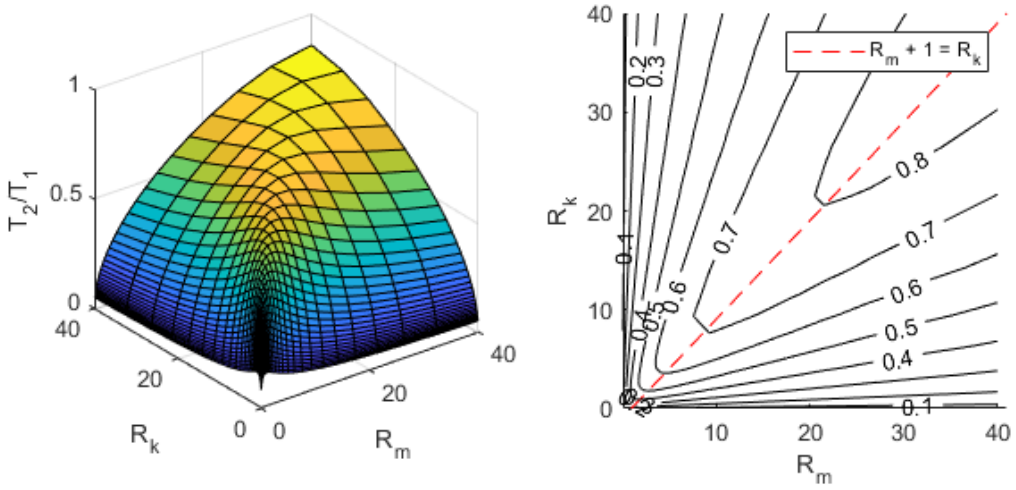

Figure B.8: Variation of T_2/T_1 relative to R_k and R_m

If $R_k = R_m + 1$ is substituted into Equation (B.6), the maximum T_2/T_1 can be determined for any value of R_m (Yuan, 2016):

$$\left(\frac{T_2}{T_1}\right)_{max} = \sqrt{\frac{\left(\sqrt{1 + R_m} - 1\right)\left(R_m + 1 - \sqrt{1 + R_m}\right)}{R_m\sqrt{1 + R_m}}} \quad \text{(B.7)}$$

Considering that the limitations given in Section 1.3.2 have changed relative to Yuan & Xu (2016) and Yuan (2016), the maximum and minimum values of T_2/T_1 and ρ are different. For the current study, the maximum R_m is 55, corresponding to $r_m = 5$, $N_U = 1$ and $N_L = 11$, and the minimum R_m is

0.09, corresponding to $r_m = 1$, $N_U = 11$ and $N_L = 1$. For $R_m = 55$, the maximum T_2/T_1 given by Equation (B.7) is 0.874, as opposed to 0.826 according to Yuan (2016). Using Equation (3.6), the maximum ρ is therefore 0.35. The previous maximum used in Yuan (2016) was 0.22. As the change in scope has increased the range of possible R_m, the potential for modal interaction (as indicated by ρ) has significantly increased. If T_2/T_1 is defined using Equation (B.6), ρ can be plotted as a function of R_m and R_k for 5% damping as in Figure B.9. The relationship is like that of Figure B.3 and M_{U1} and M_{U2}. Specifically, the increase in the absolute values M_{U1} and M_{U2} coincides directly with an increase in ρ, which can be explained via the increase in between-mode interaction which ρ expresses. In addition, $R_k = R_m + 1$ coincides with the maximum value of ρ.

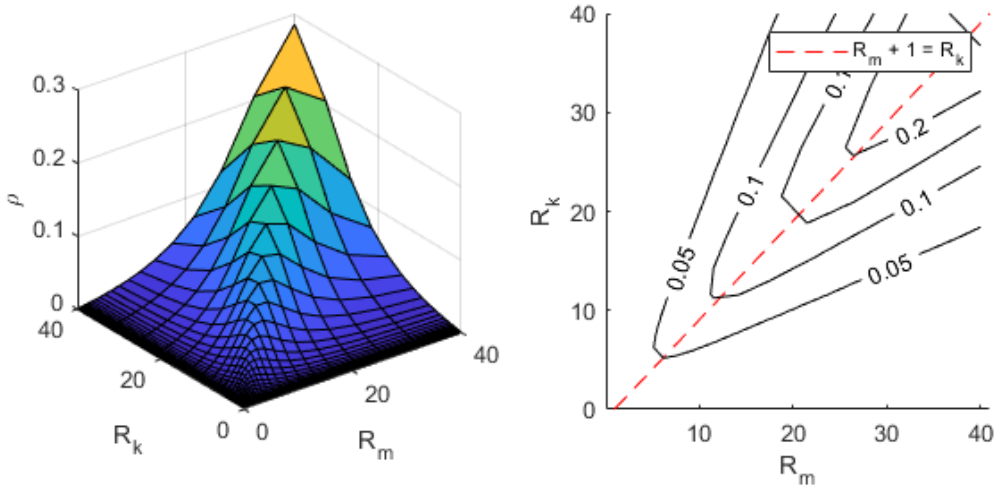

Figure B.9: Variation of ρ as relative to R_m and R_k

It should however be emphasized that the choice of damping ratio will affect the value of ρ and therefore the relative necessity of the CQC method versus the SRSS method. For this study, it is assumed that damping is 5% of critical damping in all modes, but real structures may experience anywhere between 2% and 20% damping, depending on the type and condition of the structure (Newmark & Hall, 1982). As illustrated by Figure B.10, this can significantly change the behaviour of ρ in the 2DOF model and the MDOF model, and thus designers must carefully assess the validity of the model for a given structure. In general, however, the trend is the same – ρ is relatively low for well-spaced periods, and quickly increases as the period ratio exceeds 0.7 (for $\zeta = 5\%$).

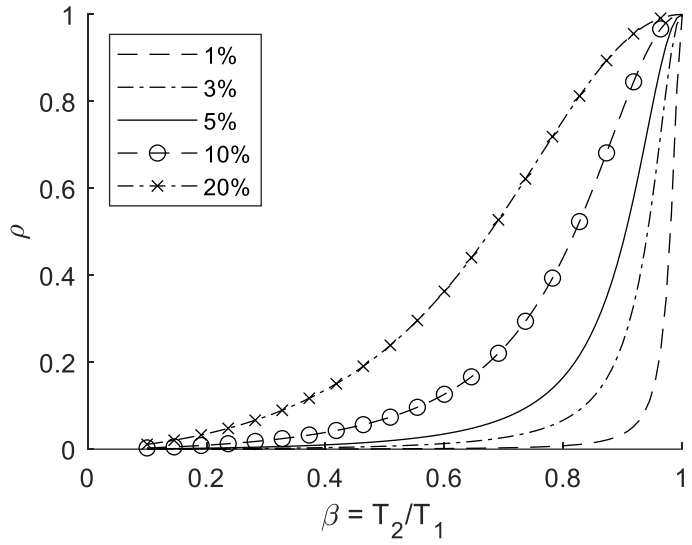

Figure B.10: Effect of period ratio T_2/T_1 and damping ratio ζ on ρ

B.2.6 Effect of R_k and R_m on α_U

Based on the forthgoing sections, an increase of R_k from zero with R_m held constant corresponds to:

1. A decrease in φ_{L1} from unity at a decreasing rate until φ_{L1} asymptotically approaches zero. Simultaneously, φ_{L2} increases in magnitude at an increasing rate, resulting in negative values of large magnitude for large values of R_k and small values of R_m.

2. At first, an increase in the magnitude of effective modal masses M_{U1} and M_{U2} as R_k approaches from $R_k = R_m + 1$. As R_k continues to increase beyond $R_k = R_m + 1$, the magnitudes decrease, with M_{U1} approaching unity and M_{U2} approaching zero. The rate of change with respect to R_k is largest for small distances from $R_k = R_m + 1$, and decreases as the distance from the line $R_k = R_m + 1$ increases.

3. As R_k increases from zero, T_U approaches the value of T_1 and grows increasingly distant from T_2. The value of $S_a(T_1)/S_a(T_U)$ also increases, reaching its maximum value of one at approximately $R_k = R_m + 1$.

4. As R_k increases from zero, the distance between T_2 and T_1 increases from zero, reaching its maximum at $R_k = R_m + 1$. As R_k increases further, the ratio T_2/T_1 approaches zero. The rate of change with respect to R_k increases as the distance to the line $R_k = R_m + 1$ increases. ρ behaves similarly, with its maximum value achieved at $R_k = R_m + 1$, except that the rate of

change decreases as the distance from $R_k = R_m + 1$ increases, with ρ approaching zero at the limit.

The relationships with R_m being varied and R_k held constant follow approximately the same patterns as that for R_k being varied for most of the variables. This is except for φ_{L1}, T_U/T_1 and T_U/T_2, for which an increase in R_m produces a similar result as a decrease of R_k.

From this, it can be inferred that the line $R_k = R_m + 1$ is associated with the maximum amplification factor α_{Umax} and that α_U decreases for values of R_m and R_k which increase the distance from this line. Note, however, that the interpretation of $R_k = R_m + 1$ is that of Yuan (2016) is adopted for consistency. It could be argued that $R_m = R_k$ is an equally valid boundary based on the previous sections' figures. However, this difference is small and $R_k = R_m + 1$ is used instead.

Appendix C
Determination of Revised Critical Stiffness Ratios and Amplification Factors

C.1 Introduction

To characterize the R_m-α_U distribution assumed for this study as it appears in Chapter 3.3.4, four critical stiffness ratios R_k are required, similarly to Yuan & Xu (2016) and Yuan (2016):

1. R_{kU1} – this stiffness ratio identifies the value of R_k below which the interstorey drift is largest in the lower structure, and above which the interstorey drift is largest in the upper structure. This is therefore the minimum stiffness ratio. Values of $R_k < R_{kU1}$ are outside the scope of this study.
2. R_{kU2} and R_{kU3} – as a pair, these stiffness ratios represent the range of stiffness ratios within which the maximum amplification α_{Umax} is assumed to occur. With R_{kU2} as the lower bound and R_{kU3} as the upper bound, $\alpha_U = \alpha_{Umax}$ for values of R_k within this range.
3. R_{kU2stg} – this stiffness ratio identifies the limit beyond which the two-stage assumption similar to that appearing in ASCE 7 is applicable. R_{kU2stg} and R_{k2stg} as defined by Yuan (2016) have been consolidated into a single variable.

Likewise, each of the critical R_k is associated with a corresponding amplification factor α_U:

1. R_{kU1} and α_{U1}
2. R_{kU2} and R_{kU3} and α_{Umax}
3. R_{kU2stg} and α_{U2stg}

This chapter intends to present the background for each new proposed definition, to compare them to those given by Yuan (2016), and to elaborate on differences where they exist. First, for the stiffness ratios R_k and then for the revised amplification ratios α_U.

C.2 Revised stiffness ratios

C.2.1 Minimum overall stiffness ratio R_{kU1}

The proposed design criterion, Equation (3.9), is derived based on Δ_{Ulim}, the code-specified interstorey drift limit (e.g. per Clause 4.1.8.2 11 in NBCC 2015 (NRCC, 2015c)), and according to the definition

of α_U given by Equation (3.5). However, to use this amplification implicitly assumes that the drift limit is governed by the drift at the base of the upper structure. For a regular structure, this is not the case – the maximum storey drift occurs at the base of the structure. Yet as the storey stiffness and mass of the upper structure decrease relative to the lower structure, the drift at the base of the upper structure becomes more dominant until a transition occurs at which it becomes larger than elsewhere in the structure. This transition can be associated with the overall stiffness ratio R_k – this value is referred to as the minimum overall stiffness ratio R_{kUI}.

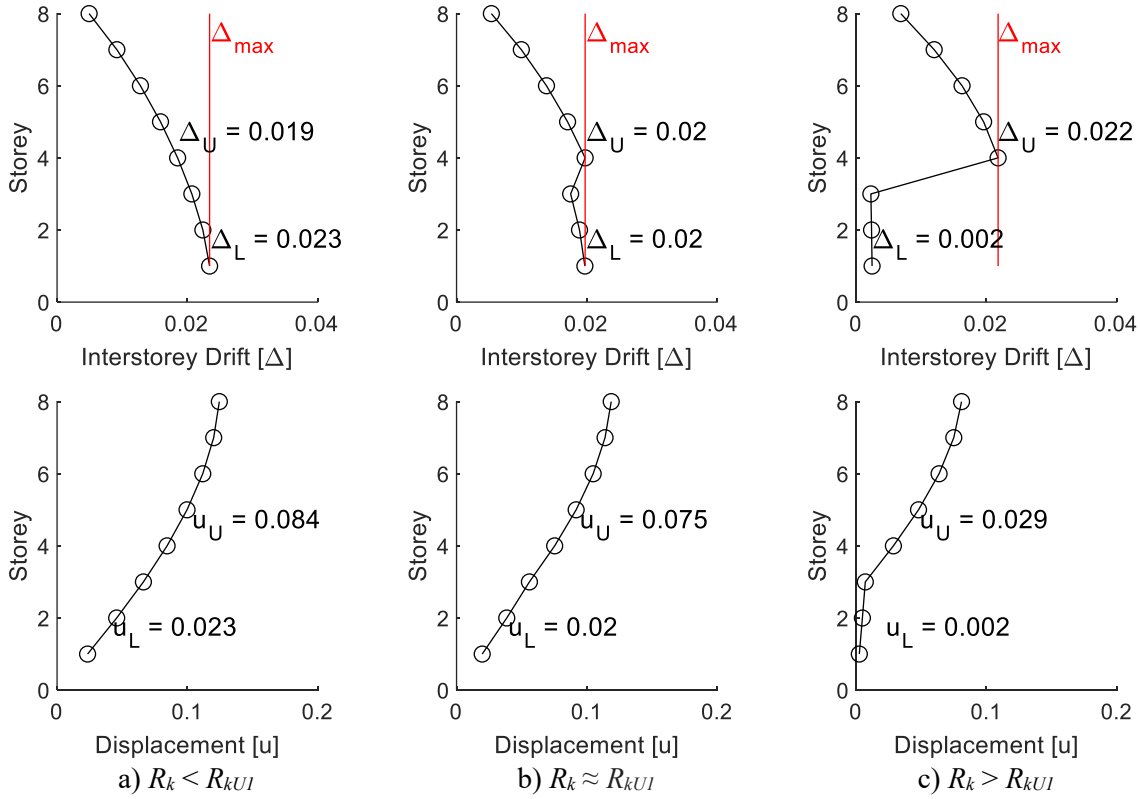

a) $R_k < R_{kUI}$ b) $R_k \approx R_{kUI}$ c) $R_k > R_{kUI}$

Figure C.1: Interstorey drift and Displacement Transition Characterizing R_{kUI}

Figure C.1 illustrates the effect using a sample structure with a three-storey lower structure and a five-storey upper structure, each of equal height, and with other parameters selected arbitrarily. The specific values are not important, as the intent is to illustrate the trend rather than the specific values of storey drift. From left to right, the stiffness ratio is increased with all else kept constant, and the relative importance of the upper structure's drift increases until it is dominant.

The interstorey drift Δ is calculated according to the following procedure derived from Chopra (2012):

$$\Delta_{jn}(t) = \Delta_{jn}^{st} A_n(t) = \frac{\Gamma_n}{\omega_n^2}(\phi_{j,n} - \phi_{j-1,n})A_n(t) \tag{C.1}$$

$$\Delta_{no} = \Delta_n^{st} A_n(T_n, \zeta_n) = \Delta_n^{st} S(T_n) \tag{C.2}$$

$$\Delta_{jo} \approx \sqrt{\Sigma_{i=1}^{N} \Sigma_{n=1}^{N} \rho_{in} \Delta_{io} \Delta_{no}} \tag{C.3}$$

Where:

$$\Gamma_n = \frac{\phi_n^T \boldsymbol{M}\mathbf{1}}{\phi_n^T \boldsymbol{M} \phi_n} \tag{C.4}$$

Proceeding from Equation (C.1), the drift at DOF (storey) j is described in terms of modal properties Γ_n, $\phi_{j,n}$, $\phi_{j-1,n}$ and ω_n, and pseudo-acceleration $A_n(t)$, where $\boldsymbol{M}$ is the mass matrix of the MDOF model. Using the code-specified pseudo-acceleration spectral value $S(T_n)$ to approximate the peak response of $A(T_n,\zeta_n = 5\%)$, the peak modal drift at storey j, Δ_{jo}, is computed according to Equation (C.3), which uses the CQC method to combine each the peak drift Δ_{no} in each mode. ρ is defined by Equation (3.6). Using this procedure, the storey stiffness ratio r_k is increased until the transition described by Figure C.1 occurs. The corresponding R_k is taken as R_{kU1}, which is tabulated in Table E.1.

Conversely, R_{kU1} as previously proposed in Xu & Yuan (2015) and Yuan (2016) is defined based on an assumed value of the mode shape φ_{L1}:

$$\phi_{L1} = \frac{0.88N_L}{N_L + N_U} \tag{C.5}$$

which is an approximation based on the same procedure given above. By substituting this into the form of φ_{L1} given by Equation (A.13) and using the definitions of R_m and R_k given by Equations (3.18) and (3.19), the definition of r_{kU1} given by Yuan (2016) is:

$$r_{kU1} = \left[\frac{r_m N_L(0.12N_L + N_U)}{(N_L + N_U)N_U} + \frac{0.12N_L + N_U}{0.88N_L}\right]\frac{N_U}{N_L}\left(\frac{\bar{\omega}_{1U}}{\bar{\omega}_{1L}}\right)^2 \tag{C.6}$$

However, the form of Equation (C.6) is inconvenient for comparison on account of being for r_k rather than R_k, which is used as the basis of the definition of α_U. While the expression for r_{kU1} can be helpful to determine whether a structure is within the scope of the method at-a-glance (i.e. $1 \leq r_k \leq$

20), the remainder of the critical stiffness ratios are expressed as a function of the overall ratio R_k. With a reversal of some of the substitutions, Equation (C.6) can be re-expressed as:

$$R_{kU1} = \left[\frac{R_m(0.12N_L + N_U)}{(N_L + N_U)} + \frac{0.12N_L + N_U}{0.88N_L}\right] \tag{C.7}$$

Or, even more generally:

$$R_{kU1} = -R_m\phi_{L1} - 1 + R_m + \frac{1}{\phi_{L1}} \tag{C.8}$$

Where φ_{L1} is defined according to Equation (C.5).

However, the formulation of Equation (C.5) is only an approximation, and there is room for improvement, as evident in Figure C.2. In Figure C.2, the value of φ_{L1} associated with a variety of inputs in the MDOF model is plotted against the mode shape proposed by Yuan (2016) given in Equation (C.5). At-a-glance, the Yuan (2016) assumption measurably overestimates the minimum mode shape value at low values of $N_L/(N_U + N_L)$ and underestimates it at intermediate values where the storey count of the upper and lower structure are approximately equal. Moreover, the comparison to $N_L/(N_U + N_L)$ obscures the differences between disparate combinations having the same value of $N_L/(N_U + N_L)$ – for example, it is not necessarily the case that R_{kU1} for $N_U = 1$ and $N_L = 1$ will resemble that of $N_U = 6$ and $N_L = 6$, despite $N_L/(N_U + N_L)$ being of equal value. Accordingly, Figure C.3 compares the values of the minimum mode shape value φ_{L1} (= $\varphi_{L1,min}$) as calculated versus the Yuan (2016) formulation as a function of each permissible storey combination, with each pair of points associated with a given combination of N_U and N_L connected by a black line for easier interpretation. From Figure C.3, it is observed that, in general, lower values of N_U (and thus, higher $N_L/(N_U + N_L)$) are associated with larger underestimates of $\varphi_{L1,min}$, whereas larger values of N_U are generally associated with Yuan (2016) more closely estimating $\varphi_{L1,min}$ albeit with some points being overestimated. Nevertheless, this relationship is not consistent – some adjacent points have a significant variation in the difference between Yuan (2016) and the calculated minimum. One example is (N_U,N_L) = (1,1) and (2,1). Despite a one-storey difference, the ratio of $N_L/(N_U+N_L)$ changes significantly, and thus the estimate of $\varphi_{L1,min}$ given by Yuan (2016), despite only a minor difference between the two calculated values of $\varphi_{L1,min}$.

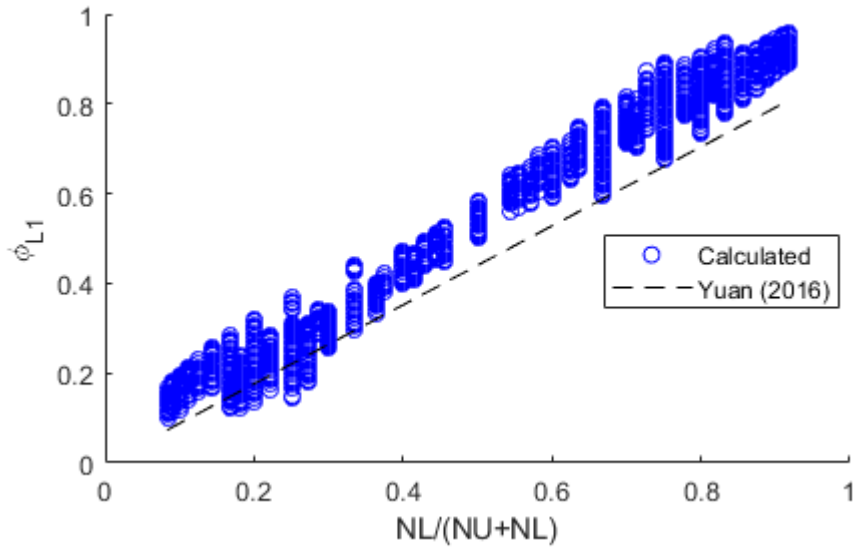

Figure C.2: Mode shape associated with R_{kU1} - Yuan (2016) vs calculated as $f(N_L/(N_U + N_L))$

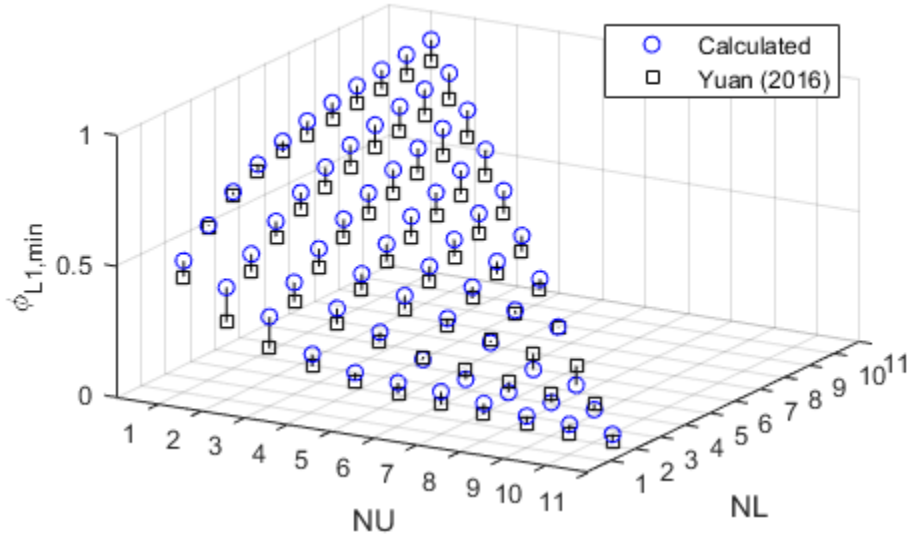

Figure C.3: Mode shape associated with R_{kU1} - Yuan vs calculated as $f(N_U, N_L)$

Therefore, while it serves as an effective rule of thumb, the estimate of φ_{L1} given by Equation (C.5) can be improved by instead formulating R_{kU1} in a tabular format, similar to α_{U11}, α_{U12}, α_{Umax1} and α_{Umax2} in the original formulation of the α_U appearing in Xu & Yuan (2015) and Yuan (2016). While this increases slightly the complexity of calculating R_{kU1} by replacing a closed-form equation with tabular input and linear interpolation, the discrete nature of N_L and N_U means that the relationship

need not work for intermediate, fractional values of N_U and N_L. Given that there is a limited range of points, discretely tabulating the values can therefore give a more accurate but not excessively onerous representation of R_{kU1}.

To determine the tabulated values of R_{kU1}, the calculated values of φ_{L1} are computed as before for approximately 500,000 combinations of N_U, N_L, r_m, T_{singU} and $S_a(T)$ which lie within the scope of the study and by using Equation (C.8) the values of φ_{L1} are converted into the equivalent value of R_{kU1}. Then, two tabular configurations are considered – either as tabulated only as a function of N_L and N_U, or as a function of N_L, N_U, and r_m. For each configuration, the maximum R_{kU1} is recorded for each combination of N_U and N_L (and r_m, as applicable) to construct the table, since the requirement that $R_{kU1} \leq R_k$ is most conservative for larger R_{kU1}. These two cases are referred to as $f(N_U, N_L)$ and $f(N_U, N_L, r_m)$ for brevity. In the case of $f(N_U, N_L)$, R_{kU1} is based only on N_U and N_L, and for $f(N_U, N_L, r_m)$ the value is also based on r_m and interpolated for non-integer r_m.

Rather than based on the difference between the calculated and proposed R_{kU1}, the error of each formulation for R_{kU1} – Yuan (2016), $f(N_U, N_L)$ and $f(N_U, N_L, r_m)$ – is assessed based on the calculated drift ratio between the bottom of the upper structure and the bottom of the full structure in the MDOF model. As previously discussed, the theoretical formulation of R_{kU1} is predicated on predicting the value of R_k at which these two interstorey drifts are identical. Ergo, it is logical to use this to evaluate the efficacy of the proposed forms directly, rather than using R_{kU1} as a proxy. Considering a larger set of values compared to Figure C.2 and Figure C.3, the following histograms plot the error in the drift ratio between the proposed and calculated values. For each, the x-axis indicates the percentage error (i.e. between the calculated drift ratio and the ideal value of one), and the y-axis indicated the proportion of values that sit within a given bin of the histogram, and red lines indicate the 99th percentile, 1st percentile and median. Figure C.4 corresponds to R_{kU1} as defined by Yuan (2016), Figure C.5 corresponds to $f(N_U, N_L)$, Figure C.6 corresponds to $f(N_U, N_L, r_m)$ and Figure C.7 is a side-by-side comparison of the three.

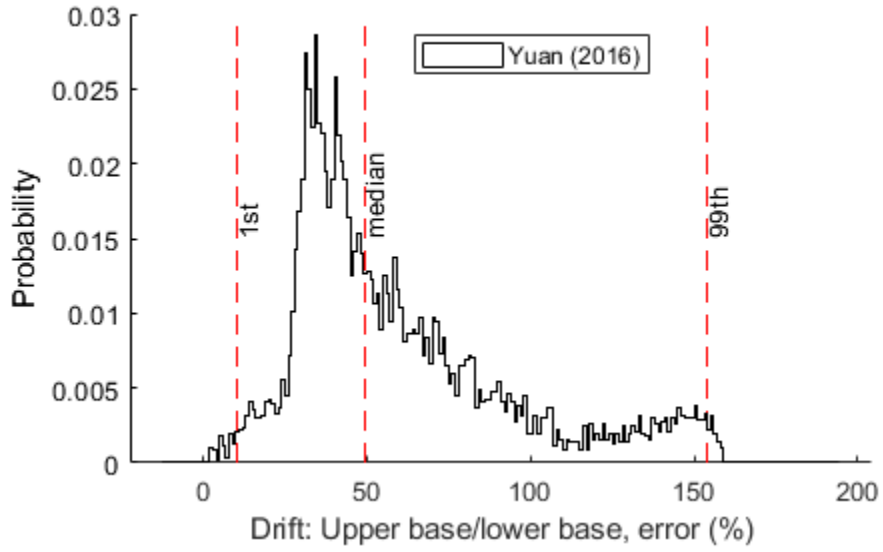

Figure C.4: Error histogram - R_{kU1} as defined by Yuan (2016)

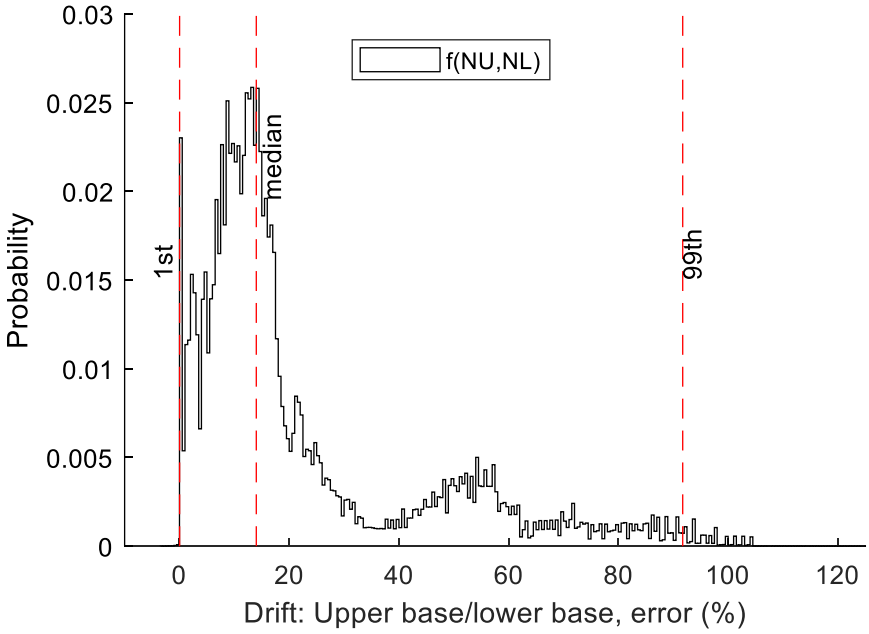

Figure C.5: Error histogram - R_{kU1} as defined by $f(N_U, N_L)$

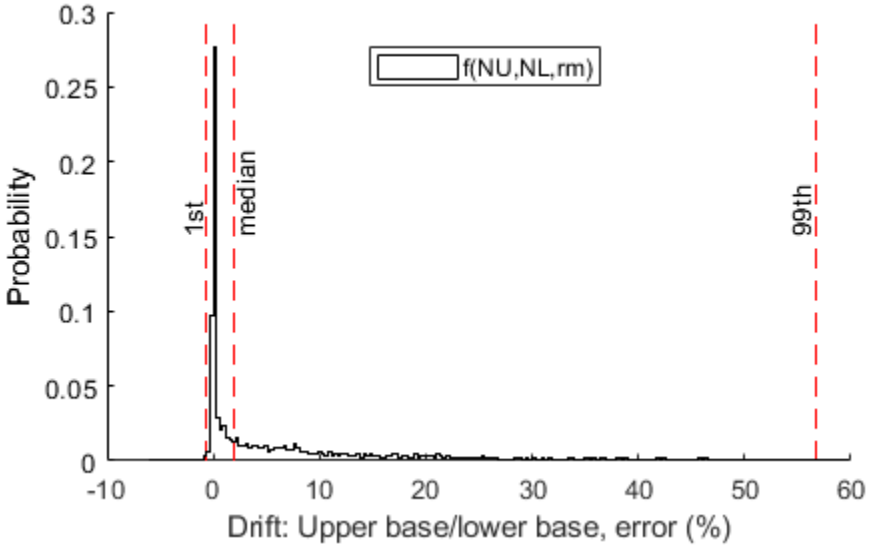

Figure C.6: Error histogram - R_{kU1} as defined by $f(N_U, N_L, r_m)$

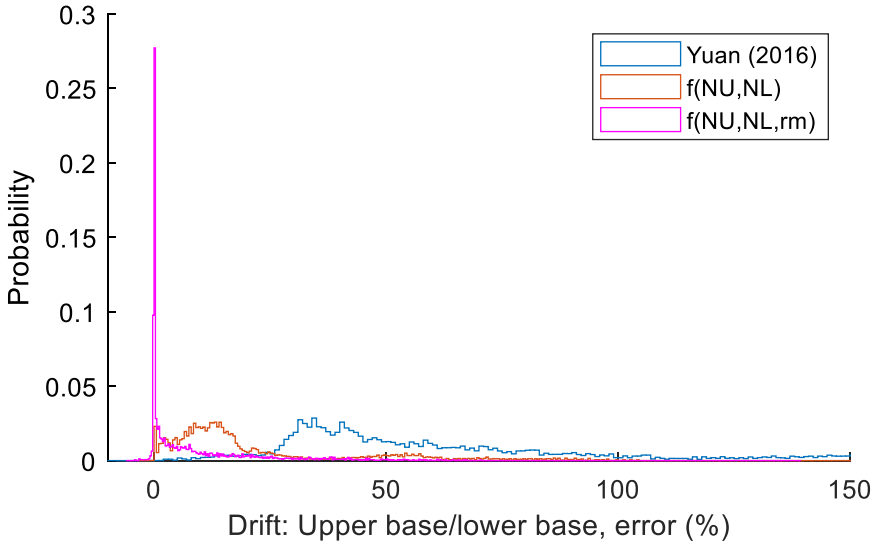

Figure C.7: Comparison of R_{kU1} error histograms

From Figure C.4 to Figure C.7, the following conclusions can be drawn:

1. The median error of the Yuan (2016) formulation is 50% (overestimate), with most values lying between a 25% and 75% overestimate of R_{kU1}. Overestimates do not generally exceed 150%.

2. The median error of R_{kU1} if defined only as a function of N_U and N_L is approximately 15% (overestimate), and most of the error is between 0% and 50%. Overestimates do not generally exceed 100%.
3. The median error of R_{kU1} defined as a function of N_U and N_L and interpolated for r_m is less than a 5% overestimate, with most error values lying between 0% and 10%. Overestimates do not generally exceed 60%.

From this comparison, $R_{kU1} = f(N_U, N_L, r_m)$ exhibits superior performance at estimating the R_{kU1} corresponding to the drift transition described by Figure C.1. The values corresponding to $R_{kU1} = f(N_U,N_L,r_m)$ appear in Table E.1.

As values taken from Table E.1 are to be used for further calculations, the question remains as to how many decimal places for calculation are appropriate. Figure C.8 indicates the difference between the results where the tabulated R_{kU1} is rounded to a different number of decimal points (dp). Of note are the blue and red lines corresponding to 1 or 5 decimal places, respectively. Clearly, 1 decimal place somewhat worsens the results of using the tabulated R_{kU1}, as expected. However, aside from 1 decimal place, the distinction between the other 4 lines is minor – the adequacy of R_{kU1} does not significantly differ based on the number of decimal places so long as at least two are used. Therefore, the values in Table E.1 are provided to three decimal places.

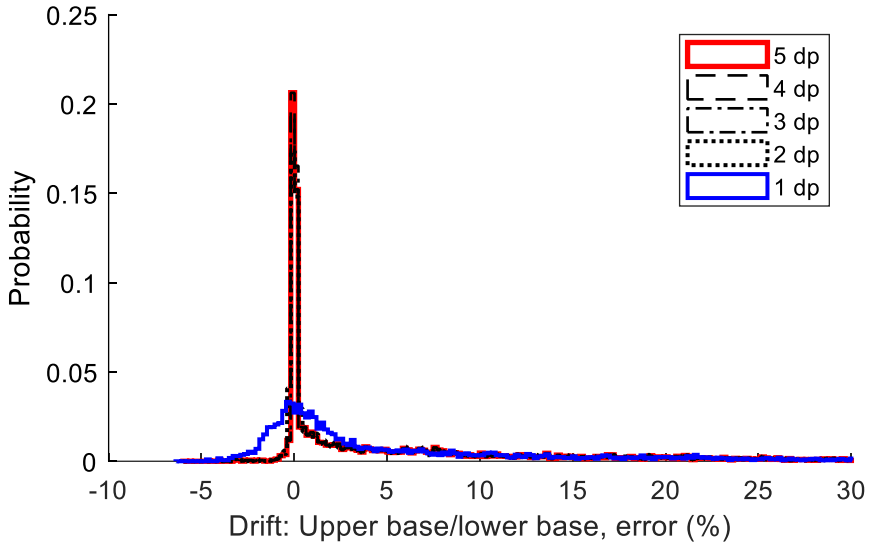

Figure C.8: Sensitivity of $R_{kU1} = f(N_U, N_L, r_m)$

C.2.2 Overall stiffness ratios associated with maximum amplification, R_{kU2} and R_{kU3}

As with Xu & Yuan (2015) and Yuan (2016), R_{kU2} and R_{kU3} delimit the bounds within which $\alpha_U \approx \alpha_{Umax}$ - R_{kU2} is the lower bound and R_{kU3} is the upper bound. Based on Appendix B.2, $S_a(T_1)/S_a(T_U)$, M_{U1} and M_{U2} generally attain their absolute maximum values for $R_k = R_m + 1$, and given that $S_a(T_1)/S_a(T_U)$ is approximately unity for all $R_k > R_m + 1$, R_{kU2} is taken as equal to $R_m + 1$, consistent with Equation (3.30) and with Xu & Yuan (2015) and Yuan (2016). However, it is clear from Figure B.6 that this is only approximately true – for $T_U \geq 0.2$ seconds, there is a small influence of T_U as T_U increases beyond the extent of the constant acceleration region (typically ≤ 0.2 seconds in NBCC 2015 (2015c)). This discrepancy is connected to $S_a(T_2)/S_a(T_U)$ – as evident in Figure B.7, $S_a(T_2)/S_a(T_U)$ is equal to one when $T_U \leq 0.2$ seconds, and otherwise increases as a function of R_k. This maximum of $S_a(T_2)/S_a(T_U)$ for T_U is neither directly connected to $R_k = R_m + 1$ nor bounded between zero and one (although the reciprocal $S_a(T_U)/S_a(T_2)$ is bounded between zero and one).

Therefore, α_U as defined by Equation (A.29) is due to two components – one, the product of M_{U1} and $S_a(T_1)/S_a(T_U)$ and two, the product of M_{U2} and $S_a(T_2)/S_a(T_U)$. It is known that M_{U1}, M_{U2} and $S_a(T_1)/S_a(T_U)$ all approximately attain their maximum values at $R_k = R_m + 1$, albeit with a minor change to $S_a(T_1)/S_a(T_U)$ based on T_U. However, this is not the case with $S_a(T_2)/S_a(T_U)$, and consequently R_{kU3}, the upper bound of the region where $\alpha_U \approx \alpha_{Umax}$, must be empirically based to ensure that the region bounded by R_{kU2} and R_{kU3} still approximately captures the R_k associated with the maximum α_U for any given combination of inputs.

This problem is acknowledged as such by Yuan (2016), which defines R_{kU3} based on an empirical investigation of the ASCE spectrum. Although not particularly clear as to how the variable is derived, they define R_{kU3} as follows:

$$R_{kU3} = \begin{cases} 0.826R_m + 4.76 & R_m \leq 0.71 \\ -0.26R_m + 5.52 & 0.71 < R_m < 2 \\ R_m + 3 & R_m \geq 2 \end{cases} \quad \text{(C.9)}$$

Note that the above equation as it appears in Yuan (2016) gives the upper bound of the second piece of the piecewise equation as 1 rather than 2. This has been changed to ensure that the equation is continuous and to ensure it is consistent with the given discussion. Likewise, R_{kU3} is partially defined for another variable in Yuan (2016) – this intermediate substitution has been made here for brevity so that R_{kU3} is only a function of R_m.

However, Yuan (2016) gives another formulation different that that referred to in their derivation, based on calibration to ensure that the MDOF results are conservatively approximated. This can be considered the final formulation:

$$R_{kU3} = \begin{cases} 4.13R_m + 2 & R_m \leq 0.8 \\ -0.26R_m + 5.52 & 0.8 < R_m < 2 \\ R_m + 3 & R_m \geq 2 \end{cases} \quad \text{(C.10)}$$

In any event, R_{kU3} as specified by Equation (C.10) is used for both the NBCC and ASCE-derived formulations given by Yuan (2016). Perplexingly, the first piece of Equations (C.9) and (C.10) are significantly different. It is unclear why this is the case – Equation (C.9) is supposedly based on the parameter survey whereas Equation (C.10) is modified to ensure the MDOF α_U is conservatively approximated. Nonetheless, in the absence of a better rationale and on account of being sufficiently performative, R_{kU2} and R_{kU3} are defined identically to Yuan (2016).

C.2.3 Overall stiffness ratio R_{kU2stg} associated with the two-stage criterion (formerly R_{kU2stg} and R_{k2stg})

In multiple previous studies published by Yuan & Xu (Xu & Yuan, 2015; Yuan, 2016; Yuan & Xu, 2016, 2014), two variables with very similar notation – R_{kU2stg} and R_{k2stg} (henceforth: $R_{kU2stg,Yuan}$ and $R_{k2stg,Yuan}$) – are used in different contexts somewhat related to the ASCE 7 two-stage procedure to capture two different phenomena. In these works, $R_{kU2stg,Yuan}$ corresponds to a lower bound of stiffness above which $\alpha_U \approx 1$, whereas $R_{k2stg,Yuan}$ delimits the stiffness ratio beyond which the two-stage criterion applies. The requirement that $\alpha_U \approx 1$ is not by itself sufficient to satisfy the assumptions of the two-stage assumption. It is therefore imperfect to identify $R_{kU2stg,Yuan}$ as related to the two-stage criterion and only invites confusion when set alongside the similarly named $R_{k2stg,Yuan}$ which is intended to identify whether the two-stage procedure applies. To alleviate this confusion, $R_{kU2stg,Yuan}$ and $R_{k2stg,Yuan}$ are consolidated in the current study, so that R_{kU2stg} refers to both phenomena. However, it should be noted that $\alpha_U \approx 1$ is only approximately true – based on the inputs to the MDOF model and as stated in Yuan (2016), α_U for $R_k > R_{kUstg}$ may in some circumstances be as high as 1.25 or so.

The following section explains the previous formulation's $R_{k2stg,Yuan}$ and $R_{kU2stg,Yuan}$ as they appear in the previous formulation and describes the changes made in the proposed formulation in two subsections. First, the focus is on $R_{k2stg,Yuan}$ beyond which the two-stage procedure is assumed to be approximately applicable. This discussion includes a characterization of the two-stage procedure and relevant research to justify the proposed criterion. Following this, the focus shifts to $R_{kU2stg,Yuan}$,

beyond which $\alpha_U \approx 1$. In more practical terms, α_U for $R_k > R_{kU2stg,Yuan}$ can exceed 1, but it is expected that $\alpha_U \leq \alpha_{U2stg}$ in this region.

Overall stiffness ratio associated with the two-stage criterion, $R_{k2stg,Yuan}$

Prior to characterizing $R_{k2stg,Yuan}$, it is necessary to define the two-stage procedure. For vertically irregular structures having a flexible upper structure and a sufficiently stiff lower structure, it is often assumed that the lower structure acts as a rigid body transmitting the ground acceleration directly to the upper structure's base. If this is true, it follows that the upper structure behaves as though fixed to the ground, and so the upper structure and lower structure can be analyzed separately via the equivalent static force procedure (ESFP) and reassembled to obtain the loads on the original structure. This assumption that the upper and lower structure can be analyzed separately and reassembled to obtain the full structure's loads is the two-stage assumption, and the procedure by which this is done is the two-stage procedure.

While this method does not appear in the NBCC aside from a brief mention in the 2015 commentary (NRCC, 2015b), it is commonly used in American design codes and has appeared in historical versions of the NBCC for setback structures (e.g. NBCC 1970 (NRCC, 1971)). First introduced in the 1988 SEAOC Blue Book and UBC (ICBO, 1988; SEAOC, 1988), the procedure appears in subsequent codes such as ASCE 7. In ASCE 7-16 (2017), it applies to structures for which the lower structure's (overall) stiffness is at least 10 times the (overall) stiffness of the upper structure, and for which the period of the full structure is less than 1.1 times that of the upper structure alone. In other words:

1. $R_k \geq 10$, which indicates that the lower structure acts as a rigid body that transmits ground accelerations directly to the base of the upper structure (SEAOC, 2019)
2. $T_1/T_U \leq 1.1$, which implies that the upper structure is dominated by the first mode as assumed by equivalent static procedures

However, American design codes have given negligible feedback on the adequacy of the limits given in ASCE 7, which are essentially unchanged since their introduction with UBC 1988, except that the stiffness ratio is considered relative to storey stiffness in 1988 UBC/SEAOC and overall stiffness in ASCE 7-16 (2017). Research using both nonlinear time history analysis (Chen & Ni, 2020) and linear modal response spectrum analysis (Yuan & Xu, 2016) concludes that the ASCE 7 criteria are not adequate to ensure the two-stage procedure can be applied.

To remedy this both Xu & Yuan (2015) and Chen & Ni (2020) propose alternative criteria given by Equations (C.12) and (C.13). If the ASCE criteria are translated into terms of R_k and R_m as proposed by Xu & Yuan (2015) and Equation (C.11), the three criteria can be readily compared:

$$R_k \geq max(0.826R_m + 4.76, 10) \quad \text{(Xu \& Yuan, 2015)} \quad \text{(C.11)}$$

$$R_k \geq 10\mathrm{R}_m \quad \text{(Chen \& Ni, 2020)} \quad \text{(C.12)}$$

$$R_k \geq R_{k2stg,Yuan} = \begin{cases} 1.637R_m + 9.07 & R_m \leq 1.23 \\ 11.029R_m - 2.5 & R_m > 1.23 \end{cases} \quad \text{(Yuan \& Xu, 2016)} \quad \text{(C.13)}$$

Note that the normalization for stiffness in Chen & Ni (2020) is slightly different than that used in Xu & Yuan (2015). However, because the formulations that are given by Equations (C.12) and (C.13) are so similar, this difference is assumed to be negligible.

If these criteria are plotted side-by-side per Figure C.9, it is evident that Chen & Ni (2020) and Yuan & Xu (2016) agree that the ASCE 7 criteria are inadequate and propose that a similar limit should be applied for $R_m > 1$. This, despite their relatively different approaches, indicates that the ASCE 7 criteria are incapable of fully capturing the two-stage phenomena. Chen & Ni (2020) attribute this to the incapability of T_I/T_U to identify whether the two-stage procedure should be applied. Instead, they argue that the masses and stiffnesses of the building itself should be used exclusively, as these parameters determine the response of the structure.

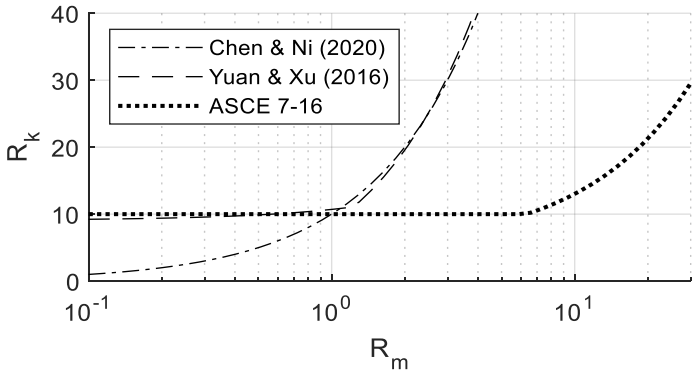

Figure C.9: Comparison of existing two-stage criteria

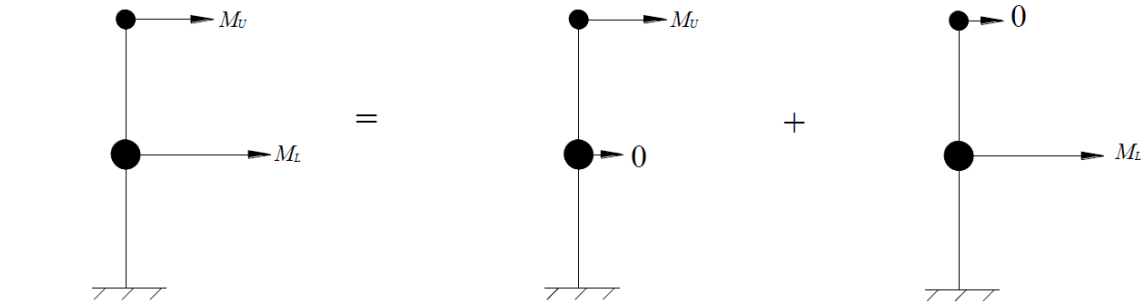

(a) mass distribution of 2DOF model (b) first mode ($T_1 \approx T_U$) (c) second mode ($T_2 \approx T_L$)

Figure C.10: Effective mass distribution of simplified 2DOF model with extremely stiff lower structure (two-stage assumption) (Yuan, 2016)

Meanwhile. Yuan (2016) does not eschew T_I/T_U entirely and instead considers also the relationship between T_2 and T_L. As interpreted by Yuan (2016) in Figure C.10, the two-stage procedure implicitly assumes that the effective mass of the upper and lower structures are approximately concentrated in well-separated first and second modes such that $T_U \approx T_I$ and $T_L \approx T_2$. In terms of the effective modal masses given by Equations (A.22) to (A.27), they interpret the two-stage requirement as associated with $T_I/T_U \leq 1.1$, $M_{LI} \leq 0.1$ and $M_{UI} \leq 1.1$. Essentially, Yuan (2016) specifies that:

$$F_U = M_U S_a(T_U) \tag{C.14}$$

$$F_U = M_L S_a(T_L) \tag{C.15}$$

i.e. that the equivalent static loads on the upper and lower structures feature no contribution from the other structure.

By amalgamating the ASCE 7-16 (2017), Chen & Ni (2020) and Yuan & Xu (2016) definitions, it is proposed that $R_{kU2stg} = 10R_m \geq 10$ as stated in Equation (3.28). The lower bound is applied based on ASCE 7-16 (2017) and Yuan & Xu (2016) and chosen to be $R_k \geq 10$ as it is very similar but much simpler than $1.637R_m$+9.07 given by Yuan & Xu (2016). Likewise, the ascending portion is applied based on Chen & Ni (2020) and Yuan & Xu (2016), with $R_k \geq 10R_m$ being chosen over $R_k \geq 11.029R_m$-2.5 for simplicity. It is true that Chen & Ni (2020) do not specify a lower bound on Equation (C.12), but given that all structures in their study with $R_k < 10$ are considered inadequate, it is reasonable to apply the oft-used lower bound of $R_k = 10$ which appears in ASCE 7. As for the adoption of simplified bounds over those proposed by Yuan & Xu (2016) and Yuan (2016), the previously-proposed coefficients are not so precise as to be worth preserving when a simpler result is

desirable. The bounds given by Yuan & Xu (2016) and Yuan (2016) are based on a theoretical application of assumed bounds on chosen parameters in the 2DOF model using the ASCE spectrum, and only approximately represent the results of the MDOF model using the NBCC spectrum. Given that the variation between the new and previously proposed R_{kU2stg} is less than the width of the range [R_{kU2}, R_{kU3}] which defines $\alpha_U = \alpha_{Umax}$ for values of R_k and R_m within the current scope of r_k, r_m and T_{singU}, it is reasonable to expect that the net impact on the accuracy of the method will be negligible.

To further justify the proposed approach, it is compared against the ratios of the modal masses given by Equations (A.22) to (A.27). If the two-stage procedure applies as interpreted by Yuan (2016) and Figure C.10, it follows that the absolute value of the ratios $|M_{U2}/M_{L2}|$ and $|M_{L1}/M_{U1}| \leq 0.1$ (10%), which implies that the effective mass of the upper structure in the second mode is much smaller than that of the lower structure and that the effective mass of the lower structure in the first mode is much smaller than that of the upper structure. As apparent from Figure C.11, the proposed criterion is effective at ensuring that the effective modal mass of the lower structure dominates the second mode (b) and that the effective mass of the upper structure dominates the first mode (a).

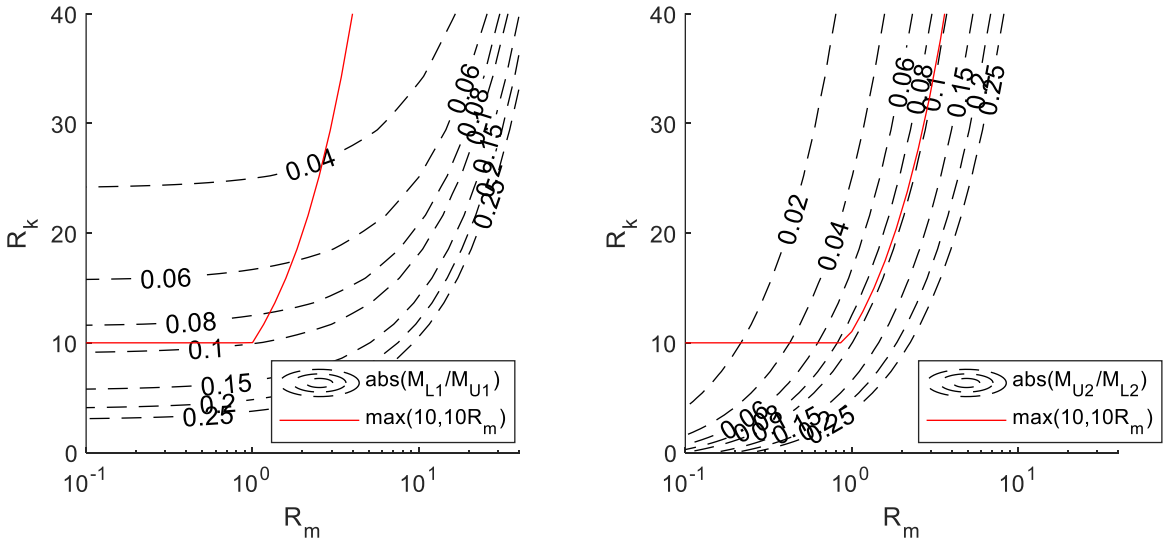

Figure C.11: Relative modal masses in the 2DOF model versus proposed R_{kU2stg}

Overall stiffness ratio associated with $\alpha_U \approx 1$, $R_{kU2stg,Yuan}$

As R_k increases beyond the maximum α_U with R_m held constant, at some point the two-stage procedure is expected to apply. According to Yuan (2016), this necessarily entails that $\alpha_U \approx 1$, for a

sufficiently stiff lower structure acts as a rigid body to transmit the ground motions without amplification to the upper structure. However, the two-stage phenomenon involves both the upper and lower structures, and so it may be that $\alpha_U \approx 1$ even for $R_k < R_{kU2stg}$ (i.e. the two-stage procedure does not apply). Assuming that $\alpha_U \approx 1$ if $T_I/T_U \leq 1.1$ and $M_{UI} < 1.1$, Yuan (2016) defines $R_{kU2st,Yuan}$ as in Equation (C.16). As $\alpha_U \approx 1$ is necessary but insufficient for the two-stage phenomenon to occur, $R_{kU2stg,Yuan}$ is potentially much smaller than $R_{2stg,Yuan}$. Later, Yuan (2016) develops Equation (C.16) for the NBCC spectrum. On account of the larger variation of $S_a(T_I)/S_a(T_U)$ using the NBCC spectrum, the limit $T_I/T_U \leq 1.1$ is reduced to $T_I/T_U \leq 1.05$ in the derivation of Equation (C.16), resulting in a much stricter limit.

$$R_{kU2stg,ASCE} = \begin{cases} 0.826R_m + 4.76 & R_m \leq 0.71 \\ 11.029R_m - 2.5 & R_m > 0.71 \end{cases} \quad \text{(C.16)}$$

$$R_{kU2stg,NBCC} = \begin{cases} 0.907R_m + 9.78 & R_m \leq 1.213 \\ 11.029R_m - 2.5 & R_m > 1.213 \end{cases} \quad \text{(C.17)}$$

Despite this difference in $R_{kU2stg,Yuan}$, the two-stage requirement $R_{k2stg,Yuan}$ from Yuan & Xu (2016) and Yuan (2016) in (C.18) is identical in either case. Perplexingly, this means that $R_{k2stg,Yuan}$ for the NBCC is larger for some values of R_m than the two-stage limit $R_{k2stg,Yuan}$. This is likely just an oversight owing to the derivation that was used – intuitively, $R_{kU2stg,Yuan} \leq R_{k2stg,Yuan}$ and given their proximity Equations (C.13) and (C.17) are effectively the same.

Strictly speaking, $\alpha_U \approx 1$ is a misnomer – R_{kU2stg_Yuan} is more appropriately the boundary beyond which $\alpha_U \leq \alpha_{U2stg}$, where α_{U2stg} at times may be larger than 1.1. This is implicitly acknowledged by Yuan (2016) – α_{U2stg} is assumed to vary as a function of R_m and at times is considered to be as large as 1.25. It is, therefore, true that the assumptions $M_{UI} \leq 1.1$ and $T_I/T_U \leq 1.1$ (or $T_I/T_U \leq 1.05$) applied to the 2DOF model ensure that $\alpha_U \approx 1$ in only a very broad sense. To some extent this is expected – the two-stage assumption entails the upper and lower structures each behave as a regular structure. However, it is known and acknowledged by NBCC 2015 that even regular structures experience some sort of higher mode effect, which is captured by M_v. M_v, as defined by Equation (3.2), is directly analogous to α_U as defined by Equation (3.4), and so if the upper structure is considered alone as a regular structure is prone to higher-mode effects indicated by $M_v \geq 1$, it follows that the same is true of α_U.

In consideration of the forthgoing discussion, it is proposed that $R_{kUstg,Yuan}$ and $R_{k2stg,Yuan}$ be merged into a single variable, R_{kU2stg}. The form of R_{kU2stg} expressed in Equation (3.28) is based on the amalgamation of the two-stage criteria given by Equations (C.11) to (C.13). The aspect that α_U attains

a constant value for large R_k is not given a separate variable and instead is implicitly incorporated into the new definition of R_{kU2stg}. Given the close similarity of $R_{kU2stg,Yuan}$ and $R_{k2stg,Yuan}$ for the NBCC, this is merely a simplification of what is already the case in Yuan (2016).

C.2.4 Amplification ratio α_{U1} (associated with R_{kU1})

Accompanying the lower-bound stiffness R_{kU1} is α_{U1}, which is the approximation to the amplification ratio α_U at $R_k = R_{kU1}$. Much the same as α_U in the 2DOF model, α_{U1} varies on account of not only R_m and R_k but also $S_a(T_1)/S_a(T_U)$, as discussed in Appendix B. Therefore, α_{U1} approximated as a function of R_m and R_k only is inadequate – the effect of $S_a(T_1)/S_a(T_U)$ must be incorporated. Broadly speaking, $S_a(T_1)/S_a(T_U)$ varies between zero and one (or more practically: a finite lower bound and one), and thus α_{U1} itself varies between some maximum and minimum value.

The original ASCE formulation of α_{U1} given by Xu & Yuan (2015) denotes these minimum and maximum values as α_{U11} and α_{U12} (see Table D.1). Accordingly, α_{U11} is therefore associated with the minimum $S_a(T_1)/S_a(T_U)$ and α_{U12} associated with the maximum $S_a(T_1)/S_a(T_U)$, and α_{U1} is assumed to vary between these endpoints via a power function fit. From this logic Xu & Yuan (2015) obtain the following form of α_{U1} as formulated for ASCE 7:

$$\alpha_{U1} = \begin{cases} \alpha_{U11} & T_U/T_S \geq 1 \\ \alpha_{U12} & T_U/T_S \leq \sqrt{\dfrac{N_U + 0.12N_L}{N_U + N_L}} \\ \alpha_{U11}(T_U/T_S)^{x_3} & \sqrt{\dfrac{N_U + 0.12N_L}{N_U + N_L}} < T_U/T_S < 1 \end{cases} \tag{C.18}$$

Where x_3 is an exponent defined as:

$$x_3 = \frac{ln\left(\frac{\alpha_{U12}}{\alpha_{U11}}\right)}{0.5ln\left(\frac{N_U + 0.12N_L}{N_U + N_L}\right)} \tag{C.19}$$

If unfamiliar with the ASCE 7 spectrum and the Xu & Yuan (2015) formulation as a whole, it is not immediately clear why α_{U1} is defined as a function of T_U/T_S rather than $S_a(T_1)/S_a(T_U)$ and for what reason the endpoints are selected. The lack of clarity is via a pair of substitutions – as previously mentioned, all values $S_a(T_1)/S_a(T_U)$ defined via the ASCE map directly to ratios of periods T_U, T_1 and T_S, whereas before T_S marks the end of the constant acceleration region in the ASCE spectrum. Consequently, the relationship between T_U/T_S and $S_a(T_1)/S_a(T_U)$ is the same: for $T_U/T_S \geq 1$,

$S_a(T_1)/S_a(T_U) = 1$ and α_{U1} reaches its maximum and thus $\alpha_{U1} = \alpha_{U12}$, and for $T_U/T_S \leq T_U/T_1 = \sqrt{(N_U + 0.12N_L)/(N_U + N_L)}$, $S_a(T_1)/S_a(T_U)$ is at its minimum and thus $\alpha_{U1} = \alpha_{U11}$. The bound $T_U/T_1 = \sqrt{(N_U + 0.12N_L)/(N_U + N_L)}$ is derived by substituting the assumed mode shape for $R_k = R_{kU1}$ given by Equation (C.5) into Equation (A.13) which relates the mode shape and period ratio. In this way, Equation (C.18) follows the logic outlined above to define α_{U1} based on $S_a(T_1)/S_a(T_U)$ using T_U/T_S as a proxy.

For the NBCC, the substitution of $S_a(T_1)/S_a(T_U)$ for T_U/T_1 is not possible, and therefore Yuan (2016) provides a slightly different albeit similar formulation where T_1 is approximated via $T_U/T_1 = \sqrt{(N_U + 0.12N_L)/(N_U + N_L)}$ as before:

$$\alpha_{U1} = \begin{cases} \alpha_{U11} & \dfrac{S_a\left[\sqrt{\dfrac{N_U + N_L}{N_U + 0.12N_L}}T_U\right]}{S_a(T_U)} = \sqrt{\dfrac{N_U + 0.12N_L}{N_U + N_L}} \\ \alpha_{U12} & \dfrac{S_a\left[\sqrt{\dfrac{N_U + N_L}{N_U + 0.12N_L}}T_U\right]}{S_a(T_U)} = 1 \\ \alpha_{U12}\left\{\dfrac{S_a\left[\sqrt{\dfrac{N_U + N_L}{N_U + 0.12N_L}}T_U\right]}{S_a(T_U)}\right\}^{-x_3} & \sqrt{\dfrac{N_U + 0.12N_L}{N_U + N_L}} < \dfrac{S_a\left[\sqrt{\dfrac{N_U + N_L}{N_U + 0.12N_L}}T_U\right]}{S_a(T_U)} < 1 \end{cases} \quad \text{(C.20)}$$

Where x_3, α_{U11} and α_{U12} are defined identically to the ASCE procedure.

However, while the substitution of T_U/T_S for $S_a(T_1)/S_a(T_U)$ is necessary to adapt the ASCE formulation to the NBCC, the resulting equation is unwieldy. In the original ASCE derivation, it is assumed that α_{U11} and α_{U12} correspond to the minimum and maximum values of α_{U1}, corresponding to $S_a(T_1)/S_a(T_U) = T_U/T_1$ and 1, respectively. The NBCC formulation is identical to the ASCE formulation and simply assumes that T_1/T_U is defined using Equations (C.5) and (A.13). These equations relate the same mode shape they use to derive R_{kU1} to the period ratio T_1/T_U. By substituting T_U/T_S for $S_a(T_1)/S_a(T_U)$ and T_1/T_U for a function of the mode shape, the NBCC formulation is derived.

Unfortunately, these substitutions obscure the relationship between the ASCE formulation and NBCC formulation. For designers not familiar with the ASCE, it is not immediately clear how T_U/T_S translates to $S_a(T_1)/S_a(T_U)$, and given that the corresponding equations are spread throughout the thesis, not immediately clear that T_1/T_U is used to derive the revised limits. More significantly, the form of Equation (3.18) comes off as somewhat contrived for the NBCC on account of the non-

monotonic relation between the ratio of two periods and the ratio of the corresponding spectral values. The relationship is convenient for ASCE 7, as any two periods can be related directly to the spectral values such that an increase in the period ratio T_U/T_S directly corresponds to a decrease in the spectral ratio $S_a(T_1)/S_a(T_U)$. It is consequently the case that the minimum value of α_U does not necessarily correspond to $T_1/T_U = S_a(T_1)/S_a(T_U)$ for the NBCC spectrum. Since the endpoints of the relationship between $S_a(T_1)/S_a(T_U)$ and α_{U1} are less clear for the NBCC spectrum, it makes less sense to define it using α_{U11} and α_{U12}. This is further complicated by the changed definition of R_{kU1}, which has changed from the one-size-fits-all definition which arises from the assumed mode shape given by Equation (C.5) to a variable defined via N_U, N_L and r_m. As R_{kU1} has changed, so too must α_{U1}.

Therefore, the proposed Equation (3.29) differs from the prior Equation (C.20) in two primary ways:

1. The form of the equation is no longer a piecewise power function fit between two fixed endpoints and is now a simpler exponential fit. Rather than α_{U11} and α_{U12} being the parameters defining the fit, coefficients A_{U1} and B_{U1} are introduced. A_{U1} and B_{U1} are tabulated in the same fashion as α_{U11} and α_{U12} and appear in Appendix E. The fit is therefore not between two set endpoints but based on two set fit parameters.
2. $S_a(T_1)$ is no longer defined according to an assumed mode shape. Instead, it is defined via Equation (3.30) and R_{kU1} (Table E.1). Equation (3.30) is based on Equation (A.13).

As a consequence of the change, the formulation is more intuitive and requires fewer calculations. For the same number of inputs, it is clear from the form of Equation (3.29) that α_{U1} (approximately) increases monotonically as a function of $S_a(T_1)/S_a(T_U)$. The proposed formulation also clearly relates the value of R_{kU1} and the ratio of T_U/T_1 (albeit obliquely via $S_a(T_1)/S_a(T_U)$) and is no longer piecewise.

To calculate the proposed α_{U1}, values of $S_a(T_1)/S_a(T_U)$ and α_U corresponding to the MDOF model are calculated for each combination of N_U, N_L and (integer) r_m for a range of inputs (e.g. $S_a(T)$ and T_{singU}) within the scope. An exponential fit is then applied to the resulting $S_a(T_1)/S_a(T_U)$-α_U, with post-processing to ensure that α_{Umax} is not underestimated. An example of this is shown in Figure C.12 for $N_U = 4$, $N_L = 5$ and $r_m = 2$. By adjusting the least-squares exponential fit, the proposed values of A_{U1} and B_{U1} are obtained and tabulated in Table E.2 and Table E.3.

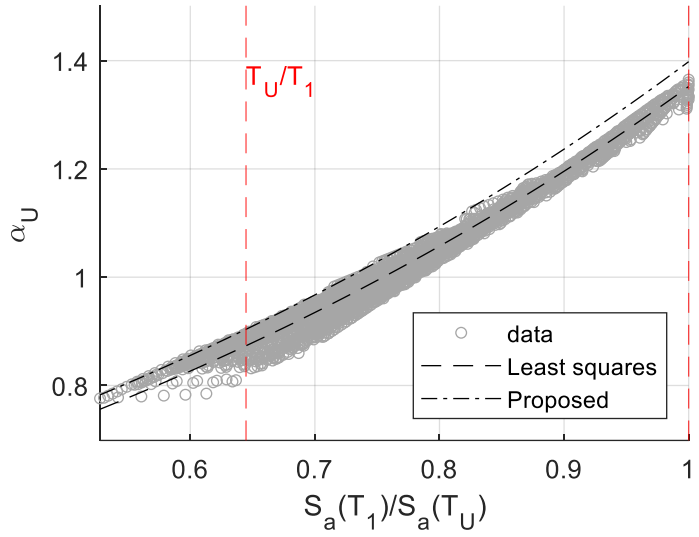

Figure C.12: Comparison between calculated and proposed α_{U1} ($N_U = 4$, $N_L = 5$, $r_m = 2$)

C.2.5 Amplification ratio α_{Umax} (associated with R_{kU2} and R_{kU3})

The maximum amplification factor, α_{Umax}, associated with R_{kU2} and R_{kU3}, is analogously defined in both the previous and the new proposed formulations. Xu & Yuan (2015) define the ASCE 7 formulation of α_{Umax} in the same manner as α_{U1}, with α_{Umax1}, α_{Umax2} and x_4 acting as direct counterparts to α_{U11}, α_{U12} and x_3 which appear in Equation (C.18):

$$\alpha_{Umax} = \begin{cases} \alpha_{Umax1} & T_U/T_S \geq 1 \\ \alpha_{Umax2} & T_U/T_S \leq 0.769(R_m)^{0.059} \\ \alpha_{Umax1}(T_U/T_s)^{x_4} & 0.769(R_m)^{0.059} < T_U/T_S < 1 \end{cases} \quad \text{(C.21)}$$

Where x_4 is an exponent defined as:

$$x_4 = \frac{ln\left(\frac{\alpha_{Umax2}}{\alpha_{Umax1}}\right)}{ln(0.769(R_m)^{0.059})} \quad \text{(C.22)}$$

Equations (C.21) and (C.22) are nigh-identical to Equations (C.18) and (C.19), except that T_U/T_1 is instead assumed to be $0.769R_m^{0.059}$ and α_{Umax1} and α_{Umax2} are defined by piecewise functions rather than drawn from a table of values. Per Yuan (2016):

$$\alpha_{Umax1} = \begin{cases} 0.03R_m + 1 & R_m \leq 0.71 \\ 0.17R_m + 0.9 & 0.71 < R_m \leq 4.5 \\ -0.005R_m^2 + 0.19R_m + 0.91 & 4.5 < R_m \leq 16 \\ 0.047R_m + 1.918 & R_m > 16 \end{cases} \quad \text{(C.23)}$$

$$\alpha_{Umax2} = \begin{cases} 1.1 & R_m \leq 0.4 \\ 0.35R_m + 0.96 & 0.4 < R_m \leq 71 \\ 0.209R_m + 1.061 & 0.71 < R_m \leq 4.5 \\ -0.0025R_m^2 + 0.145R_m + 1.4 & 4.5 < R_m < 21 \\ 0.0335R_m + 2.639 & R_m \geq 21 \end{cases} \quad \text{(C.24)}$$

The formula for α_{Umax} is likewise adapted for the NBCC, with α_{Umax1} and α_{Umax2} defined via a table of values instead of Equations (C.23) and (C.24):

$$\alpha_{Umax} = \begin{cases} \alpha_{Umax1} & \dfrac{S_a[1.30(R_m)^{-0.059}T_U]}{S_a(T_U)} = 0.769(R_m)^{0.059} \\ \alpha_{Umax2} & \dfrac{S_a[1.30(R_m)^{-0.059}T_U]}{S_a(T_U)} = 1 \\ \alpha_{Umax2}\left\{\dfrac{S_a[1.30(R_m)^{-0.059}T_U]}{S_a(T_U)}\right\}^{-x_3} & 0.769(R_m)^{0.059} < \dfrac{S_a[1.30(R_m)^{-0.059}T_U]}{S_a(T_U)} < 1 \end{cases} \quad \text{(C.25)}$$

For the same reasons discussed in Section C.3.1, the exponential form of Equation (3.31) is adopted, with coefficients A_{max} and B_{max} being defined analogously to A_{U1} and B_{U1}, with $S_a(1.30(R_m)^{-0.059}T_U)$ being replaced with Equation (3.32). $T_1 = 1.30(R_m)^{-0.059}T_U$ is not immediately connected to the formulations given in Appendix A and its rationale is somewhat poorly-articulated in Yuan (2016), and so Equation (3.32) is adopted to more clearly align with Appendix A and to mirror the formulation for α_{U1}. In the same fashion as Figure C.12, Figure C.13 illustrates the relationship between the proposed fit given by A_{Umax} and B_{Umax} for $N_U = 4$, $N_L = 5$ and $r_m = 2$. The proposed values of A_{Umax} and B_{Umax} are given in Table E.4 and Table E.5. Specifically, A_{max} and B_{max} are derived for values of α_U lying between R_{kU2} and R_{kU3}. Occasionally, α_U reaches its maximum value for $R_k > R_{KU3}$ – for these situations α_{U2stg} is large enough that α_U remains conservative.

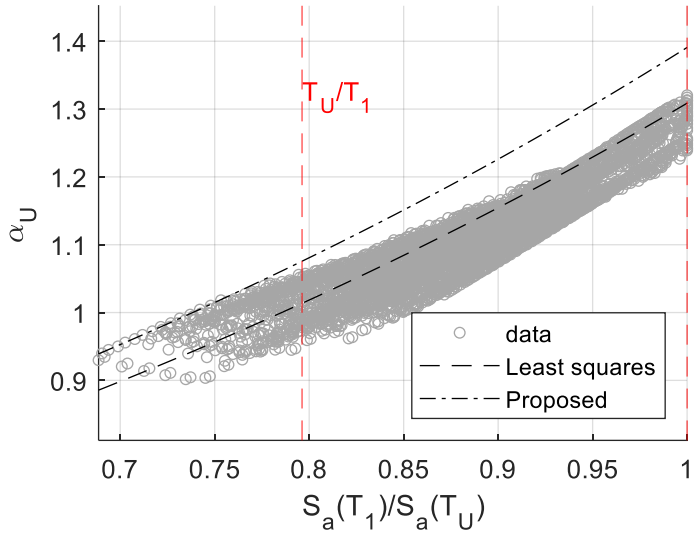

Figure C.13: Comparison between calculated and proposed α_{Umax} (N_U = 4, N_L = 5, r_m = 2)

C.2.6 Amplification ratio α_{U2stg} (associated with R_{kU2stg})

As discussed in Section C.2.3, α_{U2stg} is the upper bound on α_U for $R_k > R_{kU2stg}$ beyond which $\alpha_U \approx 1$. However, this is only approximately true, since even in the Yuan (2016) α_{U2stg} can take on values as large as 1.25 depending on R_m. The expectation is that α_U will not exceed α_{U2stg} for $R_k > R_{kU2stg}$, rather than specifically a value of one.

In Yuan (2016), α_{U2stg} is defined as a function of R_m, according to Equation (C.26):

$$\alpha_{U2stg} = \begin{cases} 1.1 & R_m \leq 1.4 \\ 0.14R_m + 0.918 & 1.4 < R_m \leq 2.3 \\ -0.08R_m + 1.424 & 2.3 < R_m < 4.1 \\ 1.1 & R_m \geq 4.1 \end{cases} \quad \text{(C.26)}$$

In essence, it is assumed that α_{U2stg} = 1.1 (theoretically 1 with a 10% surcharge for conservatism), with a spike between R_m = 1.4 and 4.1 to account for an increase in α_{U2stg} owing to higher mode effects not considered by the 2DOF model. This formulation is used for both the NBCC and ASCE 7 formulations.

However, it is somewhat misleading to state that the relationship given by Equation (C.26) applies for $R_m > 3$. In Yuan (2016), the maximum storey count is ten, and the maximum r_k and r_m are 20 and 3, respectively. Considering the definition of R_{kU2stg} given by Equation (C.16), if e.g. R_m = 3, $R_k \geq$ 30.6. Using Equation (3.19), if r_k lies between 1 and 20, this implies that $1.5 \leq (N_L/N_U)(\bar{\omega}_{1L}/\bar{\omega}_{1U})^2 \leq 30.6$. But for N_U+$N_L \leq 10$, this is only true for a few combinations of N_U and N_L, all of which have

$N_L/N_U \leq 0.5$. By Equation (3.18), if $r_m \leq 3$ there is no combination in the scope where both $R_m \geq 3$ and Equation (C.16) are satisfied. Therefore, by working from the 2DOF model and not enforcing the scope being used, the output can be potentially misleading.

As elsewhere, α_{U2stg} is computed based on a range of input values for N_U, N_L, r_m, etc. for $R_k \geq R_{kU2stg}$, where R_{kU2stg} is defined by Equation (3.28). These values are plotted alongside the Yuan (2016) and newly proposed formulations for α_{U2stg}, i.e. Equations (C.26) and (3.28) in Figure C.14. In general, the newly proposed formulation more closely matches the calculated values of α_{U2stg} in a more concise form. However, as alluded to, the proposed formulation is not valid for $R_m > 3$ due to the results having been truncated according to the scope.

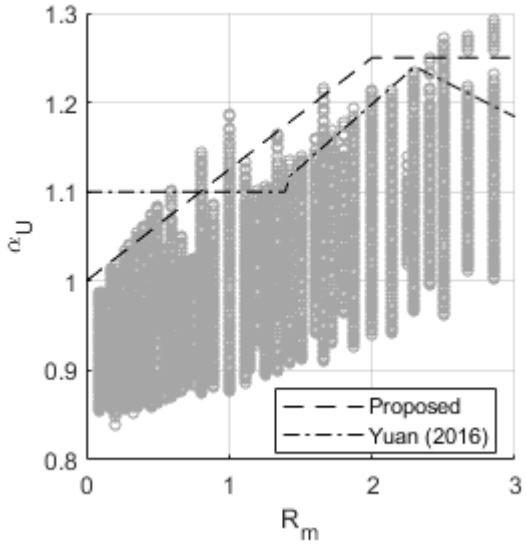

Figure C.14: Comparison between proposed and Yuan (2016) α_{U2stg}

Appendix D

α_U-k_U Relationship Derived by Yuan (2016)

D.1 Introduction

The latter half of Chapter 3, in which the approximated α_U relationship is used to derive limits on the storey stiffness k_U, is adapted from Yuan (2016). However, the original formulation is based on ASCE 7-10 (2010) and is adapted in an expedited manner to suit NBCC 2010 (NRCC, 2010). Correspondingly, the need to suit the relationships produced for ASCE 7 leads to several novel transformations by Yuan (2016) to the form of the NBCC 2010 spectrum. The current study heavily modifies these derivations and thus this appendix provides the relevant original equations so that they can be referred to without requiring the full text of Yuan (2016). In the following order, this Appendix provides a reference for three aspects of the Yuan (2016) formulation:

1. The Yuan (2016) approximation for α_U, both for ASCE 7-10 and NBCC 2010
2. The EXP-2 approximation for NBCC 2010's spectral acceleration, $S_a(T)$
3. The derivation of design stiffnesses k_U based on α_U and the EXP-2 approach.

This Appendix is only a partial account of Yuan (2016) – for example, as part of the adaptation of the ASCE 7 procedure to NBCC 2010, Yuan (2016) proposes four alternative transformations to the NBCC 2010 spectrum. Of these, the EXP-2 approach is identified as the preferred approach by Yuan (2016) and so is given exclusive attention here. For the remaining three alternatives, refer to Yuan (2016).

However, while the EXP-2 formulation is discussed in the current thesis, note that it is based on NBCC 2010 rather than NBCC 2015. In NBCC 2010, the spectral acceleration is defined by values at T = 0.2, 0.5, 1.0 and 2.0 seconds, while in NBCC 2015 values at T = 5.0 and 10.0 seconds are also used. Therefore, the fits proposed by Yuan (2016) are not directly applicable to NBCC 2015.

D.2 Equations proposed to evaluate shear-force-amplification factor α_U

So that the previously-proposed formulation can be referenced elsewhere, the Yuan (2016) formulation for α_U is given here, in Equations (D.1) to (D.17). The intent of each variable is analogous to the newly proposed procedure given in Section 3.3.4, and the changes are discussed in detail in Appendix C. Both those equations for the ASCE 7-10 and NBCC 2010 formulations are

given, and except for α_{U1}, α_{Umax}, and R_{kU2stg} are identical between the two formulations. For ASCE 7, $S_a(T)$ is defined as specified by the code, and for NBCC 2010 $S_a(T)$ is defined according to one of the four alternatives proposed by Yuan (2016) (in this case, the EXP-2 formulation is discussed in Appendix D.3).

ASCE Formulation

$$\alpha_U = \begin{cases} \alpha_{U1}\left(\frac{R_k}{R_{kU1}}\right)^{x_1} & R_{kU1} \le R_k < R_{kU2} \\ \alpha_{Umax} & R_{kU2} \le R_k \le R_{kU3} \\ \alpha_{Umax}\left(\frac{R_k}{R_{kU3}}\right)^{x_2} & R_{kU3} < R_k < R_{kU2stg} \\ \alpha_{U2stg} & R_{kU2stg} \le R_k \end{cases} \tag{D.1}$$

$$x_1 = \frac{ln\left(\alpha_{Umax}/\alpha_{U1}\right)}{ln\left(R_{kU2}/R_{kU1}\right)} \tag{D.2}$$

$$x_2 = \frac{ln\left(\alpha_{U2stg}/\alpha_{Umax}\right)}{ln\left(R_{kU2stg}/R_{kU3}\right)} \tag{D.3}$$

$$\alpha_{U1} = \begin{cases} \alpha_{U11} & 1 \le T_U/T_S \\ \alpha_{U12} & T_U/T_S \le \sqrt{(N_U + 0.12N_L)/(N_U + N_L)} \\ \alpha_{U11}\left(\frac{T_U}{T_S}\right)^{x_3} & \sqrt{(N_U + 0.12N_L)/(N_U + N_L)} < T_U/T_S < 1 \end{cases} \tag{D.4}$$

$$x_3 = \frac{ln\left(\alpha_{U12}/\alpha_{U11}\right)}{0.5ln\left((N_U + 0.12N_L)/(N_U + N_L)\right)} \tag{D.5}$$

$$\alpha_{Ymax} = \begin{cases} \alpha_{Umax1} & 1 \le T_U/T_S \\ \alpha_{Umax2} & T_U/T_S \le 0.769(R_m)^{0.059} \\ \alpha_{Umax1}\left(\frac{T_U}{T_S}\right)^{x_4} & 0.769(R_m)^{0.059} < T_U/T_S < 1 \end{cases} \tag{D.6}$$

$$x_4 = \frac{ln\left(\alpha_{Umax2}/\alpha_{Umax1}\right)}{ln\left(0.769(R_m)^{0.059}\right)} \tag{D.7}$$

$$\alpha_{Umax1} = \begin{cases} 0.03R_m + 1 & R_m < 0.71 \\ 0.17R_m + 0.9 & 0.71 \le R_m \le 4.5 \\ -0.005R_m^2 + 0.19R_m + 0.91 & 4.5 < R_m < 16 \\ 0.047R_m + 1.918 & 16 \le R_m \end{cases} \tag{D.8}$$

$$\alpha_{Umax2} = \begin{cases} 1{,}1 & R_m \leq 0.40 \\ 0.35R_m + 0.96 & 0.40 < R_m \leq 0.71 \\ 0.29R_m + 1.061 & 0.71 < R_m \leq 4.5 \\ -0.0025R_m^2 + 0.145R_m + 1.40 & 4.5 < R_m < 21 \\ 0.0335R_m + 2.639 & 21 \leq R_m \end{cases} \quad \text{(D.9)}$$

$$\alpha_{U2stg} = \begin{cases} 1.1 & R_m \leq 1.4 \\ 0.14R_m + 0.918 & 1.4 < R_m \leq 2.3 \\ -0.08R_m + 1.424 & 2.3 < R_m < 4.1 \\ 1.1 & 4.1 \leq R_m \end{cases} \quad \text{(D.10)}$$

$$R_{kU1} = \frac{R_m(0.12N_L + N_U)}{N_L + N_U} + \frac{0.12N_L + N_U}{0.88N_L} \quad \text{(D.11)}$$

$$R_{kU2} = R_m + 1 \quad \text{(D.12)}$$

$$R_{kU3} = \begin{cases} 4.13R_m + 2 & R_m \leq 0.8 \\ -0.26R_m + 5.52 & 0.8 < R_m < 2 \\ R_m + 3 & 2 \leq R_m \end{cases} \quad \text{(D.13)}$$

$$R_{kU2stg} = \begin{cases} 0.826R_m + 4.76 & R_m \leq 0.71 \\ 11.029R_m - 2.5 & 0.71 < R_m \end{cases} \quad \text{(D.14)}$$

NBCC Formulation (otherwise identical to ASCE formulation)

$$\alpha_{U1} = \begin{cases} \alpha_{U12}\left(\dfrac{S_a\left(\sqrt{\dfrac{N_U + N_L}{N_U + 0.12N_L}}T_U\right)}{S_a(T_U)}\right)^{-x_3} & \sqrt{\dfrac{N_U + N_L}{N_U + 0.12N_L}}T_U > 0.2\ s \\ \alpha_{U12} & \sqrt{\dfrac{N_U + N_L}{N_U + 0.12N_L}}T_U \leq 0.2\ s \end{cases} \quad \text{(D.15)}$$

$$\alpha_{Umax} = \begin{cases} \alpha_{Umax2}\left(\dfrac{S_a(1.30R_m^{-0.059}T_U)}{S_a(T_U)}\right)^{-x_4} & 1.30R_m^{-0.059} > 0.2\ s \\ \alpha_{Umax2} & 1.30R_m^{-0.059} \leq 0.2\ s \end{cases} \quad \text{(D.16)}$$

$$R_{kU2stg} = \begin{cases} 0.907R_m + 9.78 & R_m \leq 1.213 \\ 11.029R_m - 2.5 & 1.213 < R_m \end{cases} \quad \text{(D.17)}$$

The relevant values of α_{U11}, α_{U12}, α_{Umax1} and α_{Umax2} given by Yuan (2016) appear in Table D.1, Table D.2 and Table D.3. α_{U11} and α_{U12} are identical whether the ASCE 7 or NBCC 2010 formulations are used, and α_{Umax1} and α_{Umax2} are evaluated either by Equations (D.8) and (D.9) (for ASCE 7) or by Table D.2 and Table D.3 (for NBCC 2010).

Table D.1: Values of α_{U12} and α_{U12} for the case where $R_{kU1} < R_{kU2}$ (Yuan, 2016)

		α_{U11}			α_{U12}		
		r_m			r_m		
N_U	N_L	1	2	3	1	2	3
1	1	0.986	1.162	1.281	1.258	1.435	1.572
1	2	0.990	1.179	1.296	1.468	1.681	1.818
1	3	0.979	1.165	1.267	1.550	1.757	1.874
1	4	0.985	1.163	1.253	1.609	1.801	1.899
1	5	0.993	1.165	1.248	1.652	1.826	1.910
1	6	1.007	1.175	1.252	1.686	1.846	1.921
1	7	0.929	1.077	1.145	1.556	1.692	1.754
1	8	0.942	1.086	1.154	1.575	1.703	1.761
1	9	0.956	1.100	1.168	1.593	1.716	1.771
2	2	0.905	1.086	1.222	1.237	1.412	1.555
2	3	0.893	1.088	1.221	1.314	1.516	1.663
2	4	0.944	1.150	1.283	1.452	1.674	1.823
2	5	0.943	1.147	1.269	1.500	1.720	1.586
2	6	0.948	1.148	1.260	1.541	1.754	1.877
2	7	0.954	1.148	1.250	1.574	1.778	1.888
2	8	0.959	1.145	1.239	1.600	1.793	1.892
3	3	**0.920**	1.051	1.190	1.223	1.391	1.532
3	4	0.869	1.064	1.200	1.278	1.470	1.617
3	5	0.921	1.127	1.267	1.400	1.615	1.769
3	6	0.925	1.131	1.267	1.441	1.661	1.809
3	7	0.927	1.134	1.262	1.476	1.696	1.836
4	3	0.918	1.066	1.204	1.231	1.373	1.502
4	4	0.905	1.092	1.240	1.285	1.459	1.605
4	5	0.903	1.106	1.250	1.331	1.525	1.678
4	6	0.907	1.114	1.256	1.370	1.577	1.732
5	4	0.901	1.054	1.197	1.223	1.383	1.515
5	5	0.892	1.077	1.225	1.193	1.385	1.548

Note: Table D.1 is to be interpolated for intermediate values of r_m. In addition, the bolded value of 0.920 differs from Yuan (2016) and is given to correct a mismatch between the original MATLAB code used by Yuan (2016) and the text of Yuan (2016).

Table D.2: Values of α_{Umax1} for NBCC 2010 (Yuan, 2016)

		α_{Umax1}					α_{Umax1}		
		r_m					r_m		
N_L	N_U	1	2	3	N_L	N_U	1	2	3
1	1	1.070	1.240	1.410	3	7	0.900	1.046	1.119
1	2	1.015	1.070	1.155	4	1	1.580	2.110	2.470
1	3	1.010	1.040	1.080	4	2	1.240	1.580	1.870
1	4	1.008	1.015	1.060	4	3	1.050	1.353	1.580
1	5	1.006	1.012	1.018	4	4	1.010	1.151	1.410
1	6	1.005	1.010	1.015	4	5	0.990	1.142	1.232
1	7	1.004	1.009	1.013	4	6	0.940	1.043	1.141
1	8	1.004	1.008	1.011	5	1	1.735	2.310	2.635
1	9	1.003	1.007	1.010	5	2	1.325	1.735	2.054
2	1	1.240	1.580	1.870	5	3	1.082	1.467	1.735
2	2	1.070	1.240	1.410	5	4	1.040	1.224	1.538
2	3	1.020	1.127	1.240	5	5	1.000	1.198	1.293
2	4	1.015	1.070	1.155	6	1	1.870	2.470	2.764
2	5	1.012	1.036	1.104	6	2	1.410	1.870	2.215
2	6	1.010	1.020	1.070	6	3	1.102	1.580	1.870
2	7	1.009	1.017	1.046	6	4	1.050	1.295	1.665
2	8	0.900	1.015	1.028	7	1	1.995	2.590	2.905
3	1	1.410	1.870	2.215	7	2	1.495	1.995	2.354
3	2	1.155	1.410	1.665	7	3	1.152	1.688	1.995
3	3	1.020	1.240	1.410	8	1	2.110	2.670	3.046
3	4	0.990	1.155	1.283	8	2	1.580	2.110	2.470
3	5	0.965	1.050	1.123	9	1	2.215	2.764	3.187
3	6	1.015	1.070	1.155					

Note: Table D.2 is to be interpolated for intermediate values of r_m.

Table D.3: Values of α_{Umax2} for NBCC 2010 (Yuan, 2016)

		α_{Umax2}					α_{Umax2}		
		r_m					r_m		
N_L	N_U	1	2	3	N_L	N_U	1	2	3
1	1	1.270	1.479	1.688	3	7	1.030	1.180	1.330
1	2	1.135	1.270	1.375	4	1	1.897	2.400	2.780
1	3	1.100	1.193	1.270	4	2	1.479	1.897	2.180
1	4	1.100	1.135	1.230	4	3	1.280	1.618	1.897
1	5	1.100	1.100	1.170	4	4	1.240	1.350	1.688
1	6	1.100	1.100	1.135	4	5	1.240	1.395	1.520
1	7	1.100	1.100	1.110	4	6	1.100	1.230	1.479
1	8	1.100	1.100	1.100	5	1	2.063	2.600	3.013
1	9	1.100	1.100	1.100	5	2	1.584	2.063	2.347
2	1	1.479	1.897	2.180	5	3	1.274	1.758	2.063
2	2	1.270	1.479	1.688	5	4	1.285	1.436	1.845
2	3	1.193	1.340	1.479	5	5	1.220	1.479	1.550
2	4	1.135	1.270	1.375	6	1	2.180	2.780	3.200
2	5	1.100	1.228	1.312	6	2	1.688	2.180	2.503
2	6	1.100	1.193	1.270	6	3	1.320	1.897	2.180
2	7	1.100	1.140	1.160	6	4	1.260	1.540	2.002
2	8	1.000	1.080	1.130	7	1	2.293	2.940	3.343
3	1	1.688	2.180	2.503	7	2	1.763	2.293	2.647
3	2	1.375	1.688	2.002	7	3	1.365	2.022	2.293
3	3	1.180	1.479	1.688	8	1	2.400	3.080	3.443
3	4	1.127	1.375	1.531	8	2	1.897	2.400	2.780
3	5	1.080	1.198	1.291	9	1	2.503	3.200	3.544
3	6	1.135	1.270	1.375					

Note: Table D.3 is to be interpolated for intermediate values of r_m.

D.3 Approximation of spectral acceleration relationship $S_a(T)$

A key difference between the ASCE 7 and NBCC codes is the spectral shape used. In the case of ASCE 7 (2010, 2017), the spectrum is similar to that of Newmark & Hall (1982), while the NBCC (NRCC, 2010, 2015c) uses a piecewise uniform hazard spectrum that is intended to describe more accurately a uniform hazard across the full range of considered periods. Each is defined by different parameters and produces a different shape, as demonstrated by Figure 1.2 (NBCC 2015), Figure 1.3 (ASCE 7), and Figure D.1 (NBCC 2010). For comparison, the approximated EXP-2 and the NBCC 2010 spectrum appear in Figure D.2.

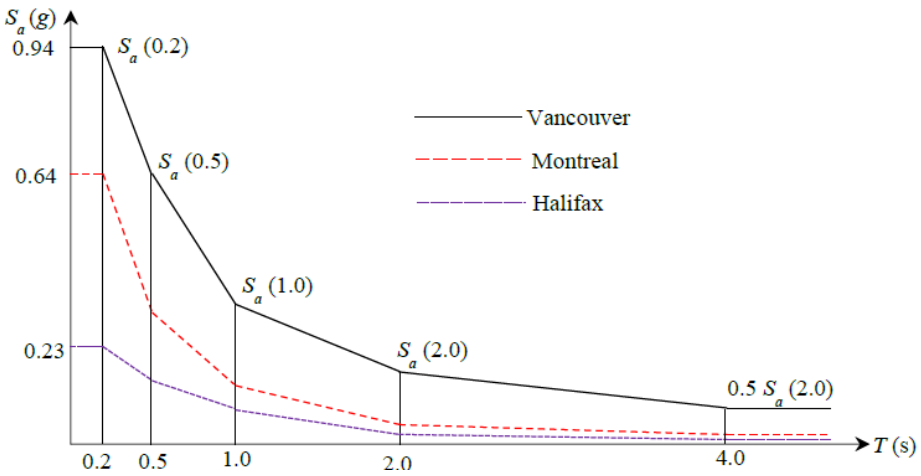

Figure D.1: NBCC 2010 design spectrum (Yuan, 2016)

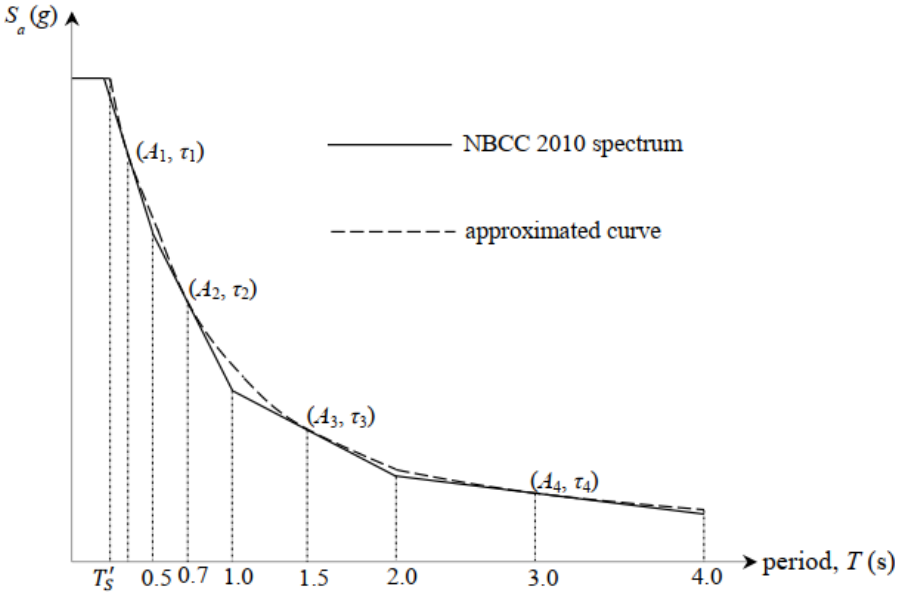

Figure D.2: EXP-2 design spectrum (Yuan, 2016)

One key advantage of the ASCE 7 spectrum utilized by Xu & Yuan (2015) is that any ratio of two spectral accelerations calculated using ASCE 7 can be directly related to the ratio of two related periods. Consequently, the relationships between R_m, R_k, α_U, and k_U are readily expressed in terms of the structural periods directly, without the intermediate calculation of the spectral accelerations. Due to the piecewise nature of the NBCC spectrum, this is not the case, and therefore some expression to

calculate the ratio of spectral accelerations is required. To suit the ASCE 7-based expressions, Yuan (2016) proposes two alternative approximations to the NBCC spectrum such that the ratio of spectral accelerations can be expressed analogously to ASCE 7. The first approximation expresses the spectral values $S_a(T)$ using a power function as in Equation (D.19) and the second uses an exponential function as in Equation (D.20). Equation (D.18) corresponds to the form of $S_a(T_1)/S_a(T_U)$ given by ASCE 7, for comparison.

$$\frac{S_a(T_1)}{S_a(T_U)} = \begin{cases} 1 & T_U/T_S \le T_U/T_1 \\ T_S/T_1 & T_U/T_1 < T_U/T_S \le 1 \\ T_U/T_1 & 1 < T_U/T_S \end{cases} \tag{D.18}$$

$$S_a(T) = \begin{cases} S_a(0.2) & T \le T_s' \\ A_1(T)^{\tau_1} & T_s' < T \le 0.5s \\ A_2(T)^{\tau_2} & 0.5s < T \le 1.0s \\ A_3(T)^{\tau_3} & 1.0s < T \le 2.0s \\ A_4(T)^{\tau_4} & 2.0s < T \le 4.0s \end{cases} \tag{D.19}$$

$$S_a(T) = \begin{cases} S_a(0.2) & T \le T_s' \\ A_1 e^{(\tau_1 T)} & T_s' < T \le 0.5s \\ A_2 e^{(\tau_2 T)} & 0.5s < T \le 1.0s \\ A_3 e^{(\tau_3 T)} & 1.0s < T \le 2.0s \\ A_4 e^{(\tau_4 T)} & 2.0s < T \le 4.0s \end{cases} \tag{D.20}$$

In Equations (D.19) and (D.20), A, τ and T_s' are curve fitting parameters specified by Yuan (2016). These parameters are evaluated in one of two different ways for each of Equations (D.19) and (D.20), as they can be calibrated either according to the midpoint or the endpoints of each segment. The differences significantly affect the calculated results, but those associated with the preferred EXP-2 (read: 2nd alternative, exponential form) alternative are sufficient to discuss the characteristics of the fitting functions. The fitting parameters for the EXP-2 fit are as follows:

$$\tau_i = \begin{cases} \dfrac{S_a(0.5) - S_a(0.2)}{0.3 S_a(0.35)} & i = 1 \\ \dfrac{ln[exp(0.15\tau_1)(S_a(0.35)/S_a(0.75))]}{0.5 - 0.75} & i = 2 \\ \dfrac{ln[exp(0.25\tau_2)(S_a(0.75)/S_a(1.5))]}{1.0 - 1.5} & i = 3 \\ \dfrac{ln[exp(0.5\tau_3)(S_a(1.5)/S_a(3.0))]}{2.0 - 3.5} & i = 4 \end{cases} \tag{D.21}$$

$$A_i = \begin{cases} S_a(0.35)\, exp(-0.35\tau_1) & i = 1 \\ S_a(0.75)\, exp(-0.75\tau_2) & i = 2 \\ S_a(1.5)\, exp(-1.5\tau_3) & i = 3 \\ S_a(3.0)\, exp(-3.0\tau_4) & i = 4 \end{cases} \tag{D.22}$$

$$T_s' = \frac{ln[S_a(0.2)/A_1]}{\tau_1} \tag{D.23}$$

Note that the form of Equation (D.21) differs from that given in Yuan (2016). The coefficients that are given to calculate τ in Yuan (2016) do not match the MATLAB code originally used to demonstrate the adequacy of the fit and do not produce satisfactory results. Equation (D.21) provides the correct values. This aside, Equation (D.21) is not appropriate for $S_a(0.2) \leq S_a(0.5)$ as sometimes occurs in NBCC 2010, and will produce nonsensical results. For $S_a(0.2) \leq S_a(0.5)$, T_s' should be taken as 0.5 seconds and the term corresponding to 0.2 to 0.5 seconds should be omitted.

Altogether, Equations (D.21) to (D.23) are cumbersome for several reasons. For example, τ is defined recursively and so requires that each prior term must also be calculated for larger periods. Therefore, even for a hypothetical structure where all the essential periods are at longer periods, the function must be evaluated for shorter periods notwithstanding that $S_a(T)$ itself at those periods is not required. The formulation also requires that several new variables be defined beyond those required to calculate α_U and to those familiar to users of the NBCC equivalent static force procedure. Finally, the formulation is based only on NBCC 2010 and would require updating for use with NBCC 2015, and the imminent NBCC 2020.

D.4 Critical upper structure stiffnesses k_U for EXP-2 fit

By using the exponential form for $S_a(T)$, $S_a(T_1)/S_a(T_U)$ can be re-expressed to be similar to that of ASCE 7 (i.e. Equation (D.18)). Via the design requirement given by Equation (3.9), the approximate form of α_U given by Yuan (2016) in Equation (D.1), the form of $S_a(T)$ given by Equations (D.20) to (D.23) and a significant amount of algebraic manipulation, the following expressions can be derived for the various critical k_U which correspond to the critical points (R_k, α_U) of the R_k-α_U distribution (e.g. R_{kU1}). Said equations are derived by substituting the form of α_U into Equation (3.9) and then rearranging to solve for k_U. The form of $S_a(T)$ given by Equations (D.20) to (D.23) (corresponding to the EXP-2 fit) is then substituted into the equation. What results is a series of equations for each critical value of k_U. For the EXP-2 fit, the solution that is given by Yuan (2016) is the following:

$$k_{\alpha U1}=\begin{cases}\alpha_{U12}m_U N_U\dfrac{S_a(0.2)}{\Delta_{Ulim}} & k_{U03}\le k_{\alpha U1}\\ m_U\left(\dfrac{2\pi}{\bar{\omega}_{1U}}\right)^2\left(\dfrac{N_U+N_L}{N_U+0.12N_L}\right)\left(\dfrac{\tau_1 x_3}{y_1}\right)^2 & k_{U01}\le k_{\alpha U1}<k_{U03}\\ m_U\left(\dfrac{2\pi}{\bar{\omega}_{1U}}\right)^2\left((1-C_1)x_3+1\right)^2\left(\dfrac{\tau_1}{y_2}\right)^2 & \dfrac{k_{U03}(T_s')^2}{0.25}\le k_{\alpha U1}<k_{U01}\\ m_U\left(\dfrac{2\pi}{\bar{\omega}_{1U}}\right)^2\left((\tau_1-\tau_2C_1)x_3+\tau_1\right)^2\left(\dfrac{1}{y_3}\right)^2 & \dfrac{k_{U01}(T_s')^2}{0.25}\le k_{\alpha U1}<\dfrac{k_{U03}(T_s')^2}{0.25}\\ m_U\left(\dfrac{2\pi}{\bar{\omega}_{1U}}\right)^2\left((1-C_1)x_3+1\right)^2\left(\dfrac{\tau_2}{y_4}\right)^2 & k_{U03}(T_s')^2\le k_{\alpha U1}<\dfrac{k_{U01}(T_s')^2}{0.25}\\ m_U\left(\dfrac{2\pi}{\bar{\omega}_{1U}}\right)^2\left((\tau_2-\tau_3C_1)x_3+\tau_2\right)^2\left(\dfrac{1}{y_5}\right)^2 & k_{U01}(T_s')^2\le k_{\alpha U1}<k_{U03}(T_s')^2\\ m_U\left(\dfrac{2\pi}{\bar{\omega}_{1U}}\right)^2\left((1-C_1)x_3+1\right)^2\left(\dfrac{\tau_3}{y_6}\right)^2 & \dfrac{k_{U03}(T_s')^2}{4}\le k_{\alpha U1}<k_{U01}(T_s')^2\\ m_U\left(\dfrac{2\pi}{\bar{\omega}_{1U}}\right)^2\left((\tau_3-\tau_4C_1)x_3+\tau_3\right)^2\left(\dfrac{1}{y_7}\right)^2 & \dfrac{k_{U01}(T_s')^2}{4}\le k_{\alpha U1}<\dfrac{k_{U03}(T_s')^2}{4}\end{cases} \quad \text{(D.24)}$$

$$k_{\alpha Umax}=$$

$$\begin{cases}\alpha_{U12}m_U N_U\frac{S_a(0.2)}{\Delta_{Ulim}} & k_{U03}\le k_{\alpha Umax}\\ m_U\left(\frac{2\pi}{\bar{\omega}_{1U}}\right)^2(1.691R_m^{-0.118})\left(\frac{\tau_1 x_4}{y_1}\right)^2 & k_{U01}\le k_{\alpha Umax}<k_{U03}\\ m_U\left(\frac{2\pi}{\bar{\omega}_{1U}}\right)^2\left((1-1.30R_m^{-0.059})x_4+1\right)^2\left(\frac{\tau_1}{y_2}\right)^2 & \frac{k_{U02}(T_s')^2}{0.25}\le k_{\alpha Umax}<k_{U01}\\ m_U\left(\frac{2\pi}{\bar{\omega}_{1U}}\right)^2\left((\tau_1-1.30\tau_2R_m^{-0.059})x_4+\tau_1\right)^2\left(\frac{1}{y_3}\right)^2 & \frac{k_{U01}(T_s')^2}{0.25}\le k_{\alpha Umax}<\frac{k_{U02}(T_s')^2}{0.25}\\ m_U\left(\frac{2\pi}{\bar{\omega}_{1U}}\right)^2\left((1-1.30R_m^{-0.059})x_4+1\right)^2\left(\frac{\tau_2}{y_4}\right)^2 & k_{U02}(T_s')^2\le k_{\alpha Umax}<\frac{k_{U01}(T_s')^2}{0.25}\\ m_U\left(\frac{2\pi}{\bar{\omega}_{1U}}\right)^2\left((\tau_2-1.30\tau_3R_m^{-0.059})x_4+\tau_2\right)^2\left(\frac{1}{y_5}\right)^2 & k_{U01}(T_s')^2\le k_{\alpha Umax}<k_{U02}(T_s')^2\\ m_U\left(\frac{2\pi}{\bar{\omega}_{1U}}\right)^2\left((1-1.30R_m^{-0.059})x_4+1\right)^2\left(\frac{\tau_3}{y_6}\right)^2 & \frac{k_{U02}(T_s')^2}{4}\le k_{\alpha Umax}<k_{U01}(T_s')^2\\ m_U\left(\frac{2\pi}{\bar{\omega}_{1U}}\right)^2\left((\tau_3-1.30\tau_4R_m^{-0.059})x_4+\tau_3\right)^2\left(\frac{1}{y_7}\right)^2 & \frac{k_{U01}(T_s')^2}{4}\le k_{\alpha Umax}<\frac{k_{U02}(T_s')^2}{4}\end{cases} \quad \text{(D.25)}$$

$$k_{\alpha U2stg} = \begin{cases} \alpha_{U2stg} m_U N_U \dfrac{S_a(0.2)}{\Delta_{Ulim}} & k_{U01} \le k_{\alpha U2stg} \\ m_U \left(\dfrac{2\pi}{\bar{\omega}_{1U}}\right)^2 \left(\dfrac{\tau_1}{y_1}\right)^2 & \dfrac{k_{U01}(T_s')^2}{0.25} \le k_{\alpha U2stg} < k_{U01} \\ m_U \left(\dfrac{2\pi}{\bar{\omega}_{1U}}\right)^2 \left(\dfrac{\tau_2}{y_2}\right)^2 & k_{U01}(T_s')^2 \le k_{\alpha U2stg} < \dfrac{k_{U01}(T_s')^2}{0.25} \\ m_U \left(\dfrac{2\pi}{\bar{\omega}_{1U}}\right)^2 \left(\dfrac{\tau_3}{y_3}\right)^2 & \dfrac{k_{U01}(T_s')^2}{4} \le k_{\alpha U2stg} < k_{U01}(T_s')^2 \end{cases} \tag{D.26}$$

$$C_1 = \sqrt{\frac{N_U + N_L}{N_U + 0.12N_L}} \tag{D.27}$$

$$k_{U01} = m_U \left(\frac{2\pi}{\bar{\omega}_{1U} T_s'}\right)^2 \tag{D.28}$$

$$k_{U02} = 1.691(R_m)^{-0.118} k_{U01} \tag{D.29}$$

$$k_{U03} = \left(\frac{N_U + N_L}{N_U + 0.12N_L}\right) k_{U01} \tag{D.30}$$

$$exp(y_i) y_i^2 = b_i \tag{D.31}$$

$$b_{\alpha U1,i} = \begin{cases} \left[\dfrac{N_U + N_L}{N_U + 0.12N_L}\right] \tau_1^2 x_3^2 \left(\dfrac{2\pi}{\bar{\omega}_{1U}}\right)^2 \left(\dfrac{S_a(0.2)}{A_1}\right)^{x_3} \dfrac{\Delta_{Ulim}}{\alpha_{U12} N_U S_a(0.2)} & i = 1 \\ \left[\left(1 - \sqrt{\dfrac{N_U + 0.12N_L}{N_U + N_L}}\right) x_3 + 1\right]^2 \tau_1^2 \left(\dfrac{2\pi}{\bar{\omega}_{1U}}\right)^2 \dfrac{\Delta_{Ulim}}{\alpha_{U12} N_U A_1} & i = 2 \\ \left[\left(\tau_1 - \tau_2 \sqrt{\dfrac{N_U + 0.12N_L}{N_U + N_L}}\right) x_3 + \tau_1\right]^2 \left(\dfrac{2\pi}{\bar{\omega}_{1U}}\right)^2 \left(\dfrac{A_2}{A_1}\right)^{x_3} \dfrac{\Delta_{Ulim}}{\alpha_{U12} N_U A_1} & i = 3 \\ \left[\left(1 - \sqrt{\dfrac{N_U + 0.12N_L}{N_U + N_L}}\right) x_3 + 1\right]^2 \tau_2^2 \left(\dfrac{2\pi}{\bar{\omega}_{1U}}\right)^2 \dfrac{\Delta_{Ulim}}{\alpha_{U12} N_U A_2} & i = 4 \\ \left[x_3 \left(\tau_2 - \tau_3 \sqrt{\dfrac{N_U + 0.12N_L}{N_U + N_L}}\right) + \tau_2\right]^2 \left(\dfrac{2\pi}{\bar{\omega}_{1U}}\right)^2 \left(\dfrac{A_3}{A_2}\right)^{x_3} \dfrac{\Delta_{Ulim}}{\alpha_{U12} N_U A_2} & i = 5 \\ \left[\left(1 - \sqrt{\dfrac{N_U + 0.12N_L}{N_U + N_L}}\right) x_3 + 1\right]^2 \tau_3^2 \left(\dfrac{2\pi}{\bar{\omega}_{1U}}\right)^2 \dfrac{\Delta_{Ulim}}{\alpha_{U12} N_U A_3} & i = 6 \\ \left[\left(\tau_3 - \tau_4 \sqrt{\dfrac{N_U + 0.12N_L}{N_U + N_L}}\right) x_3 + \tau_3\right]^2 \left(\dfrac{2\pi}{\bar{\omega}_{1U}}\right)^2 \left(\dfrac{A_4}{A_3}\right)^{x_3} \dfrac{\Delta_{Ulim}}{\alpha_{U12} N_U A_3} & i = 7 \end{cases} \tag{D.32}$$

$$b_{\alpha \mathrm{U}max,i} = \begin{cases} [1.169\mathrm{R_m^{-0.118}}]\tau_1^2 x_4^2 \left(\frac{2\pi}{\bar{\omega}_{1U}}\right)^2 \left(\frac{S_a(0.2)}{A_1}\right)^{x_4} \frac{\Delta_{Ulim}}{\alpha_{Umax2} N_U S_a(0.2)} & i = 1 \\ [(1 - 1.3R_m^{-0.059})x_4 + 1]^2 \tau_1^2 \left(\frac{2\pi}{\bar{\omega}_{1U}}\right)^2 \frac{\Delta_{Ulim}}{\alpha_{Umax2} N_U A_1} & i = 2 \\ [(\tau_1 - 1.3\tau_2 R_m^{-0.059})x_4 + \tau_1]^2 \left(\frac{2\pi}{\bar{\omega}_{1U}}\right)^2 \left(\frac{A_2}{A_1}\right)^{x_4} \frac{\Delta_{Ulim}}{\alpha_{Umax2} N_U A_1} & i = 3 \\ [(1 - 1.3R_m^{-0.059})x_4 + 1]^2 \tau_2^2 \left(\frac{2\pi}{\bar{\omega}_{1U}}\right)^2 \frac{\Delta_{Ulim}}{\alpha_{Umax2} N_U A_2} & i = 4 \\ [(\tau_2 - 1.3\tau_3 R_m^{-0.059})x_4 + \tau_2]^2 \left(\frac{2\pi}{\bar{\omega}_{1U}}\right)^2 \left(\frac{A_3}{A_2}\right)^{x_4} \frac{\Delta_{Ulim}}{\alpha_{Umax2} N_U A_2} & i = 5 \\ [(1 - 1.3R_m^{-0.059})x_4 + 1]^2 \tau_3^2 \left(\frac{2\pi}{\bar{\omega}_{1U}}\right)^2 \frac{\Delta_{Ulim}}{\alpha_{Umax2} N_U A_3} & i = 6 \\ [(\tau_3 - 1.3\tau_4 R_m^{-0.059})x_4 + \tau_3]^2 \left(\frac{2\pi}{\bar{\omega}_{1U}}\right)^2 \left(\frac{A_4}{A_3}\right)^{x_4} \frac{\Delta_{Ulim}}{\alpha_{Umax2} N_U A_3} & i = 7 \end{cases} \quad \text{(D.33)}$$

$$b_{\alpha \mathrm{U}2stg,i} = \begin{cases} \tau_1^2 \left(\frac{2\pi}{\bar{\omega}_{1U}}\right)^2 \frac{\Delta_{Ulim}}{\alpha_{U2stg} N_U A_1} & i = 1 \\ \tau_2^2 \left(\frac{2\pi}{\bar{\omega}_{1U}}\right)^2 \frac{\Delta_{Ulim}}{\alpha_{U2stg} N_U A_2} & i = 2 \\ \tau_3^2 \left(\frac{2\pi}{\bar{\omega}_{1U}}\right)^2 \frac{\Delta_{Ulim}}{\alpha_{U2stg} N_U A_3} & i = 3 \end{cases} \quad \text{(D.34)}$$

In the above, each $k_{\alpha U}$ is the storey stiffness of the upper structure corresponding to the relevant α_U (i.e. $k_{\alpha U1}$ is associated with the Yuan (2016) formulation for $\alpha_{U1}\backslash R_{kU1}$). The formulation is defined in three parts - $k_{\alpha U}$, with which the final value of $k_{\alpha U}$ is defined, y_i, an intermediate variable which must be solved numerically via Equation (D.31), and $b_{\alpha U}$, a coefficient associated with each $k_{\alpha U}$ and used to solve for y_i. For $k_{\alpha U1}$ and $k_{\alpha Umax}$, the derivation assumes that $T_1/T_U = \sqrt{N_U + N_L/N_U + 0.12N_L}$ and $1.30R_m^{-0.059}$ respectively as part of the transformations performed. Note that the variables C_1, k_{U01}, k_{U02} and k_{U03} are used to make the equations more concise and that each $k_{\alpha U}$ is referred to as simply k_U in the newly proposed formulation.

To continue and evaluate each $k_{\alpha U}$ requires the solution of the transcendental equation, Equation (D.31), for y_i based on $b_{\alpha U,i}$. This Equation (D.31) is derived from the same procedure as $k_{\alpha U}$ but has no direct physical interpretation. It can therefore only be said that the relationship may produce multiple results based on the value of $b_{\alpha U,I}$, which can be interpreted as having an exponential part and a quadratic part. Where multiple solutions exist, no guidance is provided by Yuan (2016) but that y_i is

to be evaluated according to Table D.4. While not stated explicitly by Yuan (2016), it appears that the tabulated solutions correspond to the negative-valued root closest in value to zero.

Table D.4: Numerical solution of y_i (Yuan, 2016)

y_i	b_i	y_i	b_i
-0.100	0.009	-1.100	0.403
-0.200	0.033	-1.200	0.434
-0.300	0.067	-1.300	0.461
-0.400	0.107	-1.400	0.483
-0.500	0.152	-1.500	0.502
-0.600	0.198	-1.600	0.517
-0.700	0.243	-1.700	0.528
-0.800	0.288	-1.800	0.536
-0.900	0.329	-1.900	0.540
-1.000	0.368	-2.000	0.541

The development of Equations (D.24) to (D.34) is an involved procedure. It may not be obvious where various elements arise from when compared to the initial formulation of α_U and the original design criterion. In particular, the limits expressed concerning stiffness $k_{\alpha U}$ are not directly related to the prior limits given for R_k, T_U and T_1, and y_i is not clearly related to either the original formulation or some physical intuition. Little guidance is provided for the transcendental equation in particular, which is integral to the solution for $k_{\alpha U}$ and arises due to a transformation partway through the derivation. Specifically, each $k_{\alpha U}$ can be expressed as an exponential function of the period T_U of the form given by (D.35). Assuming that the exponent is equal to y_i and assuming that the form of $k_{\alpha U}$ can be represented similarly to Equation (D.24) to (D.26), the numerical solution is derived according to Equation (D.31). What is not obvious from the Equations given by Yuan (2016) is that y_i is directly related to T_U based on the fitting parameters τ, A and T_S', as well as the exponent x (x_3 or x_4 as applicable). In fact, the intermediate exponential form can be generically expressed as:

$$k_{\alpha U} = C_1 e^{C_2 \times T_U} = C_1 e^{\left(\frac{C_3}{\sqrt{k_{\alpha U}}}\right)} \tag{D.35}$$

where C_i represents various constants defined with respect to the model and fit parameters (e.g. τ, $S_a(T)$).

Note that compared to Yuan (2016) x_3^2 has been added to the first term of Equation (D.32) for consistency with the original MATLAB code and with Equation (D.32). Likewise, the limits on stiffness on the seventh term of Equation (D.25) have been revised so that they vary continuously,

and the eighth term of Equation (D.25) has been corrected from 1.301 to 1.30 to be consistent with elsewhere.

Appendix E

Tabulated values of R_{kU1}, A_{U1}, B_{U1}, A_{Umax} and B_{Umax}

The following tabulated values are used as part of the α_U formulation given in Chapter 3.3.4.

Table E.1: Values of R_{kU1}

		r_m							r_m				
N_U	N_L	1	2	3	4	5	N_U	N_L	1	2	3	4	5
1	1	1.496	1.978	2.457	2.936	3.414	4	3	1.691	2.032	2.351	2.705	3.054
1	2	1.506	2.223	2.937	3.652	4.367	4	4	1.461	1.846	2.252	2.654	3.055
1	3	1.463	2.315	3.165	4.016	4.868	4	5	1.302	1.751	2.194	2.635	3.076
1	4	1.433	2.368	3.301	4.231	5.159	4	6	1.210	1.685	2.158	2.632	3.105
1	5	1.412	2.398	3.374	4.342	5.303	4	7	1.141	1.639	2.137	2.635	3.134
1	6	1.395	2.411	3.399	4.366	5.316	4	8	1.088	1.605	2.123	2.642	3.160
1	7	1.382	2.408	3.385	4.320	5.216	5	1	2.725	3.113	3.594	4.142	4.723
1	8	1.370	2.395	3.351	4.246	5.091	5	2	2.327	2.872	3.315	3.598	3.762
1	9	1.359	2.381	3.320	4.201	4.907	5	3	1.941	2.351	2.608	2.860	3.120
1	10	1.349	2.369	3.307	4.200	5.071	5	4	1.670	2.005	2.331	2.693	3.051
1	11	1.341	2.362	3.313	4.098	5.135	5	5	1.462	1.833	2.234	2.632	3.028
2	1	1.618	1.915	2.180	2.456	2.732	5	6	1.313	1.743	2.172	2.600	3.027
2	2	1.460	1.900	2.330	2.756	3.182	5	7	1.222	1.678	2.131	2.584	3.037
2	3	1.322	1.848	2.368	2.888	3.408	6	1	3.152	3.613	4.193	4.901	5.684
2	4	1.230	1.814	2.397	2.980	3.563	6	2	2.616	3.214	3.856	4.417	4.778
2	5	1.167	1.794	2.420	3.046	3.672	6	3	2.185	2.711	3.060	3.272	3.476
2	6	1.122	1.781	2.437	3.092	3.746	6	4	1.868	2.258	2.531	2.795	3.109
2	7	1.089	1.770	2.447	3.118	3.786	6	5	1.641	1.978	2.312	2.676	3.040
2	8	1.063	1.761	2.448	3.125	3.794	6	6	1.463	1.824	2.222	2.616	3.009
2	9	1.043	1.751	2.442	3.116	3.776	7	1	3.543	3.998	4.553	5.161	5.841
2	10	1.026	1.741	2.430	3.095	3.736	7	2	2.919	3.558	4.365	5.306	6.370
3	1	1.947	2.257	2.524	2.747	2.940	7	3	2.426	3.041	3.533	3.867	4.139
3	2	1.692	2.040	2.352	2.686	3.017	7	4	2.071	2.545	2.861	3.091	3.309
3	3	1.453	1.865	2.280	2.690	3.099	7	5	1.815	2.203	2.477	2.754	3.092
3	4	1.301	1.773	2.240	2.706	3.172	8	1	3.939	4.386	4.952	5.579	6.247
3	5	1.204	1.715	2.222	2.730	3.238	8	2	3.219	3.881	4.736	5.681	6.671
3	6	1.135	1.675	2.214	2.753	3.293	8	3	2.657	3.313	4.000	4.574	5.078
3	7	1.084	1.647	2.210	2.774	3.337	8	4	2.274	2.846	3.273	3.556	3.728
3	8	1.044	1.626	2.208	2.789	3.369	9	1	4.342	4.798	5.381	6.029	6.709
3	9	1.013	1.610	2.205	2.798	3.388	9	2	3.535	4.164	4.954	5.900	6.983
4	1	2.319	2.663	3.039	3.383	3.675	9	3	2.919	3.616	4.482	5.276	6.148
4	2	1.982	2.386	2.681	2.918	3.148	10	1	4.763	5.260	5.905	6.670	7.507

		r_m							r_m					
N_U	N_L	1	2	3	4	5	N_U	N_L	1	2	3	4	5
10	2	3.881	4.583	5.376	6.255	7.322	11	1	5.193	5.744	6.461	7.315	8.306

Table E.2: Values of A_{U1}

		r_m							r_m					
N_U	N_L	1	2	3	4	5	N_U	N_L	1	2	3	4	5
1	1	0.433	0.516	0.575	0.618	0.65	4	4	0.291	0.39	0.471	0.533	0.582
1	2	0.396	0.518	0.593	0.64	0.674	4	5	0.307	0.410	0.49	0.549	0.593
1	3	0.444	0.564	0.629	0.669	0.697	4	6	0.321	0.427	0.504	0.56	0.601
1	4	0.478	0.595	0.657	0.696	0.722	4	7	0.335	0.443	0.515	0.567	0.603
1	5	0.505	0.624	0.691	0.735	0.768	4	8	0.347	0.457	0.525	0.571	0.605
1	6	0.527	0.656	0.737	0.800	0.852	5	1	0.386	0.409	0.423	0.434	0.443
1	7	0.547	0.692	0.798	0.891	0.974	5	2	0.276	0.310	0.351	0.402	0.464
1	8	0.567	0.731	0.865	0.982	1.085	5	3	0.262	0.327	0.403	0.477	0.537
1	9	0.586	0.768	0.917	1.039	1.126	5	4	0.266	0.356	0.441	0.511	0.566
1	10	0.604	0.800	0.947	1.058	1.142	5	5	0.278	0.377	0.463	0.528	0.58
1	11	0.619	0.821	0.960	1.037	1.127	5	6	0.289	0.393	0.478	0.541	0.588
2	1	0.382	0.446	0.510	0.565	0.611	5	7	0.301	0.407	0.490	0.549	0.593
2	2	0.329	0.428	0.509	0.570	0.617	6	1	0.406	0.436	0.474	0.511	0.550
2	3	0.344	0.458	0.534	0.589	0.629	6	2	0.274	0.301	0.326	0.353	0.387
2	4	0.364	0.483	0.555	0.603	0.638	6	3	0.248	0.297	0.354	0.423	0.492
2	5	0.384	0.503	0.572	0.616	0.648	6	4	0.244	0.319	0.399	0.470	0.529
2	6	0.413	0.536	0.601	0.645	0.677	6	5	0.25	0.343	0.423	0.489	0.542
2	7	0.433	0.549	0.619	0.669	0.709	6	6	0.262	0.362	0.442	0.505	0.556
2	8	0.444	0.565	0.648	0.709	0.758	7	1	0.427	0.462	0.509	0.570	0.634
2	9	0.456	0.588	0.682	0.756	0.818	7	2	0.270	0.300	0.324	0.345	0.367
2	10	0.468	0.612	0.719	0.806	0.882	7	3	0.234	0.271	0.313	0.360	0.416
3	1	0.375	0.406	0.452	0.503	0.553	7	4	0.226	0.282	0.347	0.417	0.479
3	2	0.279	0.354	0.424	0.486	0.539	7	5	0.238	0.316	0.402	0.474	0.525
3	3	0.291	0.391	0.465	0.524	0.573	8	1	0.449	0.488	0.542	0.619	0.72
3	4	0.319	0.421	0.497	0.553	0.595	8	2	0.268	0.300	0.334	0.365	0.394
3	5	0.340	0.448	0.521	0.571	0.609	8	3	0.251	0.262	0.284	0.315	0.348
3	6	0.359	0.468	0.538	0.584	0.618	8	4	0.252	0.294	0.343	0.401	0.469
3	7	0.376	0.487	0.554	0.597	0.630	9	1	0.465	0.512	0.570	0.653	0.764
3	8	0.390	0.504	0.569	0.612	0.644	9	2	0.305	0.344	0.388	0.434	0.486
3	9	0.402	0.513	0.579	0.626	0.663	9	3	0.268	0.300	0.325	0.347	0.372
4	1	0.369	0.388	0.406	0.432	0.465	10	1	0.507	0.565	0.641	0.737	0.871
4	2	0.282	0.332	0.395	0.459	0.513	10	2	0.313	0.360	0.421	0.496	0.597
4	3	0.278	0.362	0.441	0.506	0.559	11	1	0.632	0.547	0.438	0.307	0.165

Table E.3: Values of B_{UI}

N_U	N_L	r_m 1	2	3	4	5
1	1	1.033	0.976	0.944	0.925	0.914
1	2	1.234	1.086	1.018	0.981	0.957
1	3	1.176	1.036	0.977	0.945	0.924
1	4	1.125	0.994	0.937	0.904	0.882
1	5	1.087	0.953	0.889	0.849	0.821
1	6	1.055	0.909	0.832	0.779	0.738
1	7	1.025	0.864	0.769	0.699	0.643
1	8	0.998	0.820	0.711	0.631	0.570
1	9	0.973	0.783	0.669	0.592	0.542
1	10	0.951	0.755	0.646	0.578	0.533
1	11	0.933	0.737	0.637	0.590	0.542
2	1	1.063	1.007	0.955	0.918	0.891
2	2	1.310	1.158	1.073	1.021	0.987
2	3	1.327	1.153	1.069	1.020	0.989
2	4	1.310	1.133	1.052	1.008	0.979
2	5	1.285	1.110	1.033	0.989	0.961
2	6	1.244	1.077	1.002	0.958	0.927
2	7	1.206	1.048	0.970	0.921	0.886
2	8	1.179	1.020	0.936	0.879	0.836
2	9	1.159	0.993	0.898	0.832	0.780
2	10	1.140	0.966	0.861	0.786	0.725
3	1	1.028	1.010	0.965	0.916	0.876
3	2	1.429	1.283	1.179	1.113	1.066
3	3	1.459	1.265	1.163	1.098	1.054
3	4	1.399	1.216	1.122	1.066	1.029
3	5	1.353	1.179	1.093	1.043	1.010
3	6	1.321	1.151	1.071	1.025	0.995
3	7	1.294	1.128	1.051	1.007	0.977
3	8	1.272	1.109	1.034	0.987	0.956
3	9	1.254	1.093	1.014	0.963	0.928
4	1	1.011	1.002	0.994	0.968	0.933
4	2	1.374	1.291	1.193	1.113	1.058
4	3	1.448	1.284	1.173	1.102	1.054
4	4	1.442	1.252	1.150	1.087	1.044
4	5	1.418	1.228	1.131	1.073	1.034
4	6	1.394	1.206	1.114	1.059	1.024
4	7	1.375	1.188	1.100	1.048	1.015
4	8	1.358	1.174	1.088	1.040	1.008
5	1	0.955	0.932	0.923	0.915	0.909
5	2	1.360	1.308	1.240	1.161	1.083
5	3	1.479	1.343	1.212	1.120	1.060
5	4	1.505	1.307	1.181	1.104	1.054
5	5	1.497	1.281	1.167	1.098	1.052
5	6	1.483	1.263	1.154	1.090	1.047
5	7	1.466	1.248	1.144	1.083	1.043
6	1	0.888	0.845	0.788	0.731	0.669
6	2	1.350	1.302	1.262	1.216	1.162
6	3	1.520	1.410	1.293	1.181	1.096
6	4	1.587	1.402	1.250	1.156	1.097
6	5	1.607	1.372	1.237	1.160	1.108
6	6	1.582	1.338	1.220	1.150	1.100
7	1	0.824	0.771	0.696	0.605	0.515
7	2	1.350	1.283	1.231	1.183	1.134
7	3	1.576	1.477	1.384	1.289	1.196
7	4	1.663	1.517	1.368	1.249	1.170
7	5	1.636	1.433	1.273	1.177	1.118
8	1	0.766	0.703	0.618	0.505	0.372
8	2	1.351	1.265	1.174	1.102	1.038
8	3	1.519	1.488	1.444	1.379	1.311
8	4	1.547	1.463	1.364	1.258	1.156
9	1	0.723	0.645	0.554	0.436	0.296
9	2	1.222	1.135	1.041	0.946	0.842
9	3	1.408	1.339	1.291	1.253	1.203
10	1	0.670	0.588	0.483	0.365	0.216
10	2	1.185	1.079	0.955	0.822	0.662
11	1	0.632	0.547	0.438	0.307	0.165

Table E.4: Values of A_{Umax}

N_U	N_L	r_m 1	2	3	4	5	N_U	N_L	r_m 1	2	3	4	5
1	1	0.449	0.570	0.687	0.797	0.899	4	4	0.287	0.394	0.506	0.611	0.710
1	2	0.405	0.609	0.793	0.960	1.113	4	5	0.304	0.437	0.570	0.692	0.806
1	3	0.445	0.713	0.948	1.156	1.343	4	6	0.323	0.481	0.633	0.771	0.897
1	4	0.502	0.826	1.103	1.344	1.557	4	7	0.343	0.525	0.694	0.845	0.982
1	5	0.564	0.938	1.251	1.518	1.753	4	8	0.364	0.569	0.753	0.917	1.063
1	6	0.627	1.046	1.390	1.680	1.931	5	1	0.34	0.359	0.382	0.409	0.438
1	7	0.690	1.150	1.520	1.830	2.095	5	2	0.266	0.308	0.356	0.408	0.462
1	8	0.752	1.249	1.643	1.969	2.244	5	3	0.258	0.324	0.395	0.470	0.546
1	9	0.813	1.344	1.759	2.099	2.382	5	4	0.263	0.352	0.447	0.544	0.638
1	10	0.872	1.435	1.868	2.218	2.511	5	5	0.276	0.386	0.504	0.620	0.732
1	11	0.929	1.521	1.972	2.331	2.631	5	6	0.292	0.424	0.562	0.696	0.821
2	1	0.38	0.447	0.519	0.590	0.658	5	7	0.307	0.462	0.620	0.769	0.907
2	2	0.328	0.449	0.572	0.688	0.796	6	1	0.337	0.352	0.370	0.392	0.415
2	3	0.347	0.516	0.679	0.828	0.966	6	2	0.251	0.286	0.326	0.367	0.413
2	4	0.381	0.593	0.790	0.968	1.129	6	3	0.237	0.292	0.352	0.414	0.479
2	5	0.421	0.672	0.898	1.100	1.280	6	4	0.238	0.313	0.392	0.475	0.558
2	6	0.461	0.749	1.002	1.223	1.419	6	5	0.247	0.341	0.439	0.540	0.639
2	7	0.503	0.825	1.101	1.341	1.550	6	6	0.259	0.371	0.488	0.606	0.715
2	8	0.544	0.897	1.195	1.449	1.673	7	1	0.328	0.341	0.357	0.374	0.393
2	9	0.585	0.968	1.286	1.553	1.785	7	2	0.248	0.271	0.299	0.331	0.365
2	10	0.626	1.036	1.370	1.652	1.893	7	3	0.238	0.270	0.314	0.361	0.411
3	1	0.360	0.399	0.446	0.494	0.542	7	4	0.238	0.284	0.342	0.406	0.472
3	2	0.278	0.355	0.437	0.519	0.596	7	5	0.239	0.303	0.377	0.455	0.535
3	3	0.274	0.387	0.499	0.607	0.709	8	1	0.321	0.331	0.341	0.355	0.370
3	4	0.289	0.435	0.573	0.704	0.826	8	2	0.253	0.275	0.302	0.331	0.360
3	5	0.312	0.486	0.648	0.800	0.939	8	3	0.245	0.281	0.324	0.365	0.409
3	6	0.337	0.539	0.724	0.893	1.047	8	4	0.246	0.299	0.353	0.410	0.466
3	7	0.364	0.591	0.797	0.982	1.149	9	1	0.319	0.329	0.338	0.349	0.359
3	8	0.391	0.642	0.868	1.068	1.247	9	2	0.254	0.276	0.296	0.323	0.352
3	9	0.419	0.693	0.937	1.149	1.34	9	3	0.245	0.277	0.315	0.355	0.398
4	1	0.342	0.367	0.398	0.432	0.466	10	1	0.319	0.327	0.335	0.344	0.354
4	2	0.277	0.331	0.391	0.453	0.512	10	2	0.251	0.271	0.289	0.310	0.336
4	3	0.275	0.357	0.444	0.529	0.610	11	1	0.318	0.326	0.334	0.341	0.349

Table E.5: Values of B_{Umax}

N_U	N_L	r_m 1	2	3	4	5	N_U	N_L	r_m 1	2	3	4	5
1	1	1.003	0.906	0.828	0.767	0.719	4	4	1.462	1.261	1.116	1.011	0.931
1	2	1.232	1.020	0.892	0.806	0.743	4	5	1.440	1.212	1.061	0.954	0.875
1	3	1.237	0.987	0.851	0.764	0.702	4	6	1.411	1.165	1.010	0.904	0.826
1	4	1.196	0.937	0.803	0.719	0.661	4	7	1.377	1.119	0.965	0.862	0.788
1	5	1.147	0.888	0.760	0.681	0.627	4	8	1.343	1.078	0.925	0.824	0.754
1	6	1.099	0.846	0.723	0.649	0.598	5	1	1.111	1.096	1.073	1.042	1.012
1	7	1.056	0.810	0.693	0.622	0.574	5	2	1.419	1.335	1.244	1.165	1.097
1	8	1.016	0.777	0.666	0.599	0.555	5	3	1.503	1.354	1.223	1.119	1.037
1	9	0.981	0.749	0.643	0.580	0.539	5	4	1.516	1.319	1.167	1.053	0.966
1	10	0.949	0.724	0.623	0.563	0.524	5	5	1.501	1.270	1.107	0.990	0.900
1	11	0.920	0.703	0.605	0.549	0.512	5	6	1.473	1.218	1.050	0.932	0.845
2	1	1.070	1.004	0.935	0.876	0.826	5	7	1.442	1.171	1.000	0.883	0.797
2	2	1.312	1.131	1.002	0.908	0.836	6	1	1.109	1.099	1.081	1.056	1.030
2	3	1.332	1.095	0.948	0.848	0.775	6	2	1.479	1.395	1.310	1.231	1.160
2	4	1.298	1.038	0.887	0.789	0.718	6	3	1.590	1.440	1.307	1.198	1.109
2	5	1.251	0.981	0.834	0.739	0.673	6	4	1.618	1.415	1.255	1.132	1.036
2	6	1.204	0.931	0.788	0.698	0.636	6	5	1.613	1.367	1.192	1.064	0.969
2	7	1.158	0.887	0.749	0.663	0.604	6	6	1.589	1.316	1.134	1.004	0.914
2	8	1.116	0.849	0.716	0.635	0.578	7	1	1.136	1.125	1.107	1.085	1.062
2	9	1.077	0.815	0.686	0.609	0.557	7	2	1.493	1.446	1.387	1.322	1.258
2	10	1.041	0.785	0.661	0.586	0.537	7	3	1.593	1.508	1.411	1.316	1.233
3	1	1.083	1.044	0.992	0.944	0.899	7	4	1.628	1.505	1.378	1.265	1.166
3	2	1.436	1.277	1.148	1.051	0.978	7	5	1.637	1.477	1.329	1.202	1.102
3	3	1.511	1.276	1.117	1.007	0.925	8	1	1.162	1.156	1.146	1.131	1.112
3	4	1.505	1.227	1.059	0.948	0.866	8	2	1.457	1.410	1.355	1.299	1.247
3	5	1.468	1.171	1.004	0.893	0.813	8	3	1.533	1.447	1.359	1.281	1.215
3	6	1.425	1.118	0.952	0.845	0.768	8	4	1.553	1.433	1.324	1.233	1.158
3	7	1.379	1.070	0.908	0.803	0.730	9	1	1.165	1.160	1.154	1.142	1.127
3	8	1.334	1.028	0.868	0.767	0.697	9	2	1.444	1.400	1.351	1.299	1.251
3	9	1.293	0.988	0.833	0.736	0.669	9	3	1.519	1.434	1.353	1.278	1.210
4	1	1.117	1.094	1.059	1.021	0.985	10	1	1.163	1.162	1.156	1.146	1.135
4	2	1.396	1.297	1.200	1.120	1.053	10	2	1.452	1.411	1.369	1.323	1.277
4	3	1.460	1.300	1.171	1.073	0.995	11	1	1.162	1.161	1.155	1.147	1.139

Appendix F
The Yuan (2016) two-stage procedure

F.1 Introduction

In Yuan (2016), a modification of the ASCE 7-10 two-stage procedure is proposed to address structures beyond having a stiffness ratio larger than the two-stage stiffness ratio R_{kU2stg} (note: R_{k2stg} is the nomenclature used by Yuan). Their approach uses an additional top storey force analogous to that used by NBCC 2015, defined in terms of a *regular* component and an *irregular/interactional* component. The regular component is associated with the modal masses and period of the perfectly uniform upper structure considered alone, and the irregular/interactional component considers the remaining proportion of the top shear. This is unlike the newly-proposed method given in Chapter 4.5, which instead changes the force distribution to match a proposed top storey shear. Replaced by the newly-proposed method in this thesis, the Yuan (2016) two-stage procedure is given here so that it can be referenced in Chapter 4. Note also that, technically, the method first appears in Yuan & Xu (2016) – however, this method exclusively references ASCE 7-10. The method is only adapted to NBCC 2010 within Yuan (2016), which is the exclusive source of the content in this appendix.

F.2 The rationale of the two-stage procedure

The rationale associated with the two-stage procedure given by Yuan (2016) is already discussed in the context of R_{kU2stg} in Chapter C.2.3. To not belabour this point, Yuan (2016) associates the two-stage phenomena with the upper structure and lower structure responses being delineated clearly into the first and second modes, respectively. This manifests as $T_U \approx T_1$ and $T_L \approx T_2$, and therefore the force applied at the upper and lower DOF of the 2DOF model arises only from the respective mass. In other words, the upper structure only contributes an equivalent static force to itself, and likewise to the lower structure – the masses do not interact whatsoever, theoretically.

F.3 Seismic load distribution

F.3.1 Upper structure

As with the ASCE 7 two-stage procedure, Yuan (2016) assumes that the upper structure acts as though fixed to the ground. However, despite the theoretical rationale for the two-stage procedure,

there is in practical terms some magnification of the upper structure's base shear. Given that $R_k > R_{kU2stg}$, $\alpha_U = \alpha_{U2stg}$, and so the assumed base shear on the upper structure is:

$$V_{Ub} = \alpha_{U2stg} M_U g S_a(T_U) \tag{F.1}$$

where α_{U2stg} is defined by Equation (D.10) and R_{kU2stg} by Equation (D.17). Based on this V_{Ub}, Yuan (2016) assumes that the storey forces are defined in the same manner as the NBCC, i.e. by Equation (4.3), except that the top storey shear F_t is redefined to account for irregular structures.

F.3.2 Lower structure

For the lower structure, Yuan (2016) assumes that the storey forces are computed based only on the mass and period of the lower structure and according to the default NBCC distribution without a top storey force applied, i.e.:

$$F_x = (M_L S_a(T_L)) \frac{W_x h_x}{\sum_{i=1}^{n=N_L} W_i h_i} \tag{F.2}$$

where F_x is the top storey shear on each storey of the lower structure. This definition of the storey force applies only to the lower structure – those in the upper structure are defined using V_{Ub} and the (forthcoming) definition of the additional top storey shear F_t. Having established the storey forces on the upper structure and lower structure, Yuan (2016) proposes that the storey shears in the i-th storey of the lower structure, V_{Li}, be defined by combining the upper structure base shear V_{Ub} given by Equation (F.1) with the storey forces F_x given by Equation (F.2) via the square-root-sum-of-squares (SRSS) method:

$$V_{Li} = \sqrt{(V_{Ub})^2 + \left(\sum_{x=i}^{N_L} F_x\right)^2} \tag{F.3}$$

By using the SRSS method to combine the responses for the lower structure, Yuan (2016) differs from the two-stage procedure given by ASCE 7 (2010, 2017). ASCE 7 makes no explicit mention of how the reaction force from the upper structure is to be applied to the lower structure. Given that, ASCE 7 presumably intends that the absolute sum (ABSSUM) method be used, rather than the SRSS, to combine the two structures' responses. This appears to be the approach, for example, used by SEAOC (2015) in their 2015 IBC seismic design manual.

F.3.3 Top storey loading

While Sections F.3.1 and F.3.2 describe the assumed force distribution used in the Yuan (2016), these components are comparable to those given by the NBCC (NRCC, 2010, 2015c) and ASCE 7 (2010, 2017) and of comparatively less significance to the method than its linchpin, the top storey shear F_t. Yuan (2016) identifies that the top storey of the upper structure is very susceptible to the likes of higher mode effects such as those embodied by α_U, such that the top storey shear may significantly exceed that of the uniform upper structure considered alone. Surmising that the response of the top storey associated with the uniform upper structure is more likely to be affected by higher-mode effects due to the presence of the lower structure, Yuan (2016) proposes that an additional top force be applied similarly to that of the NBCC. As in Equation (4.4), Yuan (2016) specifies that the top storey force is to a proportion of the base shear of the upper structure:

$$F_t = \gamma V_{Ub} \tag{F.4}$$

where γ denotes the proportion of the base shear V_{Ub} defined by Equation (F.1). Specifically, Yuan (2016) defines γ as the sum of two parts: γ_{reg}, the component associated with the perfectly-uniform upper structure, and γ_{intr}, the portion associated with the interaction between the top storey and the rest of the structure in excess of the regular component. γ_{intr}, therefore, can be thought of as the component attributed to the irregularity of the structure and the presence of the lower structure, such that:

$$\gamma = \gamma_{reg} + \gamma_{intr} \tag{F.5}$$

F.3.3.1 The regular component, γ_{reg}

In either the NBCC (NRCC, 2010, 2015c) or ASCE 7 (2010, 2017), higher-mode effects on the top storey of a regular structure are already captured by code formulas. In the case of NBCC 2015, F_t via Equation (4.4) fulfills this role, and in ASCE 7 the exponent k given by Equation (4.8) serves as its counterpart. In both cases, the factor is only a function of the fundamental period. However, as noted by Yuan (2016) and as discussed in Chapter 2, the predominant period of the seismic excitation influences the response. This is not captured in either the ASCE 7 or NBCC approaches. To address this, Yuan (2016) proposes that γ_{reg} be based on modal masses of a uniform structure, combined using the SRSS method, as follows:

$$\gamma_{reg} = \frac{\sqrt{\sum_{i=1}^{n=N_U} \left(\frac{M_{Ni} S_a(T_i)}{N_U S_a(T_1)}\right)^2} - \frac{m_U h_N}{\sum_{i=1}^{n=N_U}(m_U h_i)}}{1 - \frac{m_U h_N}{\sum_{i=1}^{n=N_U}(m_U h_i)}} \quad \text{(F.6)}$$

where M_{Ni} and T_i are the normalized effective modal mass of the top storey and the period associated with the i-th mode. The structure is assumed to be perfectly uniform, and therefore M_{Ni} and T_i are constant as a function of the number of storeys. M_{Ni} and T_i are tabulated in Table F.1 and Table F.2, which have been expanded compared to Yuan (2016) to accommodate the expanded scope of 12 storeys. Note that if $N_U = 1$, the full mass of the upper structure acts at the storey, and Equation (F.6) does not apply.

Table F.1: *i*-th mode normalized effective modal masses M_{Ni} for top storey of uniform structure

i / N_U	1	2	3	4	5	6	7	8	9	10	11
2	1.171	-0.171	N/A	N/A	N/A	N/A	N/A	N/A	N/A	N/A	N/A
3	1.220	-0.280	0.060	N/A	N/A	N/A	N/A	N/A	N/A	N/A	N/A
4	1.241	-0.333	0.120	-0.028	N/A	N/A	N/A	N/A	N/A	N/A	N/A
5	1.252	-0.362	0.159	-0.063	0.015	N/A	N/A	N/A	N/A	N/A	N/A
6	1.258	-0.379	0.183	-0.090	0.036	-0.009	N/A	N/A	N/A	N/A	N/A
7	1.262	-0.390	0.200	-0.110	0.057	-0.024	0.006	N/A	N/A	N/A	N/A
8	1.264	-0.398	0.212	-0.124	0.072	-0.038	0.017	-0.004	N/A	N/A	N/A
9	1.266	-0.403	0.220	-0.135	0.084	-0.050	0.027	-0.012	0.003	N/A	N/A
10	1.267	-0.407	0.226	-0.143	0.093	-0.060	0.037	-0.020	0.009	-0.002	N/A
11	1.268	-0.410	0.231	-0.149	0.101	-0.068	0.045	-0.028	0.015	-0.007	0.002

Table F.2: *i*-th mode normalized circular frequencies $\bar{\omega}_i$ of uniform structures

i / N_U	1	2	3	4	5	6	7	8	9	10	11
2	0.618	1.618	N/A	N/A	N/A	N/A	N/A	N/A	N/A	N/A	N/A
3	0.445	1.247	1.802	N/A	N/A	N/A	N/A	N/A	N/A	N/A	N/A
4	0.347	1.000	1.532	1.879	N/A	N/A	N/A	N/A	N/A	N/A	N/A
5	0.285	0.831	1.310	1.683	1.919	N/A	N/A	N/A	N/A	N/A	N/A
6	0.241	0.709	1.136	1.497	1.771	1.942	N/A	N/A	N/A	N/A	N/A
7	0.209	0.618	1.000	1.338	1.618	1.827	1.956	N/A	N/A	N/A	N/A
8	0.185	0.547	0.892	1.205	1.478	1.700	1.865	1.966	N/A	N/A	N/A
9	0.165	0.491	0.803	1.094	1.355	1.578	1.759	1.892	1.973	N/A	N/A
10	0.150	0.445	0.731	1.000	1.247	1.466	1.653	1.802	1.911	1.978	N/A
11	0.137	0.407	0.670	0.920	1.153	1.365	1.551	1.709	1.834	1.926	1.981

Equation (F.6) represents the difference between the ratio of the MRS-derived shear force and MRS-derived first-mode shear force (i.e. the term in the square root) and the proportion of the base shear specified by the NBCC's default load distribution. This difference is normalized by another representing the proportion of the upper structure's mass that the NBCC force distribution does not contribute to the top storey. The top storey force, F_t, indicated by NBCC is not included, for the intent of the proposed proportion is to replace that component altogether. In this way, Equation (F.6) captures the component of the top shear force associated with the uniform upper structure which is not captured by the default NBCC distribution.

For the above, the period T_i is calculated similarly to T_U:

$$T_i = \frac{2\pi}{\bar{\omega}_i}\sqrt{\frac{m_U}{k_U}} \tag{F.7}$$

where each period $\bar{\omega}_i$ is provided in Table F.2.

F.3.3.2 The irregular component, γ_{intr}

To address the interactional component as it affects the upper structure, Yuan (2016) introduces γ_{intr} and its counterpart, η_{intr}. γ_{intr} is defined as before by Equation (F.5) and η_{intr} is defined relative to γ_{intr}:

$$\gamma_{intr} = 1 - \eta_{intr} \tag{F.8}$$

Similarly to γ_{intr}, η_{intr} represents a proportion of a whole and is bounded between zero and unity. It has the inverse meaning to γ_{intr}: whereas $\gamma_{intr} = 1$ indicates that the full base shear is applied at the top storey, $\eta_{intr} = 1$ indicates that the interaction of the first mode of the lower structure and the higher modes of the upper structure does not induce an additional top storey force, i.e. that $\gamma_{intr} = 0$. Correspondingly, a smaller η_{intr} corresponds to a larger top storey force.

The calibration of η_{intr} is performed by Yuan (2016). They observe that the error of the top storey considering no additional top-storey force is associated (in the ASCE 7 formulation) with T_U/T_S and T_U/T_L. Specifically, T_U/T_S is related to the relative value of $S_a(T_U)$ and the maximum $S_a(T)$, and T_U/T_L is related to the relative closeness of the upper and lower structures' fundamental periods. Considering these variables, Yuan (2016) proposes that η_{intr} decreases as a T_U/T_S increases, attaining some minimum, η_{min}, where T_U/T_S exceeds T_U/T_L. In the NBCC formulation where period ratios are exchanged for spectral acceleration ratios, η_{intr} is defined as:

$$\eta_{intr} = \begin{cases} 1 & \frac{S_a(T_L)}{S_a(T_U)} \leq \left(\frac{T_U}{T_S}\right)_{CRT} \\ \eta_{\min}\left[\frac{S_a(T_L)/S_a(T_U)}{T_U/T_L}\right]^{x_5} & \left(\frac{T_U}{T_S}\right)_{CRT} < \frac{S_a(T_L)}{S_a(T_U)} < \frac{T_U}{T_L} \\ \eta_{\min} & \frac{S_a(T_L)}{S_a(T_U)} = \frac{T_U}{T_L} \end{cases} \quad \text{(F.9)}$$

where $(T_U/T_S)_{CRT}$ is a tabulated critical value, provided in Table F.4, and x_5 is an exponent defined as follows:

$$x_5 = \frac{\ln(\eta_{min})}{\ln\left[\frac{T_U/T_L}{\left(\frac{T_U}{T_S}\right)_{CRT}}\right]} \quad \text{(F.10)}$$

The minimum value of η_{intr}, η_{min}, is said to vary as a function of T_U/T_L between 1 and two values - η_{min1} and η_{min2}:

$$\eta_{min} = \begin{cases} \eta_{\min 1}\left[\frac{T_U/T_L}{\sqrt{R_{k2stg}/R_m}}\right]^{x_6} & \frac{T_U}{T_L} < \left(\frac{T_U}{T_L}\right)_{CRT1} \\ \eta_{min2} & \left(\frac{T_U}{T_L}\right)_{CRT1} \leq \frac{T_U}{T_L} \leq \left(\frac{T_U}{T_L}\right)_{CRT2} \\ \eta_{\min 2}\left[\frac{T_U/T_L}{(T_U/T_L)_{CRT2}}\right]^{x_7} & \left(\frac{T_U}{T_L}\right)_{CRT2} < \frac{T_U}{T_L} < \left(\frac{T_U}{T_L}\right)_{CRT3} \\ 1 & \left(\frac{T_U}{T_L}\right)_{CRT3} \leq \frac{T_U}{T_L} \end{cases} \quad \text{(F.11)}$$

where R_{k2stg} is defined according to Equation (C.13), the critical values $(T_U/T_L)_{CRT}$ are provided by Table F.3, η_{min1} and η_{min2} are given in Table F.3 and Table F.4, and x_6 and x_7 are defined as:

$$x_6 = \frac{\ln(\eta_{min2}/\eta_{min1})}{\ln\left[\frac{(T_U/T_L)_{CRT1}}{\sqrt{R_{k2stg}/R_m}}\right]} \quad \text{(F.12)}$$

$$x_7 = \frac{\ln(\eta_{min2})}{\ln\left[\frac{(T_U/T_L)_{CRT2}}{(T_U/T_L)_{CRT3}}\right]} \quad \text{(F.13)}$$

Using Equations (F.4) to (F.13), the loads on any structure for which $R_k \geq R_{kU2stg}$ can be estimated using the Yuan (2016). However, the definitions of the critical T_U/T_L, T_U/T_S and η are based on the

ASCE 7 spectrum. Consequently, they exploit the fact that the Newmark-Hall spectrum explicitly relates ratios of spectral accelerations to periods – if this were not applied, T_U/T_L should be replaced by $S_a(T_U)/S_a(T_L)$ and T_U/T_S with $S_a(T_U)/S_a(T_S)$. Therefore, for the application of these equations to the NBCC, the EXP-2 formulation given in Appendix D should be used. Unfortunately, this relationship does not apply to the NBCC 2015 spectrum, and so some sort of equivalency must be assumed to apply this method to the NBCC 2015 spectrum.

Table F.3: Empirical values of critical T_U/T_L and T_U/T_S (Yuan, 2016)

N_U	$(T_U/T_L)_{CRT1}$	$(T_U/T_L)_{CRT2}$	$(T_U/T_L)_{CRT3}$	$(T_U/T_S)_{CRT}$
3	2.34	3.18	4.71	1.00
4	3.06	4.25	7.44	1.00
5	3.74	4.61	9.30	1.05
6	4.44	5.87	10.92	1.24
7	4.60	6.40	10.70	1.43
8	4.83	6.64	12.97	1.63
9	4.86	7.82	13.08	1.82

Table F.4: Values of η_{min1} and η_{min2} for two-stage analysis procedure (Yuan, 2016)

		η_{min1}					η_{min2}		
		r_m					r_m		
N_U	N_L	1	2	3	N_U	N_L	1	2	3
1	1	1.00	1.00	1.00	1	1	1.00	1.00	1.00
2	1	1.00	1.00	1.00	2	1	1.00	1.00	1.00
2	2	1.00	1.00	1.00	2	2	1.00	1.00	1.00
2	3	1.00	1.00	1.00	2	3	1.00	1.00	1.00
3	1	1.00	0.91	0.70	3	1	1.00	0.91	0.70
3	2	0.95	0.57	0.55	3	2	0.95	0.57	0.55
3	3	0.68	0.49	N/A	3	3	0.68	0.49	N/A
3	4	0.60	0.46	N/A	3	4	0.60	0.46	N/A
4	1	1.00	0.86	0.74	4	1	1.00	0.86	0.74
4	2	0.90	0.68	0.55	4	2	0.90	0.68	0.55
4	3	0.78	0.56	0.55	4	3	0.78	0.56	0.55
4	4	0.72	0.42	N/A	4	4	0.72	0.42	N/A
4	5	0.68	0.51	N/A	4	5	0.65	0.51	N/A
5	1	1.00	0.89	0.79	5	1	1.00	0.89	0.79
5	2	0.91	0.70	0.63	5	2	0.91	0.70	0.63
5	3	0.83	0.63	0.53	5	3	0.83	0.61	0.53
5	4	0.77	0.55	0.47	5	4	0.75	0.55	0.47
5	5	0.68	0.49	N/A	5	5	0.68	0.49	N/A
6	1	1.00	0.90	0.83	6	1	1.00	0.90	0.83
6	2	0.93	0.81	0.70	6	2	0.93	0.78	0.69
6	3	0.88	0.73	0.52	6	3	0.86	0.68	0.52
6	4	0.84	0.60	0.50	6	4	0.78	0.59	0.50
7	1	1.00	0.92	0.87	7	1	1.00	0.92	0.85
7	2	0.95	0.84	0.74	7	2	0.95	0.80	0.72
7	3	0.88	0.77	0.62	7	3	0.87	0.74	0.58
8	1	1.00	0.92	0.86	8	1	1.00	0.92	0.86
8	2	0.95	0.82	0.73	8	2	0.95	0.82	0.73
9	1	1.00	0.94	0.89	9	1	1.00	0.94	0.89

Note: N/A indicates that the two-stage analysis procedure is not applicable. The table should be interpolated for intermediate values of r_m.

F.4 Design procedure

As an alternative to the two methods provided in this study, structures for which $R_k \geq R_{kU2stg}$ can be evaluated according to the Yuan (2016) two-stage procedure set out in the prior sections of this appendix. The procedure is set out below, but note that the original procedure is calibrated only for 1

$\leq r_m \leq 3$, $N_U + N_L \leq 10$ and the NBCC 2010 spectrum, specifically via the EXP-2 approximation. The method is only approximately applicable to the NBCC 2015 spectrum, and there are no guarantees that the method is accurate or even defined for values of r_m, N_U and N_L outside the originally considered scope (i.e. that of Yuan (2016)).

1. Based on the selected building configuration, identify the value of each of these parameters: m_U, k_U, m_L, k_L, N_U, N_L, $S_a(T)$
2. Evaluate $\bar{\omega}_{1L}$ and $\bar{\omega}_{1U}$ from Table 3.1, corresponding to $N = N_L$ and $N = N_U$
3. Calculate r_m, r_k, R_m and R_k based on Equations (3.16) to (3.19)
4. Determine R_{kU1}, R_{kU2}, R_{kU3} and R_{kU2stg} according to Equations (3.25) to (3.28) and Appendix E, as well as A_{U1}, B_{U1}, A_{Umax}, and B_{Umax} from Appendix E. If $R_k \geq R_{kU2stg}$, it is possible to use the Yuan (2016) two-stage procedure detailed in Appendix F, subject the conditions listed in that appendix.
5. Evaluate α_{U1} according to Equations (3.29) and (3.30) (if applicable, i.e. $R_{kU1} < R_{kU2}$), α_{Umax} according to Equations (3.31) and (3.32) and α_{U2stg} according to Equation (3.33). $S_a(T_U)$ is evaluated according to Equation (3.37) and φ_{L1} according to Equation (A.13). As with the definition of α_U given in Chapter 3, if $R_{kU1} \geq R_{kU2}$, α_U does not require α_{U1} to be calculated, only α_{U2stg} and α_{Umax} are required. In such a case, R_{kU1} is only used as a lower bound on R_k, i.e. it is required that $R_{kU1} \leq R_k$.
6. Evaluate α_U according to Equations (3.21) to (3.24). Recall that R_k must be larger than R_{kU1}. If α_U is larger than desired, repeat steps 1-6 with a modified set of properties. Note that the estimate of α_U will never be greater than the maximum of α_{U1}, α_{U2stg} and α_{Umax}, nor less than the minimum. If a lower value is desired, dynamic analysis (e.g. MRS analysis) can be used.
7. Evaluate V_{Ub} according to Equation (3.7). It should not be less than Equation (4.2).
8. Confirm $R_k \geq R_{kU2stg}$, R_{kU2stg} is defined by Yuan (2016) according to Equation (D.17), and that $N_U + N_L \leq 10$, $r_m \leq 3$.
9. Evaluate α_{U2stg} according to the Yuan (2016) definition, Equation (D.10).
10. Evaluate the base shear of the upper structure, V_{Ub}, according to Equation (F.1). Use the value of α_{U2stg} evaluated in the previous step, rather than according to the newly-proposed definition.

11. Select the appropriate $S_a(T)$ – strictly speaking, Yuan (2016) requires that the EXP-2 approximation be used based on NBCC 2010. The calculation for the relevant parameters is given in Appendix D. However, the direct substitution of the NBCC 2015 $S_a(T)$ is most likely adequate.

12. Evaluate T_L according to Equation (3.15), and the resulting storey forces on the lower structure according to Equation (F.2). The storey shears on the lower structure are defined by Equation (F.3).

13. Evaluate the regular component of the top storey shear, γ_{reg}, according to Equation (F.6). The required normalized effective modal masses M_{Ni} and normalized circular frequencies $\bar{\omega}_i$ are provided by Table F.1 and Table F.2, and T_i is defined by Equation (F.7).

14. Evaluate η_{intr} according to Equation (F.9). This requires $(T_U/T_S)_{\text{CRT}}$, $(T_U/T_L)_{\text{CRT1}}$, $(T_U/T_L)_{\text{CRT2}}$, and $(T_U/T_L)_{\text{CRT3}}$, obtained from Table F.3, and x_5, x_6, x_7, η_{min}, η_{min1} and η_{min2}, defined by Equations (F.10), (F.12), (F.13), (F.11) and Table F.4 (for η_{min1} and η_{min2}), in that order.

15. Evaluate the irregular/interactional component of the top storey shear, γ_{intr} via Equation (F.8).

16. Evaluate the top storey shear F_t according to Equation (F.4). This replaces the NBCC 2010/2015 definition of F_t.

17. The storey shears and forces on the upper structure are defined using Equation (4.3), with V = V_{Ub}.

Appendix G

Stiffness of CFS shear wall and RC moment-resisting frame

G.1 Introduction

Rather than elaborate on the calculation of SFRS element stiffnesses in the Chapter 3 and 4 examples, this appendix describes the rationale used to estimate the member stiffnesses. The CFS shear wall stiffnesses are estimated based on AISI S400-15 (AISI, 2015) and the reinforced concrete moment-resisting frame column stiffnesses are estimated based on CSA A23.3-19 (CSA Group, 2019). The intention of these calculations is not to provide an exact value for the stiffness – this is impractical, as the stiffness will vary based on the members selected, whether an initial or secant stiffness is used, and based on the effects of non-structural members. Instead, the intent is to provide a semi-realistic baseline value for the examples' stiffness.

G.2 CFS stiffness

In Yuan (2016), the CFS shears walls are assumed to be oriented strand board (OSB) sheathed CFS shear walls corresponding to tests 25A, 25B, and 25C in Branston (2004). These shear wall configurations have back-to-back 362S162-43 CFS chord studs (F_y = 230 MPa, 33 ksi) backed by one 11 mm sheet of OSB, and are tested in 1220 x 2440 mm segments. The OSB is subject to CSA O325 (Canadian Standards Association, 1992) and is fastened at 3" increments (75 mm). Per Branston (2004), these specimens have an average elastic stiffness of 1960 kN/m. Meanwhile, Yuan (2016) assumes that two sheets of sheathing are provided, and thus that the stiffness is doubled - 3836 kN/m. In doing so, they assume that the failure of the studs, particularly at the ends of the wall, does not control the design.

However, it is not necessarily practical to use tested values as design values, despite that AISI S400 cites Branston (2004). Stiffness of shear walls is not well-addressed by AISI S400-15 - to estimate the stiffness for an OSB-sheathed shear wall, the formulation for design deflection is used:

$$\delta = \frac{2vh^3}{3EA_c b} + \frac{\omega_1\omega_2 vh}{\rho G t_{sheathing}} + \omega_1^{\frac{5}{4}}\omega_2\omega_3\omega_4\left(\frac{v}{\beta}\right)^2 + \frac{h}{b}\delta_v \qquad \text{(G.1)}$$

For Equation (G.1), the material properties for the CFS studs are based on Clark-Dietrich specifications (2017), the OSB properties are based on Louisiana Pacific specifications (2012) and the American Wood Council (2017, 2018), and the remaining variables are per AISI S400-15 (AISI,

2015). The chord studs are back-to-back 362S162-43 and thus t_{stud} = 0.0451 in (1.15 mm), A_c = 2×0.340 in^2 (439 mm^2) and E = 203000 MPa. The OSB panels are 11 mm thick (7/16") and are assumed to have a 24/16 span rating, and so $t_{sheathing}$ = 22 mm. Per the AWC, 24/16 panels have a rigidity-through the thickness of 83500 lb$_f$/in (14600 N/mm), and thus it is assumed that the shear modulus G = 1329 MPa (rigidity-through-the-thickness $G_v t_v$ can be used to approximate G per AISI S400). It is assumed that the walls are 1220 mm by 2440 mm and thus b = 1220 mm and h = 2440 mm with a fastener spacing of s = 75 mm (3"). The remaining variables are defined by AISI S400 for OSB: β = 1.91 N/mm$^{1.5}$, ρ = 1.05, ω_1 = 0.492, ω_2 = 0.732, ω_3 = 1 and ω_4 = 1.

Left outstanding are δ_v, V and v. δ_v corresponds to the vertical deformation expected from the anchorage attachment details – this is assumed to be negligible. Meanwhile, V and v are the total shear and shear flow and thus depend on the condition being considered. Having defined all other variables, the shear is dictated by the displacement and vice versa. Two conditions are considered – the wall as stressed to the interstorey drift ratio, and the wall at its factored resistance. Considering the interstorey drift limit of 2.5% of the storey height applied to a 3-metre storey, the limiting drift is 75 mm, and the corresponding force is 35.7 kN. The secant stiffness is therefore 475.8 kN/m, or 390 kN/m per metre of wall. But this exceeds the factored strength of the wall segment – per AISI S400, the nominal resistance for this type of wall is 18.5 kN/m per metre, and so the factored resistance is 15.8 kN for this 1.2 metre-long wall segment. Considering instead that V = 15800 N, the stiffness is 1000 kN/m, or 822 kN/m/m for a one-panel wall, or 2000 kN/m (1640 kN/m/m) for a two-panel wall.

G.3 RC frame stiffness

The resistance of the reinforced concrete moment frame is estimated according to CSA A23.3-19 (2019), albeit with some simplifying assumptions. For one, A23.3-19 specifies that the effective area of a column for seismic analysis is defined as between 0.5 and 1.0 times the gross area, defined as a function of the dead load applied to the column. In lieu of a more specific analysis, the effective area is taken as 50% of the gross area, and the stiffness is assumed to be $12EI/L^3$, corresponding to the theoretical fixed end moment for a fixed-fixed column experiencing a lateral displacement. The modulus of elasticity is assumed to be equal to $4500\sqrt{f_c'}$, and the columns are assumed to be equal, square columns.